THE METAL PHOTODISSOLUTION EFFECT IN SPIN-COATED As-S FILMS AND ITS APPLICATION IN GRATING FABRICATION

by

Eva Hajto

A thesis presented for the degree of
Doctor of Philosophy at the
University of Edinburgh

December 1991

DECLARATION

This thesis is the original composition of the author's work, unless stated otherwise, and has not been submitted previously for any other degree.

ACKNOWLEDGEMENTS

I would like to thank the following people for their help and assistance throughout:

Prof. Alan Owen for his guidance;

my supervisors, Dr. P. J. S. Ewen and Dr. R. E. Belford for their interest and advice;

the Science and Engineering Research Council and Pilkington Plc. for providing the CASE studentship.

I am most grateful to my family for their support and encouragement.

ABSTRACT

The deposition of chalcogenides from their solutions using the spin-coating technique offers a new possibility for preparing technologically useful thin films in an easier way than the conventional vacuum techniques. This study describes the use of the spin-coating technique to prepare chalcogenide thin films from their propylamine solutions. The composition range $As_{15}S_{85}-As_{40}S_{60}$ was investigated.

Infrared transmittance measurements show that the main structural unit of the spin-coated films is the AsS_3 pyramid. IR Spectroscopy also indicates that the amine group of the solvent propylamine molecule plays the dominant role in the dissolution process. The solvent / chalcogenide interaction was found to occur at the S-sites of the AsS_3 structural units of the chalcogenide.

The dispersion of the refractive index, $n(\lambda)$, for undoped and Ag-doped spin-coated As-S films was measured and shows that these films are transparent in the $\lambda = 1\text{-}10$ μm spectral region. The refractive index values were fitted with the single oscillator expression and the oscillator energy, E_o, and the oscillator dispersion energy, E_d, for spin-coated films were determined. These values provide further information about the structure of these films. The values of the absorption coefficient, α, for a range of compositions of spin-coated As-S films and also for silver photodoped spin-coated As-S films at the optical absorption edge were calculated, and the band gap energy, E_g, for these films determined. The compositional dependence of E_g is explained by the bond strengths of the different bonds in the films.

The kinetics of silver photodissolution was also studied as this is a promising method for high resolution image formation in spin-coated As-S films. Simultaneous transmittance and reflectance measurements indicate a diffusion controlled process. Higher photodissolution rate was obtained with increasing illumination intensity and shorter illumination wavelength.

The preparation of holographic diffraction gratings in spin-coated As-S films by silver photodissolution and subsequent selective etching using CF_4 plasma is described. The diffraction efficiency of the surface relief gratings yielded a similar value to that for gratings prepared in vacuum-evaporated films.

CONTENTS

CHAPTER 1

INTRODUCTION

1.1 THE AMORPHOUS STATE

The position of atoms in a solid may be considered from the point of view of short and long range order. The short range order is associated with the interatomic distances (determined by the bond lengths) and the coordination number (determined by the valency and the bond angle) around a given atom with respect to its nearest neighbours. In *crystals* the position of atoms or molecules is determined by the unit cell. The unit cell in a crystal repeats itself periodically in three dimensions, that is to say the crystalline material has translational symmetry. This translational symmetry means that any structural element of the lattice, a given atom for example, can be found in any particular direction at regular intervals. An *amorphous* solid does not have long range order in its structure, in contrast to the crystalline counterpart, but there is short range order determined by the chemical bonding. The term amorphous solid is a general one, applicable to any solid having a non-periodic atomic array described above. The term *glass* has conventionally been associated with amorphous solids prepared by quenching from the liquid state, but both terms are often used synonymously. Other terms are also used in the literature in place of amorphous solid, such as non-crystalline solid or vitreous solid.

Amorphous solids, like crystalline solids, can be metals, insulators or semiconductors. Amorphous solids can be formed from all of the main types of bonding: covalent, ionic, metallic, van der Waals and hydrogen. Based on their constituent elements the amorphous solids are usually divided into the following main categories:

a) SiO_2 and silicate based glasses,

b) transition-metal oxide glasses,

c) chalcogenide glasses,

d) amorphous tetrahedral semiconductors,

e) polymeric glasses,

f) fluoride glasses,

g) metallic glasses.

This work describes the structure and physico-chemical properties of As-S chalcogenide glass thin films deposited by the spin-coating technique.

1.2 PREPARATION OF AMORPHOUS SOLIDS

Materials in the liquid state can solidify in two different ways: either discontinuously to a crystalline solid or continuously to an amorphous solid as shown in Figure 1.1 [1]. At the liquid-to-crystal transition there is a marked change in the volume (the crystal is more dense). During the preparation of amorphous solids fast cooling enables the crystallization to be bypassed and the liquid state persists until a lower temperature, the glass transition temperature, T_g, is reached. At temperatures below T_g the super-cooled liquid solidifies with no sharp change in its volume. In order to prepare amorphous solids the crystallization has to be avoided. According to Turnbull [2], nearly all materials can, if cooled fast enough to a suitable temperature, be prepared as amorphous solids. There are several generally applied methods for forming amorphous solids such as: quenching, splat-cooling, vacuum-evaporation, and RF-sputtering [3]. In addition to these techniques, several other methods have been introduced recently such as the plasma-induced decomposition of a molecular species, a technique employed to deposit amorphous silicon from silane (SiH_4) vapour [4], or chemical vapour deposition [5]. Amorphous thin films can also be prepared from solutions by the spin-coating technique [6]. The spin-coating technique and its application for chalcogenide thin film deposition is described in detail in Section 2.5. This technique is applied in the present project to prepare amorphous chalcogenide thin films.

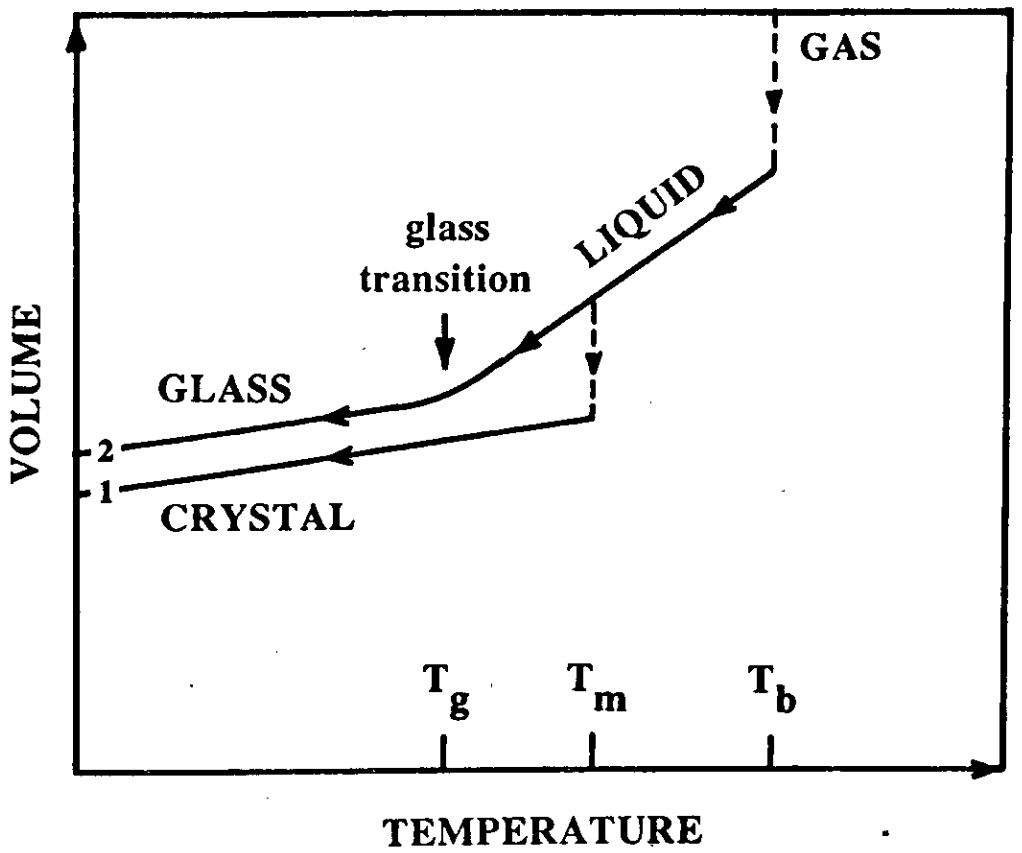

Figure 1.1 The two cooling paths for a material leading to the solid state: path 1 to the crystalline, and path 2 to the amorphous form [1].

1.3 STRUCTURE OF CHALCOGENIDE GLASSES

Chalcogenide glasses are solid phase materials which are formed by the combination of the chalcogen elements (S, Se, Te) with one or more elements of group III, IV or V of the periodic table. These materials, similarly to their crystalline counterparts, belong to the category of *molecular solids*. Molecular solids are characterised by the coexistence of strong (mainly covalent) and weak (primarily van der Waals) bonds in their structure. Molecular solids can be further categorised by the degree of the molecular network dimensionality [7] which is defined as the number of dimensions in which the covalently bonded molecular unit is macroscopically extended. The network dimensionality of chalcogenide based solids (crystalline or amorphous) can have a different value. For example, orthorhombic sulphur is a typical molecular solid with zero-dimensionality because the network is based on disconnected rings formed from eight sulphur atoms. On the other hand trigonal selenium is a one-dimensional molecular solid because the molecular unit Se_N ($N \sim 10^7$) is macroscopically extended in one dimension resulting in long chains [7].

Crystalline As_2S_3 (or $As_{40}S_{60}$ in terms of atomic percent) has a monoclinic structure formed by threefold coordinated As and twofold coordinated S atoms [8], as shown in Figure 1.2 (a). The chemical bonding consists of strong covalent bonds between As and S atoms, and weaker van der Waals bonds formed between layers of AsS_3 "molecular" units. The structure has short range order because the bond distances and the bond angles are the same throughout the crystal. The long range periodicity (long range order) of the crystal can also be seen. This material is a two-dimensional network molecular solid because the $(As_2S_3)_N$ macro-molecular units, containing $\sim 10^{14}$ atoms, are extended in two dimensions, forming layers.

In contrast, in amorphous As_2S_3, there is no long range periodicity, although there is a well defined short range order determined by the valency and the coordination number of the constituent As and S atoms as illustrated in Figure 1.2 (b). The S atom in the As_2S_3 glass is twofold-coordinated and the As atom is threefold-coordinated.

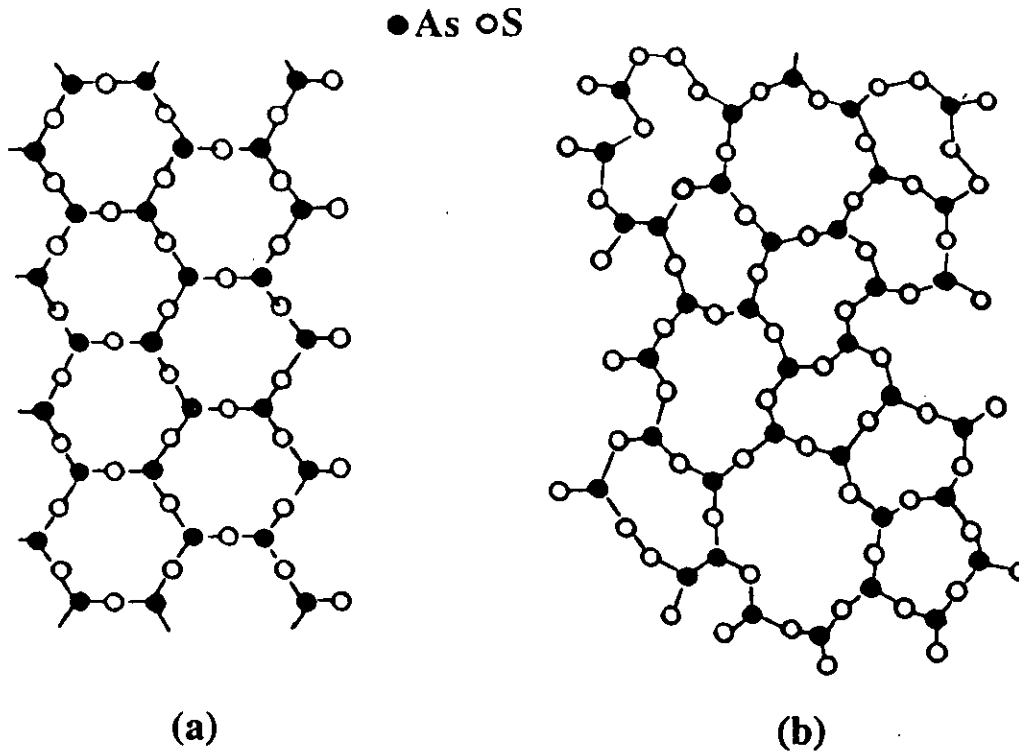

Figure 1.2 A two dimensional representation of the structure of As_2S_3 in: (a) the crystalline, and (b) the amorphous form.

It was confirmed by X-ray diffraction [9] and Raman scattering [10] that the nearest neighbour coordination and valency (that is the short range order associated with the covalent bonds) are retained in the network of As_2S_3 glass. Thus amorphous As_2S_3 has, in common with the corresponding crystal, a short range order. On the other hand, there is a marked absence of long range order because, for amorphous As_2S_3, distinguishable peaks in the X-ray diffraction spectra do not occur beyond those for the third nearest neighbours [11].

Another distinctive characteristic feature of this material is the presence of the chalcogen S atom which has a unique electronic structure. Apart from the electrons involved in forming the covalent bonds with the As atoms, the S atoms (like other chalcogenide elements) also have two localized non-bonding p electrons in the outer shell forming the lone-pair electrons. The top of the valence band is formed from these

lone-pair non-bonding electrons [12] and the optical energy gap corresponds to the separation of the lone-pair - antibonding states. The high energy lone-pair electrons are very versatile and can be easily excited to form various local atomic configurations. Figure 1.3 shows typical forms for the density of electronic states in: (a) a crystalline, and (b) an amorphous semiconductor. In the crystalline semiconductor the band edges are discontinuous and separated by the forbidden energy gap, E_g. In the case of the amorphous semiconductor distortions of bond angle and length occur to a greater or lesser extent, and this results in a "tailing" of band edges into a "pseudo-gap" which contains a finite density of allowed states. In the structure of amorphous solids there are also deviations from the "ideal" random network such as homo-bonds or defects where the atomic distances and/or the bond angles are quite different from those generally found in the network. The existence of such defects in the glass structure will result in the appearance of additional localized states in the forbidden gap between the valence and conduction bands of these materials [13].

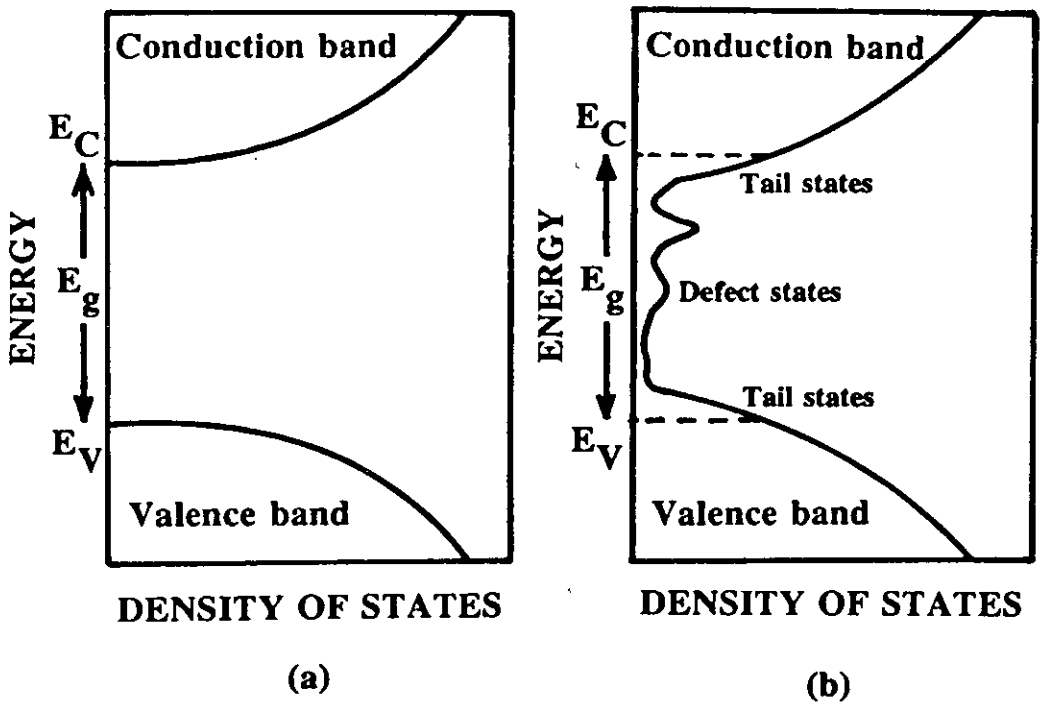

Figure 1.3 The band structure of: (a) a crystalline, and (b) an amorphous semiconductor.

The structure of chalcogenide glasses, due to their preparation technique, is far from thermodynamic equilibrium, yet it is stable up to the glass transition temperature, T_g [14]. T_g is always smaller than the melting temperature, T_m of the same material as seen in Figure 1.1. A typical value of T_g/T_m for chalcogenides is ~0.7. Above T_g the motion of the atoms within the amorphous network becomes liquid-like, which means that the atoms gain a greater degree of translational freedom. This circumstance in turn makes possible the formation of crystalline nuclei and their growth. Therefore in the temperature range from T_g to T_m the amorphous structure converts to a crystalline form. Below T_g the movement of the atoms in the amorphous network consists of vibrations around equilibrium positions just as in a crystal. This structure corresponds to a local minimum of the free energy and there is no relaxation towards a thermodynamically more stable configuration.

1.4 OPTICAL PROPERTIES OF CHALCOGENIDE GLASSES

The interaction with light provides an experimental method for probing the electronic and vibrational structure of a solid. By measuring the reflectance and the transmittance of the material its characteristic energy spectrum can be obtained. The optical response function of the solid is described by the frequency dependent complex refractive index $\bar{n}(\nu) = n+i\kappa$ where n is the refractive index and κ is the extinction coefficient. The refractive index, n, is associated with the polarization induced by the light, and usually obtained from reflectance measurements. The exctinction coefficient, κ, is associated with the optical absorption process in which a single elementary excitation (excited electronic or vibrational state) occurs. κ is related to the absorption constant, α, as: $\alpha = (4\pi/\lambda)\kappa$, and can be obtained from transmittance measurements [15].

The sharp features seen in the optical response function of crystals are absent for the corresponding amorphous material because they are associated with the long range translational periodicity [16]. However, as a consequence of the *same* short range order existing for the amorphous and the corresponding crystalline chalcogenide glasses, their optical response is similar. For example, for both forms of material the position and magnitude of the fundamental absorption bands are similar and the long

wavelength refractive indices are the same [16].

In chalcogenide glasses there are two characteristic energy ranges in which interaction with light occurs in the optical part of the spectrum. In the infrared region the absorption of light is associated with vibrational excitations (phonons) of the constituent atoms or molecules. On the other hand, in the visible part of the optical spectrum, light absorption causes the excitation of electrons from filled states in the valence band to empty states in the conduction band. Between these two characteristic absorption bands the chalcogenide glasses are transparent for a broad range of the optical spectrum and therefore can be used as optical "window" materials.

In the visible part of the optical spectrum, where the fundamental absorption occurs, the absorption edge of chalcogenide glasses is slightly different from that of the corresponding crystalline material. The absorption edge is less sharp and, in most cases, displays an exponential rise with photon energy from the onset of optical absorption to about $\alpha = 10^4$ cm^{-1}. This so-called Urbach edge [17] is described by the empirical relationship:

$$\alpha = \alpha_0 \exp[\gamma (h\nu - E_o)/kT] \qquad (1)$$

where γ is a constant and T is the temperature. Thus the optical absorption edge becomes broader as the temperature increases. The origin of the Urbach edge is still uncertain but it may be due to internal electric fields produced by charged defects or impurities in the amorphous state [18].

Although the existence of the Urbach tail in the chalcogenide glasses means that the absorption cutoff below the optical band gap energy, E_g, is not as sharp as in the corresponding crystal, its exponential decrease results in very low values of α at lower photon energies. Chalcogenide glasses, and particularly As_2S_3 can be used therefore in many applications as an infrared window material [19].

In the absence of any clear-cut sharp feature on the Urbach absorption edge, the determination of the optical band gap energy, E_g, is not as straightforward as in the case of the crystal. Tauc [20] suggested that in the higher absorption region where $\alpha > 10^4$ cm^{-1}, the absorption coefficient rises less steeply with photon energy and can be described by the following relationship:

$$\alpha h\nu = B(h\nu - E_g)^2 \qquad (2)$$

where B is a constant and E_g is defined as the optical band gap energy. This arises from the spectral dependence of the absorption coefficient in this region being attributed to electronic transitions between valence band and conduction band states (interband transitions) [21]. If the form of the density of states at both band edges is parabolic then the photon energy dependence of the absorption takes on the form expressed by the above equation. The value of the optical energy gap, E_g, can be obtained by extrapolating $\alpha^{1/2}$ towards zero [22].

1.5 THE AIMS OF THE PROJECT

The deposition of chalcogenide films from their solutions by the spin-coating technique offers a new possibility for preparing technologically useful films in an easier and less expensive way than the conventionally used vacuum evaporation method. The spin-coating technique may be a more suitable method to obtain thin films of chalcogenides for applications in, for example high resolution lithography and optical imaging, including holographic recording. Spin-coating is a technique that is widely used in the IC fabrication industry for depositing photoresist and is also used in the optics industry for depositing organic coatings such as di-chromated gelatin.

The metal photodissolution effect in chalcogenide glasses is possibly the most interesting of the light induced phenomena observed in these materials because it produces the most significant change in the structural and physico-chemical properties of the chalcogenide. In the present work the silver photodissolution effect is investigated as a means of fabrication of grating structures in spin-coated As-S films. The principal aim of this project is to investigate the physical and chemical properties of As-S films deposited by spin-coating, and to observe in these films the various light-induced effects characteristic of chalcogenides, in particular silver photodissolution. The optimal deposition conditions necessary to provide different compositions of spin-coated As-S films with reproducible properties need to be established. In order to assess the quality of the spin-coated As-S films the composition, structure and optical properties of the spin-coated films need to be investigated. The silver photodissolution

process provides a useful technique to pattern these films and therefore the rate at which the silver diffuses into the spin-coated As-S films must be measured as this governs the exposure required to produce an image in these materials. The sensitivity of the Ag / As-S system for imaging applications is a key parameter and must be determined. The final objective of this study is to fabricate grating structures in spin-coated As-S chalcogenide films using the silver photodissolution process and to evaluate the performance of the gratings produced. Because of the IR-transmitting properties of these materials, such grating structures may be used as diffractive components (lenses, beam combiners etc.) in IR systems for use in, for example, thermal imaging.

The work carried out in the present study is organised as follows. A general introduction to the preparation, structure and optical properties of the chalcogenide glasses has been presented in this chapter. A review of previous work on the photo-induced effects in chalcogenide glasses and their applications is presented in Chapter 2. The characterisation and applications of spin-coated chalcogenide glasses are also found in Chapter 2. Chapter 3 describes the method used for the preparation of amorphous As-S films in the present work using the spin-coating technique and also the various experimental methods employed to study the structure and optical properties of the films, the kinetics of silver photodissolution, the etching properties, and the holographic illumination arrangement used for grating preparation in spin-coated As-S films. The results of the compositional and structural analysis are summarised in Chapter 4 while Chapter 5 describes the optical properties of undoped and silver doped films. Chapter 6 describes the results obtained on the kinetics of silver photodissolution in spin-coated As-S films and Chapter 7 summarises the results obtained on the dry etching process used to create surface relief structures. Chapter 8 describes the results obtained for the preparation and evaluation of the diffraction gratings and, finally the conclusions reached in this study and suggestions for further work are presented in Chapter 9.

1.6 REFERENCES

[1] R. Zallen, "The Physics of Amorphous Solids", 1983, published by John Willey, New York, p. 2.

[2] D. Turnbull, Contemp. Phys. 1969, 10, p. 473.

[3] R. Zallen, "The Physics of Amorphous Solids", 1983, Willey, New York, p. 9.

[4] W. E. Spear and P. G. LeComber, Phyl. Mag. 1976, Vol. 33, No. 6, pp. 935-949.

[5] H. Shimizu, S. Nakao, H. Kusakabe and M. Noda, J. Non-Cryst. Sol. 1989, 114, pp. 196-198.

[6] G. C. Chern and I. Lauks, J. Appl. Phys. 1982, 53(10), pp. 6979-6982.

[7] R. Zallen, "The Physics of Amorphous Solids", 1983, Willey, New York, p. 86.

[8] R. Zallen, "The Physics og Amorphous Solids", p. 92.

[9] L. Cervinka, "The structure of Non-Crystalline Materials", 1982, ed. by P. H. Gaskell, Taylor, New York, p. 255.

[10] G. Lucovsky and R. M. Martin, J. Non-Cryst. Solids, 1972, 8-10, p. 185.

[11] A. C. Wright and A. J. Leadbetter, Phys. Chem. Glasses, 1976, Vol. 17, p. 122.

[12] M. Kastner, D. Adler and H. Fritzsche, Phys. Rev. Lett. 1976, Vol. 37, p. 1504.

[13] M. Kastner, Proc. of the 7th Int. Conf. on Amorphous and Liquid Semicond. 1977, Edinburgh, p. 504.

[14] R. Zallen, "The physics of Amorphous Solids", 1983, p. 16.

[15] R. Zallen, "The physics of Amorphous Solids", 1983, publ. J. Wiley, p. 261.

[16] R. Zallen and F. Blossey, "Optical and Electrical Properties of Materials with Layered Structures", 1976, ed. by P. A. Lee, Reidel, Dordrecht, p. 231.

[17] N. F. Mott and E. A. Davis, "Electronic Processes in Non-Crystalline Materials", 1971, Caledonian Press, Oxford, p. 240.

[18] M. A. Afromowitz and D. Redfield, Proc. 9th Intern. Conf. on the Phys. of Semiconductors", 1968, Moscow, p. 98.

[19] A. M. Andries, V. V. Ponomar, V. L. Smirnov and A. V. Mironos, Sov. J. Quantum Electron. 1986, 16(6), pp. 721-736.

[20] J. Tauc, "Optical Properties of Solids", 1970, ed. by F. Abeles, Nort-Holland, Amsterdam.

[21] N. F. Mott and E. A. Davis, "Electronic Processes in Non-crystalline Materials", 1971, published by Clarendon Press, Oxford, p. 242.

[22] S. R. Elliott, "Physics of Amorphous Materials" 1983, published by Longman, London, p. 234.

CHAPTER 2

BACKGROUND: PHOTO-INDUCED EFFECTS AND THE SPIN-COATING TECHNIQUE IN CHALCOGENIDE GLASSES

The amorphous state is not simply one more possible configuration of the substance in addition to its crystalline forms. The terms *amorphous state* or *glass state* refer to a continuous set of microscopically different configurations. The actual structure of an amorphous material is dependent on the preparation conditions. For instance, the density of a melt-quenched chalcogenide glass is gradually increased as the cooling rate is decreased. The glass is therefore stable (i.e. metastable) in a whole range of densities, and hence free energies. From the thermodynamic point of view, they can exist in a range of non-equilibrium states. Therefore their bonding configuration and structure can be modified easily by applying the appropriate energy in the form of electromagnetic irradiation. The irradiation induced structural changes are manifested in certain changes in the physical and chemical properties of the solid such as optical edge shifts, changes in the refractive index, volume changes, changes in microhardness, enhanced chemical reactivity, solubility changes, etc. These photo-induced effects in chalcogenide glasses are discussed in this chapter.

Photo-induced effects have been observed in a wide variety of chalcogenides, for example a-Se, a-As_2S_3, a-As_2Se_3, a-$GeSe_2$, a-As_4Se_5Ge, a-GeTe and many others. The important elements in these materials as far as light-induced effects are concerned are the chalcogens S, Se and Te because of their electronic structure and low coordination number.

The various photo-induced phenomena observed in amorphous chalcogenides are usually classified according to whether they are reversible or irreversible, reversible here meaning that the original structure, and hence the original properties of the solid can be regained by annealing subsequent to irradiation, at a temperature close to, but below the glass transition temperature, T_g. The reversible changes are generally observed in well annealed vacuum-deposited films, or melt-quenched glasses, which are comparatively well annealed as a consequence of their method of preparation. In contrast, the irreversible changes are found mainly in non-annealed vapour-deposited films where the initial structure is rather different from the structure of the well annealed films. Owen et al.[1] proposed a further, more detailed, classification of the photostructural changes according to whether the changes are structural or physico-chemical, as seen in Table 2.1.

a) Structural changes	b) Physico-chemical changes
Reversible	Reversible
1) Changes in local atomic configurations	1) Decomposition
Irreversible	Irreversible
2) Polymerization	2) Vaporization
3) Crystallization	3) Metal photodissolution
4) Morphological changes	

Table 2.1 Classification of photo-induced structural and physico-chemical phenomena in amorphous chalcogenide semiconductors [1].

2.1 REVERSIBLE PHOTO-INDUCED EFFECTS

Reversible photo-induced effects are usually observed in melt-quenched bulk glasses or in thin films of the chalcogenides. However, most of the publications describing the reversible light-induced changes, refer to thin As–S, As–Se, or Ge–Se films [2, 3, 4]. These reversible photostructural changes are accompanied by a nearly parallel shift of the absorption edge to lower energies, which is therefore termed *photodarkening*. Figure 2.1 shows the reversible photodarkening observed in evaporated (EV) and melt-quenched (MQ) As_2S_3 after repeated cycles of illumination and annealing at 170° C. The edge-shifts for both samples are similar in magnitude, but no change was observed in crystalline As_2S_3 samples, showing that photodarkening is a phenomenon uniquely associated with the amorphous structure [5].

Together with the absorption edge shift, a photo-induced increase of the refractive index has also been observed in amorphous chalcogenides. It was found that the refractive index (n) of an annealed $As_{40}S_{60}$ film increases to a saturation value (n_1) after illumination with light of energy higher than the optical band-gap energy, as a result of reversible photostructural change. If the irradiation stops, a relaxation to n_2 results ($n \leq n_2 \leq n_1$). The time constant of this relaxation has been found to be around 100 sec [6].

The evidence for the structural changes responsible for the reversible photodarkening in amorphous As_2S_3 films came first from X-ray diffraction measurements [7]. These measurements suggest that there is a small change in the short range order, namely that the As–S bond length might be affected as a result of illumination. However, other experimental results indicate that the reversible photostructural changes can be associated with larger scale effects such as bond breaking and the creation of new bonds in the amorphous network. Frumar et al. [8] investigated the reversible photodarkening effect in As–S thin films and bulk glasses. Comparing the Raman spectra of the photodarkened and annealed samples, they found that photodarkening enhanced the Raman bands associated with As–As and S–S vibrations, which suggests that additional homo-bonds are formed by illumination. The absorption edge shift in this case would be due to the increased absorption associated with clusters of As atoms and the volume increase accompanying the photodarkening could be explained by the appearance of the longer As-As bonds.

An interesting aspect of the reversible photostructural changes is that illumination with polarized light can generate structural anisotropy in amorphous chalcogenides. Anisotropy of the absorption coefficient and refractive index were found to develop in $GeSe_2$ films under the influence of linearly polarized light. Irradiation by circularly polarized or unpolarized light results in the disappearance of the anisotropy [9, 10].

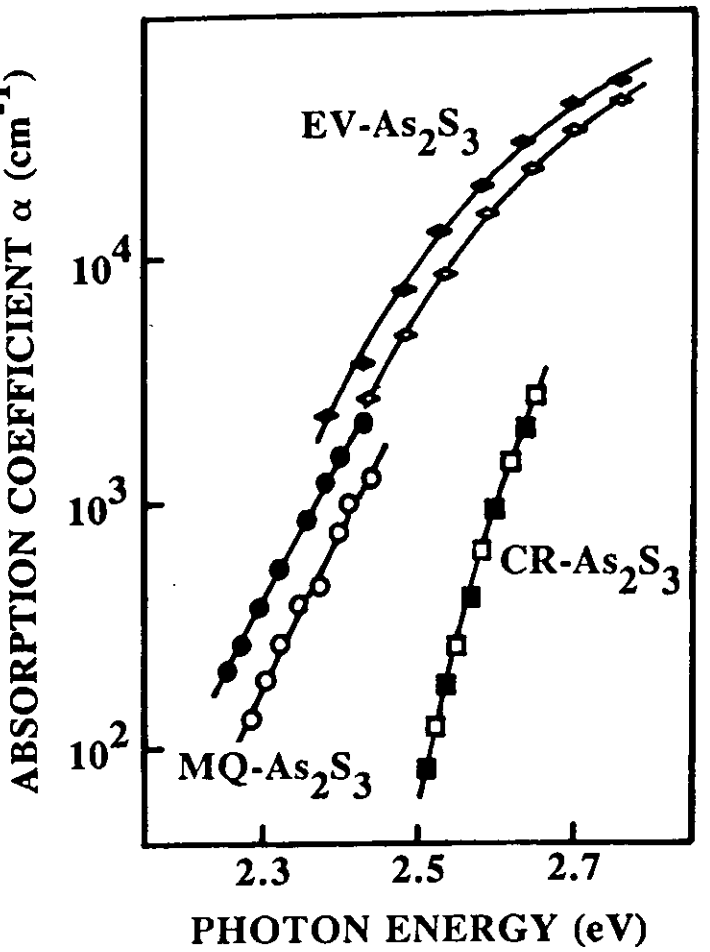

Figure 2.1 The absorption edge spectra of evaporated (EV), melt quenched (MQ) and crystalline (CR) As_2S_3 before (open symbols) and after (solid symbols) band gap illumination [5].

2.2 IRREVERSIBLE PHOTO-INDUCED EFFECTS

Irreversible photo-induced effects are usually observed in thin chalcogenide films which have a different structure from that of the melt-quenched bulk material, the structural difference being mainly due to the fast deposition rate during their preparation. The irreversible light-induced effects are usually explained by some larger scale structural rearrangements in the film. For example, in the case of the As-S system, polymerization of the existing molecular-like As_4S_4 units in the amorphous As–S network was observed under the influence of illumination [11]. It is generally believed that irreversible photo-induced structural changes tend to result in a structure in the vacuum-evaporated film that is similar to that of the melt-quenched glass.

Photo-induced irreversible changes in the morphology were also observed in thin films of Ge-Se compositions which, during vapour-phase deposition, grow on the supporting substrate in an amorphous but columnar structure [12]. On illumination, particularly with UV light the film remains amorphous but contracts in volume. Contractions in volume of up to 12% can occur. The effect is thought to be due to a collapse of the columnar morphology of the films brought about by a photo-electric excitation of the electronic defect states which are characteristic of amorphous chalcogenides.

2.3 METAL PHOTODISSOLUTION IN AMORPHOUS CHALCOGENIDES

2.3.1. The phenomenon of photodissolution

The phenomenon of the dissolution of a metal into an amorphous chalcogenide under the influence of light can be considered as a unique irreversible photo-induced effect. Much work has been carried out on the metal photodissolution effect since Kostyshin et al. [13] first reported that when a thin film of amorphous As_2S_3 deposited on a silver (Ag) substrate is illuminated the metal rapidly diffuses into the chalcogenide layer. Figure 2.2 is a schematic illustration of the basic arrangement used to produce

the effect.

Various terms have been used in the literature for this effect. Sakuma et al. [14] suggested the term *photodoping* for the phenomenon and it has been widely used, although, as pointed out later, this is not strictly correct since the amount of metal introduced into the chalcogenide may exceed 30 atomic %. As a result, the term *photodissolution* has appeared. Many authors use the term *light-enhanced silver diffusion or dissolution*. A recent review paper on this phenomenon uses the term *photodissolution* to refer to the disappearance of the metallic layer and *photodiffusion* to refer to the propagation of the metal in the chalcogenide [15]. In most reports the region of the chalcogenide film containing metal introduced by the photodissolution process is called the *photodoped* or *Ag-doped* layer and the metal-free region is referred to as the *undoped* chalcogenide layer.

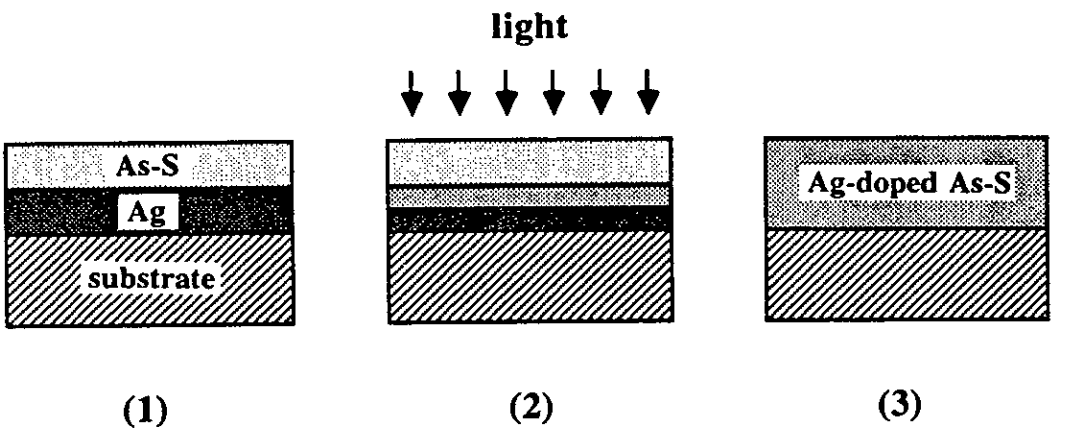

Figure 2.2 Schematic illustration of the photodissolution of a metal film into a chalcogenide layer under the influence of light: (1) The initial film structure; (2) The process during illumination; (3) The final structure.

The photodissolution of metals, like photodarkening, probably occurs only in chalcogenides having an amorphous structure. Usually the effect is studied in samples consisting of a thin metallic layer deposited either on top of, or beneath the chalcogenide film, the usual thickness ratio of the metal and chalcogenide films in the

double layer structure being ~ 1:3. Photodissolution has been observed in numerous metal / glass systems. In most cases silver is used as the metal source, but some studies have also investigated the use of copper and zinc for photodissolution [16, 17]. Usually vacuum-evaporated elemental metal is used but in some cases an evaporated metal salt, such as silver nitrate or silver chloride, or a solution of a silver compound provide the metal source for photodissolution [18, 19]. Photodissolution has also been observed in a chalcogenide deposited on a bulk silver-containing substrate (Ag_2S) [20].

The photodissolution effect has been studied mainly in the amorphous As–S, As–Se, Ge–S, and Ge–Se systems [1, 63, 21, 9]. The thin films of amorphous chalcogenide material are usually prepared by vacuum-evaporation or sputtering. Recently a new chalcogenide deposition technique has been reported in which the films were obtained from solution by spin-coating [22]. This project applies the spin-coating technique to prepare thin films of chalcogenides from their amine solutions. From a technological viewpoint, the spin-coating technique offers several advantages over thermal deposition for producing thin films of chalcogenides. A detailed account of the spin-coating technique is discussed later in Section 2.5.

2.3.2 The rate of silver photodissolution

In studying the photodissolution effect, the kinetics of the reaction and the effects of different factors on the rate are of key importance and have been extensively investigated. Various methods have been developed to monitor the progress of the process with time. These techniques usually measure either the changing amount of reactants (silver or chalcogenide) during the reaction, or the amount of reaction product (photodoped chalcogenide) generated by the reaction in a given time.

The change in the metallic layer thickness during the reaction can be measured by monitoring the electrical resistance of the metal film and converting the measured data to thickness change using a calibration curve [23]. Another measuring technique which gives information about the metal thickness change is to monitor the change in the optical transmission through the sample, which depends primarily on the thickness of the metal film [24]. An absolute method for measuring the thickness of the silver

layer during photodissolution was proposed by Rennie et al. This measurement is based on the fact that crystalline silver has a characteristic X-ray diffraction signature and monitoring the strength of its (111) Bragg peak makes it possible to determine the thickness of the silver layer accurately [25].

The kinetics of the decrease in the undoped chalcogenide film thickness during the reaction can be measured by monitoring the variations in the intensity of the light reflected from the chalcogenide surface of the sample. The propagation rate of the undoped / metal-photodoped interface can be calculated directly from the recorded interference pattern [26].

The propagation of the undoped / silver-photodoped interface under the influence of light can be monitored indirectly by using an interesting method developed by Yaji et al. [27]. They prepared a holographic grating in an Ag / As_2S_3 sample by generating photodiffusion with interfering beams yielding a spatially periodic intensity profile. The decrease in the diffraction efficiency of the grating was then monitored while the grating was subsequently illuminated with a beam of uniform light intensity profile.

The kinetics of photodissolution has also been studied by directly measuring the thickness of the reaction product generated during different reaction times. In these experiments the thickness of the photodoped chalcogenide was determined using the selective etching properties of the undoped and photodoped chalcogenides in alkaline solution [28, 29].

In studies of the kinetics of the photodissolution of silver into amorphous chalcogenides it is found that the reaction rate changes during the process. The time dependence curve for the photodissolution process consists of three well distinguished parts, as shown in Figure 2.3. It starts with an induction period where the dissolution rate is small. This is followed by a stage associated with the effective photodissolution, and in the final part a decreasing dissolution rate is found [23].

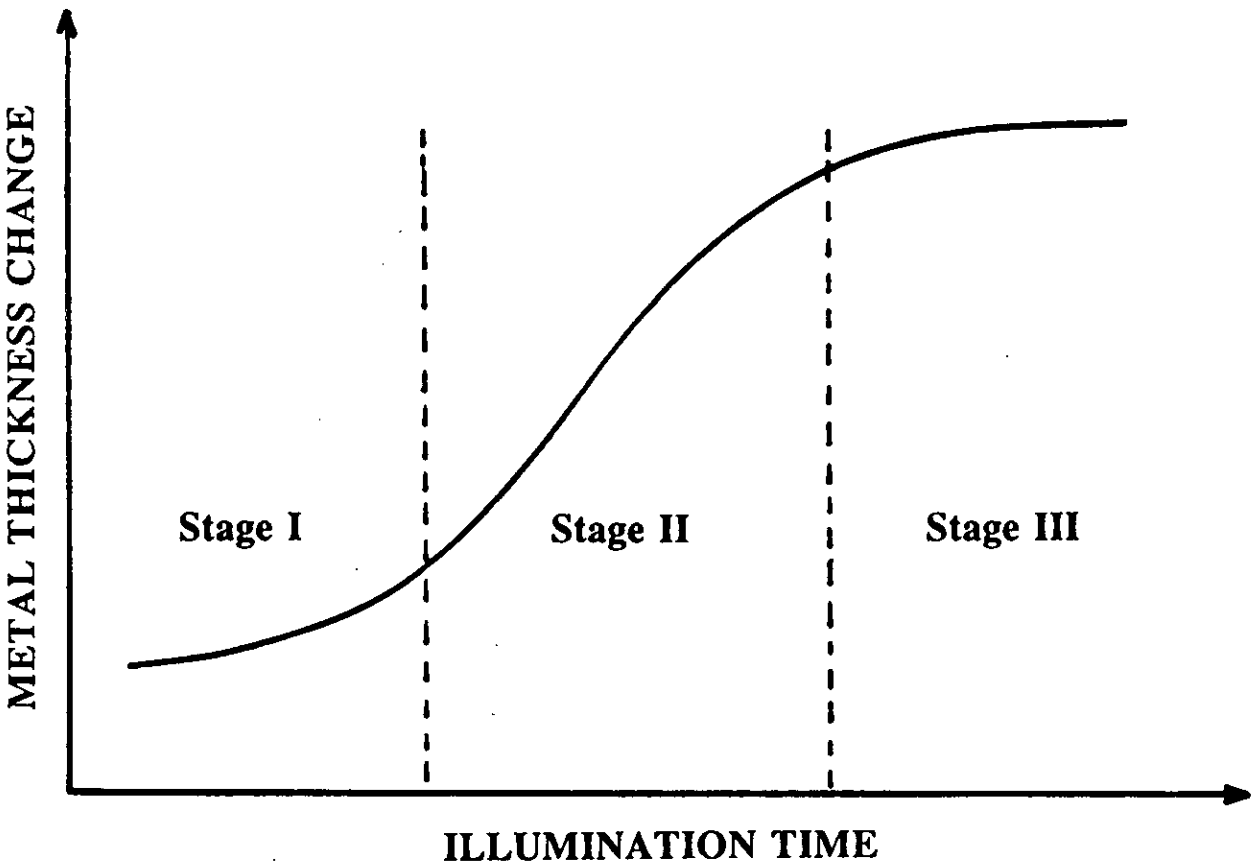

Figure 2.3 Kinetics of the silver photodissolution process.

The induction period (stage I in Figure 2.3) is observed in most cases, except when a photodoped layer is introduced artificially between the silver and the chalcogenide film [30]. An extended induction period is observed when a barrier oxide layer is formed between the metal and chalcogenide during preparation [31]. It is also found that the length of the induction period is inversely proportional to the illumination intensity [32]. From these observations Elliott and co-workers [33] proposed a model for the origin of the induction period in which they suggest that the metal photodissolves in the chalcogenide film in an inhomogeneous fashion. The photodissolution reaction starts at the grain boundaries in the metallic film and a continuous silver-doped chalcogenide film is eventually formed by lateral photodiffusion between these grain boundaries as seen in Figure 2.4. When a continuous layer of silver-doped chalcogenide is formed the photodissolution rate will rapidly increase towards a maximum value. Any intermediate oxide layer acts as a barrier to the lateral photodiffusion and hence increases the induction period. An increase in the light intensity will increase the rate of the lateral diffusion and as a result the induction period decreases.

The stage during which effective photodissolution occurs (stage II in Figure 2.3) is the part of the photodissolution process where the reaction rate is the highest. Basically two types of time dependence for this stage of the silver photodissolution have been reported in the literature. In some cases the photodissolution change is linearly dependent on the illumination time [34], in other cases a square-root time dependence is observed [35]. These contradictory results might be explained by considering different rate-limiting factors for the different experiments. The linear time dependence would occur when the rate-limiting step was the chemical reaction between metal and chalcogenide [33]. This is usually found when the sample is illuminated with low intensity light ($\sim$10 mW/cm^2). In the case of high intensity illumination ($\sim$100 mW/cm^2) diffusion of metal ions or electrons through the intermediate metal-doped layer is the rate limiting step [36].

Janai explained the various time dependences of the photodissolution rate by assuming that the light intensity reaching the metal / doped chalcogenide interface decreases during the reaction because of the increasing absorption of the expanding layer of reaction product [37]. He suggested that the light has to reach the silver / chalcogenide interface to generate Ag^+ ions during the first step of the reaction. In the second step, these Ag^+ ions react with the chalcogenide.

In the final stage of photodissolution (stage III in Figure 2.3) the reaction rate decreases and the reaction eventually stops because one of the reactants (metal or chalcogenide) is exhausted. However, it was also reported that photodiffusion continues even when there is no metallic silver left, the suggestion being that there is a redistribution of silver under the influence of illumination [38].

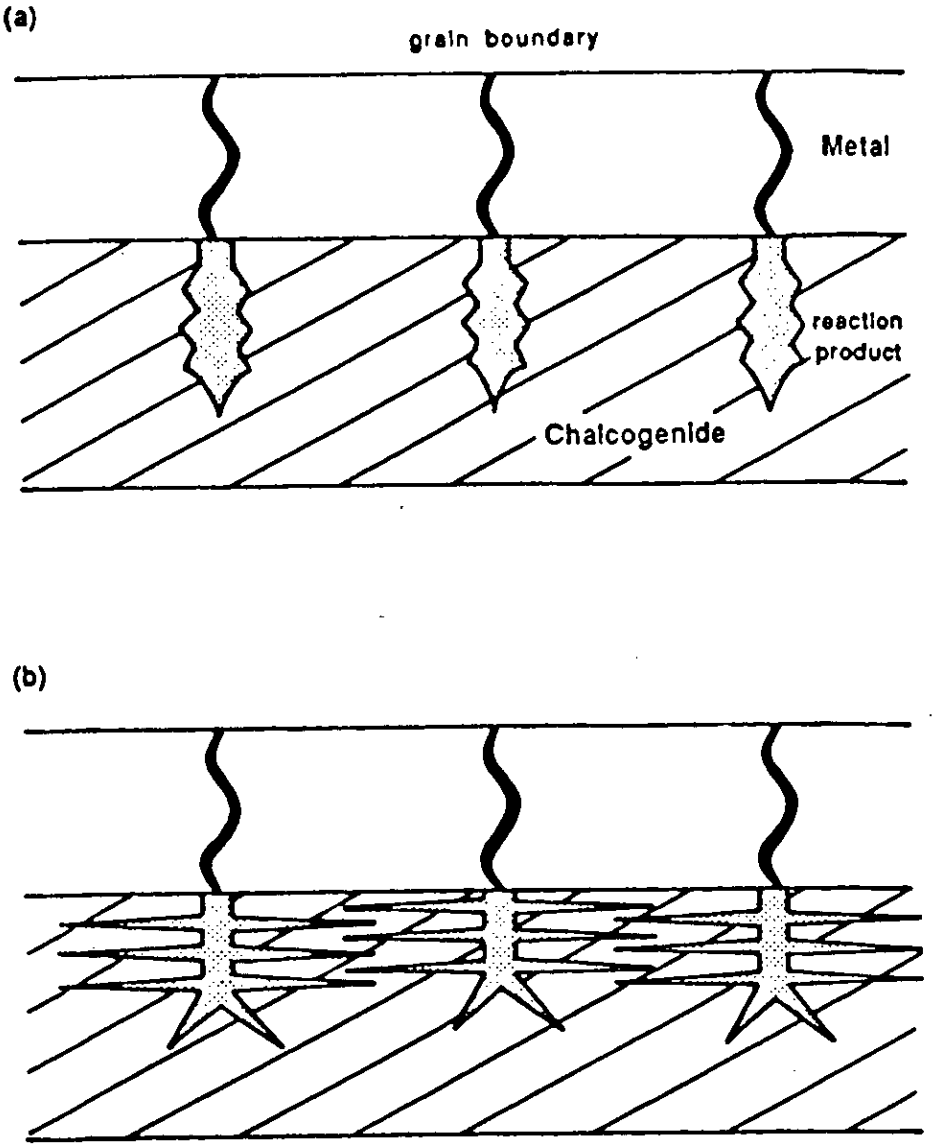

Figure 2.4 Lateral diffusion during the induction period [33].

2.3.3 Effect of different factors on the metal photodissolution rate

The metal photodissolution rate has been found to be dependent on a variety of factors. The effect of the light intensity on the dissolution rate was investigated by several authors although the experimental results obtained are not conclusive. It is agreed that the length of the induction period is inversely proportional to the illumination intensity. As stated above, Elliott and co-workers suggested that the reason for this is the higher lateral diffusion rate caused by higher illumination intensity.

In most cases it was reported that stage II is linearly dependent on the illumination intensity [23, 34]. However, Buroff and co-workers observed a superlinear dependence ($I^{1.54}$) of the photodissolution rate for silver in As_2S_3 at low illumination intensities and a sublinear dependence ($I^{0.9}$) at higher intensities [39].

The reported results for the wavelength dependence of the silver photodissolution rate are also contradictory, although it is agreed that photodissolution is most effective with the illumination energy is approximately equal to the band-gap of the chalcogenide. Kokado et al. reported that the sensitivity of the process coincides with the absorption edge of the chalcogenide and decreases at longer wavelengths [40]. However, it has also been reported that the photodissolution rate is quite large even at wavelengths which have negligible absorption in the chalcogenide [23]. Recently Kolobov et al. [36] have demonstrated experimentally that photodissolution of silver does not occur with light having a wavelength absorbed only in the undoped chalcogenide layer. It was also shown that light absorption in the metal is not important but that light absorption at the doped / undoped interface is a crucial factor. In the same study it was shown experimentally that the silver migrates through the intermediate doped layer as Ag^+ ions during photodissolution. It was also demonstrated that the dissolution-limiting step is the penetration of the metal ions from the doped region into the undoped chalcogenide.

The effect of temperature on silver photodissolution in amorphous As_2S_3 has also been studied and activation energies of 0.01-0.4 eV were obtained for the reaction depending on the light wavelength and the temperature range [41]. Plocharski and co-workers have measured the activation energies of the light-induced reaction and the

thermal reaction between Ag and As_2S_3, obtaining values of 0.18 eV and 1.5 eV respectively [42].

The effect of the composition of the As-S film on the silver photodissolution rate was investigated and the maximum rate was measured at the composition of $As_{33}S_{67}$ [43]. This behaviour was explained by the observation that this composition yields a homogeneous As-S-Ag glass, hence the diffusion through this photodoped layer is not delayed by the phase-separated regions in the structure.

The effects of other factors on the photodissolution rate such as pressure, external electric field, pre-treatment, different chalcogenide / metal thickness combinations, and the effect of atmosphere have also been investigated and are described in a recent review [15].

2.3.4 Mechanism of the silver photodissolution

Many authors have proposed models to explain the mechanism of metal photodissolution into amorphous chalcogenides. The key difference between the suggested mechanisms is where the actinic light is believed to be absorbed in the sample, in other words, the exact role of the light in the photodissolution process. In the first proposed model it was suggested that the light is absorbed in the silver layer, generating silver ions by the photo-emission of electrons. The silver ions then move by diffusion into the chalcogenide film and react with it [13]. The observation that photodissolution can occur for illumination with photon energies less than the chalcogenide band-gap supports the assumption that light absorption in the metal is the important factor for photodissolution to proceed [44].

However, the idea that the light is absorbed in the undoped chalcogenide film is also supported by experimental observation. The fact that the photodissolution process is most efficient when the incident photon-energy corresponds to, or is slightly higher than, the chalcogenide band-gap energy suggests that absorption in the chalcogenide glass is also responsible for the reaction by creating charged defects in the chalcogenide structure [45, 46].

Kokado et al. suggested that light absorption at the chalcogenide / silver interface is necessary for metal photodissolution to proceed. They argued that the conduction and valence bands of the chalcogenide are bent near the chalcogenide / silver interface with the result that photo-generated electrons move into the chalcogenide where they are trapped. This leads to a space charge which provides the driving force for the silver ion diffusion [47].

The observation of lateral photodiffusion, where the silver migrates horizontally through the chalcogenide layer, convinced many authors that the light necessary for the reaction to proceed is absorbed at the undoped / photodoped interface [1, 48, 49].

It has also been suggested that photodiffusion is a photochemical tarnishing reaction [50]. In this case the effect was compared to the reaction between silver and sulphur, one of the simplest examples of such a reaction. The reaction between the solid reagents can proceed only if the intermediate layer of reaction product allows at least one of the reagent ion species to penetrate through it. It was suggested that this requirement is satisfied for the photodissolution process because the doped chalcogenide is a good ionic conductor.

Recently Kluge [51] has developed a model which explains most of the phenomena observed in photodoping. He interprets the effect in terms of an intercalation reaction, a mechanism which was originally applied to crystalline group VI compounds. The intercalation reaction involves an ion and an electron transfer from outside into a host matrix and leads to a reversible insertion of the guest ions into the host. According to Kluge, photodoping can be considered as an intercalation reaction between the amorphous host and the silver ions, according to the following equation:

$$C_2^o + e^- + M^+ \rightarrow C_1^- M^+$$

The initially twofold coordinated covalently bonded chalcogen atom (C_2^o) transforms into a C_1^- charged unit possessing only a single covalent bond and an excess electron which establishes an ionic bond with the metal (M^+). The host chalcogenide matrix provides the empty interatomic volumes for the accommodation of the guest ions in regions of weak Van der Waals bonding. Light absorption in the metal layer will result in Ag^+ ion formation and at the same time the photoemission of electrons over

the potential barrier at the metal / doped chalcogenide interface. Light absorption also occurs within the intercalation product and generates electron-hole pairs which are separated by the interface space charge potential. These conditions lead to the intercalation of metal ions with the negatively charged C_I^- atoms because of the high ion mobility in the intercalation product and the electrostatic attraction of the separated ions. Figure 2.5 depicts the generation of electron-hole pairs by light absorption within the intercalation product and the separation of the electrons and holes by the interface space charge potential. The generation of Ag^+ ions and electrons due to the light absorption in the metal layer is also shown.

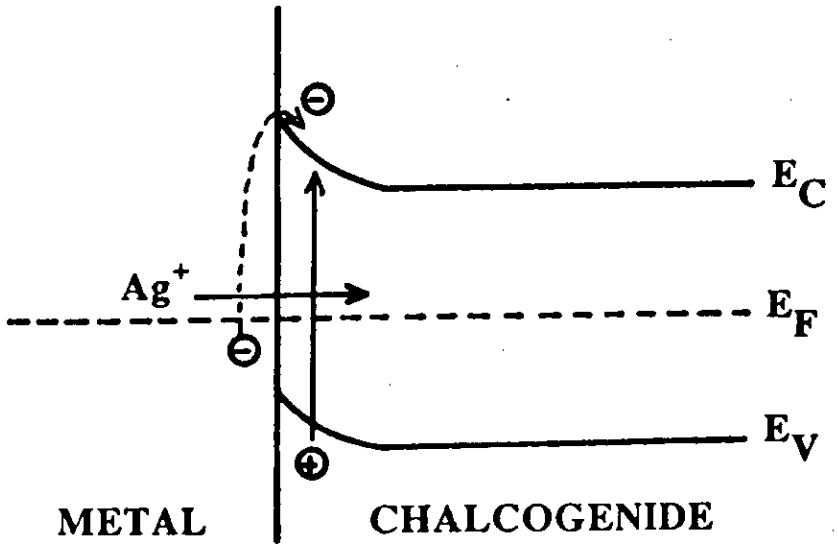

Figure 2.5 Scheme of the electron-ion generation at the metal / metal-doped chalcogenide interface [51].

The most recent attempts to explain the mechanism of photodissolution of silver into chalcogenide films have been made by Kolobov et al. and Elliott et al. The model proposed by Kolobov is based on the idea that the doped / undoped chalcogenide boundary is a p-n junction and the electric field associated with this junction pulls the metal ions into the undoped region. The ion movement in the chalcogenide film occurs via sites of voids in the chalcogenide structure. The voids are formed by photo-generated electrons through lattice deformation or breaking of existing bonds. As soon as an ion leaves the doped region its absence will be immediately compensated from the metallic source. The process will continue until the metallic layer is exhausted. The above considerations are valid if the ionic conductivity of the reaction product is

less or comparable to its electronic conductivity. If the opposite is true, the doped / undoped boundary should be regarded as an interface between a solid electrolyte and a semiconductor. In this case, the advance of the photodoping front can be regarded as an analogue to the photo-corrosion behaviour of a semiconductor in contact with a liquid electrolyte [36].

Elliot et al. proposed models for the photodissolution process for the case when the Ag-doped chalcogenide is a p-type semiconductor and also for when it is n-type [33]. He suggests that the basic photodissolution process occurring between silver and amorphous chalcogenides is a redox reaction, involving the oxidization of silver atoms (Ag) to silver ions and reducing the chalcogen atoms (C) of the glass to a negatively charged, non-bridging configuration, as shown in the following equation:

$$Ag(0)+C(II)\rightarrow Ag(I)+C(I)$$

The amount of chalcogen available to react determines the amount of photodissolved silver. As a result of the redox reaction the arsenic would become phase separated. If the Ag-doped material is p-type, holes are the dominant carriers. There is an Ag^+ ion flux from the metallic reservoir towards the doped / undoped chalcogenide interface during the photodissolution process, consequently there is a flux of holes in the reverse direction to maintain overall charge neutrality. These holes originate from the electron-hole pairs created by the absorption of photons. The electrons serve to reduce the chalcogen atoms to form charged, non-bridging configurations. From these considerations the actinic light is expected to be absorbed at the doped / undoped chalcogenide interface where the chalcogen bond breaking and reduction to form non-bridging sites takes place. On the other hand, the oxidation of silver takes place at the metal / doped chalcogenide interface, where the photo-created holes, having drifted through the doped layer from the actinic light absorption site, react with the metal atoms producing metal ions.

This process is illustrated in Figure 2.6 together with a schematic illustration of the proposed model for the case when the doped chalcogenide is an n-type semiconductor. In this case, the holes from the electron-hole pairs created by the absorption of photons at the metal interface will create Ag^+ ions as before, which will then drift through the doped layer to the advancing doping front. Electrons will also drift through the doped material in the same direction as the ions, and on arrival at the

doped / undoped interface will reduce the chalcogen atoms to form charged non-bridging configurations. In this model the actinic light is absorbed at the metal / doped chalcogenide interface, but some may also be absorbed at the doped / undoped boundary to break bonds to enable the photodissolution reaction to proceed.

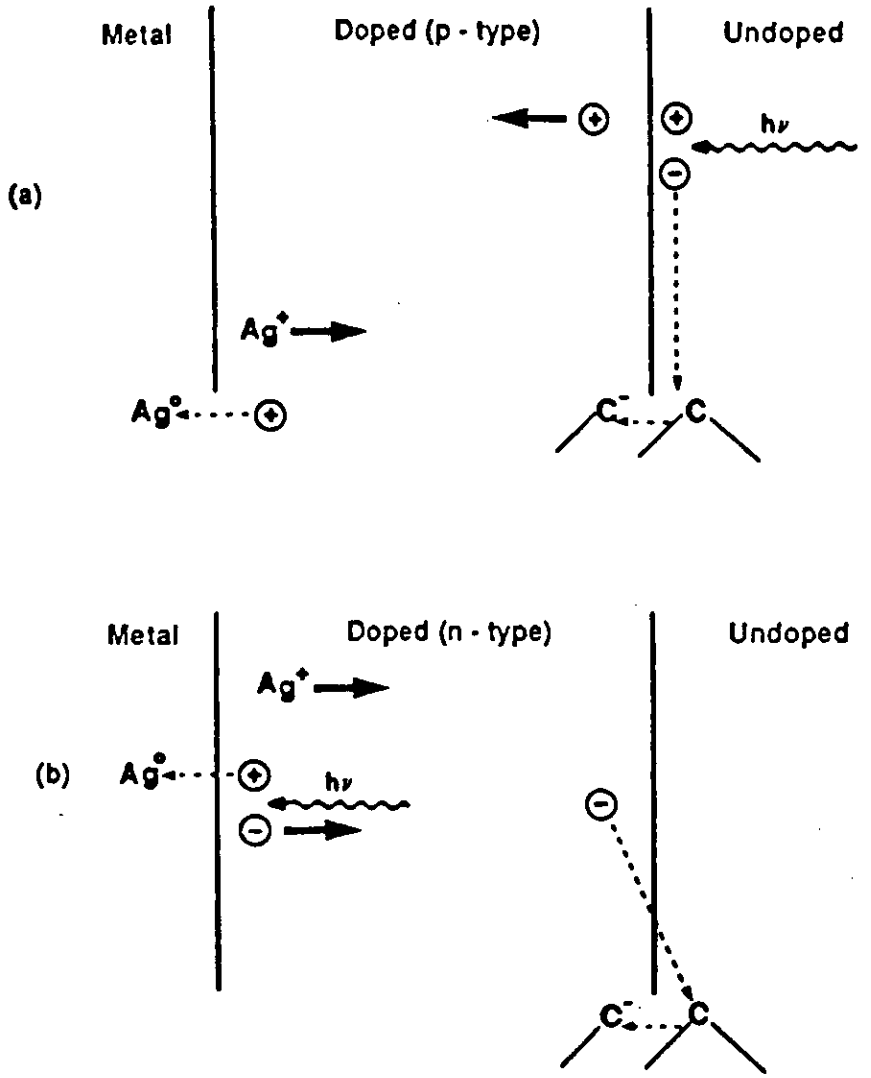

Figure 2.6 Schematic illustration of the metal photodissolution effect when the doped material is assumed to be: (a) p-type; (b) n-type [33].

2.4 APPLICATIONS OF THE LIGHT-INDUCED EFFECTS

Specific properties of glassy chalcogenide semiconductors like high transparency in a broad range of the spectrum, light sensitivity, ultra-high resolution capability, ease of manufacture, physical and chemical durability has made these materials attractive for various applications.

Chalcogenide glasses are used in infrared technology because they are highly transparent in this region of the spectrum. Prisms and lenses are fabricated from bulk glasses and also thin film waveguides are used in a variety of integrated-optics components. Also their high transparency in the infrared region together with the ability to draw long filaments from these materials open up opportunities for their use as fiber waveguides for infrared operation [52]. These applications do not involve light-induced structural effects and are therefore not discussed in this work.

It has been established that the majority of chalcogenide glasses exhibit structural changes under the influence of illumination which, makes them suitable for different types of application such as photoresists, holographic recording, and optical memories [52, 53]. In this section the applications based on light induced structural changes are summarized because these are the applications most relevant to the present work.

2.4.1 High resolution microlithography

Illumination of chalcogenide glasses results in changes in their optical, electrical, mechanical and, also, their chemical properties. Among these, light-induced effects in chemical properties can be utilized for applications such as photoresists. Light induced chemical changes, which are related to the light-induced structural changes, were first observed in As-S and Ge-Se chalcogenide films [54]. It has been reported that the illuminated areas of chalcogenide films dissolve faster than the unilluminated areas in alkaline solutions and also that they can be selectively etched by plasma etching [53, 55].

The photodissolution of metals is another important photo-chemical effect which can be used for microlithography [53]. Large amounts of metal such as zinc, copper and particularly silver can be dissolved into chalcogenide glass under the influence of illumination. As a result of photodissolution there is a drastic change in the solubility of chalcogenide glasses. These glasses can dissolve relatively easily in alkaline solutions, but when metal is diffused into the chalcogenide structure they become almost insoluble in alkaline solutions [53, 56].

The binary system Ge–Se was the first to be investigated as an inorganic photoresist [53]. In this system both the photodarkening and silver photodissolution effects were found to be effective. In the case of photodarkening, the etch rate of the illuminated area has been found to be ~15% larger than that of the unilluminated area. Therefore this effect yields a positive type of photoresist, in contrast to photodissolution since the silver photodoped Ge-Se films hardly dissolve at all in alkaline solutions. Photodissolution can therefore be used for negative type photoresist applications. Figure 2.7 shows the photolithographic process based on the photodarkening (positive process) and metal photodissolution (negative process) effects.

An advantageous feature of the Ge-Se based photoresist is that it has a strong resistance to many acid solutions, such as HF, HF–NH_4F, H_3PO_4, HCl and H_2SO_4 which are extensively used in microlithographic applications [53].

The resolving power of the Ge–Se based inorganic photoresist has also been investigated, and an ultrafine resolution of about 10 Å was confirmed using a fine-particle shadowing technique [57].

The sensitivity of the photoresist based on Ag photodissolution into evaporated As_2S_3 films was reported to be improved by overcoating with a vacuum deposited AgCl layer instead of elemental silver [18]. The As_2S_3 based resist has been further improved by sensitizing with a chemically deposited Ag_2S layer which overcomes the resolution limitation involved in the use of evaporated silver halides as a source of silver [19]. Both of these inorganic resist systems (AgCl / As_2S_3 and Ag_2S / As_2S_3) were successfully used as electron and X-ray resists as well as photoresist [18, 19].

It has also been reported that high quality chromium photomasks can be produced using As_2S_3 films as the photo-recording medium. It was claimed that the high resolution capability and the reproducibility of the As_2S_3 photoresist make it suitable for the fabrication of high quality Fresnel lenses [58]. High quality lines in the 0.5-100 μm scale have been reproduced in evaporated As_2S_3 film using a laser pattern generator.

In some systems it has been reported that there is lateral migration of silver from the unilluminated to the illuminated region of the sample, which is referred to as *edge sharpening* since it removes some of the smearing effect of diffraction at mask edges. This improves feature definition and is an additional advantage of these resists in high resolution applications [59].

A significant improvement in the use of inorganic photoresists was the discovery of selective dry etchants for the doped and undoped regions. Selective removal of the undoped chalcogenide in CF_4 and also in SF_6 plasmas has been reported [55, 60]. Sulphur plasma was reported to be used successfully to remove the Ag-As-S product of photodissolution in the Ag / As-S system [61].

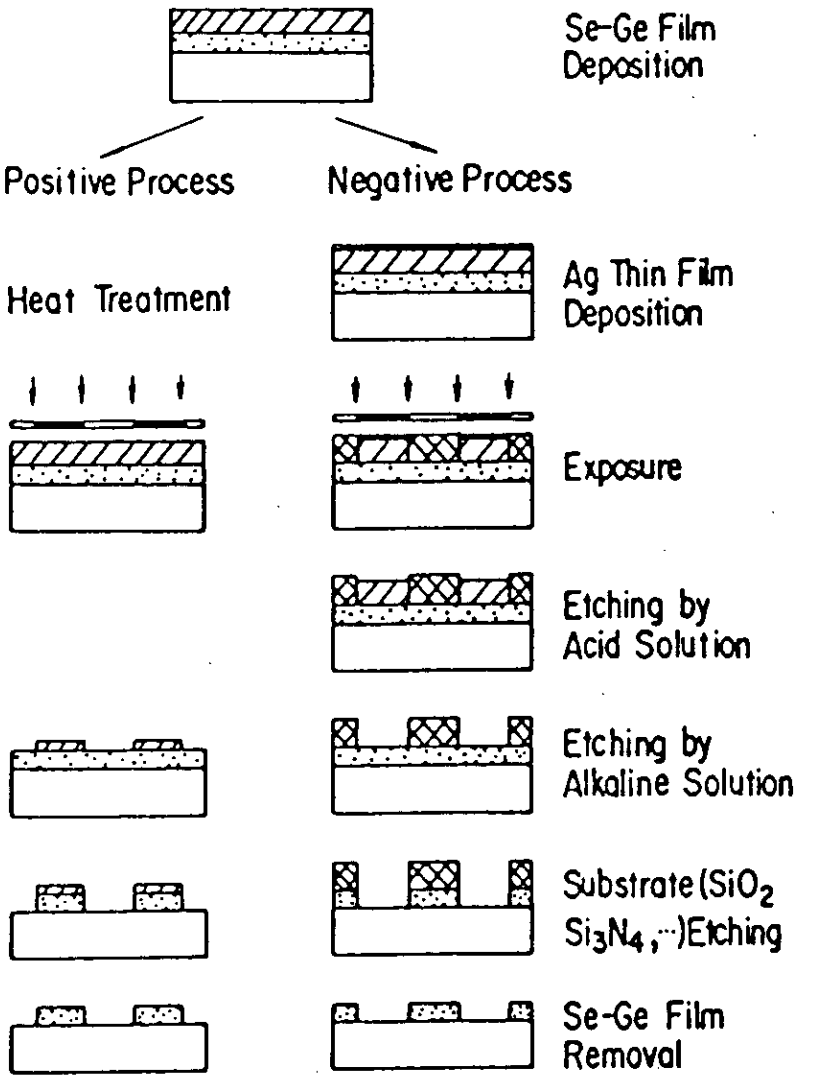

Figure 2.7 Schematic illustration of the photolithographic processes based on the photodarkening (positive process) and metal photodissolution (negative process) effects [53].

2.4.2 Holographic recording

One of the most attractive properties of chalcogenide glasses is the ability to change the absorption coefficient and the refractive index of these materials by illumination [6, 52, 62]. The spectral sensitivity of the light-induced effects corresponds to the absorption band of the chalcogenide and therefore covers a rather wide range, including X-ray, UV and Visible regions [62]. If there is a change in the refractive index under the influence of light it is possible to use chalcogenide films or bulk glasses to record not only the amplitude but also the phase of the illuminating light. This is particularly important in holographic recording applications. The magnitude of the change of the refractive index Δn can be as large as 0.05-0.1 in the visible wavelength region [6]. Such a large change in the refractive index makes these materials suitable as holographic recording media [52]. The fundamental holographic recording characteristics are usually investigated by producing a grating pattern in the chalcogenide film using a two-beam holographic technique.

For gratings produced in thin films of As-Se-S-Ge glass a diffraction efficiency of $\sim 8\%$ was obtained experimentally with a He-Ne laser ($\lambda = 0.6328 \mu m$). It was also concluded that the resolving power of these thin films was more than 2700 lines/mm. The sensitivity increases with increasing S/Se ratio in the As-Se-S-Ge system and can reach 400 mJ/cm^2 [63]. An advantage of these materials is the ability to erase and re-write because the refractive index change is reversible as it is associated with a reversible photostructural change.

Holographic gratings have been recorded in As_2S_3 films using the refractive index change induced by $\lambda = 514.5$ nm light of an Ar-ion laser. The samples in this case were illuminated with various beam ratios and a maximum diffraction efficiency of 30 % was found when equal writing beam intensities were used. A resolution of 1000 lines/mm was achieved. The effect of temperature on the diffraction efficiency has also been studied and it was concluded that the chalcogenide films are unsuitable for optical recording above 100° C [64].

In the As-Se-Ge system a difference of chemical etching rate between the heat treated state and the illuminated state has been observed. Utilizing this effect a surface relief-type diffraction grating has been obtained with a grating period of 0.86 μm [65].

The diffraction efficiency, defined as the ratio of the first order diffraction intensity to the incident light intensity, was found to be increased significantly after etching because of the larger difference of refractive indices between the photodarkened chalcogenide and air. The surface relief type grating (irradiated with 15.3 J/cm^2) achieved a relatively high diffraction efficiency of 15.8% which was about 10 times larger than that obtained before chemical etching.

The holographic applications described above are based on reversible photostructural changes. The silver photodissolution effect can also be used to obtain phase and amplitude holographic recordings or surface relief type gratings. The holographic recording properties of the evaporated $As_{16}S_{80}Te_4$ / Ag system have been investigated [66], metal dissolution being induced by irradiation with $\lambda = 488$ nm light at room temperature. It was concluded that this material can be used to make a thin amplitude or phase hologram because both the absorption coefficient and the refractive index change significantly when silver is dissolved into the chalcogenide. A surface relief type hologram can also be made by etching the sample after illumination using an alcoholic solution of sodium hydroxide. The relief mechanism is negative, that is, the etching rate is negligible in the silver-doped part. The sensitivity of this material was estimated to be ~25mJ/cm^2.

Holographic gratings have also been prepared in Ag / As_2S_3 sandwich structures. It was concluded that both the refractive index and the absorption coefficient of the sample changes as a result of silver photodissolution, consequently mixed phase and amplitude holograms were produced [67].

The extension of holographic techniques from the visible to the infrared part of the spectrum is also important from the applications point of view. It has been stated that the silver photodissolution effect in chalcogenides shows promise as one of the few techniques for fabricating low loss holographic materials for use at any given wavelength from 0.6μm to beyond 16 μm [68]. For efficient diffraction, the main requirement of the grating material is that it should be of low loss in the wave band of operation. The amorphous chalcogenides, both the undoped and the silver-doped, usually have rather low values of absorption coefficient in the infrared part of the spectrum. Consequently both undoped and silver-doped samples show high transmission from ~ 0.7 μm to beyond 13 μm (for the Ag / As_2S_3 system). The refractive index of the silver-doped regions has been found to be directly related to the

amount of silver in the chalcogenide [69]. Therefore by suitable choice of the silver thickness relative to that of the chalcogenide, the refractive index modulation of the gratings can be varied as required.

2.4.3 Optical memories

Due to the existence of reversible photostructural changes in chalcogenide glasses they can be used to fabricate optical memory elements, because their optical properties such as absorption coefficient and refractive index change reversibly when the film is illuminated and subsequently heat treated. Therefore this effect can be used to fabricate reprogrammable optical memory elements [70]. It was demonstrated that optical mass memories can be fabricated using a holographic Fourier transformation technique based on the reversible refractive index change in $As_{40}Se_{15}S_{35}Ge_{10}$ chalcogenide thin films [63]. About 400 holograms (microfiche pages) were written in an area of 5 cm x 3 cm. Experimental results have shown that 2500 pages can be written in a microfiche with 10^5 or 10^6 bits within each page. This suggests the memory capacity of these systems is $2.5x10^8$ - 10^9 bits.

Irreversible light induced structural changes in As-Te chalcogenide films have been used to fabricate optical video recording discs [71]. The information is stored by creating cleanly shaped holes in the surface of the film using pulsed Ar-ion laser irradiation (the pulse duration being 22 ns). The hole formation is due to a partial evaporation of the material at the illuminated spot. The holes are approximately 0.8μm in diameter and there is about the same distance between them, so a very high storage density can be achieved. They show stable storage characteristics and a high signal-to-noise ratio.

2.5 SPIN-COATED AMORPHOUS CHALCOGENIDE FILMS

All the work described in the previous sections was concerned with properties and light-induced effects observed in amorphous chalcogenide films which were deposited using a vacuum-coating technique, i.e. either thermal evaporation or sputtering. In 1982 Chern et al. reported a new class of amorphous chalcogenide thin films which were deposited from solution by spin-coating [22]. The deposition of amorphous chalcogenide thin films by this technique provides an opportunity to combine the ease and low cost of a technology commonly used for depositing organic photoresists or holographic recording materials, with the technologically useful properties of amorphous chalcogenide films.

2.5.1 Deposition of thin films by spin-coating

The objective of the spin-coating technique is to obtain a thin film of solute on the surface of a substrate. This deposition technique is most commonly used in the semiconductor industry in resist processing. Spin-coating has been accepted as the best coating method for obtaining an adherent and defect-free film which is uniform over the entire surface. Spin-coating is accomplished by flooding the substrate with a resist solution and rapidly rotating it at a constant speed between 1000 and 10000 revolutions per minute (rpm) until the film is dry. The spin-coating process consists of three steps:

1) flooding the substrate with resist solution

2) acceleration to a desired rpm

3) spinning at a constant rpm to near dryness.

The initial resist application can be accomplished either by flooding the entire wafer with resist solution prior to spinning or depositing a small quantity of resist in the centre of the wafer, spinning at low rpm to produce a uniform liquid film and then accelerating to the desired final spinning speed. Both approaches are designed to obtain an initial liquid film of uniform thickness. Once the uniform liquid film has developed, the remainder of the process consists of solvent evaporation to produce the solid film.

The most important parameter regarding the quality of the deposited film is its uniformity, both across a single substrate and from substrate to substrate. The fundamental parameters which govern film uniformity and thickness include molecular weight of solute, solution concentration and acceleration of the spinner. The physical and chemical properties of the solvent are also important. For a given molecular weight and constant solution concentration the film thickness depends only on the spinning parameters [72]. The deposited film quality is also affected by the solvent. A solvent should be chosen which has the correct solution properties to yield a uniform film. The solute should remain in solution throughout the entire spinning phase, otherwise aggregation may occur which can lead to opaque spots, pinholes or irregular lines. Solvent volatility also has an effect on film uniformity. Solvents which are highly volatile evaporate rapidly resulting in an increase in viscosity thereby preventing the achievement of uniform thickness over the whole substrate. Solvents with a too low volatility may result in too long drying times and increase the probability of particles sticking to the film and creating a potential defect site.

2.5.2 Spin-coated chalcogenide films

A number of chalcogenide thin films such as As_2S_3, As_2Se_3, As_2Te_3 and GeSe have been deposited from solutions, prepared by dissolving the appropriate bulk glass in organic alkaline solvents like ethylene-diamine, n-propylamine, n-butylamine, n-pentylamine, diethylamine, triethylamine or aniline. This deposition technique is analogous to the sol-gel deposition process used to obtain silicate-glass from solutions [22]. Chern et al. were the first to apply the technique of spin-coating to chalcogenide materials and their solvation in $R-NH_2$ organic solvents. The exact mechanism of the dissolution process is not established as yet. It was found that ethylene diamine and n-propylamine dissolved larger quantities of As_2S_3 glass powder, so these solutions are more suitable for thicker (several μm) film preparation. Diethylamine and triethylamine dissolved less glass material hence the solutions prepared with these solvents are more appropriate for depositing thinner films [22].

The spin-coating technique is a quick and simple process and does not require expensive vacuum equipment to obtain thin films of chalcogenides. Usually the

technique involves pipetting a few mls of centrifuged or filtered solution onto the substrate surface and spinning for a few seconds at an average rate of ~3000 rpm, depending on the viscosity of the solution. Subsequent soft baking in vacuum or in an inert atmosphere ensures the removal of the solvent from the film.

2.5.3 Characterisation of spin-coated As-S films

X-ray diffraction studies of spin-coated films show amorphous peaks whose shape and positions are dependent on the type of solvent used for dissolving the chalcogenide glass [22]. It is reported that spin-coated chalcogenide films can be deposited with more controlled stoichiometry than vacuum-evaporated films in cases where the composition, morphology and film structure are more difficult to control [22].

IR transmission spectra of spin-coated As_2S_3 films show solvent-related absorption peaks whose characteristics are dependent on the solvent used to prepare the chalcogenide solutions and also on the post-deposition heat treatment. It was reported that IR transmission spectra in the 400-200 cm^{-1} wavelength region indicate that the structure of these films is more similar to that of the bulk glass than to the structure of as-evaporated As_2S_3 films, because the absorption band characteristic of the As–S vibration in the As_4S_4 structural element is present only in the spectra of as-evaporated films [73]. The same authors reported an absorption band at ~410 cm^{-1} which was present only in the spectrum of the spin-coated As_2S_3 films but no assignment was given to this band [73].

The visible-UV transmission spectra of spin-coated As_2S_3 films indicate an absorption edge at an energy near to the absorption edge of the bulk glass. The position of the absorption edge was found to be dependent on the solvent used to prepare the solutions of As_2S_3 [22].

Based on proton NMR spectroscopy, it was suggested that the dissolution of the powdered As_2S_3 glass results in the formation of alkyl ammonium arsenic sulfide [73]. Transmission electron microscopy showed the structure of the freshly deposited spin-coated As_2S_3 films to consist of amorphous domains about 70-100 A in diameter [73].

It was suggested that during dissolution the bulk glass structure is fragmented by the solvent molecules, possibly at the weak Van der Waals bonds. The surface of the chalcogenide clusters is surrounded by the solvent molecules to form an amine salt. The alteration of the polarity of the cluster surface allows subsequent dissolution of the solid in the solvent.

Based on thermogravimetric analysis and mass spectrometric analysis, it was suggested that the decomposition of the amine salt during the heat treatment to remove the organic component from the film occurs in two steps. Annealing at lower temperatures (80–90° C) leaves hydrogenated arsenic sulphide and annealing at higher temperatures (~130° C) results in As_2S_3 formation when H_2S gas leaves the film [74].

Because the spin-coated chalcogenide / amine layer tends to dissolve if another layer is deposited on top, a new solvent-cast deposition technique has been tried, which involves a two-step preparation of the chalcogenide solution. The chalcogenide powders were dissolved in amines as a first step to obtain the amine salt of the chalcogenide. Then an amide solvent was used in the second step to dissolve the dried chalcogenide-amine salt. The resulting chalcogenide-amide solution was then used to deposit multilayer films by spin-coating, the final multilayer thickness achieved was ~5 μm. The films obtained by this technique were planar, although it was found that the surface of the multilayer film was rougher than that of the single layer [75].

The effect of annealing on the properties of spin-cast multilayer chalcogenide films was also studied and it was found that the thickness decreased and refractive index increased with increasing annealing time and temperature [75]. It was also found that the refractive index of As_2S_3 films deposited by this technique is smaller than that of sputtered or thermally evaporated films, probably because of the incorporation of some solvent residue. It was also claimed that spin-coated films are more stable to light irradiation than chalcogenide films deposited by other techniques. Smaller refractive index and absorption coefficient increases were measured when the spin-coated As_2S_3 samples were irradiated with UV, visible and IR light sources in vacuum, compared with the changes in the optical constants for evaporated As_2S_3 films for the same conditions. Oxidation and photo-decomposition was also observed during illumination in air [75].

2.5.4 Applications of spin-coated chalcogenide films

An entirely spin-coated inorganic resist system has been reported involving spin-coated As_2S_3 deposited from propylamine solutions. The chalcogenide film was sensitized by dipping into an aqueous solution of $AgNO_3$ or by spin-coating a thin film of silver halide on the surface of the spin-coated chalcogenide film [76]. Using UV illumination, 1-2 μm lines and spaces were printed in these resist systems. The illumination energy required to expose these spin-coated inorganic photoresists (3 Jcm^{-2}) was reported to be comparable with the fastest vacuum evaporated As_2S_3 resists [22]. It was reported that the edge sharpening mechanism is also present in these spin-coated resists [22].

Spin-coated As_2S_3 films have been used as a barrier layer in a trilayer resist process for use in optical and electron beam submicron lithography. Due to the low reflectivity of the intermediate spin-coated As_2S_3 film, it was possible to eliminate the anomalous standing wave effect and random light scattering in the top organic resist layer [77]. A high differential etch rate was found between the organic resist and the intermediate spin-coated As_2S_3 film in SF_6+O_2 plasma, which makes possible very precise pattern transfer in the trilayer resist system. The high resistance of the spin-coated As_2S_3 film to O_2 plasma has made possible the use of spin-coated As_2S_3 as a mask during the etching of the underlying PMMA planarizing layer [77].

Spin-coated As_2S_3 films have another advantage in multilayer lithographic processes if a thick spin-coated As_2S_3 layer is applied under the organic resist film as a planarizer. Due to the high differential etch rate of As_2S_3 compared to the imaging organic resist layer, the pattern can be directly transferred from the photoresist to the spin-coated As_2S_3 layer by reactive ion etching in SF_6+O_2 plasma. Using electron beam exposure a 0.25 μm pattern was transferred into a 2.2 μm thick spin-coated As_2S_3 planarizer layer. The thick patterns obtained had a vertical wall profile [77]. It was also pointed out that wet chemical etching as well as reactive ion etching can be used in the trilayer resist system for pattern transfer because alkaline photoresist developer and also SF_6+O_2 plasma removes spin-coated As_2S_3 films [77].

2.6 REFERENCES

[1] A. E. Owen, A. P. Firth and P. J. S. Ewen, 1985, Phil. Mag. B, Vol. 52, No. 3, pp. 347-362.

[2] K. Tanaka, 1980, "Fundamental Physics of Amorphous Semiconductors" ed. by F. Yonezava, (Springer Verlag).

[3] T. Igo and Y. Toyoshima, 1973, Proc. 5th Conf. of Solid State Devices, Tokio p. 106.

[4] K. Tanaka, S. Iijima, K. Aoki and S. Minomura, 1976, Proc. 6th Intern. Conf. Amorphous and Liquid Semicon. Leningrad.

[5] H. Hamanaka, K. Tanaka and S. Iijima, Solid State Comm. 1977, Vol. 23, p.63.

[6] K. Tanaka, 1980, Thin Solid Films, 66, pp. 271-279.

[7] K. Tanaka, 1975, Appl. Phys. Lett. Vol. 26, p. 243.

[8] M. Frumar, A. P. Firth and A. E. Owen, 1984, Phil. Mag. B, 50, p. 463.

[9] J. Hajto and P. J. S. Ewen, 1979, Phys. Stat. Sol. (a), 54, p. 385.

[10] V. G. Zhdanov, B. T. Kolomiets, V. M. Lyubin and V. K. Malinovski, 1979, Phys. Stat. Sol. (a), 52, p. 621.

[11] D. J. Treacy, U. Strom, P. B. Klein, P. C. Taylor and T. P. Martin, 1980, J. Non-Cryst. Solids, 35-36, p. 1035.

[12] B. Singh, S. Rajagopolan, P. K. Bhat, D. K. Pandya and K. L. Chopra, 1980, J. Appl. Phys. 51, 1768.

[13] M. T. Kostyshin, E. V. Mihkailovskaya and P. F. Romanenko, 1966, Fiz. Tverd. Tela, 571.

[14] H. Sakuma, I. Shimizu, H. Kokado and E. Inoue, 1971, Bulletin of Jap. Chem. Soc. 44, p. 1448.

[15] A. V. Kolobov and S. R. Elliott, Adv. Phys. in print.

[16] H. Kokado, J. Shimizu and E. Inoue, 1976, J. Non-Cryst. Solids, 20, p.131.

[17] A. V. Kolobov and V. M. Lyubin, 1984, Fiz. Tverd. Tela, 26, 2522.

[18] K. D. Kolwicz and M. S. Chang, 19880, J. Electrochem. Soc. Vol. 127, No. 1, pp. 135-138.

[19] B. Singh, S. P. Beaumont, P. G. Bower and C. D. W. Wilkinson, 1982, Appl. Phys. Lett. 41(9), pp. 889-891.

[20] P. J. S. Ewen, W. Y. Taylor and G. L. Paul, 1983, J. Phis. C. 16, p. 6475.

[21] J. M. Oldale, J. H. S. Rennie and S. R. Elliott, 1988, Thin Solid Films, 164, 467.

[22] G. C. Chern and I. Lauks, 1982, J. Appl. Phys. 53(10), pp. 6979-6982.

[23] D. Goldschmidt and P. S. Rudman, 1976, J. Non-Cryst. Sol. Vol. 22 pp. 229-243.

[24] A. V. Kolobov, B. T. Kolomiets, V. M. Lyubin and M. A. Tagirdzhanov, 1984, Sol. State Comm. Vol. 54, No. 5, pp. 379-382.

[25] J. H. S. Rennie and S. R. Elliott, 1985, J. Non-Cryst. Solids, 77-78, 1164.

[26] A. P. Firth, P. J. S. Ewen and A. E. Owen, 1985, J. Non-Cryst. Solids, 77&78, pp. 1153-1156.

[27] T. Yaji and S. Kurita, 1982, J. Appl. Phys. 54(2), pp. 647-651.

[28] E. Inoue, H. Kokado and I. Shimizu, 1974, Proceed. of the 5th Conf. on Solid State Devices, Tokyo, p. 101.

[29] R. E. Belford, E. Hajto and A. E. Owen, 1989, Thin Solid Films, 173, 129-137.

[30] T. Wagner and M. Frumar, 1990, J. Non-Cryst. Solids, 116, 269.

[31] K. Chatani, I. Shimizu, H. Kokado and E. Inoue, 1977, Jap. J. Appl. Phys. 16, 389.

[32] T. Yaji and S. Kurita, 1983, Jap. J. Appl. Phys. 22, 400.

[33] S. R. Elliott, 1991, J. Non-Cryst. Solids, in press.

[34] T. Yaji and S. Kurita, 1983, J. Appl. Phys. 54, 647.

[35] P. J. S. Ewen, A. Zakery, A. P. Firth and A. E. Owen, 1988, Philos. Mag. B, 57, 1.

[36] A. V. Kolobov and S. R. Elliott, 1990, Phil. Mag. B. Vol. 6, No. 5, 859-865.

[37] M. Janai, 1981, Phys. Rev. Lett. 47, p. 726.

[38] O. P. Kasyarum and A. A. Kudriavtsev, 1990, Proc. Int. Conf. of Non-Cryst. Semicond. Uzhgorod, p. 227.

[39] A. Buroff and R. Baeva, 1975, Proc. VI. Int. Conf. of Amorph. and Liquid Semic. Leningrad.

[40] A. Kokado, I. Shimizu and E. Inoue, 1976, J. Non-Cryst. Solids, 20. p. 531.

[41] M. T. Kostyshin, O. P. Kasyarum and A. A. Kudryavtsev, 1984, Ukr. Fiz. Zh. 29, p. 581.

[42] J. Plocharski, J. Przyluski and M. Teodorczyk, 1984, J. Non-Cryst. Solids, 93, pp. 303-310.

[43] P. J. S. Ewen, A. Zakery, A. P. Firth and A. E. Owen, 1987, J. Non-Cryst. Solids, 97-98, 1127.

[44] M. Janai, 1981, Phys. Rev. Letters, 47, 726.

[45] R. A. Street and N. F. Mott, 1975, Phys. Rev. Letters, 35, 1293.

[46] M. Kastner, D. Adler and H. Fritzsche, 1976, Phys. Rev. Letters, 37, 1504.

[47] H. Kokado, I. Shimizu and E. Inoue, 1976, J. Non-Cryst. Solids, 20, 131.

[48] M. Yamaguchi, I. Shimizu and E. Inoue, 1982, J. Non-Cryst. Solids, 47, 341.

[49] T. Wagner and M. Frumar, 1989, Proc. Int. Conf. of Non-Cryst. Semicond. Uzhgorod . 240.

[50] J. Malinowski and A. Buroff, 1978, Contemp. Phys. 19, 99.

[51] G. Kluge, 1987, Phys. Stat. Sol. a101, 105.

[52] A. M. Andries, V. V. Ponomar, V. L. Smirnov and A. V. Mironos, 1986, Sov. J. Quantum Electron. 16 (6), pp. 721-736.

[53] Y. Mizushima and A. Yoshikawa, 1982, Jap. Ann. Rev. in Electronics, Computers and Telecomm. ed. by Y. Hamakawa, pp. 277-295.

[54] J. P. DeNeufville, 1975, "Optical Properties of Solids", ed. by B. O. Seraphin, North-Holland Pub. Co. p. 437.

[55] K. Kase, G. C. Chern and I. Lauks, 1984, Thin Solid Films, 116, L53-L54.

[56] M. Mitkova and Z. Boncheva, 1987, J. Non-Cryst. Solids, 90, pp. 589-592.

[57] A. Yoshikawa, S. Hirota, O. Ochi, A. Takeda and Y. Mizushima, 1981, Jap. J. Appl. Phys. Vol. 20, No. 2, pp. L81-L83.

[58] A. G. Poleschuk, E. G. Churin and Y. Yurlov, 1986, J. Imaging Science, Vol. 30, No. 3, pp. 132-135.

[59] K. L. Tai, R. G. Vadimsky, C. T. Kemmerer, J. S. Wagner, V. E. Lamberti and A. G. Timko, 1980, J. Vac. Sci. Technol. 17(5), pp. 1169-1176.

[60] B. Singh, G. C. Chern and I. Lauks, 1984, Appl. Phis. Lett. 45(1), pp. 74-76.

[61] R. E. Belford, E. Hajto and A. E. Owen, 1989, Thin Solid Films, 173, pp. 129-137.

[62] M. I. Kostyshin, E. P. Krasnojonov, V. A. Makeev and G. A. Sobolev, 1970, Proc. Intern. Symp. of Holography, ed by J. C. Vienot (France).

[63] S. Zembutsu, Y. Toyoshima, T. Igo and H. Nagai, 1975, Appl. Optics, 14, p. 3073.

[64] A. Singht, R. A. Lessard and M. Samson, 1984, Optica Acta, Vol. 31, No. 10. pp. 1161-1165.

[65] Y. Utsugi and S. Zembutsu, 1975, Appl. Phys. Lett. Vol. 27, No. 9, pp. 508-509.

[66] T. Fukaya, S. Matsumura, J. Tsujiuchi, E. Inoue and H. Kokado, 1972, Optics Communications, Vol. 7, No. 2, pp. 98-102.

[67] A. Buroff and M. Georgiev, 1977, Optics Communications, Vol. 24, No. 1, pp. 67-71.

[68] C. W. Slinger, A. Zakery P. J. S. Ewen and A. E. Owen, 1991, Applied Optics, in press.

[69] P. J. S. Ewen, C. W. Slinger, A. Zakery, A. Zekak and A. E. Owen, 1991, Proc. Intern. Congress on Optical Science and Engineering, in press.

[70] S. Zembitsu, 1982, "Amorphous Semiconductor Technologies and Devices" ed. by Y. Hamanaka, p. 296.

[71] M. Terao, K. Shigematsu, M. Ojima, Y. Tanaguchi and S. Yonezawa, 1979, J. Appl. Phys. Vol. 50, No. 11, p. 6881.

[72] L. F. Thompson, "Introduction to Microlithography", 1983, Proc. 185th Meeting of the American Chemical Soc. p. 190.

[73] G. C. Chern and I. Lauks, 1983, J. Appl. Phys. 54(5), pp. 2701-2705.

[74] G. C. Chern and I. Lauks, 1983, J. Appl. Phys. 54(8), pp. 4596-4601.

[75] J. J. Santiago, M. Sano, M. Hamman and N. Chen, 1987, Thin Solid Films, 147, pp. 275-284.

[76] I. Lauks, G. C. Chern and K. Y. Toh, 1984, J. Appl. Phys.

[77] B. Singh, G. C. Chern and I. Lauks, 1984, Appl. Phys. Lett. 45(1), pp. 74-76.

CHAPTER 3

SAMPLE PREPARATION AND EXPERIMENTAL TECHNIQUES

3.1 PREPARATION OF BULK SAMPLES AND SPIN-COATED FILMS

The As_xS_{100-x} materials studied were prepared first in bulk form by direct synthesis from elements of 5N purity. Appropriate amounts of the constituent elements were measured into quartz ampoules. The evacuated and sealed ampoules were heated at 900° C for 12 hours in a rocking furnace. After synthesis the melts were air quenched, resulting in bulk glasses of the required compositions.

Solutions of the chalcogenides were made by dissolving the powdered glass in anhydrous n-propylamine and were always stored in anhydrous conditions. Before deposition the solutions were filtered with a 0.5μm pore-size filter to ensure that the solution did not contain solid particles. The thin films of the chalcogenides were deposited using the spin-coating technique. This deposition technique involves feeding a few drops of the solvent onto the surface of the substrate and spinning. In this project the thin films of As-S materials were obtained by spinning the samples for 20 seconds at 3000 rpm. This gives an acceleration of $1x10^4$ rev min^{-2}. The filtered solutions of the chalcogenides were deposited by spin-coating onto a number of different planar substrates, depending on the type of experiments undertaken. It was found that the resulting film thickness varied with the concentration of the solutions, the spinning time and the spinning rate. Typically 2 gm of chalcogenide glass dissolved in 10 ml n-propylamine and spin-coated at 3000 rpm for 20 s resulted in a uniform film of ~ 1 μm thickness.

Subsequent to the deposition the films were subjected to a thermal annealing treatment in order to evaporate the remains of the solvent from the film. Annealing was done at 120° C for 30 minutes or at 160° C for 30 minutes in a vacuum oven (Gallenkamp Vacuum Oven OVL-570). Examination by optical and scanning electron microscopy showed these films to be continuous, homogeneous and free of microstructure. The above detailed deposition conditions resulted in good quality As-S films with reproducible properties.

Figure 3.1 SEM photograph of an ~0.5 μm thick spin-coated $As_{40}S_{60}$ film (the irregular-shaped features are due to the scribing process).

3.2 SAMPLE PREPARATION AND EXPERIMENTAL TECHNIQUE FOR X-RAY MICROPROBE ANALYSIS

X-ray microprobe analysis was used to check the composition of some of the materials examined in this study. For this analysis ~4μm thick films of the compositions $As_{25}S_{75}$, $As_{30}S_{70}$, $As_{35}S_{65}$ and $As_{40}S_{60}$ were deposited by the spin-coating technique onto polished Si wafers from the corresponding saturated chalcogenide/n-propylamine solutions. The spinning was carried out at 3000 rpm for 10 seconds and the samples were subsequently annealed in a vacuum oven at 120° C for 30 minutes in order to remove any remaining solvent from the films. Polished slices from the appropriate bulk sources were also analyzed for the purpose of comparison.

These experiments were carried out in the Geology Department of the University of Edinburgh, using a Wavelength Dispersive X-Ray Spectrometer (Camebax Microbeam), all measurements being performed with an electron gun potential of 20 kV and probe current of 20 mA. The average of five parallel measurements was taken for each sample as the result of the compositional analysis. The estimated precision of the measurements was ~ ±1 atomic%.

3.3 SAMPLE PREPARATION AND EXPERIMENTAL TECHNIQUE FOR INFRARED SPECTROSCOPY

Information on the structure and the purity of the spin-coated films was obtained by infrared spectroscopy. These measurements were carried out using a Perkin-Elmer 598 Infrared Spectrophotometer. The transmittance spectra of spin-coated films of composition $As_{25}S_{75}$, $As_{30}S_{70}$ and $As_{40}S_{60}$ and spin-coated films of pure sulphur (also deposited from solutions of n-propylamine) were recorded in the 2.5-50.0 μm (4000-200 cm^{-1}) spectral range. The films were deposited onto CsI substrates which are transparent in the required spectral region. A CsI cell was also used for obtaining the IR spectra of liquid samples such as n-propylamine and solutions of various As–S compositions.

In order to monitor the removal of the solvent from the spin-coated As–S films, infrared transmittance spectra were recorded from samples in the as-deposited state and also after annealing in a vacuum oven at 100° C for 2 hours or at 160° C for 2 hours.

The effect of silver diffusion on the structure of the spin-coated $As_{33}S_{67}$ films was also investigated using infrared spectroscopy. For this purpose a silver film of ~0.3 μm thickness was first vacuum evaporated (at 10^{-6} Torr) onto a CsI substrate and then a ~1μm thick $As_{33}S_{67}$ film was deposited by spin-coating on top of the silver. The samples were annealed at 120° C for 30 minutes in the dark. It was found that annealing at the given conditions caused only negligible thermal diffusion of silver, but produced solvent-free samples which could be used for pattern fabrication using the silver photodissolution effect. After annealing, the silver / chalcogenide structure was illuminated with the mercury lamp of a Carl Suss Illumination System for 1 hour, which resulted in spin-coated As–S films uniformly doped with silver. The undoped chalcogenide film from the sample surface was removed by dissolving in methanol saturated with ammonia. Infrared transmittance spectra in the spectral range of 400-200 cm^{-1} were recorded from the samples prepared this way.

3.4 SAMPLE PREPARATION AND EXPERIMENTAL METHOD FOR OBTAINING THE OPTICAL CONSTANTS

The optical constants (refractive index, n, and absorption coefficient, α) of the undoped and the Ag-doped spin-coated As–S films were calculated from the measured transmittance and reflectance of these films. The optical transmittance and reflectance spectra of spin-coated $As_{15}S_{85}$, $As_{25}S_{75}$, $As_{30}S_{70}$, $As_{35}S_{65}$, $As_{40}S_{60}$ and also of the Ag-doped $As_{40}S_{60}$ films were obtained at room temperature in the spectral region of 0.2-2.5 μm using an UV-VIS-NIR spectrophotometer (Perkin-Elmer Lambda 9). For this purpose thin films (~1μm) of the required compositions of As–S were deposited by spin-coating onto Corning glass 7059 substrates. Silver photodoped samples were prepared as described in Section 3.3., but again Corning glass 7059 substrates were used. The method suggested by Swanepoel [1] and Ticha et al. [2] was used to calculate the optical constants from the recorded transmittance and reflectance spectra of the films. In these calculations a thin absorbing film on a thick transparent substrate

is considered. Figure 3.2 shows the optical path of this structure.

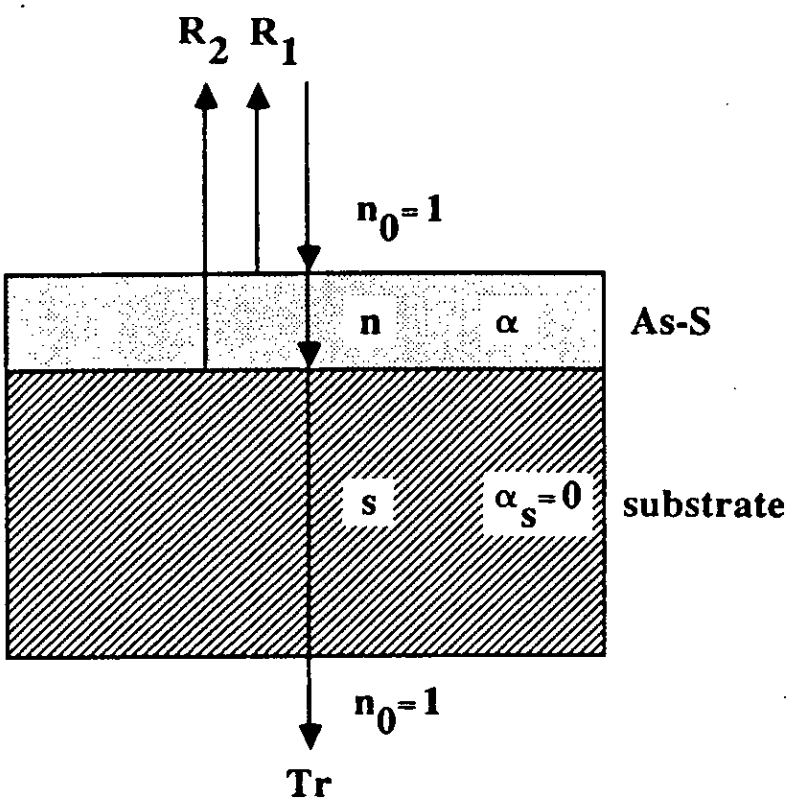

Figure 3.2 Schematic diagram of a sample structure consisting of a thin absorbing film on a thick transparent substrate.

The transparent substrate has a thickness several orders of magnitude larger than that of the thin film, it has a refractive index, s, and a negligible absorption coefficient, $\alpha_s \simeq 0$. The refractive index of the surrounding air is $n_o = 1$. The absorbing thin film has thickness, d, a complex refractive index, $n = n - i\kappa$, where n is the refractive index and κ is the extinction coefficient, which is related to the absorption coefficient, α, of the thin film by:

$$\kappa = \frac{\alpha\lambda}{4\pi} \tag{1}$$

where λ is the wavelength of the illuminating light.

The transmittance, Tr, of this structure will depend on the wavelength of the measuring light, the refractive index of the substrate, the refractive index of the thin film, the absorption coefficient of the film, and the film thickness:

$$Tr = Tr(\lambda, s, n, \alpha, d) \tag{2}$$

Figure 3.3 shows a typical transmission spectrum recorded from a 0.6 μm thick spin-coated $As_{40}S_{60}$ film in the 0.35-1.55 μm spectral range. If the thickness of the deposited film is uniform, interference effects, such as those visible in Figure 3.3 occur due to multiple reflection at the interfaces. The recorded transmission spectrum can be divided into four regions:

1) In the transparent region $\alpha \simeq 0$ and the transmission is determined by n and s through multiple reflections.

2) In the region of weak absorption α has a small but increasing value which will start to reduce the transmission.

3) In the region of medium absorption α is increasing further and as a consequence the transmission also decreases.

4) In the region of strong absorption the transmission decreases drastically and the interference is suppressed due to the high absorption of the film.

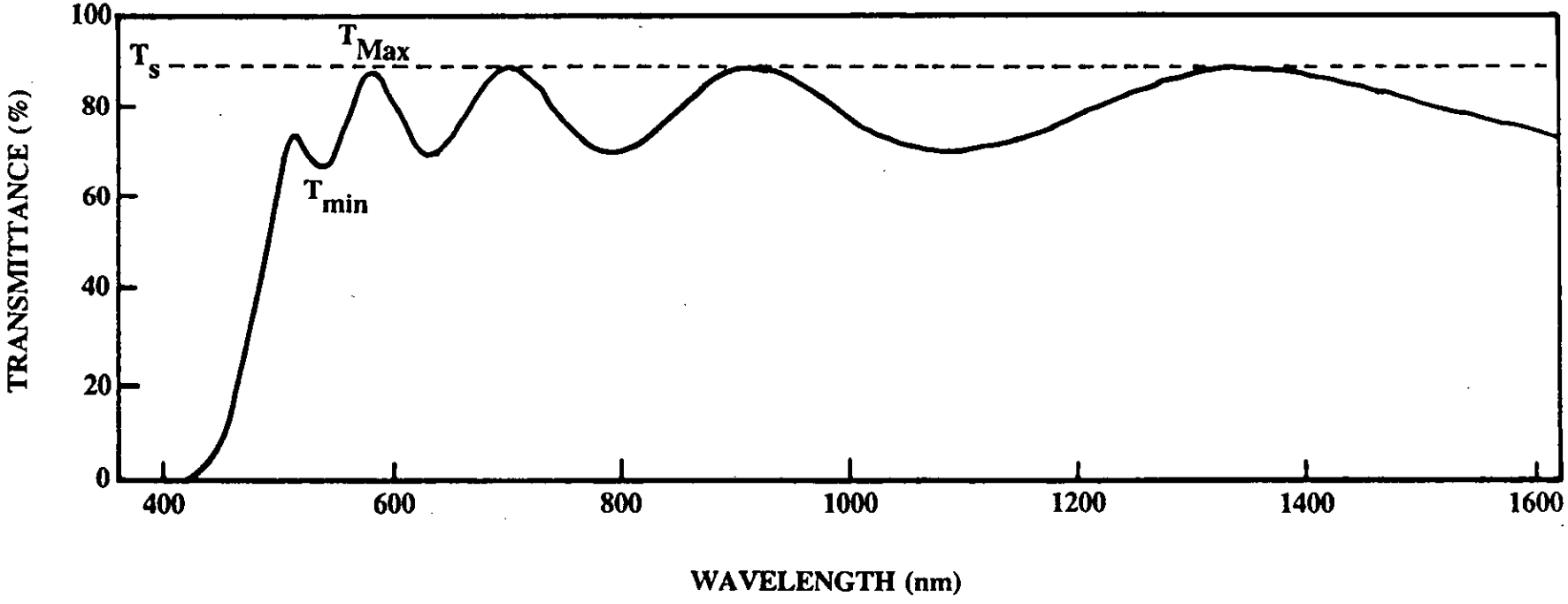

Figure 3.3 Transmission spectrum of a 0.6 μm thick spin-coated $As_{40}S_{60}$ film.

Using the calculations suggested by Swanepoel [1] the recorded interference fringes can be used to determine the optical constants (n, α) of the film in the transparent region and in the region of weak and medium absorption. In the region of strong absorption the optical constants were calculated from the interference-free transmission and reflection data of the samples using a different calculation method [2].

For the calculation of the optical constants (n, α) using the transmission spectrum of the thin film, it is necessary to know the refractive index of the substrate. The transmittance of a non-absorbing substrate, T_s, is a function of its refractive index, s, and is given by:

$$T_s = \frac{2s}{s^2+1} \tag{3}$$

Using Equation (3), s can be determined as:

$$s = \frac{1}{T_s} + \left(\frac{1}{T_s^2} - 1\right)^{1/2} \tag{4}$$

The refractive index of a thin film in the transparent region of the spectrum can be obtained using the values of the interference fringes and the refractive index of the substrate [1].

In the transparent region ($\alpha \approx 0$) the maxima of the interference fringes, T_M, are equal to the transmission of the substrate, T_s, (see Figure 3.3) and are a function of s only:

$$T_M = \frac{2s}{s^2+1} \tag{5}$$

The minima of the interference fringes, T_m, can be written as:

$$T_m = \frac{4n^2 s}{n^4 + n^2(s^2+1) + s^2} \tag{6}$$

where

$$n = [M + (M^2 - s^2)^{1/2}]^{1/2} \tag{7}$$

and

$$M = \frac{2s}{T_m} - \frac{s^2+1}{2} \tag{8}$$

T_m is a function of both n and s, and n can be calculated from T_m using Equation (7).

In the region of weak and medium absorption the interference maxima depart from T_s denoting the onset of absorption. In this region $n(\lambda)$ can also be calculated using the values of the interference maxima and minima:

$$n = [N+(N^2-s^2)^{1/2}]^{1/2} \tag{9}$$

where

$$N = 2s\frac{T_M-T_m}{T_M T_m}+\frac{s^2+1}{2} \tag{10}$$

Once $n(\lambda)$ is known, $\alpha(\lambda)$ can be calculated in various ways. To obtain α it is useful to introduce a parameter, x, as defined below:

$$x = \exp(-\alpha d) \tag{11}$$

It is possible to calculate x using the value of the interference maxima, T_M, the refractive index of the film, n and the refractive index of the substrate, s:

$$x = \frac{E_M-[E_M^2-(n^2-1)^3(n^2-s^4)]^{1/2}}{(n-1)^3(n-s^2)} \tag{12}$$

where

$$E_M = \frac{8n^2s}{T_M}+(n^2-1)(n^2-s^2) \tag{13}$$

Alternatively, x can be calculated using the minima of the interference fringes (T_m):

$$x = \frac{E_m-[E_m^2-(n^2-1)^3(n^2-s^4)]^{1/2}}{(n-1)^3(n-s^2)} \tag{14}$$

where

$$E_m = \frac{8n^2s}{T_m}-(n^2-1)(n^2-s^2) \tag{15}$$

The parameter x can also be calculated using the interference fringes in a different way. From T_M and T_m the interference-free transmission T_α can be calculated using the following expression:

$$T_\alpha = (T_M T_m)^{1/2} \tag{16}$$

It can be shown that x is given by:

$$x = \frac{[G-[G^2-(n^2-1)^6(n^2-s^4)^2]^{1/2}]^{1/2}}{(n-1)^3(n-s^2)} \tag{17}$$

where

$$G = \frac{128n^4s^2}{T_\alpha^2} + n^2(n^2-1)^2(s^2-1)^2 + (n^2-1)^2(n^2-s^2)^2 \tag{18}$$

Using this third method α can be obtained with better accuracy since both T_M and T_m are used and also because this technique is less sensitive to the effect of changes in the slit width of the spectrophotometer on the transmission spectrum (these affect the amplitude of the interference fringes) [1]. Therefore in calculating n and α in the region of weak and medium absorption Equations (16), (17), and (18) were used.

In order to obtain α from x using Equation (11) an accurate value of the film thickness, d, is necessary. Two different methods were used to determine the film thickness. First, prior to the calculations, a step was produced in the film by scribing and its depth measured using a mechanical stylus instrument (Sloan Dektak II).

The thickness of the spin-coated films was also determined using a graphical method, suggested by Swanepoel [1] based also on the interference conditions. The interference conditions equation for the extremes of the transmission spectra is:

$$2nd = (m_1 + \frac{l}{2})\lambda \tag{19}$$

where n is the refractive index of the film, d is the film thickness, m_1 is the order number of the first maximum or minimum of the interference, l is an integer (0, 1, 2, 3...) and λ is the wavelength. Equation (17) can be re-written as:

$$\frac{l}{2} = 2d(\frac{n}{\lambda}) - m_1 \tag{20}$$

Thus by plotting l/2 versus n/λ a straight line can be obtained with a slope of 2d, that is, twice the film thickness (see Figure 3.4). No substantial differences were found between the measured and calculated values of the film thickness, but for the absorption coefficient calculations, the values obtained from the graphical method have been used.

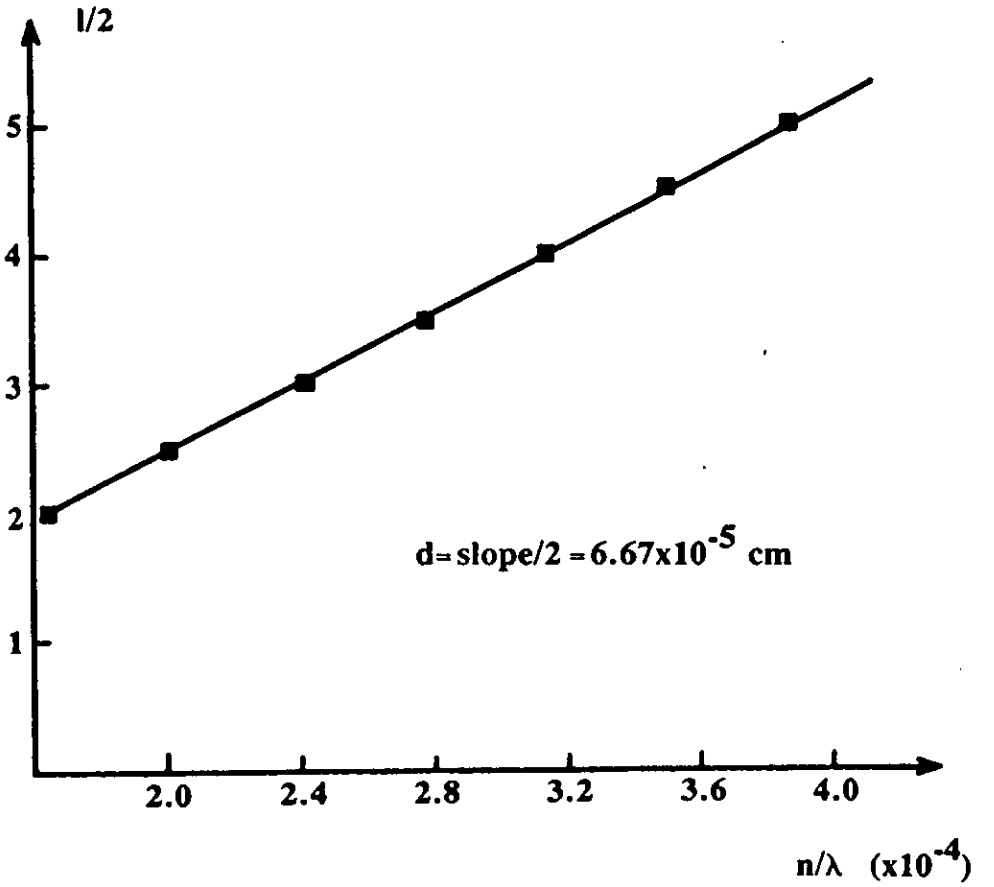

Figure 3.4 Thickness determination by plotting I/2 versus n/λ.

In the region of strong absorption in the transmission spectra the interference fringes disappear and the transmission decreases sharply in the direction of shorter wavelengths. At the same time, with decreasing wavelength, the interference fringes in the reflection spectra also disappear and the reflection begins to increase. Figure 3.5 shows a typical reflection spectrum for a ~0.6 μm thick spin-coated $As_{40}S_{60}$ film in the 0.2-1μm range of the spectrum. In this region the absorption coefficient, α, was calculated from both the measured interference free transmission, T_α, and the interference free reflection, R_α, using Equation (21) [2]:

$$\alpha = d^{-1}\ln\frac{(1-R_\alpha)^2[(1-R_\alpha)^4+4R_\alpha^2T_\alpha^2]^{1/2}}{2T_\alpha} \qquad (21)$$

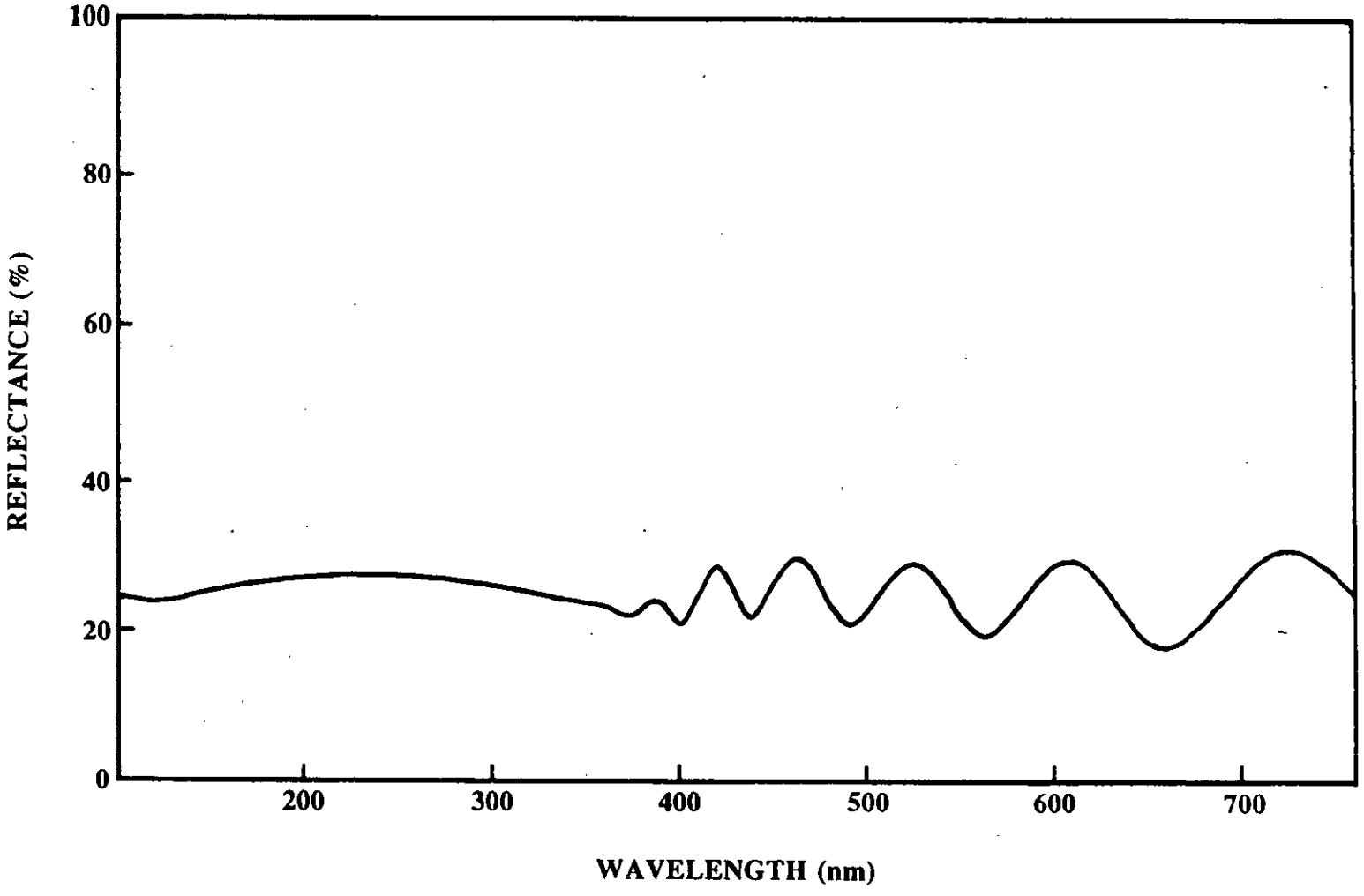

Figure 3.5 Reflection spectrum of a 0.6 μm thick spin-coated $As_{40}S_{60}$ film.

3.5 SAMPLE PREPARATION AND EXPERIMENTAL ARRANGEMENT FOR MEASURING THE REACTION KINETICS OF SILVER PHOTODISSOLUTION

For the experiments concerned with the light-induced diffusion of silver into spin-coated As-S films, a 0.04 μm Ag film was deposited by vacuum evaporation onto a silica glass substrate in a vacuum of 10^{-6} Torr. An $As_{40}S_{60}$ film of thickness 1 μm was then deposited on top of the Ag film by the spin-coating technique. The samples were finally annealed in an oven at 120° C for 30 minutes.

The samples prepared in this way were illuminated with monochromatic light at room temperature to induce the silver photodissolution. The change of the optical properties of the sample (transmittance, Tr, and reflectance, R,) were recorded in order to gain information about the kinetics of the process. The effect of different factors such as illumination intensity and wavelength on the silver photodissolution rate were also investigated.

Figure 3.6 shows the experimental arrangement used for studying the kinetics of silver photodissolution in spin-coated $As_{40}S_{60}$ films. An unfocussed cw Ar-ion laser was used to induce the reaction between the silver and the chalcogenide layers, the diameter of the illuminated area being 0.2 cm. The following single wavelengths were used to study the wavelength dependence of the process: $\lambda = 0.5145$, 0.4880, and 0.4658 μm. The incident power of the illuminating light was changed over the 13-220 mW range by neutral density filters. Simultaneously with the Ar-ion laser, a low intensity He-Ne laser was used as a monitoring source with a wavelength ($\lambda = 0.6328$ μm) that had negligible absorption in the chalcogenide layer thickness used for the experiments. The samples were illuminated from the chalcogenide side, and the reflected and the transmitted beams were filtered with red filters in order to separate the monitoring beam from the beam used to induce the silver photodissolution. The intensity changes in the monitoring He-Ne light were detected with Si photodetectors and plotted on a chart recorder. The use of a separate monitoring light made the reading of the measurement independent of the different values of absorption at the different exciting light wavelengths and the consequent differences in the transmitted light intensities through the chalcogenide film. Because of the low absorption at 0.6328 μm and the low intensity (~1mW) of the monitoring light, the He-Ne laser beam did not induce any reaction between the layers but served only to yield

information on the thickness changes of the chalcogenide and the silver films during the reaction.

The time dependence of the silver photodissolution process and also the effects of illumination intensity and wavelength on the rate were investigated using two different methods and the results were compared. During the photodissolution reaction, part of the incident light intensity is reflected from the Ag (or later, the doped As–S surface) and part is reflected from the surface of the sample. Since the thickness of the undoped chalcogenide region changes with time, the reflected intensity of the monitoring beam changes periodically, due to interference effects [3]. Using the interference condition:

$$2nd = m\lambda \tag{22}$$

where n is the refractive index of the $As_{40}S_{60}$ film (measured earlier), d is the film thickness, m is an integer and λ is the wavelength of the monitoring light, the kinetics of the change in the chalcogenide layer thickness can be calculated.

Alternatively, the change in the transmitted light intensity which accompanies the change in the thickness of the Ag layer can be used to calculate the silver diffusion rate, v, from the relation:

$$v = \frac{1}{Tr}\frac{dTr}{dt} \tag{23}$$

where Tr is the transmitted intensity of the illuminating light [4].

To obtain information about the effect of the incident intensity and wavelength on the silver photodissolution, the reaction rates measured at the same stage of the process were compared. Using the reflected intensity change of the monitoring light, the reaction rates measured between the first and second interference maxima were compared. The maximum points of the first (time) derivative curves of the transmitted intensities obtained with different illumination intensities and wavelengths were also compared.

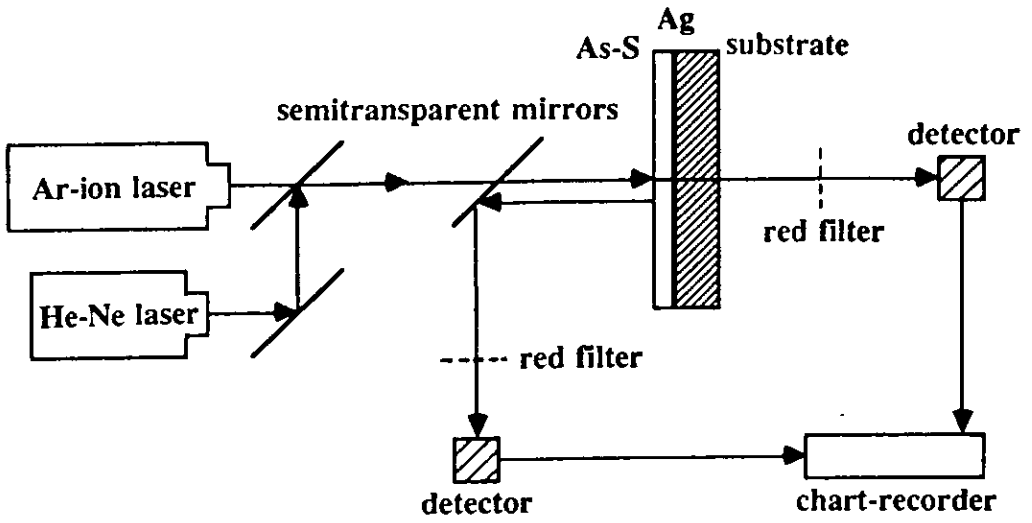

Figure 3.6 Experimental arrangement for measuring the rate of the silver photodissolution.

3.6 SAMPLE PREPARATION AND EXPERIMENTAL ARRANGEMENT FOR MEASURING THE ETCHING PROPERTIES OF SPIN-COATED As-S FILMS

Silver photodissolution and also illumination itself cause changes in the structure of the As–S films which result in an etch rate difference between the illuminated and unilluminated parts of the films in alkaline solutions [5]. The selective removal of these films by plasma etching has also been reported [6].

The etching properties of Ag-doped and undoped spin-coated $As_{40}S_{60}$ films and also the illuminated and the unilluminated spin-coated $As_{40}S_{60}$ films were investigated using CF_4 plasma. Typically ~2 μm thick $As_{40}S_{60}$ films were deposited by spin-coating onto silica glass substrates and annealed at 160° C for 30 minutes. To investigate the effect of Ag-diffusion on the etching rate, Ag-doped $As_{40}S_{60}$ thin films were prepared. Vacuum evaporated Ag films of thickness ~0.4 μm were deposited onto microscope slides in a 10^{-6} Torr vacuum then ~1 μm thick $As_{40}S_{60}$ films were deposited by spin-coating on top of the Ag film. The samples were annealed at 120° C for 30 minutes and illuminated with UV light for 1 hour, using the Carl Suss illumination system, to produce the silver photodissolution reaction.

The etching rates of the annealed, the illuminated and also the silver-doped spin-coated $As_{40}S_{60}$ films were measured using CF_4 plasma. These experiments were carried out in an International Plasma Corporation 2000 series system which is a basic barrel-type plasma etcher, powered by a 13.56 MHz RF generator. In order to establish a constant etching rate during measurement, different CF_4 gas pressures and RF power combinations were tried. The gas flow rate in the chamber was controlled by the chamber pressure. The optimum etching conditions were found to be: CF_4 gas pressure=0.7 Torr, RF power=100 W.

An "in situ" optical technique was used to measure the etching rate of the differently treated samples in the CF_4 plasma. The experimental arrangement used in these measurements is shown in Figure 3.7. A low intensity He-Ne laser (λ=0.6328 μm) beam was reflected from the surface of the sample during etching and its intensity detected by a photodiode and plotted on a chart recorder. The etching rate was evaluated from the time interval between consecutive interference maxima and minima using the interference condition (Equation 22). The etching rates of annealed,

illuminated (photodarkened) and silver-doped spin-coated $As_{40}S_{60}$ films were compared.

A surface relief grating was prepared in a spin-coated $As_{40}S_{60}$ film using the differential etch rate of the illuminated and unilluminated parts of the film. For this experiment 1 μm thick spin-coated $As_{40}S_{60}$ films were deposited onto microscope slides and annealed at 120° C for 30 min. The prepared films were illuminated with UV light from a mask alignment system through a contact mask with 4 μm equal lines and spaces. The pattern was developed by plasma etching using CF_4 gas.

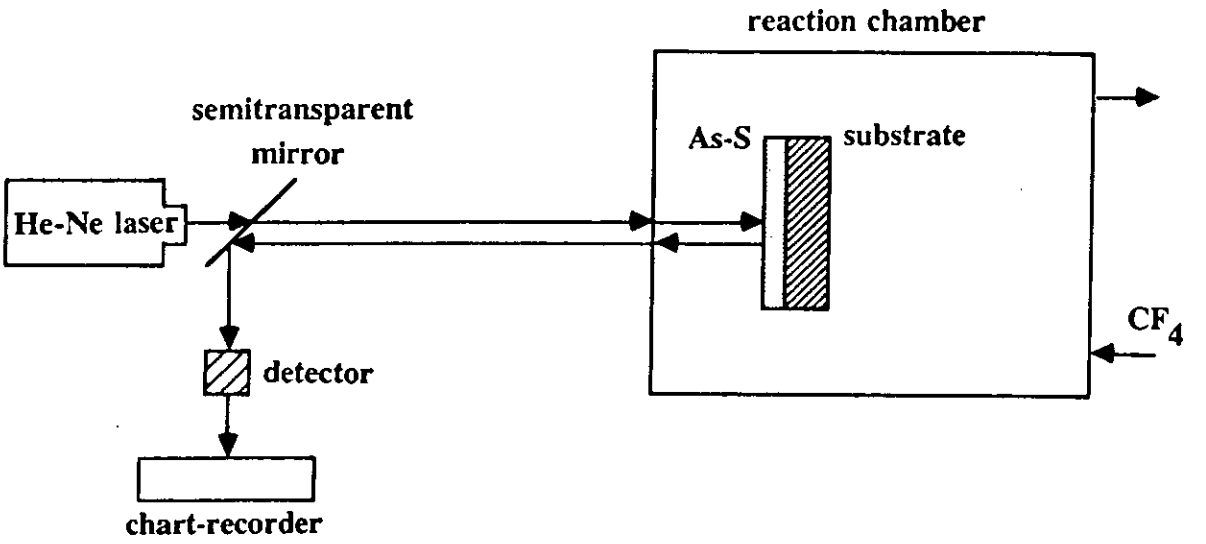

Figure 3.7 Experimental arrangement for measuring the etching rate.

3.7 SAMPLE PREPARATION AND EXPERIMENTAL ARRANGEMENT FOR PRODUCING DIFFRACTION GRATINGS IN SPIN-COATED As-S FILMS BY SILVER PHOTODISSOLUTION

In this project diffraction gratings were also prepared in spin-coated $As_{40}S_{60}$ films by the silver photodissolution. Grating patterns were generated in the samples using a holographic illumination arrangement [7].

The Ag / $As_{40}S_{60}$ double layer samples used for this experiments were prepared in two steps. First, a thin (~0.4 μm) silver layer was deposited by vacuum evaporation onto a silica glass substrate, then an $As_{40}S_{60}$ film of thickness ~1 μm was spin-coated onto the surface of the silver film. The samples were annealed in the dark at 120° C for 30 min.

Grating patterns were generated in the samples using the silver photodissolution effect. Figure 3.8 shows the scheme of the optical arrangement that was developed to illuminate the Ag / $As_{40}S_{60}$ layers. The samples were exposed to a spatially periodic intensity pattern, generated by two interfering beams of light. The beam of an Ar-ion laser was focussed through a spatial filter, expanded and collimated, and finally divided into two parts of equal intensity using a prism. As Figure 3.8 shows, the angle of the prism determines the angle of incidence of the illuminating beam, and hence determines the grating period produced in the film. According to the theory, when two coherent beams of light intersect at an angle of 2θ, they will interfere with a spacing (Λ) given by:

$$\Lambda = \lambda/2\sin\theta \qquad (24)$$

where λ is the wavelength of the illuminating light and θ is the angle of incidence [8]. Therefore the grating period generated in the sample by the above holographic illumination arrangement, is determined only by the wavelength of the illuminating light and by the angle of incidence of the interfering beams. In theory the finest spacing obtainable is $\lambda/2$, which corresponds to $\theta = 90°$. This cannot be achieved in practice since it requires both beams to be incident along the surface of the sample. A value of $\theta = 60°$ yields a spacing of 0.6λ. In the present experiments the grating period was varied by using different angles of incidence, while the illumination wavelength

remained unchanged. The illuminating wavelength used was fixed at $\lambda = 0.5145$ μm and the angle of incidence was changed by using two different prisms with different apex angles for dividing and deflecting the beam: prism 1 provided an angle of incidence of $\theta = 20°$, and prism 2 provided an angle of incidence of $\theta = 0.7°$.

After illumination, the films were developed by CF_4 plasma to produce surface relief gratings. The uniformity and the spacing of the surface relief gratings produced were assessed using a scanning electron microscope. The grating period was also determined by measuring the angles of diffraction of á low intensity He-Ne laser beam. The diffraction efficiency of the prepared holographic gratings was measured in reflection mode. For these measurements the surface relief grating was covered with a thin ($\sim$ 0.2 μm) aluminium film in order to increase the reflectance of the sample. The diffracted angles and the diffracted intensities of a He-Ne laser beam were measured with respect to the incident beam.

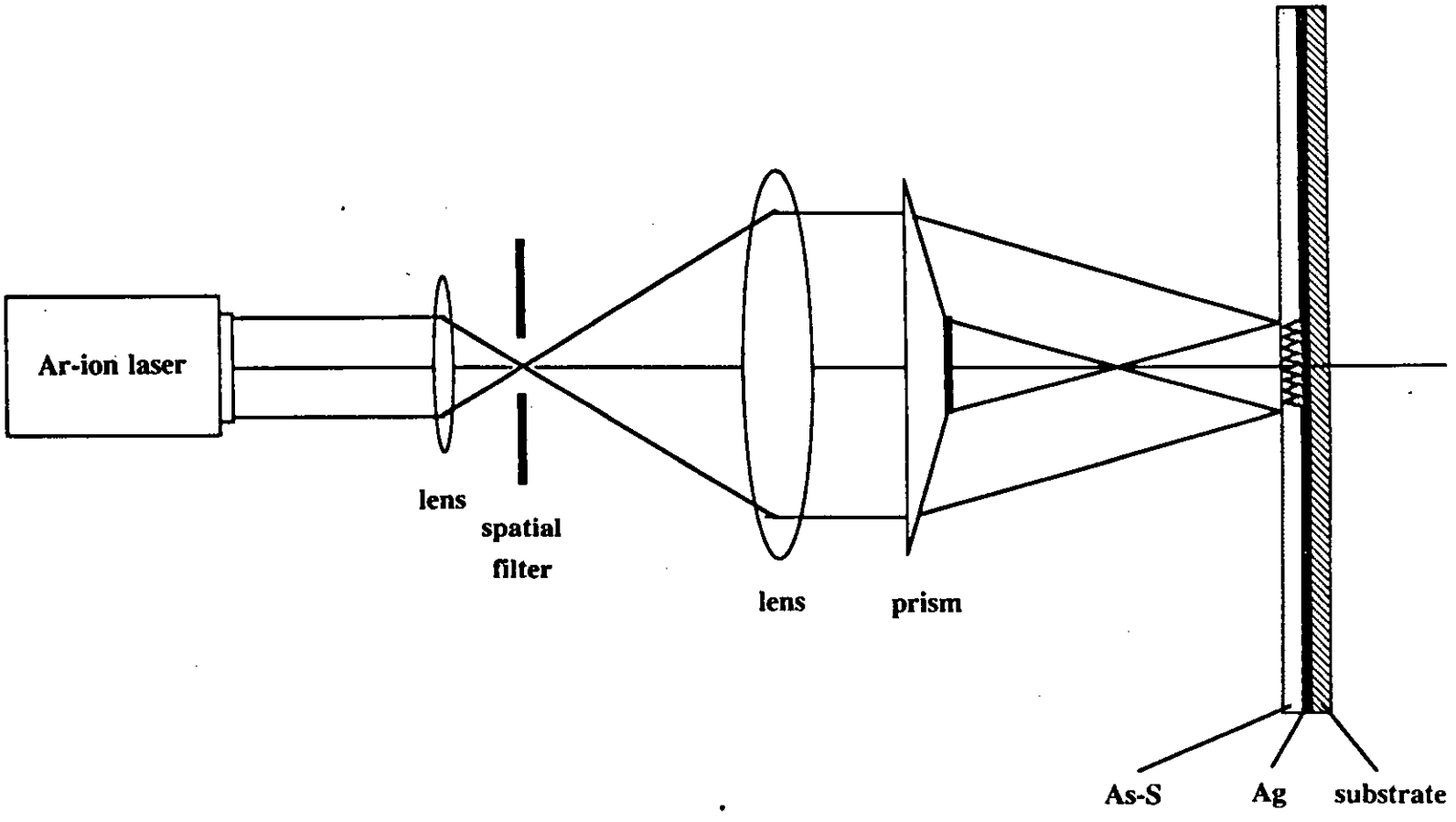

Figure 3.8 Illumination arrangement for diffraction grating production.

3.8 REFERENCES

[1] R. Swanepoel, J. Phys. E. Sci. Instrum. 1983, 16, 1214.

[2] H. Ticha, L. Tichy and M. Frumar Phys. Stat. Sol. 1979, (a) 54, K163.

[3] F. G. Smith and J. H. Thomson "Optics" Edited by F. Mandl, 1988, John Wiley & Sons Ltd. Chicester p. 205.

[4] A. V. Kolobov, B. T. Kolomiets, V. M. Lyubin and M. A. Tagirdzhanov Solid Stata Comm. 1985, Vol. 54, No. 5, pp. 379-382.

[5] B. Singh, S. P. Beaumont, P. G. Bower and C. D. W. Wilkinson, Appl. Phys. Lett. 1982, 41(9), pp. 889-891.

[6] K. Kase, G. C. Chern and I. Lauks, Thin Solid Films, 1984, 116 L53-L54.

[7] T. Fukaya, S. Matsumura, J. Tsujiuchi, E. Inoue and H. Kokado, Optics Commun. 1973 Vol. 7, No. 2, pp. 98-102.

[8] M. C. Hutley "Diffraction Gratings" 1982, Edited by N. H. March, Academic Press, London.

CHAPTER 4

COMPOSITION AND STRUCTURE OF SPIN-COATED As-S FILMS

4.1 COMPOSITIONAL ANALYSIS OF SPIN-COATED As-S FILMS AND BULK SOURCES

The compositions of the As–S films deposited by the spin-coating technique and the compositions of the bulk materials used as solutes were determined by wavelength dispersive X-ray microprobe analysis. Table 4.1 summarises the results of the analysis in atomic %. It can be seen that the compositions of the spin-coated films closely follow the compositions of the corresponding bulk glasses. In most cases the difference between the composition of the spin-coated film and that of the source bulk material was found to be ~1 atomic % (the estimated precision of the measurement was also 1 atomic %). The largest deviation was found at the composition of $As_{25}S_{75}$, which was the most sulphur rich composition examined. In this case a difference of ~4 atomic % was measured. It was found that the annealed spin-coated film of nominal composition $As_{25}S_{75}$ becomes more arsenic rich which can be explained by some sulphur loss occurring during the annealing step of the preparation process.

Nominal composition of bulk glasses (at.%)	Actual composition of bulk glasses (at.%)	Actual composition of annealed spun films (at.%)
$As_{40}S_{60}$	$As_{39.4}S_{60.6}$	$As_{38.2}S_{61.8}$
$As_{35}S_{65}$	$As_{34.3}S_{65.7}$	$As_{33.2}S_{66.8}$
$As_{30}S_{70}$	$As_{29.5}S_{70.5}$	$As_{29.4}S_{70.6}$
$As_{25}S_{75}$	$As_{23.9}S_{76.1}$	$As_{27.9}S_{72.1}$

Table 4.1 Compositions of bulk and spin-coated As–S materials.

4.2 COMPOSITIONAL AND STRUCTURAL ANALYSIS OF SPIN-COATED As-S FILMS USING INFRARED SPECTROSCOPY

4.2.1 The effect of thermal treatment on the composition of spin-coated As-S films (as determined from their middle- to far-infrared transmittance spectra)

In order to assess the amount of solvent trapped in the spin-coated As–S films and also to establish the optimum annealing temperature and duration of the annealing, transmittance spectra of the differently treated spin-coated As–S films of various compositions have been recorded in the 4000-600 cm^{-1} spectral range. Comparison of the absorption bands of the spectra also provides information about the possible dissolution process of the bulk As–S glass in propylamine.

Figure 4.1 shows the recorded transmittance spectra of propylamine, a sulphur film deposited from its solution of propylamine, an unannealed spin-coated $As_{40}S_{60}$ film, and a vacuum-evaporated $As_{40}S_{60}$ film over the 4000-600 cm^{-1} spectral range. The spectrum of the vacuum-evaporated $As_{40}S_{60}$ film does not have any characteristic absorption band in the above mentioned wavelength region, while the spectrum of the freshly deposited unannealed spin-coated $As_{40}S_{60}$ film has an extensive series of absorption bands. These are found at the characteristic vibration frequencies of the propylamine molecule, indicating that the freshly deposited spin-coated $As_{40}S_{60}$ film contains a substantial amount of solvent.

Table 4.2 summarises the positions and assignments of the absorption bands present in the middle- to far-infrared absorption spectra of Figure 4.1. The 2960, 2920 and 2870 cm^{-1} bands and the 1465 and 1390 cm^{-1} bands are characteristic of the aliphatic C-H stretch and bend respectively [1]; they are observed unchanged in both the spectrum recorded from the solvent and also from the spin-coated As-S film, indicating that the aliphatic C-H chain is not taking part in the dissolving process.

On the other hand the 3365 cm^{-1} and 3290 cm^{-1} absorption peaks and also the 900-800 cm^{-1} absorption band characteristic of $-NH_2$ stretch and out-of-plane vibrations respectively [1] are present only in the spectrum recorded from the solvent.

However, a broad absorption band can be observed in the spectra of the spin-coated sulphur and spin-coated $As_{40}S_{60}$ films at 3200-2200 cm^{-1}, which is characteristic of the $-NH_3$ unit of an amine salt. This broad band is absent in the spectrum of the solvent, but appears identically in the spectra of the spin-coated sulphur and chalcogenide films. These observations indicate that the solvent / chalcogenide interaction occurs at the sulphur sites in the amorphous network. This is the first experimental proof supporting the hypothesis that during the dissolution of the bulk As-S material the amine group of the solvent molecules bonds to the S atoms of the chalcogenide network and an amine salt is formed [2]. This assumption is further supported by the observation that the solubility of the As–S bulk material in propylamine increases with the increasing sulphur content of the chalcogenide.

The spin coated As-S films were subjected to different temperature treatments in order to investigate the removal of the solvent trapped in the chalcogenide films during deposition. The middle- to far-infrared transmittance spectra of spin-coated $As_{40}S_{60}$ films annealed at 100° C and 160° C can be seen in Figure 4.2 where they are compared with that of the unannealed spin-coated $As_{40}S_{60}$ film. The spectrum of the as-deposited $As_{40}S_{60}$ film features the absorption bands characteristic of the molecular vibrations of the solvent, whereas the spectrum of the spin-coated $As_{40}S_{60}$ film annealed at 100° C for one hour contains the same absorption bands but reduced in magnitude. This observation indicates that there is no new chemical reaction taking place during annealing, only evaporation of the solvent from the As–S film occurs. Annealing the films at 160° C for 1 hour in a vacuum oven removes most of the remaining solvent from the spin-coated films.

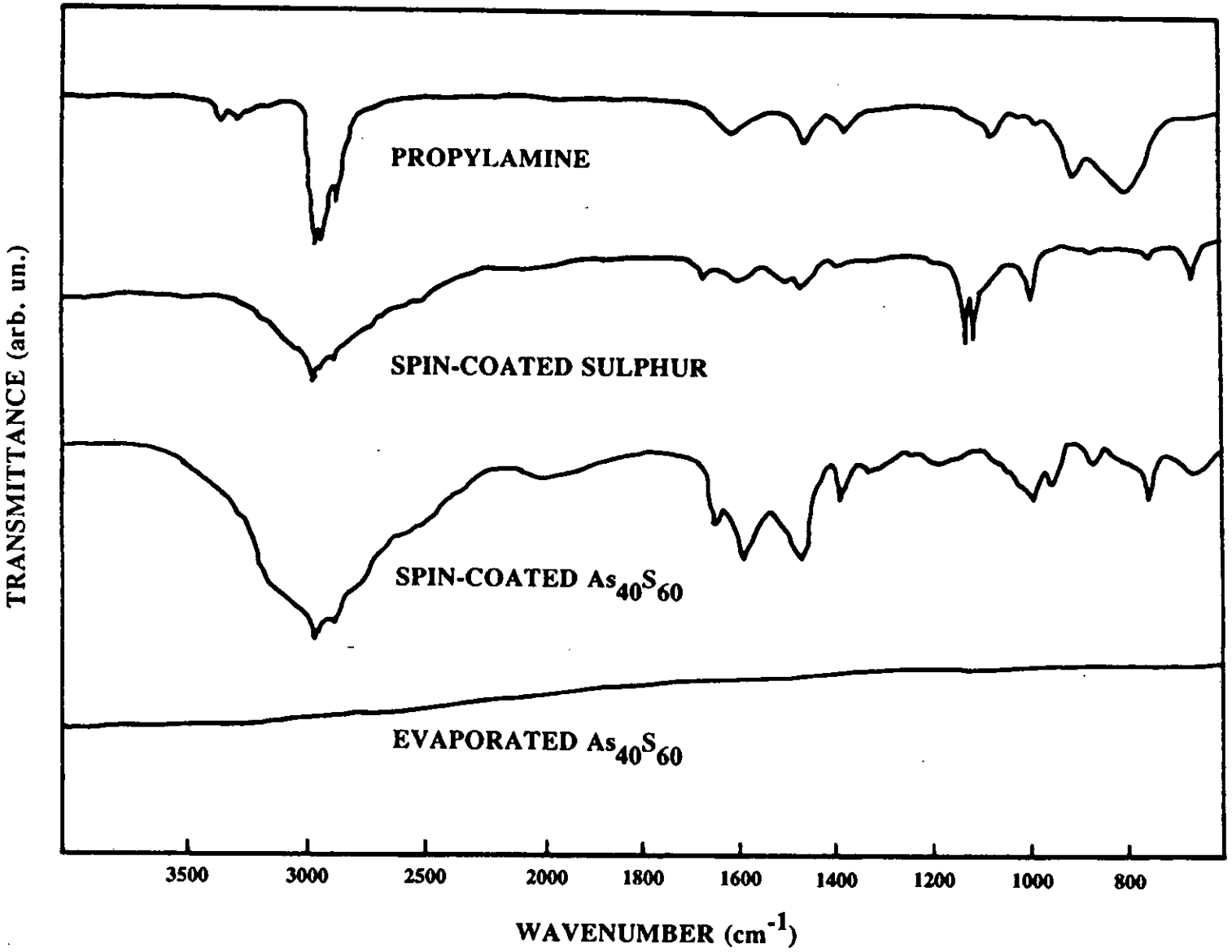

Figure 4.1 Middle- to far-infrared transmittance spectra of n-propylamine, spin-coated sulphur, spin-coated $As_{40}S_{60}$ and vacuum-evaporated $As_{40}S_{60}$.

Wavenumber (cm^{-1})	Assignment	Comment
3365 3290	NH_2 symmetric-asymmetric stretch (Doublet)	Observed in solvent, absent in spin-deposited sulphur and chalcogenide films.
900 800	NH_2 out of plane vibrations	Observed in solvent, absent in spin-deposited sulphur and chalcogenide films.
2960 2920 2870	Aliphatic C-H stretch	Observed in both solvent and spin-deposited films.
1465 1390	C-H scissor bend	Observed in both solvent and spin-deposited films.
1575	N-H scissor bend	Observed in both solvent and spin-deposited films, peak frequency is slightly different for solvent (1608 cm^{-1})
2200-3200	Broad absorption band characteristic of amine salts	Absent in solvent, present in spin-deposited films.
750	H-S stretch and wag	Absent in solvent, present in spin-deposited films.

Table 4.2 Positions and assignments of the absorption bands present in the spectra of Figure 4.1.

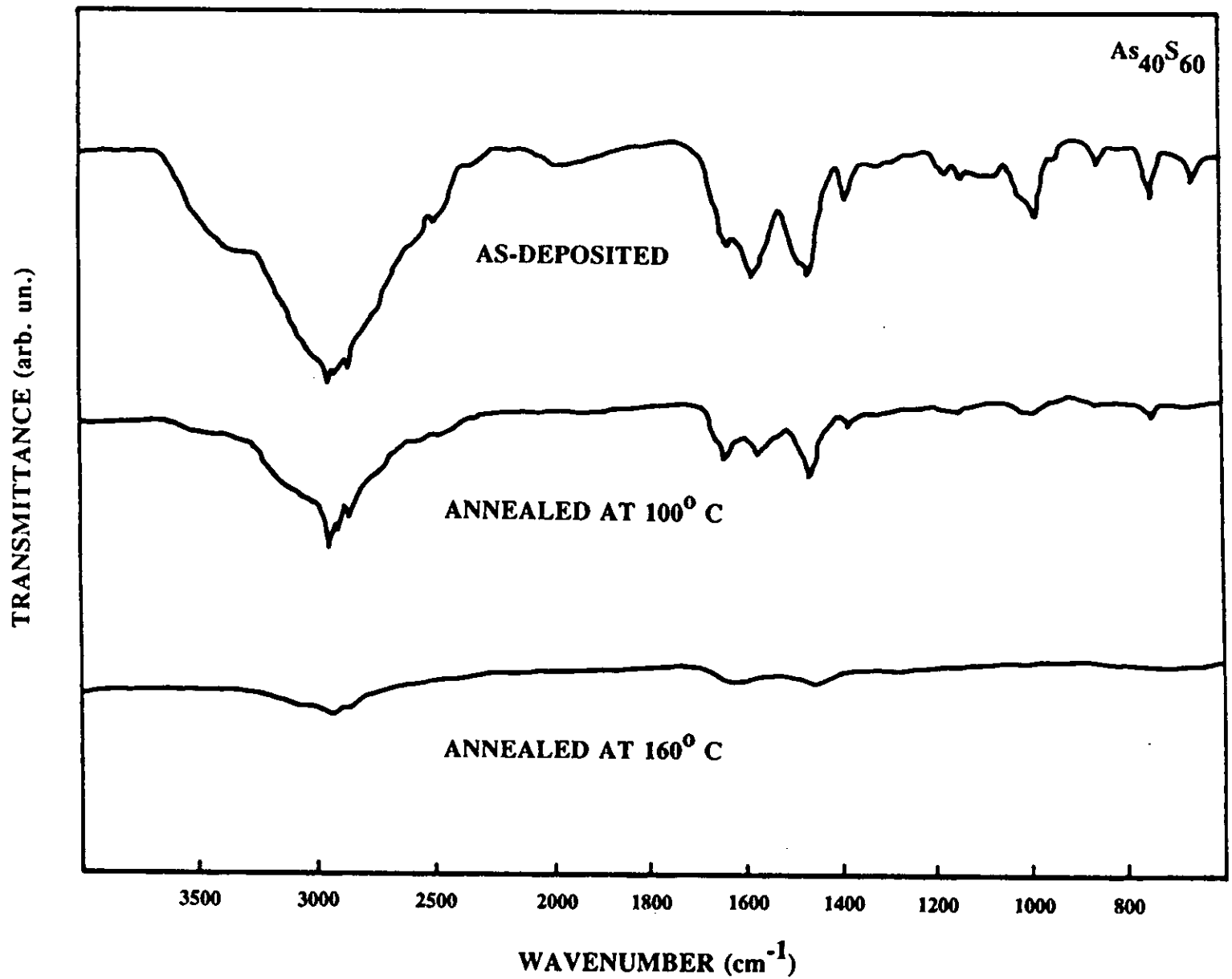

Figure 4.2 Transmittance spectra of as-deposited and annealed spin-coated $As_{40}S_{60}$ films.

4.2.2 The effect of annealing, illumination and silver photodissolution on the structure of spin-coated As-S films (as determined from their extreme far-infrared absorption spectra)

The absorption spectra of spin-coated As–S films of different compositions have been recorded in the 600-200 cm^{-1} spectral range in order to compare the composition and structure of these films with that of the bulk glasses and vacuum evaporated films.

The characteristic molecular vibration of bulk and vacuum-deposited amorphous $As_{40}S_{60}$ glasses in the extreme far-infrared region is found at a frequency of 310 cm^{-1}. It was assigned by Lucovsky [3] to one of the optical vibration modes of the AsS_3 "molecular" unit present in the structure of these glasses. A model was constructed for the structure of bulk and vacuum-evaporated $As_{40}S_{60}$ glasses based on infrared absorption and Raman scattering experiments carried out on these samples. According to this model the main structural unit in these glasses is the AsS_3 pyramid, which has four modes of vibration, ν_1 at 344 cm^{-1}, ν_2 at 162 cm^{-1}, ν_3 at 310 cm^{-1} and ν_4 at 133 cm^{-1}. All optic modes contribute to the infrared absorption spectra, but the ν_3 bond-stretching mode is dominant. According to the model, the continuous glass network of these materials is built up from the AsS_3 units by linking them together through their two-fold coordinated S atoms.

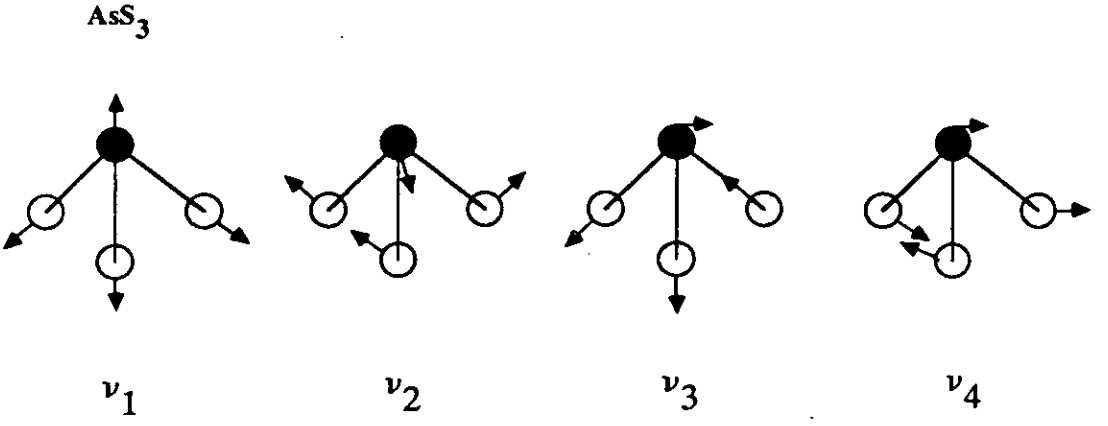

Figure 4.3 Optical vibration modes of AsS_3 pyramid [3].

Figure 4.4 shows the the transmittance spectra of unannealed spin-coated films of composition $As_{25}S_{75}$, $As_{30}S_{70}$ and $As_{40}S_{60}$ recorded in the 600-200 cm^{-1} spectral range. The spectrum of the spin-coated sulphur film deposited from its solution with n-propylamine is also presented. A strong absorption peak appears at 310 cm^{-1} for all As–S compositions, indicating that the structure of the spin-coated As–S films is also dominated by the AsS_3 units. However, for the unannealed spin-coated As–S films, another absorption band occurs at ~420 cm^{-1} which was not observed for vacuum-evaporated As–S films. The presence of this band in the absorption spectra of spin-coated As-S films was reported earlier, but no assignment was given to it [4]. It can be seen in Figure 4.4 that the intensities of the 310 cm^{-1} and 420 cm^{-1} absorption peaks change asymmetrically with the chalcogenide composition: the magnitude of the 420 cm^{-1} band is increasing with increasing sulphur content of the chalcogenide film, while the magnitude of the 310 cm^{-1} absorption band is increasing with increasing arsenic content.

Figure 4.5 shows how the annealing modifies the symmetry of these absorption bands. Transmittance spectra were recorded from the spin-coated $As_{25}S_{75}$ films in the as-deposited, annealed at 100° C and annealed at 160° C state. It can be seen that the absorption band at 420 cm^{-1} reduces as a result of annealing at 100° C for one hour. By annealing the spin-coated $As_{25}S_{75}$ thin films at 160° C for 1 hour an absorption spectrum can be obtained having only the major absorption band at 310 cm^{-1}, which can be associated with the ν_3 bond-stretching mode of the AsS_3 pyramidal units in the structure.

From the observation that the intensity of the 420 cm^{-1} peak depends on the sulphur content of the chalcogenide film (Figure 4.4) and from the fact that this absorption band gradually disappears as a result of annealing (Figure 4.5), and it is not present in the spectrum of the spin-coated sulphur film (Figure 4.4), it can be deduced that the absorption band peaking at 420 cm^{-1} can be assigned to a bond formed between the sulphur atoms of the AsS_3 structural units of the chalcogenide and the solvent molecules. This assignment would suggest that the continuous structure of the bulk glass is fragmented by the solvent molecules possibly at the sulphur sites of the AsS_3 structural units. The dissolution process would result in a material which contains fragments of the chalcogenide glass surrounded by propylamine molecules and linked to them via their amine group (shown in Section 4.2.1). The annealing process can remove most of the solvent from the spin-coated film (since only the absorption band at 310 cm^{-1} remains after annealing), so that the chalcogenide fragments then link

together, resulting in a continuous chalcogenide glass network. This hypothesis for the dissolution and the annealing process also explains the observed sulphur loss, which was observed as a result of annealing of the spin-coated As–S films with high sulphur content.

In another series of experiments spin-coated $As_{40}S_{60}$ films were subjected to illumination in order to investigate the light-induced changes that occur in the structure of spin-coated As–S films. The extreme far-infrared absorption spectrum of an as-deposited spin-coated $As_{40}S_{60}$ film is seen in Figure 4.6. As was described earlier, the main features of these films are the absorption band at 310 cm^{-1}, associated with the intramolecular asymmetric bond-stretching mode in the AsS_3 structural unit, and the absorption band at 420 cm^{-1}, which can be associated with the bond formed between the AsS_3 pyramidal units and the propylamine molecules. Illumination causes the appearance of extra features in the spectrum. As Figure 4.6 shows, the main absorption band at 310 cm^{-1} splits into two parts: beside the peak at 310 cm^{-1} a relatively strong peak appears at 340 cm^{-1}. Such change in the spectrum was associated with the irreversible structural changes which occur in the amorphous $As_{40}S_{60}$ film under illumination [5]. Furthermore, as a result of illumination, the solvent-related absorption band at 420 cm^{-1} decreases and new features appear at 480 cm^{-1} and 560 cm^{-1} which can be associated with the presence of H_2S_2 in the film [6].

After annealing the illuminated $As_{40}S_{60}$ film at 160° C for one hour the absorption band at 420 cm^{-1} is substantially reduced indicating the disappearance of the solvent from the film. Furthermore, the absorption bands associated with the presence of H_2S_2 units in the film disappear. As a result of annealing, the 340 cm^{-1} peak also disappears and the 310 cm^{-1} absorption band becomes dominant again.

The effect of illumination and annealing on the structure of the $As_{40}S_{60}$ film is different. Illumination induces the appearance of the 340 cm^{-1} band while annealing restores the originally dominant 310 cm^{-1} band. These structural transformations can be explained in different ways. It is possible that illumination causes an intramolecular charge redistribution by a small displacement of As and/or S atoms which can lead to infrared activity of the ν_1 vibration mode of the pyramidal unit at 340 cm^{-1} [3]. The light-enhanced infrared activity at 340 cm^{-1} in amorphous $As_{40}S_{60}$ due to intermolecular effects has also been reported previously [7]. However, the appearance of the 340 cm^{-1} absorption band can also be explained by the light-induced formation

of a new type of molecular unit in the film such as As_4S_4 [8]. The observed light-induced structural transformation is irreversible since further illumination of the annealed film does not restore the absorption band at 340 cm^{-1}.

The effect of silver photodissolution on the structure of spin-coated $As_{33}S_{67}$ has also been studied by monitoring changes in its infrared spectra recorded in the 600-200 cm^{-1} range. The far-infrared transmittance spectrum of silver-doped $As_{33}S_{67}$ is seen in Figure 4.7 along with those of the as-deposited and annealed films for comparison. The dominant feature of the spectrum of the annealed spin-coated $As_{33}S_{67}$ film is the absorption band at 310 cm^{-1} showing that the structure is dominated by the AsS_3 molecular units. The spectrum of the silver-doped $As_{33}S_{67}$ film is different from that of the undoped film: the main absorption band is shifted to higher frequencies (to 340 cm^{-1}) but no additional peaks appear in the spectrum. The change in the spectrum as a result of silver-doping is similar to what was observed in Raman scattering experiments on vacuum-evaporated $As_{30}S_{70}$ films [9]. It is also interesting that the magnitude of the observed band shift (310→340 cm^{-1}) is the same as in the case of the band splitting that occurs under the influence of light, as described above.

There are several possible explanations for the observed band shift in the spectra. One possibility is that a chemical reaction takes place which results in the formation of As_4S_4 and Ag_2S molecular units in the film. No characteristic feature has been observed in the spectrum of Ag_2S in this region although the characteristic vibration band of As_4S_4 occurs at 340 cm^{-1}, as deduced from the spectrum of the realgar crystal (As_4S_4) [8].

Another possibility is that silver atoms are incorporated into the AsS_3 molecular units by displacing one or more of the original atoms (substitutional doping), or can link the AsS_3 pyramids together. In the case of the substitutional doping of the pyramids, the symmetry of the unit would change considerably which would result in the appearance of more vibrational bands in the infrared spectrum but this was not observed in the experiments. The Raman results have been interpreted as evidence that the basic structural units in these Ag-doped films are similar to those of the crystalline compound smithite (Ag_3AsS_3) [10].

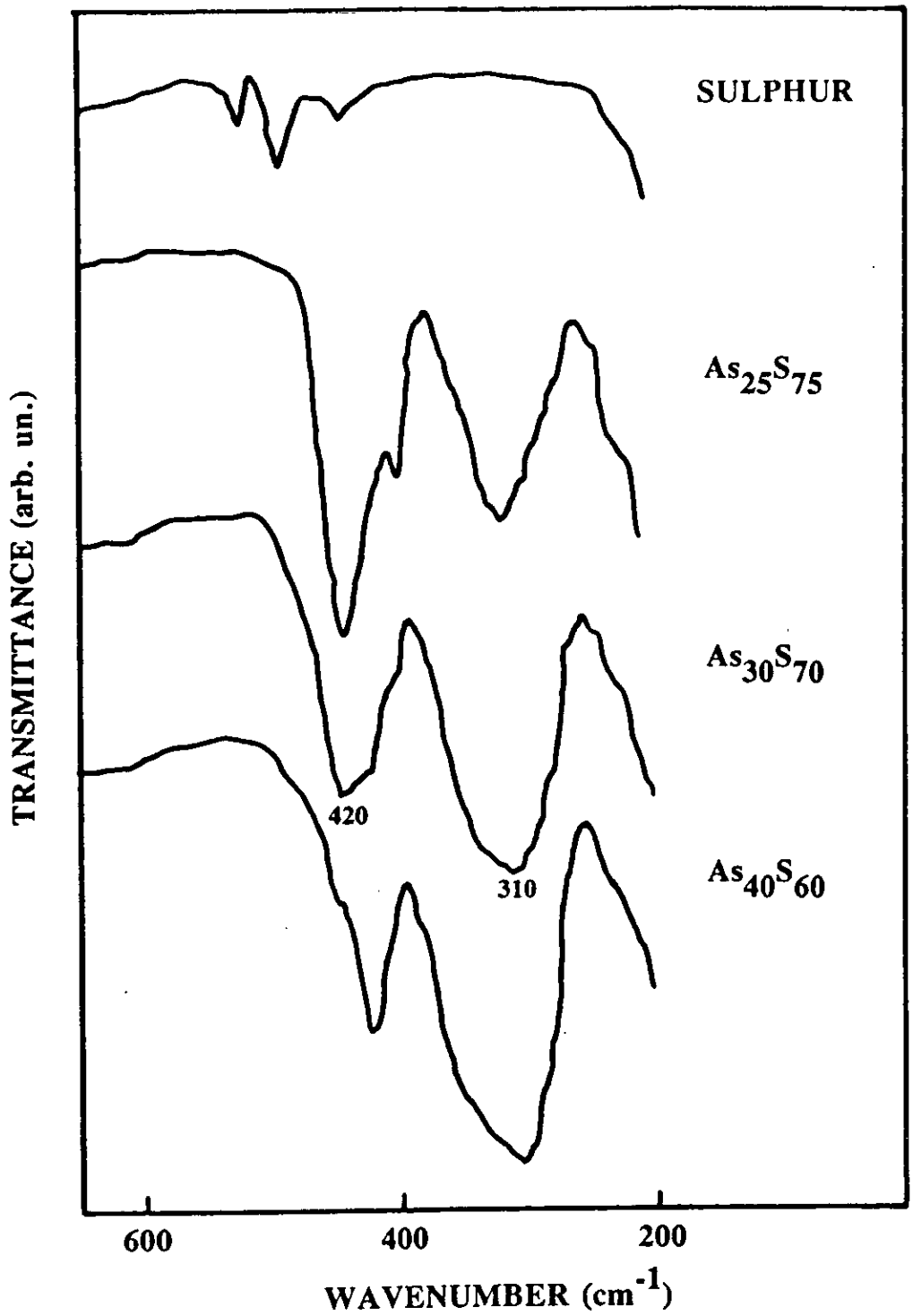

Figure 4.4 Extreme far-infrared absorption spectra of spin-coated sulphur, spin-coated $As_{25}S_{75}$, $As_{30}S_{70}$, and $As_{40}S_{60}$ films.

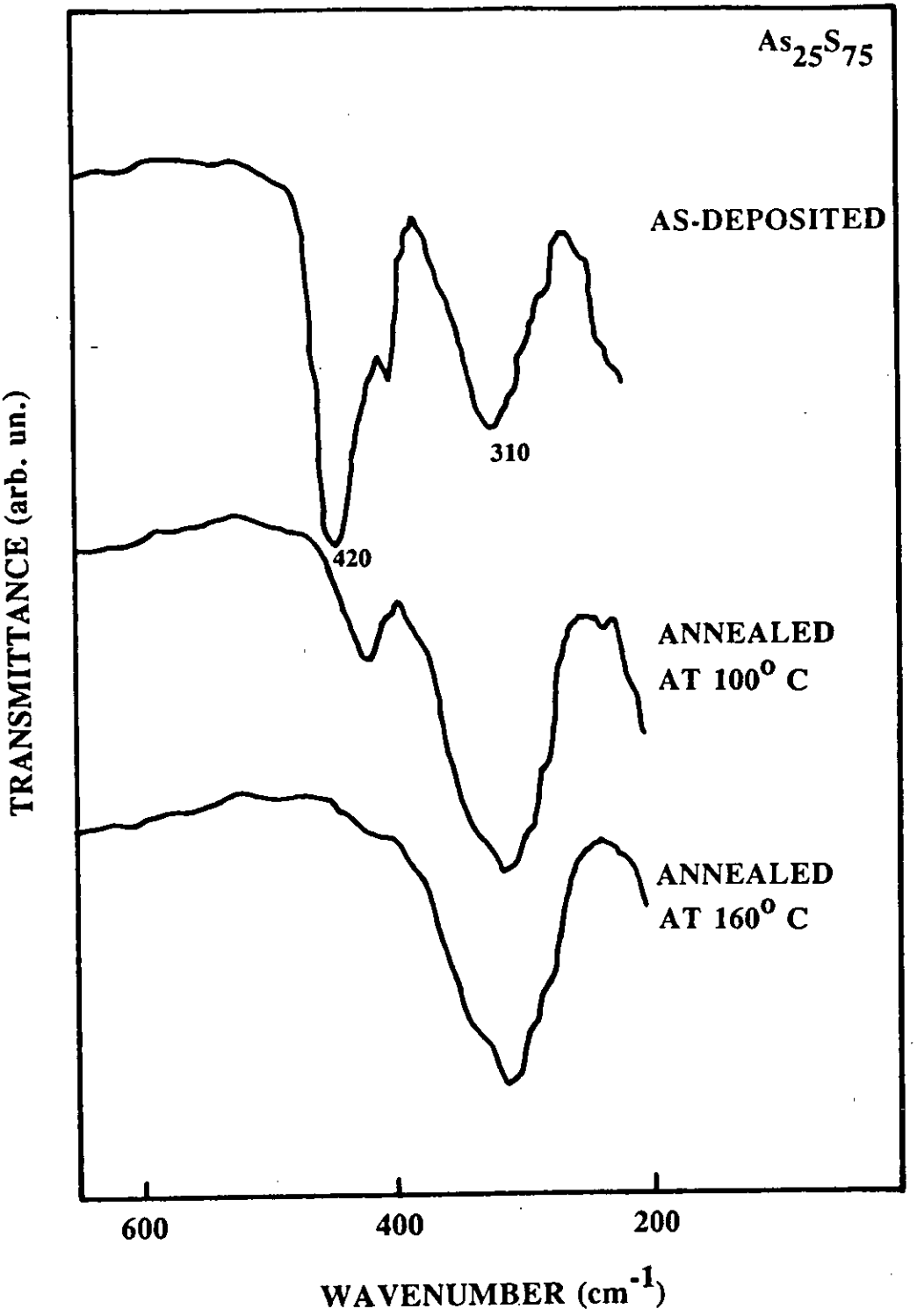

Figure 4.5 Extreme far-infrared absorption spectra of spin-coated $As_{25}S_{75}$ films annealed at 100° C and 160° C.

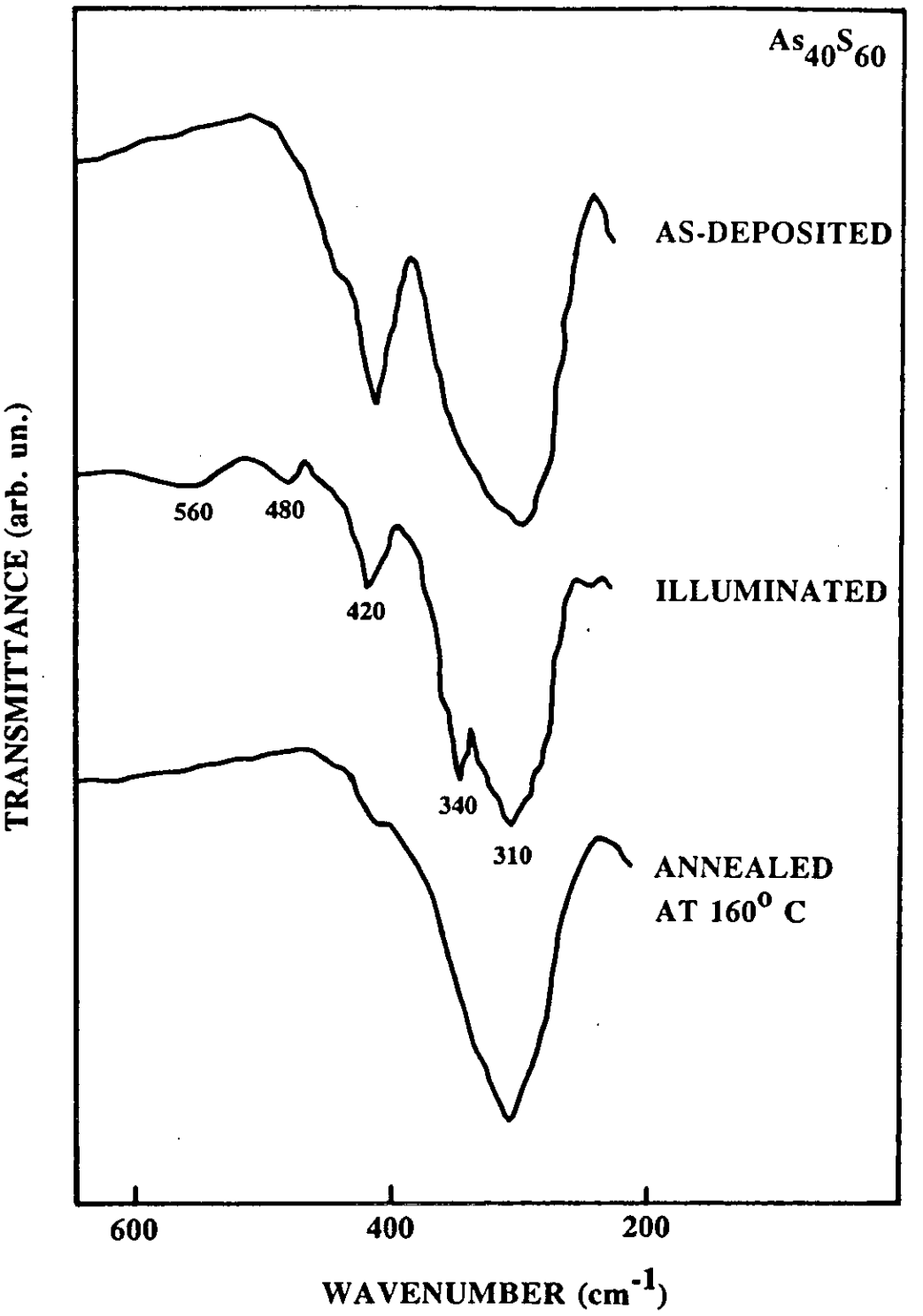

Figure 4.6 Extreme far-infrared absorption spectra of as-deposited, illuminated and annealed spin-coated $As_{40}S_{60}$ films.

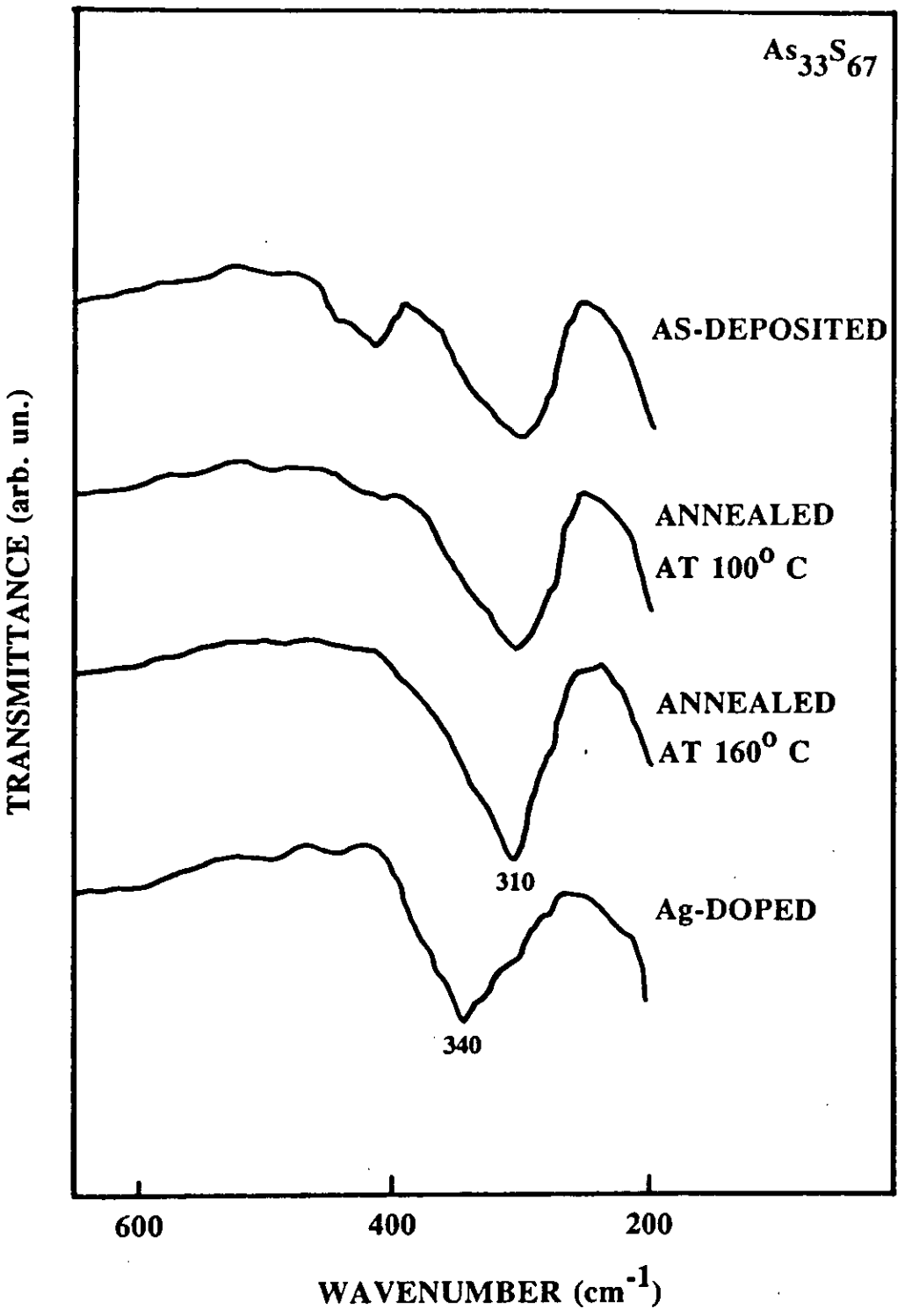

Figure 4.7 Extreme far-infrared absorption spectra of as-deposited, annealed and silver-doped spin-coated $As_{33}S_{67}$ films.

4.3 SUMMARY OF THE RESULTS OBTAINED ON THE COMPOSITION AND STRUCTURE OF SPIN-COATED As-S FILMS

Summarising the results obtained on the composition and the structure of spin-coated As–S films, it can be concluded that the compositions of the spin-coated As–S films are very similar to the compositions of their bulk sources. The deviation of the film compositions from their bulk sources was found to be only ~1 atomic %, except in the case of the composition $As_{25}S_{75}$ where a ~4 atomic % deviation was measured, possibly due to some sulphur loss occurring during annealing.

In the 4000-600 cm^{-1} wavelength region the vacuum evaporated $As_{40}S_{60}$ film is transparent, while the spin-coated $As_{40}S_{60}$ film has several solvent related absorption bands showing that the as-deposited spin-coated films contain a substantial amount of solvent. By annealing the spin-coated As–S films at 160° C for 1 hour, nearly solvent free films can be obtained.

In the extreme far-infrared region the vacuum evaporated $As_{40}S_{60}$ films show an absorption band at 310 cm^{-1} assigned to the ν_3 intramolecular bond stretching mode in the AsS_3 structural units in the glass network. Beside that, the spin-coated As–S films have another absorption band at ~420 cm^{-1}. From the experimental evidence detailed in Section 4.2.2 it can be concluded that this absorption band can be associated with the bond formed between the solvent and one or more *sulphur* atoms of the AsS_3 pyramids in the chalcogenide network. It was shown in Section 4.2.1 that the *amine group* in the propylamine molecules plays the significant role in the dissolution process. The solvent molecules would link to the AsS_3 structural units of the chalcogenide via their amine group. The absorption band at 420 cm^{-1} can be substantially reduced by annealing the spin-coated As–S films at 160° C for 1 hour, proving that the structure of the spin-coated As-S films consists mainly of AsS_3 pyramids.

Illumination of the spin-coated As–S films causes a band splitting of the main absorption band at 310 cm^{-1} resulting in the appearance of the additional absorption peak at 340 cm^{-1}, which disappears as a result of annealing. The appearance of this band was associated with the irreversible structural changes occurring in amorphous $As_{40}S_{60}$ under illumination [5].

Silver photodissolution causes a shift of the main absorption band from 310 cm^{-1} to 340 cm^{-1} in the spectra of spin-coated $As_{33}S_{67}$ films. The observed band shift was attributed to the linkage of the AsS_3 "molecular" units by silver atoms. A similar change has been observed in the Raman spectra of amorphous As_2S_3 films as a result of silver photodissolution, and it was found to be characteristic of crystalline Ag_3AsS_3 [5].

From the experiments detailed above, it can be concluded that the compositions of spin-coated As-S films are in good accordance with those of the bulk sources (except compositions far from the stoichiometric $As_{40}S_{60}$). The structure of spin-coated As-S films, similarly to that of the vacuum-evaporated As-S films, is built-up from AsS_3 "molecular" units. Illumination and also silver photodissolution cause the same changes in the structure of spin-coated As-S films as those observed in vacuum-evaporated films.

4.4 REFERENCES

[1] G. C. Chern and I. Lauks, J. Appl. Phys. 1983, 54(8), pp. 4596-4601.

[2] G. C. Chern and I. Lauks, J. Appl. Phys. 1983, 54(5), pp. 2701-2705.

[3] G. Lucovsky, Physical Review B, 1972, Vol. 6, No. 4, pp. 1480-1489

[4] G. C. Chern and I. Lauks, J. Appl. Phys. 1982, 53(10), pp. 6979-6982.

[5] P. J. S. Ewen, W. T. Taylor and G. L. Paul, 1983, J. Phys. C, 16, 6475.

[6] S. D. Ross, "Inorganic Infrared and Raman Spectra", McGraw-Hill Publ. Co. New York, 1972, p. 188.

[7] G. Lucovsky and R. M. Martin, J. Non-Cryst. Solids, 1972, 8-10, 185.

[8] U. Strom and T. P. Martin, Solid State Commun. 1979, 29, 527.

[9] A. P. Firth, P. J. S. Ewen and A. E. Owen, "The Structure of Non-Crystalline Materials" 1982, edited by P. H. Gaskell, London, p.286.

[10] A. E. Owen, A. P. Firth and P. J. S. Ewen, Phil. Mag. B, 1985, Vol. 52, No. 3, pp. 347-362.

CHAPTER 5

OPTICAL PROPERTIES OF UNDOPED AND Ag-DOPED SPIN-COATED As-S FILMS

The previous chapter described the optical response of spin-coated As-S films in the middle- to extreme-IR region. The characteristic molecular vibration of the annealed spin-coated As–S films was found to occur at 310 cm^{-1} in the extreme-far infrared region of the spectrum suggesting that the structure of these films is built up mainly from AsS_3 "molecular" species. In the middle- to far-infrared region, the annealed spin-coated As-S films were found to have similar transparency to the vacuum-evaporated As–S films.

This chapter describes the characteristic properties of spin-coated As-S films in the higher energy region of the optical spectrum. Figures 3.3 and 3.5 are transmittance and reflectance spectra of a ~0.6 μm thick spin-coated $As_{40}S_{60}$ film in the UV - Visible - Near-IR region. Similar spectra in the same wavelength region have been recorded from As-S films with different compositions and also from Ag-doped spin-coated As-S films. The optical constants (refractive index, n, and absorption coefficient, α) of the undoped and the Ag-doped As–S films were calculated from the measured transmittance and reflectance data in the λ=0.3-3 μm region using the method described in Section 3.4. The refractive index values were determined over the extended part of the spectrum (up to λ=10 μm) using the interference condition given in Equation 22 in Section 3.5.

The dispersion of the refractive index, n, of undoped and Ag-doped spin-coated As–S films is determined in the transparent region. The values of the absorption coefficient, α, for undoped and Ag-doped spin-coated As–S films near the optical absorption edge are also measured and the optical gap energy, E_g, for these films is determined.

5.1 DISPERSION OF REFRACTIVE INDEX FOR UNDOPED AND Ag-DOPED SPIN-COATED As-S FILMS

5.1.1 Refractive indices of undoped As-S films of different compositions

The compositional dependence of refractive index is shown in Figure 5.1, which plots values of n for $As_{15}S_{85}$, $As_{25}S_{75}$, $As_{30}S_{70}$, $As_{35}S_{65}$ and $As_{40}S_{60}$ spin-coated films measured at $\lambda = 1$ μm. The values of the refractive indices gradually increase towards the $As_{40}S_{60}$ stoichiometric composition. The curve is non-linear, showing that the value of the refractive index is not an additive quantity as would be the case for simple binary alloys. A similar compositional dependence of the refractive index was observed for vacuum-evaporated As–S films and the non-linearity was explained by changing short range order (valency, coordination number) with increasing arsenic content [1].

The dispersion of refractive index for $As_{30}S_{60}$, $As_{35}S_{65}$ and $As_{40}S_{60}$ spin-coated films over the $\lambda = 0.5$-10 μm spectral range is shown in Figure 5.2. All the curves are similar in shape but they are displaced to higher values of n as the As content of the films increases. The values of the refractive indices are nearly constant in the infrared region from ~2 μm to 10 μm showing that the spin-coated As–S films are transparent in this region, there is no significant absorption present, as was shown by the infrared spectra of these films (in Section 4.2.1). In the shorter wavelength part of the spectrum the values of the refractive indices begin to increase because of the influence of the increasing absorption of the film.

The dispersion of the refractive index data in the transparent part of the spectrum can be described with a single oscillator expression [2]:

$$n^2 - 1 = \frac{E_d E_o}{E_o^2 - (h\nu)^2} \qquad (1)$$

where n is the refractive index of the film, $h\nu$ is the photon energy, E_d is the dispersion energy and E_o is the oscillator energy. Equation (1) can also be written in a linearized

form as:

$$\frac{1}{n^2-1} = -\frac{1}{E_o E_d}(h\nu)^2 + \frac{E_o}{E_d} \qquad (2)$$

By plotting $(n^2-1)^{-1}$ versus $(h\nu)^2$ and fitting the data with a straight line, E_o and E_d can be obtained from the intercept (E_o/E_d) and from the slope ($-1/E_oE_d$), as seen in Figure 5.3 for spin-coated As–S films of different compositions.

The deviation from the linear behaviour at higher photon energy is a manifestation of the increase in n due to the onset of optical absorption. The refractive index values in the long wavelength region can be obtained by extrapolation up until the frequency where the lattice vibrations influence the value of n. Between these two deviations from the linear relationship, that is in the transparent part of the spectrum, E_o and E_d can be obtained with good accuracy.

The dependences of E_o and E_d on composition are summarised in Table 5.1. The observed changes are small: E_o decreases and E_d slightly increases with increasing As content towards the stoichiometric composition of $As_{40}S_{60}$. Similar dependences of E_o and E_d on composition were reported for vacuum evaporated As–S films [3]. The values of E_o obtained for spin-coated films are slightly higher than the values measured for evaporated As–S films of the same composition. On the other hand, the E_d values obtained for spin-coated As–S films are lower than those measured for the evaporated As–S films.

In order to explain the experimental observations the electronic structure of the material has to be considered. The schematic band structure of As_2S_3 is shown in Figure 5.4. The electronic band structure is obtained from a combination of the bonding characteristics of As and S and can be calculated using the tight-binding method [4]. Each As atom is covalently bonded to three S atoms in a pyramidal unit, and each S atom is shared by two As atoms. It has been found [4] that amorphous and crystalline As_2S_3 (equivalent to $As_{40}S_{60}$) have the same short range order and hence similar electronic structure. The p electron orbitals of As and S atoms are mixed in the bonding p band. However, this band is slightly lower than the lone-pair band arising from the lone-pair electron orbitals of the S atoms. It is the separation and the widths of the lone-pair and the anti-bonding bands which determines the average

energy gap, E_o, and the band gap energy, E_g. It has been demonstrated [4] that a decrease in the anti-bonding energy (also a reduction of the average band gap energy, E_o,) may be obtained if the nearest neighbour distance increases. Therefore the experimentally observed increase in E_o towards the sulphur rich compositions suggests a decrease in the "average" nearest neighbour distance which is possibly due to the increasing concentration of S–S homo-bonds in the network.

According to the model of Wemple and DiDomenico the dispersion energy, E_d, is an interband oscillator-strength parameter and it can be described by the following empirical relationship [2]:

$$E_d = N_c Z_a N_e \beta \qquad (3)$$

where N_c is the coordination number of the cation nearest neighbour to the anion, Z_a is the chemical valency of the anion, N_e is the effective number of valence electrons per anion (usually $N_e = 8$) and β is two-valued, having an "ionic" value of $\beta_i = 0.26 \pm 0.04$ eV for halides and most oxides and a "covalent" value of $\beta_c = 0.37 \pm 0.05$ eV for a range of covalently bonded structures. These observations were made for materials with crystalline structures.

The extreme far-infrared spectra of the spin-coated As–S films, presented in Section 4.2.2, showed that the main structural unit of these films is the AsS_3 pyramid, indicating that the short range order in the amorphous spin-coated films is essentially the same as in crystalline $As_{40}S_{60}$ [5]. Therefore As in the amorphous structure is threefold coordinated ($N_c = 3$), S is twofold coordinated ($Z_a = 2$), and $N_e = 8$. The decreasing E_d values with increasing sulphur content are possibly connected again with the appearance of increasing S–S homo-bonds which lower the "average" coordination. Using these values and the experimentally measured value of $E_d = 15.76$ eV (Table 5.1) for the spin-coated $As_{40}S_{60}$ film, Equation (3) yields $\beta = 0.328$, which is typical of β values found in covalent solids. Table 5.2 summarises the compositional dependence of β for spin-coated As–S films, these values being obtained from the experimental data of E_d in Table 5.1, using Equation 3. The value of β decreases with decreasing As content indicating that beside the AsS_3 "molecular" type units other, differently coordinated, structural units are formed in the amorphous network, thereby altering the overall coordination and valency when the film composition deviates from the $As_{40}S_{60}$ stoichiometric composition.

The single oscillator energy, E_o, is a measure of the average energy separation between the highest valence band and the lowest conduction band in the solid [2]. Therefore the value of E_o is significantly higher than the value of the optical band gap energy, E_g, which corresponds to the lowest direct band gap of the material. This is illustrated in Figure 5.4. Table 5.3 compares the E_o values of Table 5.1 obtained for spin-coated As–S films of different compositions with the corresponding E_g values of Figure 5.8. It can be seen from Table 5.3 that both E_o and E_g increase with increasing sulphur concentration. It can also be seen that E_o is approximately related to E_g in the case of spin-coated As–S films by:

$$E_o \sim 2.1 E_g \tag{4}$$

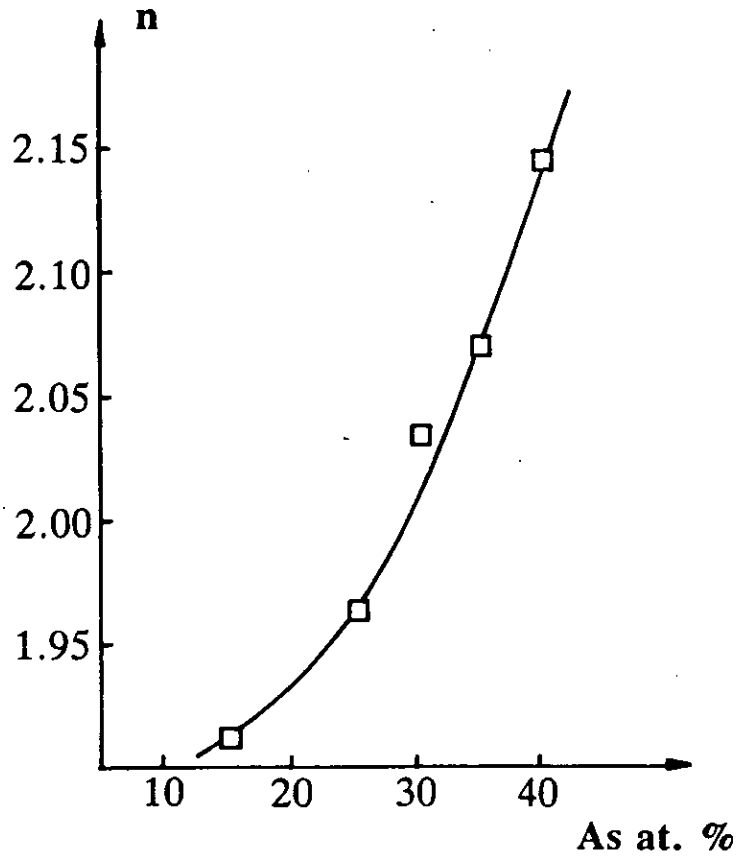

Figure 5.1 Compositional dependence of n for spin-coated As–S films measured at $\lambda = 1$ μm.

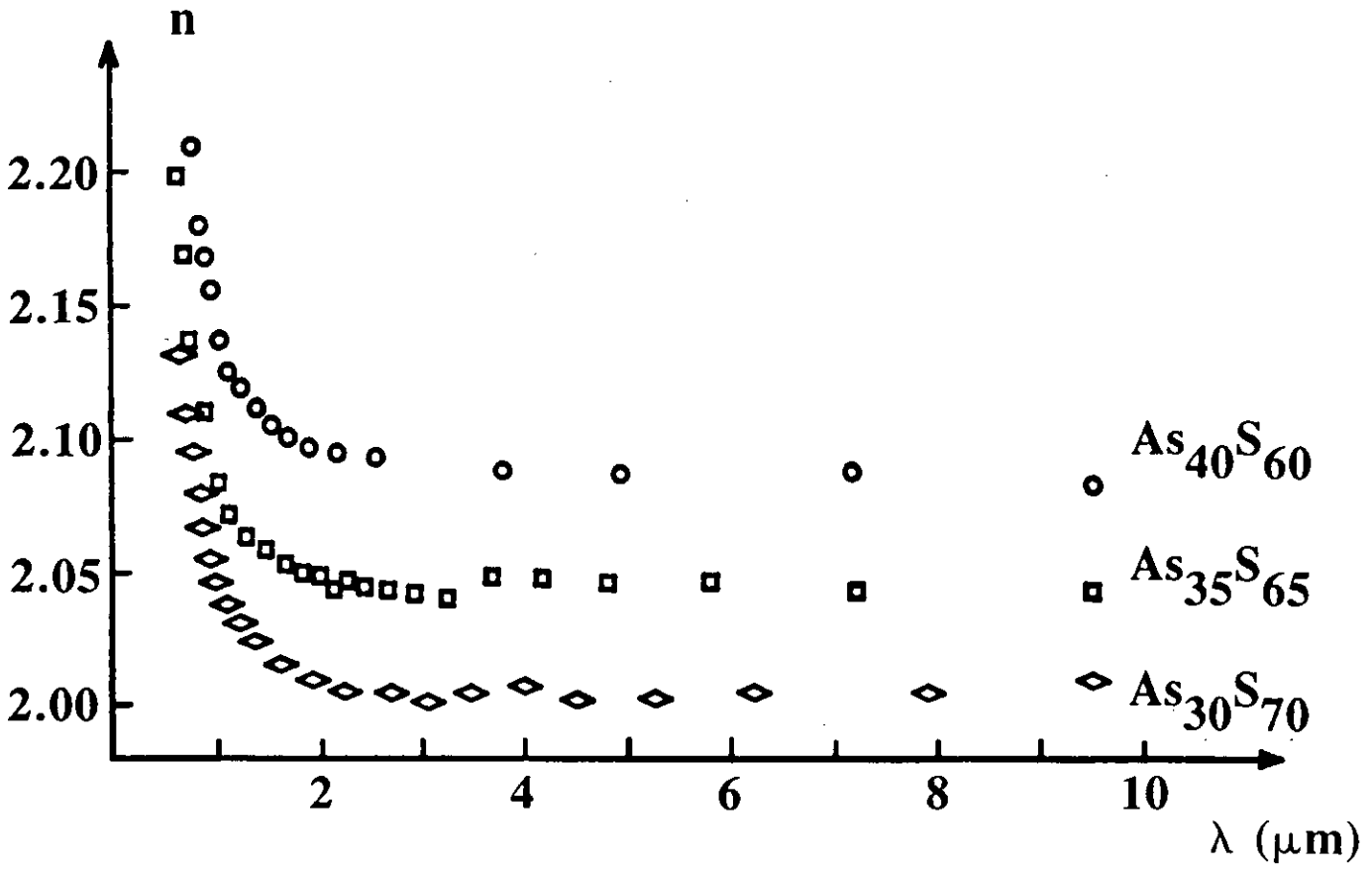

Figure 5.2 Wavelength dependence of n for spin-coated As–S films.

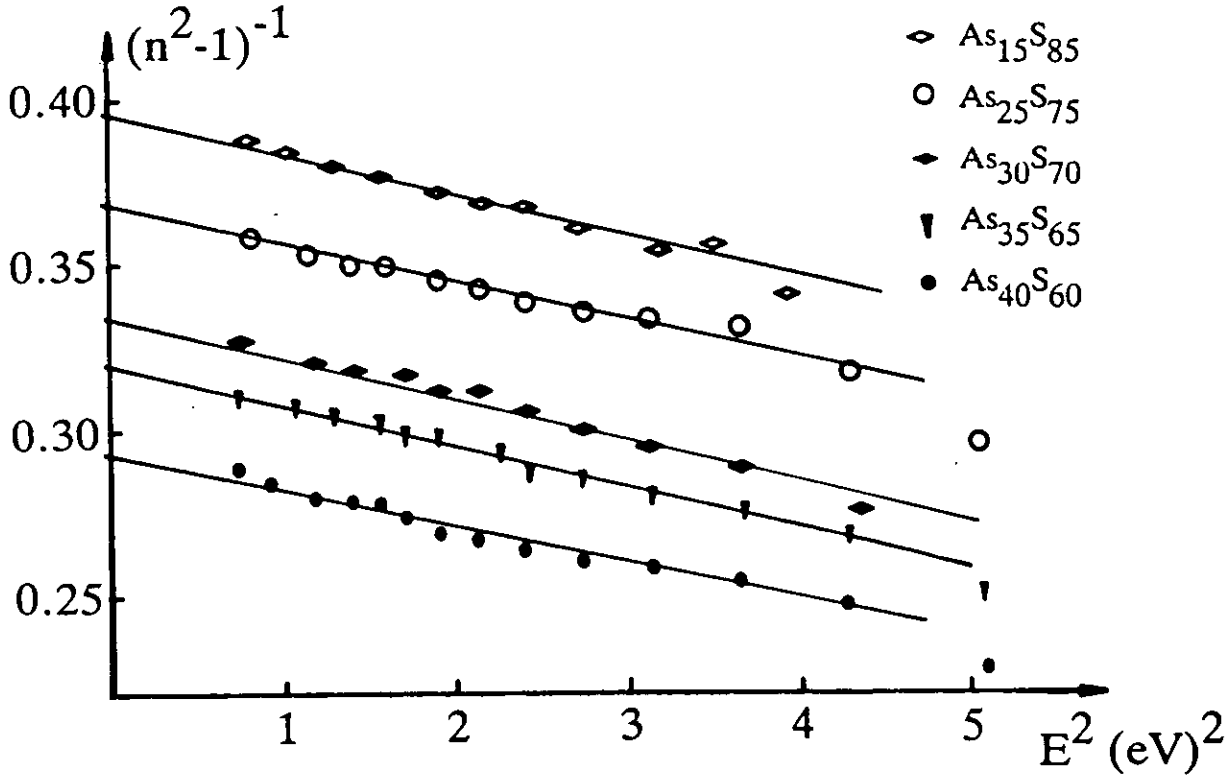

Figure 5.3 Plot of $(n^2-1)^{-1}$ vs. the square of the photon energy, E^2, for spin-coated As–S films.

Composition (at%)	E_o(eV)	E_d(eV)
$As_{40}S_{60}$	4.71	15.76
$As_{35}S_{65}$	4.88	15.23
$As_{30}S_{70}$	5.07	15.05
$As_{25}S_{75}$	5.18	14.80
$As_{15}S_{85}$	5.21	14.60

Table 5.1 E_o and E_d values for spin-coated As-S films.

Composition (at%)	β
$As_{40}S_{60}$	0.328
$As_{35}S_{65}$	0.317
$As_{30}S_{70}$	0.314
$As_{25}S_{75}$	0.308
$As_{15}S_{85}$	0.304

Table 5.2 β values for spin-coated As–S films.

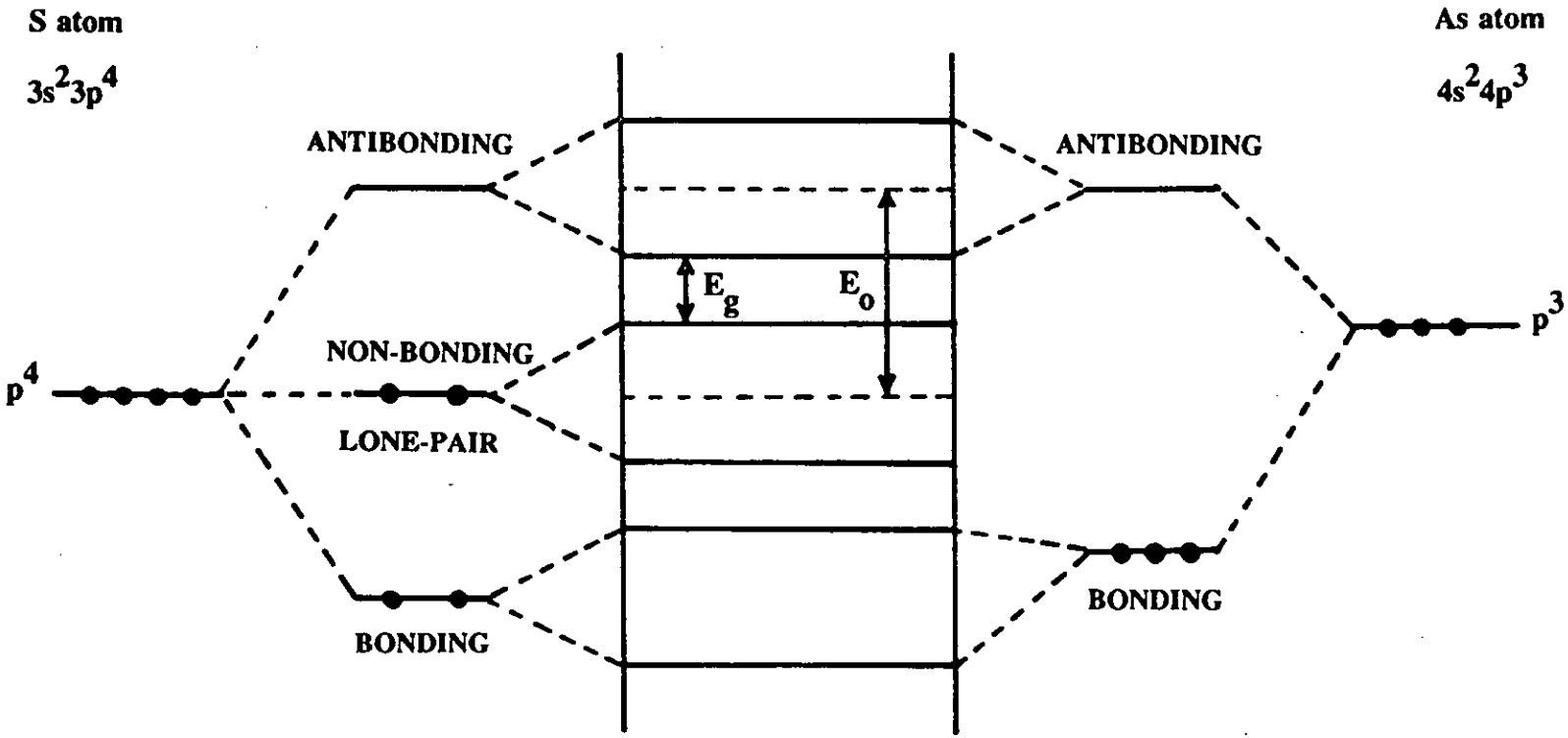

Figure 5.4 Schematic of the band structure of covalently bonded As_2S_3 solid showing the parameters E_o and E_g.

Composition(at%)	E_o(eV)	E_g(eV)	E_o/E_g
$As_{40}S_{60}$	4.71	2.35	2.00
$As_{35}S_{65}$	4.88	2.39	2.04
$As_{30}S_{70}$	5.07	2.40	2.11
$As_{25}S_{75}$	5.18	2.41	2.14
$As_{15}S_{85}$	5.21	2.43	2.14

Table 5.3 E_o and E_g data for spin-coated As−S films.

5.1.2 The effect of silver-doping on the refractive index of spin-coated As-S films

The dispersion of the refractive index was also measured for the Ag-doped spin-coated $As_{40}S_{60}$ films. The effect of silver doping on the refractive index is shown in Figure 5.5. Curve A represents the data measured for the undoped spin-coated $As_{40}S_{60}$ film and curve B shows the refractive index data of the Ag-doped $As_{40}S_{60}$ film. These results correspond to a concentration of ~22 atomic % Ag in the chalcogenide film as calculated from the initial thickness of the Ag and $As_{40}S_{60}$ films. As Figure 5.5 shows, the refractive index increases significantly (from n=2.19 to 2.74 at λ=1 μm) as a result of Ag-doping.

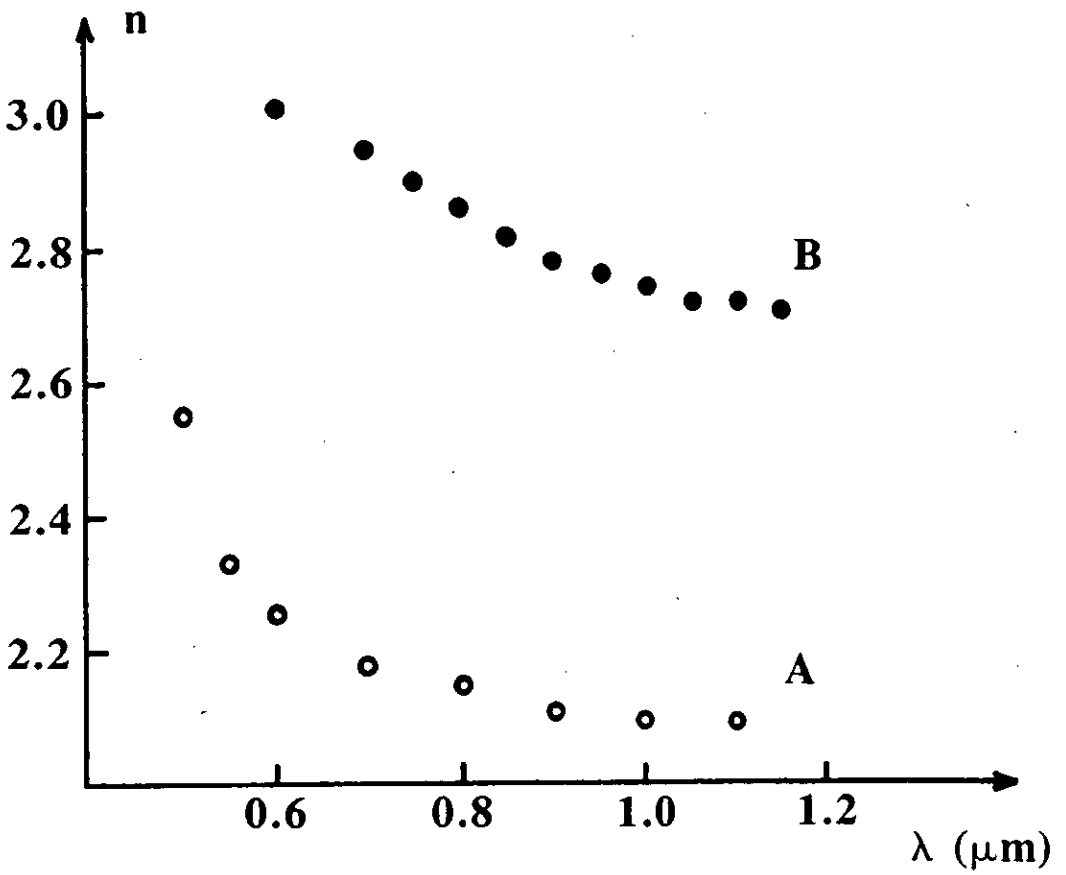

Figure 5.5 Refractive index dispersion for: (A) undoped, and (B) silver-doped spin-coated $As_{40}S_{60}$ films.

The refractive index value for Ag-doped spin-coated As-S films (n=2.74) is lower than the additive value of n=4.01, calculated from n_{Ag}=10.5 (22 at. %) and n_{As-S}=2.19 (78 at. %). This indicates that as a result of silver photodissolution a new chemical compound is formed rather than an alloy of the constituent elements.

The refractive index data of the undoped and Ag-doped $As_{40}S_{60}$ films are also plotted in the form of $(n^2-1)^{-1}$ versus the square of the photon energy (E^2) in Figure 5.6. The energy dependence of the refractive index can also be described by the single oscillator expression for the Ag-doped samples but the values of E_o and E_d are significantly different from those obtained for the undoped spin-coated films. Values of E_o=3.17 eV and E_d=17.28 eV were calculated for a Ag-doped spin-coated $As_{40}S_{60}$ film having ~22 atomic % Ag incorporated into the structure, which certainly affects the coordination number and valency in the amorphous network. Although it was suggested that the structure of Ag-As-S glasses is based on AsS_3 pyramids joined by -S-Ag-S- linkages [6], the exact coordination numbers in the structure of the reaction product are not known, but the higher E_d values obtained for Ag-doped spin-coated As-S films may suggest a β value closer to the "ionic" value.

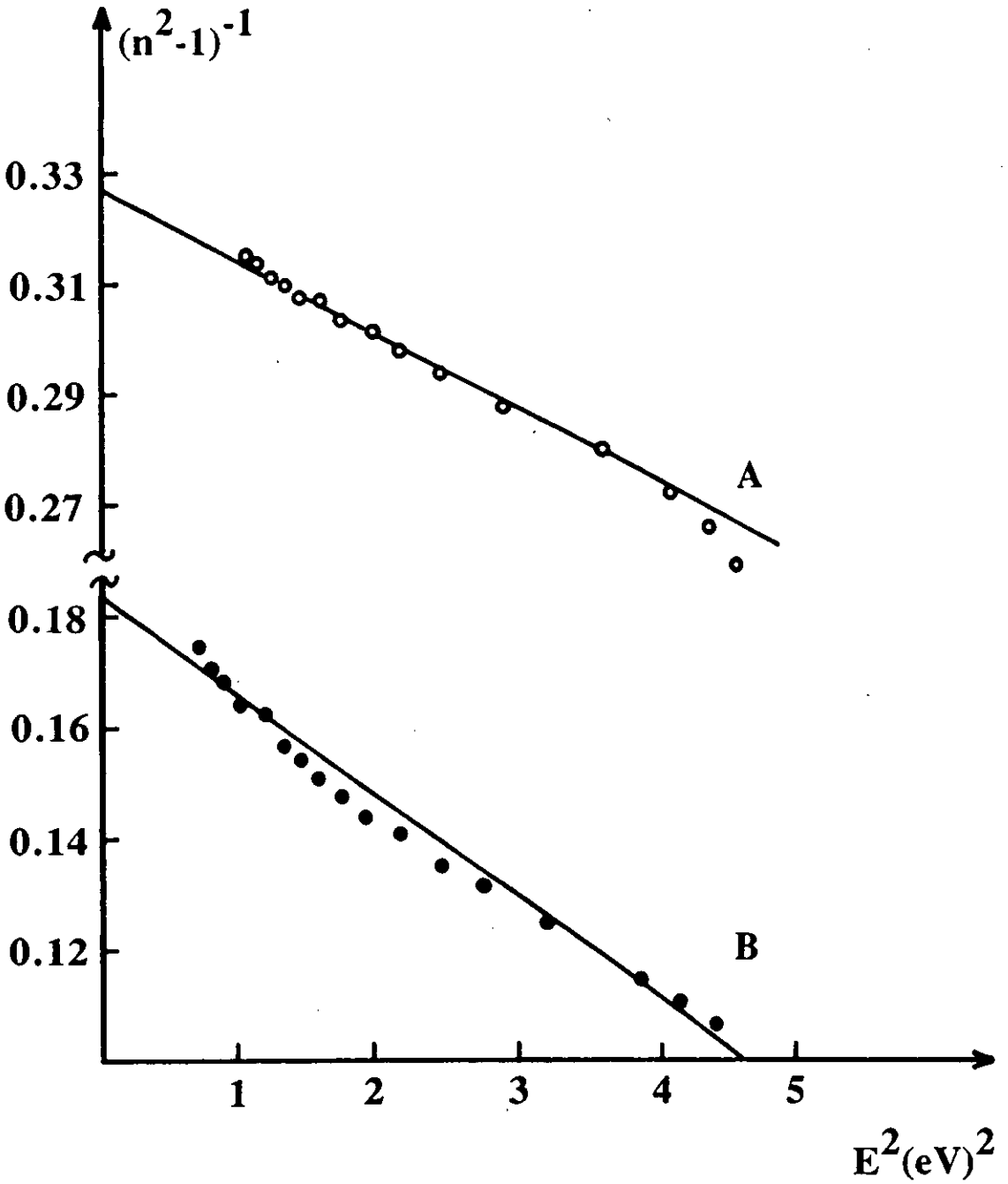

Figure 5.6 Plot of $(n^2-1)^{-1}$ vs. E^2 for: (A) undoped, and (B) Ag-doped $As_{40}S_{60}$ films.

5.2 ABSORPTION COEFFICIENT OF UNDOPED AND Ag-DOPED SPIN-COATED As-S FILMS

5.2.1 Absorption coefficient of undoped spin-coated As-S films

The absorption coefficient (α) values of amorphous $As_{40}S_{60}$ films deposited by vacuum-evaporation show a steep rise with increasing photon energy near the optical band-gap. The absorption coefficient of these films rises exponentially with increasing photon energy over the 1.5-2.7 eV region [7]:

$$\alpha = \alpha_0 \exp[B(h\nu - E_g)] \tag{5}$$

where α_0 and B are constants, $h\nu$ is the photon energy and E_g is the optical band-gap energy.

Figure 5.7 shows the optical absorption spectra of spin-coated $As_{15}S_{85}$, $As_{25}S_{75}$, $As_{30}S_{70}$, $As_{35}S_{65}$ and $As_{40}S_{60}$ films in the lower photon energy region (1-3 eV) of the absorption edge. The exponential rise of the absorption edge is restricted to a smaller region (2.4-2.6 eV) in the case of spin-coated As-S films. The slopes are less steep, ranging from 5 to 9 eV^{-1} for the compositions in the range from $As_{15}S_{85}$ to $As_{40}S_{60}$ respectively, compared to the slope of $\sim$19 eV^{-1} obtained for vacuum-evaporated $As_{40}S_{60}$ films [7]. According to theory [8], the slope of the exponential absorption edge is associated with small scale internal electric fields induced by disorder (defects) in the amorphous network. Therefore the smaller slopes in the case of spin-coated As–S films indicate a more disordered structure than in the case of vacuum-evaporated As–S films.

At lower absorption coefficient values ($\alpha \leq 10^3 cm^{-1}$) there is a broad absorption band present in the photon energy range from 1.2 to 2.3 eV. This band is not present in the absorption spectra of vacuum evaporated films and it might be associated with light scattering from inhomogeneities of the order of hundreds of angstroms in diameter [9].

At higher absorption coefficient values ($\alpha \geq 10^4$ cm^{-1}) the rise is less steep. In this region the dependence of α on the photon energy can be represented by:

$$\alpha h\nu = C(h\nu - E_g)^2 \qquad (6)$$

where C is a constant, and E_g is the value of the optical gap energy [10]. The value of E_g can be obtained by extrapolating $(\alpha h\nu)^{1/2}$ towards zero. Figure 5.8 shows plots of $(\alpha h\nu)^{1/2}$ versus photon energy for spin-coated As–S films of different compositions. Inset is a table of the optical gap energy values obtained for these compositions. The value of E_g decreases with increasing As content, being highest at the $As_{40}S_{60}$ stoichiometric composition. This compositional dependence of the band gap energy can be explained by the effect of different bond strengths. The bond strengths of the three bonds As-As, As-S and S-S are 43.4, 52.8 and 55.0 kcal mol^{-1}, respectively [12]. The short range order in amorphous $As_{40}S_{60}$ is similar to that in the crystal, containing mainly As-S bonds. By adding extra S to the stoichiometric composition the excess sulphur exists probably in chain-like form resulting in the appearance of more S-S homo-bonds in the structure. As a result, the average bond strength of the compound decreases, and hence E_g decreases [13]. The slopes of the absorption edges obtained for various As-S compositions on the other hand increases towards the stoichiometric composition indicating a narrowing of the conduction band and valence band edges and therefore representing an increasing order in the structure of the spin-coated films.

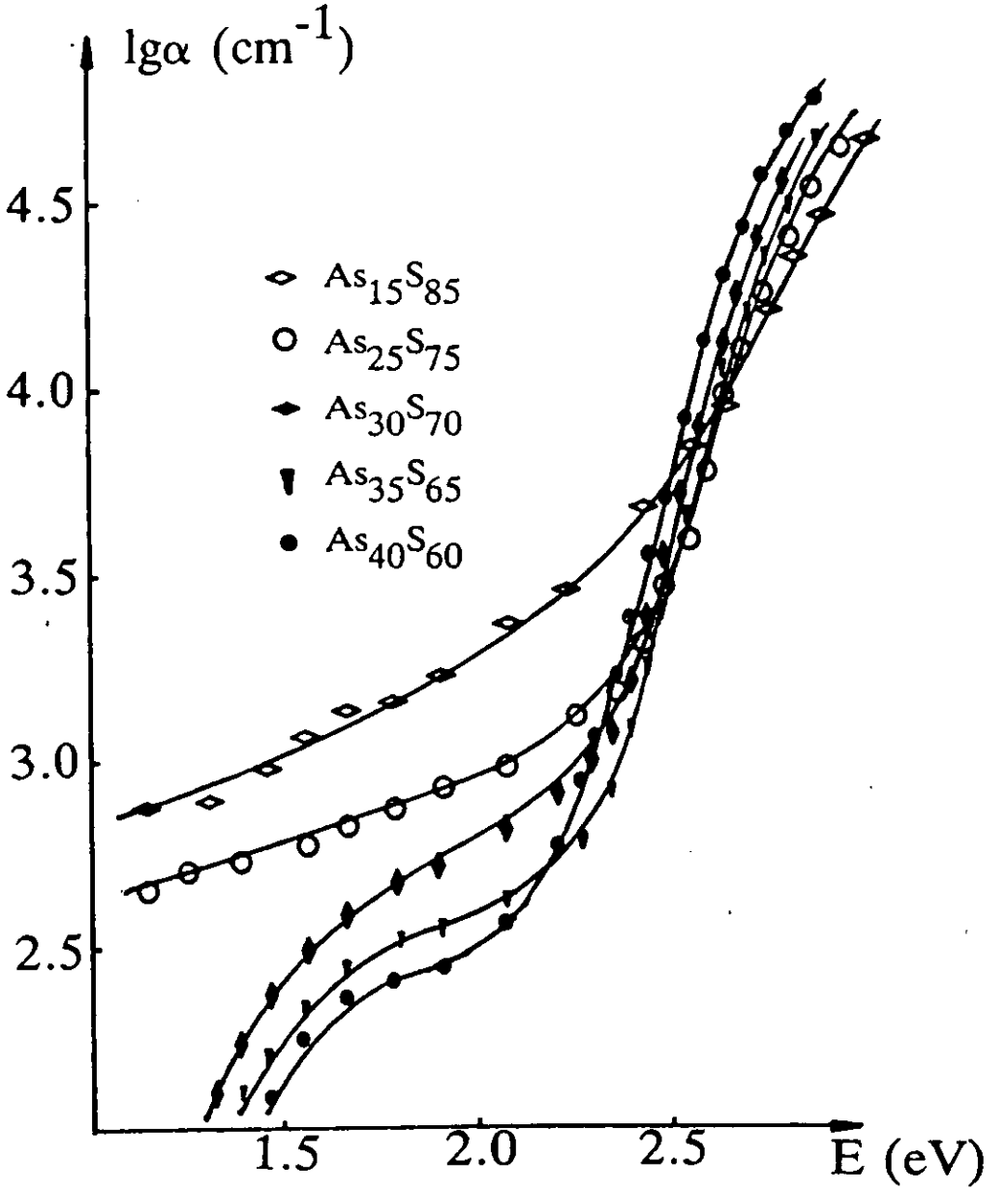

Figure 5.7 Optical absorption edge of spin-coated As-S films.

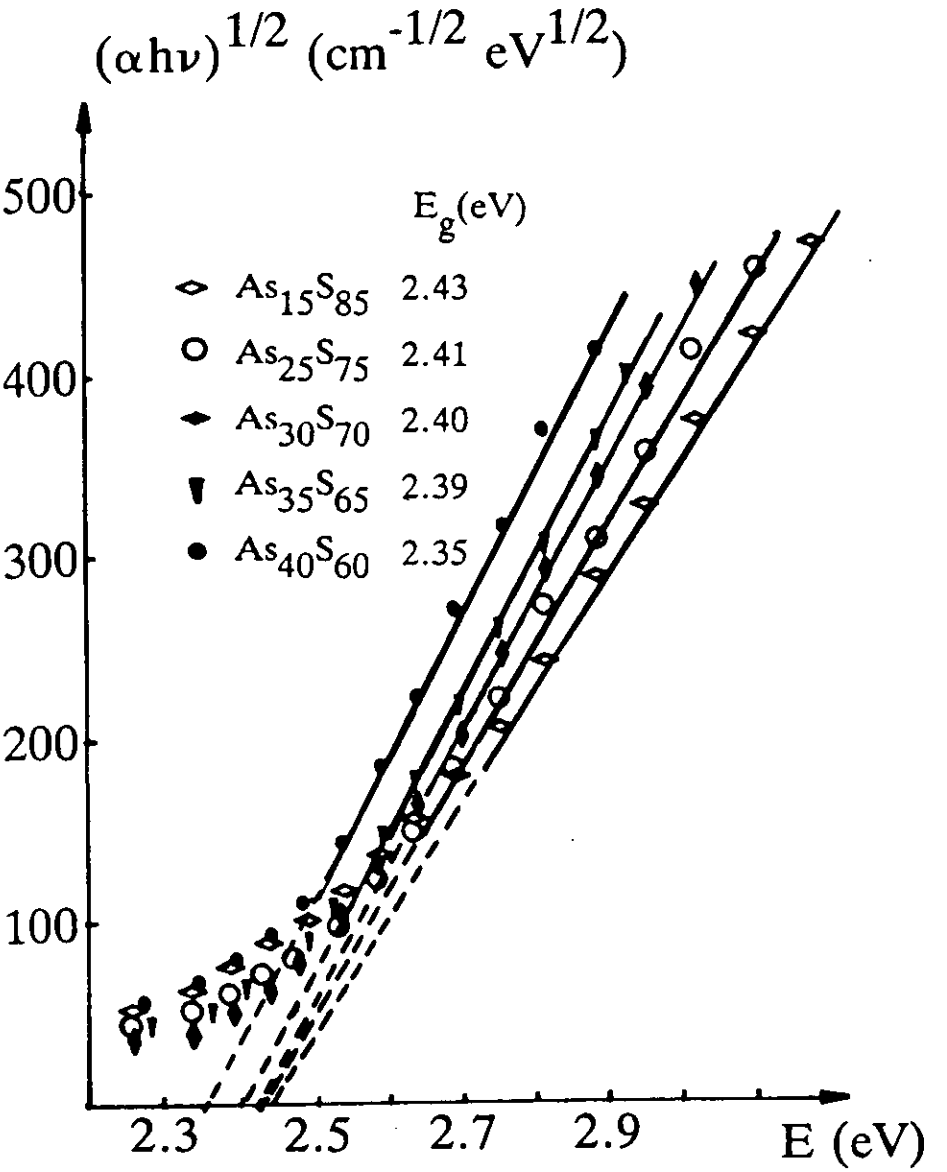

Figure 5.8 Plot of $(\alpha h\nu)^{1/2}$ vs. photon energy for spin-coated As–S films.

5.2.2 Absorption coefficient of Ag-doped spin-coated As-S films

Curve A of Figure 5.9 shows the absorption coefficient of the undoped spin-coated $As_{40}S_{60}$ film as a function of photon energy in the visible range of the optical spectrum. Curve B shows the absorption coefficient values of an Ag-doped $As_{40}S_{60}$ film (containing ~22 atomic % Ag). The optical absorption edge changes quite significantly as a result of silver incorporation into the structure of the spin-coated $As_{40}S_{60}$ film. The α value measured for the Ag-doped film is higher at any given wavelength, meaning that the optical absorption edge shifts to lower photon energies. The shift is nearly parallel at higher photon energies (i.e. at values of $E > 2.2$ eV) but the Ag-doped film retains a relatively high absorption value at lower photon energies. In the case of the silver-doped film the exponential absorption edge is shifted to higher absorption values (from $\alpha = 8x10^3$ cm^{-1} to $\alpha = 6x10^4$ cm^{-1}) as compared to the undoped film (from $\alpha = 1x10^3$ cm^{-1} to $4x10^4$ cm^{-1}).

The absorption coefficient values above the exponential rise, that is at higher photon energies, again can be described by Equation 6, and the corresponding plot is shown in Figure 5.10 for the Ag-doped spin-coated $As_{40}S_{60}$ film (curve B). The spectrum of undoped $As_{40}S_{60}$ (curve A) is also included for comparison. The value of the optical energy gap, E_g, changes from 2.35 eV to 2.19 eV as a result of Ag incorporation into the structure of the spin-coated As–S film. This could be due to the presence of Ag^+ ions, hence new bonds in the structure, which decreases the width of E_g.

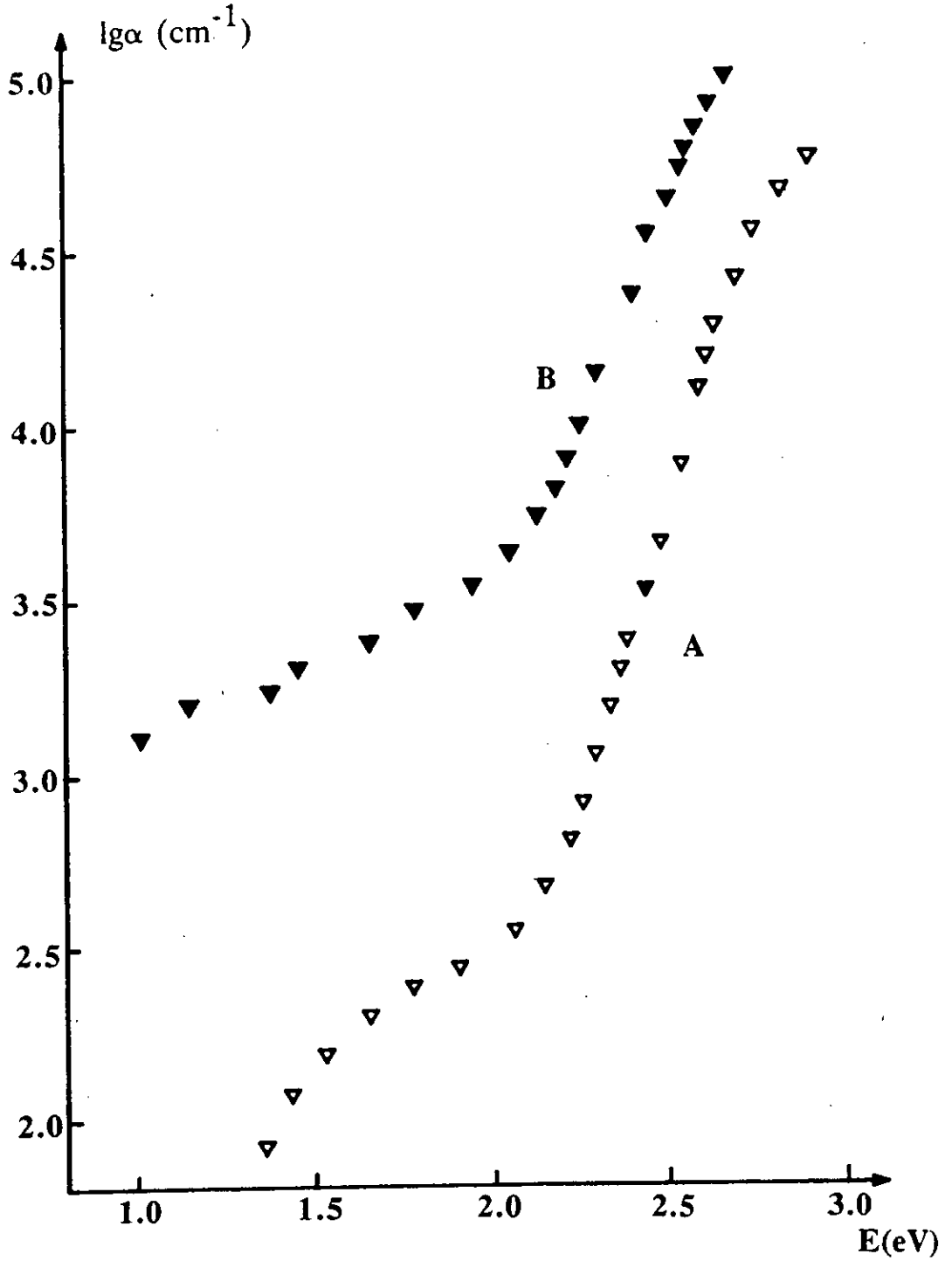

Figure 5.9 Optical absorption edge of: (A) undoped; and (B) Ag-doped spin-coated $As_{40}S_{60}$ films.

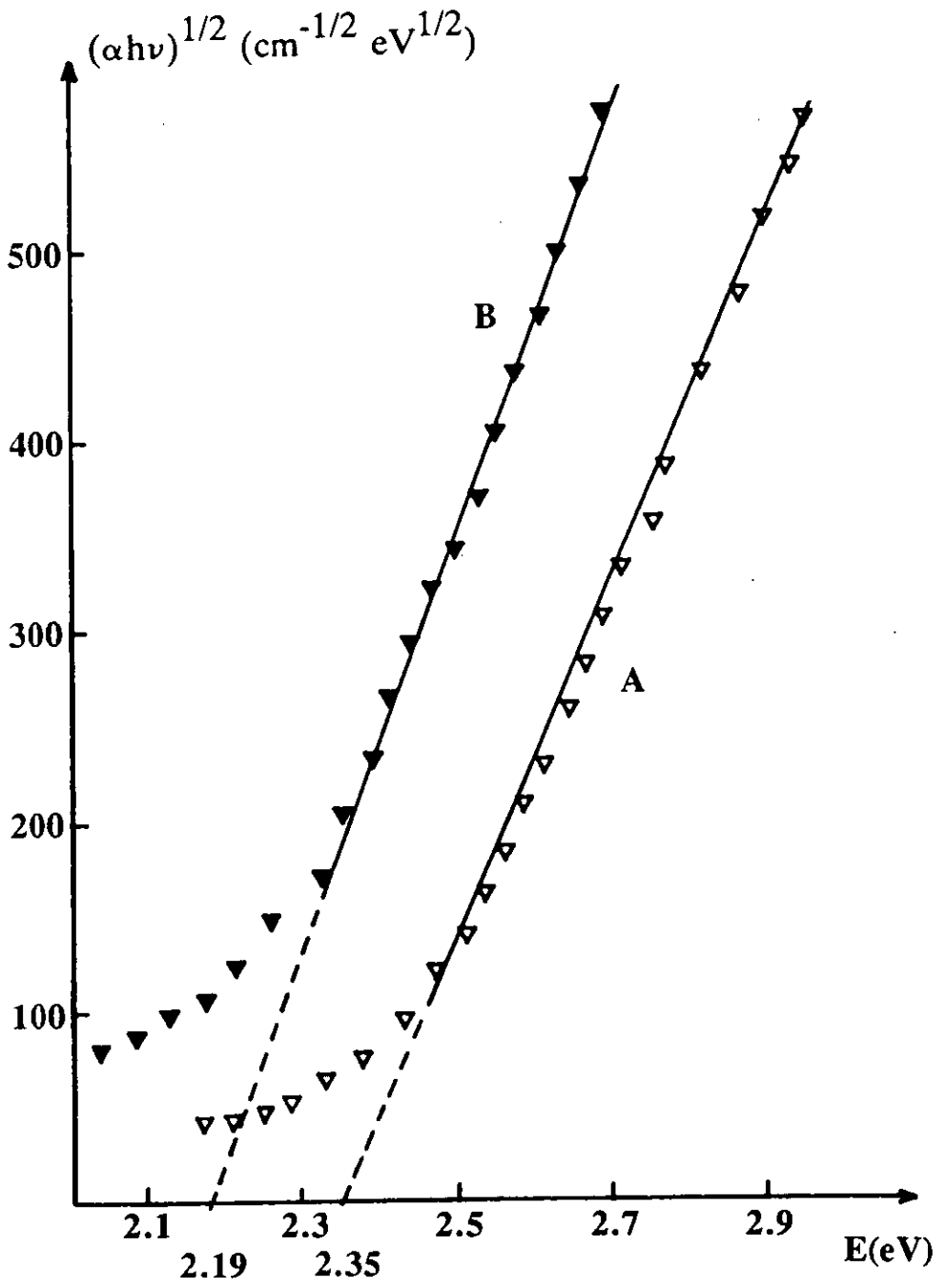

Figure 5.10 Plot of $(\alpha h\nu)^{1/2}$ vs. photon energy for: (A) undoped; and (B) Ag-doped spin-coated $As_{40}S_{60}$ films.

5.3 SUMMARY OF THE RESULTS OBTAINED ON OPTICAL PROPERTIES OF UNDOPED AND Ag-DOPED SPIN-COATED As-S FILMS

Summarising the results on the optical properties of the undoped and the Ag-doped spin-coated As–S films it can be concluded that the refractive index of spin-coated As–S films measured at $\lambda = 1$ μm gradually increases as the As content is increased towards the $As_{40}S_{60}$ stoichiometric composition. The refractive indices of spin-coated As–S films are nearly constant in the middle- to far-infrared region (measured up to 10 μm), but start to increase in the visible part of the spectrum near to the optical band gap, due to the influence of the increasing absorption of the films.

The n values obtained for different compositions of spin-coated As-S films were fitted with the single oscillator expression and E_o and E_d data were obtained. It was found that the oscillator energy, E_o, decreases and the dispersion energy, E_d, increases with increasing As content towards the $As_{40}S_{60}$ composition. It was also found that the oscillator energy values are proportional to the band gap energy values. In the case of spin-coated As-S films the E_g values are approximately half of the corresponding E_o values.

These compositional dependences can be explained by considering that E_o is determined primarily by the chemical bonding energies, but E_d is determined mainly by the valency and coordination number of the constituent atoms. At the stoichiometric composition of $As_{40}S_{60}$ the glass structure is dominated by threefold coordinated AsS_3 pyramidal units connected by twofold coordinated S atoms to form a two-dimensional network. When the S concentration increases, extra twofold coordinated S atoms are incorporated between the pyramidal units thus decreasing the average coordination number. Another reason for the decreasing coordination is that, beside the AsS_3 pyramidal units, As_4S_4 units can also be present in the structure [11] and in these units both the As and the S are twofold coordinated. The decreasing average coordination number (with larger S concentration) will result in a decreasing value of E_d as predicted by Equation 3 in Section 5.1.1.

On the other hand, the increase of the oscillator energy, E_o, and the band gap energy, E_g, with increasing S concentration can be explained by considering the effect of different bond strengths in the amorphous network. Assuming that the band gap

energy is proportional to the chemical bond strength [13] E_g increases when additional S–S bonds are incorporated into the amorphous network.

The β values calculated from the parameters E_d for the different compositions show "covalent" values for spin-coated As–S films.

The refractive index dispersion for the Ag-doped spin-coated $As_{40}S_{60}$ film is similar to that for the undoped film but is displaced to higher values (from n=2.19 for undoped $As_{40}S_{60}$ to n=2.74 for Ag-doped $As_{40}S_{60}$ films measured at $\lambda=1$ μm). The value of E_o decreased and E_d increased as a result of Ag-doping, suggesting a substantial modification of the film structure.

The absorption edge of the spin-coated As–S films rises exponentially with photon energy in the 2.4-2.6 eV region, the steepest slope being obtained for the $As_{40}S_{60}$ stoichiometric composition. In the higher energy part of the spectrum the measured absorption coefficient is proportional to E^2. The value of the optical energy gap, E_g, obtained from these plots, decreases with increasing As content, having its lowest value for the $As_{40}S_{60}$ composition. The Ag-doping shifts the optical absorption edge to lower photon energies, so that the value of E_g for the Ag-doped film decreases compared to the value obtained for the undoped $As_{40}S_{60}$ film.

5.4 REFERENCES

[1] Z. U. Borisova, "Glassy Semiconductors" Plenum Press, New York 1981, p. 136.

[2] S. H. Wemple and M. DiDomenico, Phys. Rew. B, 1971, Vol. 3, No. 4, pp. 1338-1351.

[3] K. Tanaka, Thin Solid Films, 1980, 66, 271.

[4] S. G. Bishop and N. J. Shevchik, Phys. Rev. B, 1975, 12. p. 1567.

[5] R. Zallen, "The Physics of Amorphous Solids", published by John Wiley & Sons, 1983, p. 92.

[6] Y. Kawamoto, M. Agata and S. Tsuchihashi, Journal of the Ceramics Association of Japan, 1974, 82. pp. 502-507.

[7] N. F. Mott and E. A. Davis "Electronic Processes in Non-crystalline Materials", Clarendon Press Oxford, 1971, p. 240.

[8] J. D. Dow and D. Redfield, Phys. Rev. B, 1970, 1, p. 3358.

[9] A. Vancu and R. Grigorovici, Proc. of 5th Int. Conf. on Amorphous and Liquid Semiconductors, 1971, published by Taylor and Francis London, p. 631.

[10] J. Tauc, "Optical Properties of Solids", 1970, edited by F. Abeles, North-Holland, Amsterdam.

[11] D. J. Treacy, U. Strom, P. B. Klein and P. C. Taylor, J. Non-Cryst. Solids, 1980, 35 & 36, pp. 1035-1039.

[12] R. T. Sanderson, "Chemical Bonds and Bond Energy", New York Academic Press, 1976

[13] M. Yamaguchi, Phil.Mag. B, 1985, Vol.51, No.6, p.651.

CHAPTER 6

KINETICS OF SILVER PHOTODISSOLUTION IN SPIN-COATED As-S FILMS

The kinetics of the silver photodissolution was studied in order to obtain information on the mechanism of the photodissolution effect and to determine the rate at which the reaction takes place between the Ag and the spin-coated $As_{40}S_{60}$ films under the influence of light. The effect of different illumination intensities and wavelengths on the reaction rate was also investigated. The sample preparation and the experimental set up used in the experiments are described in Section 3.5. Figure 6.1 shows the multilayer structure used in the experiments for measuring the reaction rate during photodissolution. Tr is the transmitted intensity, R_1 and R_2 are the reflected intensities from the top surface and from the Ag-doped / undoped interface respectively.

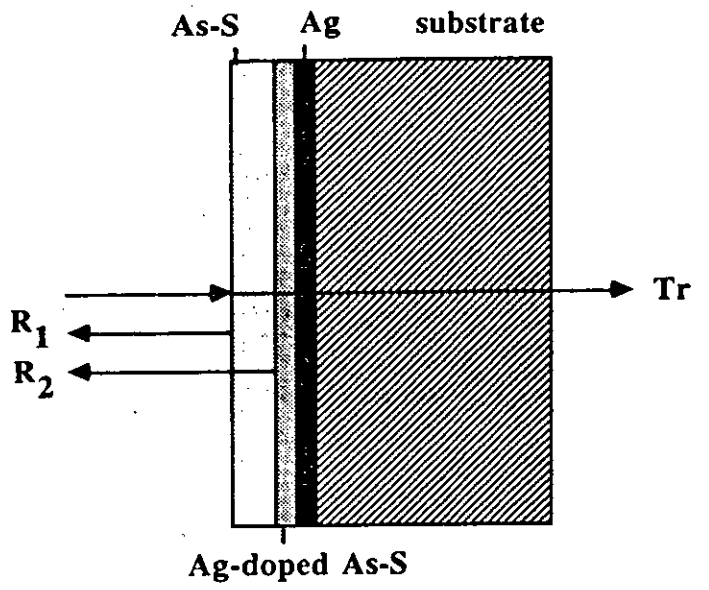

Figure 6.1 Schematic diagram of the sample structure used in the kinetics experiments.

All experiments were carried out at room temperature. The effects of wavelength and illuminating intensity on the silver photodissolution rate were studied by illuminating the samples with light of wavelength $\lambda=0.5145$, 0.4880 or 0.4658 μm of an Ar-ion laser, with incident powers varying from 6 mW to 220 mW. The diameter of the laser beam was 2 mm in all experiments described in this chapter, therefore the incident laser intensities were varied from 0.41 Wcm^{-2} to 7 Wcm^{-2}. The transmitted and reflected light intensity changes of the monitoring beam were recorded during photodissolution in order to gain information about the rate of the thickness change of the Ag and also the $As_{40}S_{60}$ films during the reaction.

When the sample is illuminated from the $As_{40}S_{60}$ side of the multilayer structure, the amount of light reaching the interface between the reactants to induce the reaction is influenced by the absorption of the $As_{40}S_{60}$ film. This is illustrated in Figure 6.2 where the transmittance of a 1.14 μm spin-coated $As_{40}S_{60}$ film (a typical chalcogenide film thickness used in the experiments concerning the reaction kinetics) is plotted as a function of wavelength.

It can be seen that the transmittance of the chalcogenide film is different at the different illumination wavelengths used in the experiments to induce the silver photodissolution effect. It was found that the transmittance of the $As_{40}S_{60}$ film is 65.8% at $\lambda=0.5145$ μm, 33.2% at $\lambda=0.4880$ μm, and 8.3% at $\lambda=0.4658$ μm. Therefore, when the intensity and wavelength dependences of the reaction rate were calculated, the incident laser powers were normalized according to the measured transmittance values.

During the photodissolution reaction, Ag^+ ions move into the $As_{40}S_{60}$ film causing a thickness reduction in both the Ag and the $As_{40}S_{60}$ films and at the same time a new layer, the Ag-doped As-S film builds up as the reaction product [1]. These changes in the sample structure result in changes in the transmitted and reflected intensities of the monitoring light. As was shown above, when the blue / green light sources are used to induce the silver photodissolution, the transmitted light intensities are influenced not only by the transmittance of the metal layer but also by the transmittance of the chalcogenide layer. In order to separate the effects of the two absorbing layers, a monitoring beam was used with wavelength $\lambda=0.6328$ μm which has a negligible absorption in the chalcogenide and also in the Ag-doped chalcogenide film formed during the reaction. In this case the transmitted intensity of the

monitoring beam was dependent only on the silver film thickness and hence contained information about the silver thickness change during reaction. Another part of the monitoring beam was reflected from the surface of the sample and also from the silver / chalcogenide interface (later from the silver-doped / undoped chalcogenide interface) causing an interference effect. From the time interval between the consecutive interference maxima and minima the rate of the chalcogenide thickness reduction was calculated. Figure 6.3 is a typical plot of the transmitted and reflected intensity changes of the monitoring light recorded during Ag photodissolution induced with a laser power of 13 mW i.e. with 0.41 Wcm^{-2} incident intensity at $\lambda = 0.5145$ μm.

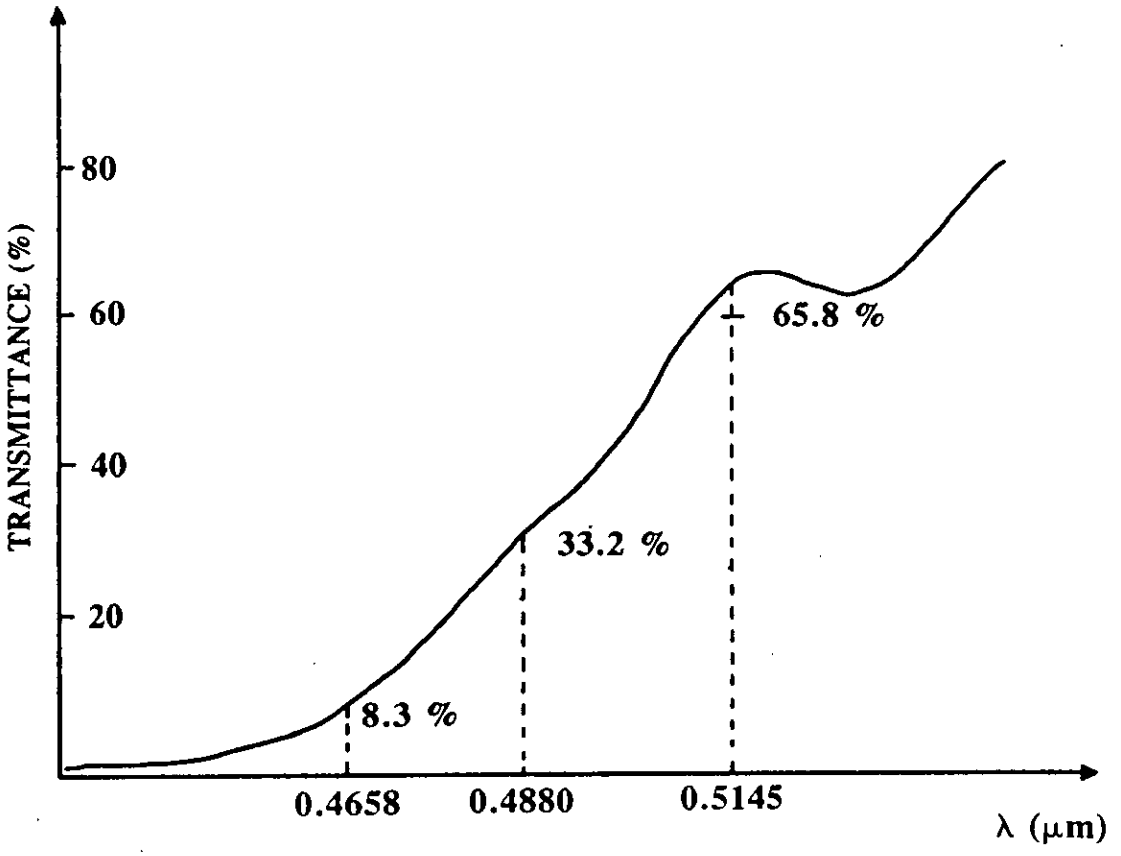

Figure 6.2 Optical transmittance of a 1.14 μm thick spin-coated $As_{40}S_{60}$ film as a function of wavelength.

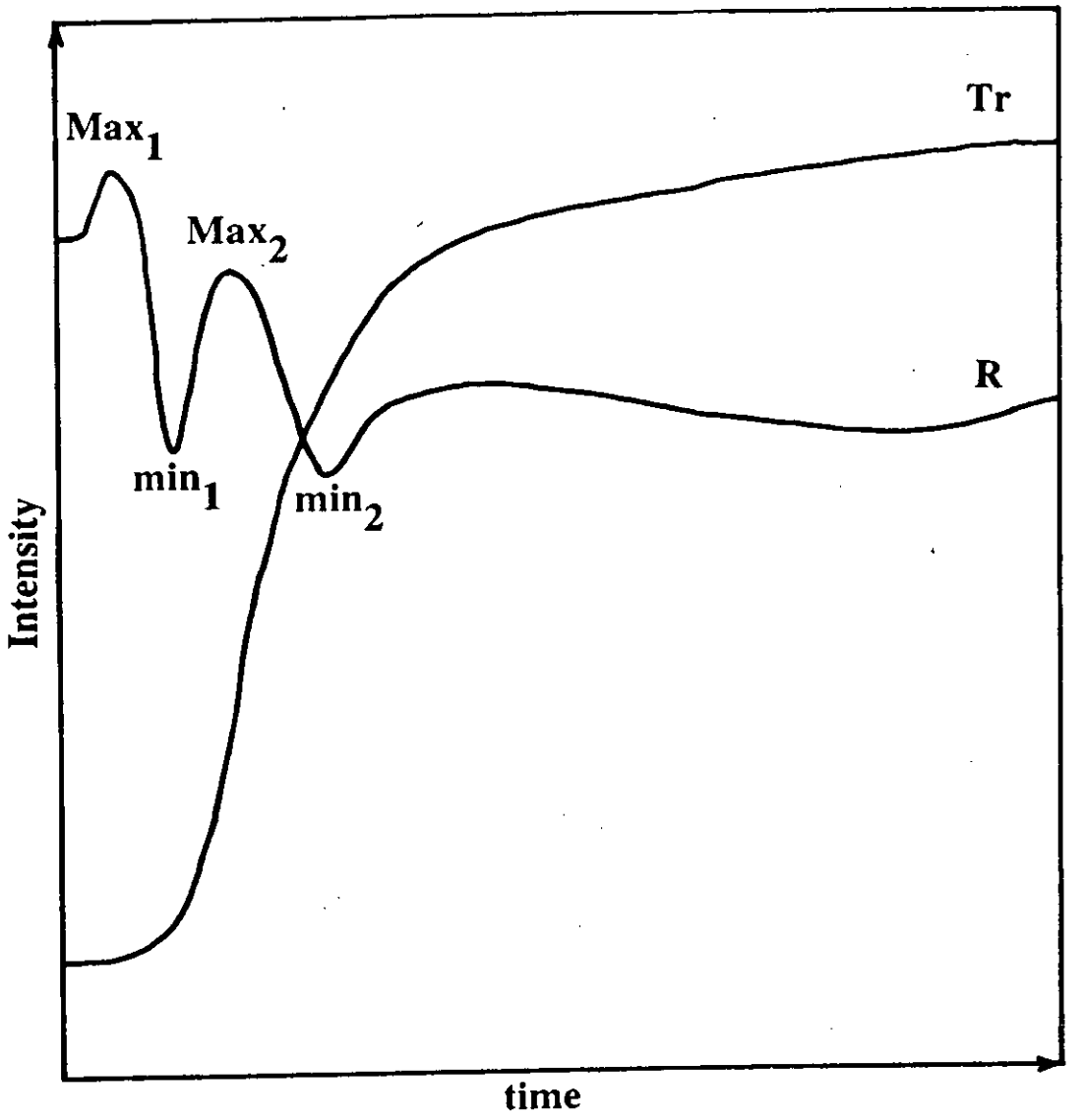

Figure 6.3 Changes in transmitted and reflected intensities of the monitoring light during photodissolution.

In evaluating the time dependence of the silver photodissolution at a constant incident light intensity, the change in the sample geometry during the reaction has to be considered. The light intensity reaching the chalcogenide / metal interface at the start of the reaction is influenced by the absorption of the chalcogenide film, as explained earlier. If the light absorption at the undoped / doped interface is the most important factor for the photodissolution to progress, the thickness reduction, and hence the changing absorption of the $As_{40}S_{60}$ film, will change the actinic light intensity during the reaction. In order to calculate the effect of the changing chalcogenide thickness on the actinic light intensity during reaction, a typical photodissolution experiment was selected in which the $As_{40}S_{60}$ film thickness reduction was calculated from the reflected light intensity change.

Figure 6.4 shows the increase in the relative intensity of the actinic light reaching the undoped / doped chalcogenide interface during a photodissolution experiment obtained with $\lambda=0.5145$ μm light with 0.41 Wcm^2 incident intensity. For this experiment the sample consisted of a 1.14 μm spin-coated $As_{40}S_{60}$ film ($\alpha=2x10^3cm^{-1}$, as discussed in Section 5.2.1) on top of a 0.04 μm Ag film. The actinic light intensity was calculated using the following relationship [2]:

$$I = (1-R)I_o\exp^{-\alpha d_{Ch}} \qquad (1)$$

where I is the intensity of the actinic light, R is the reflected light intensity, I_o is the incident light intensity, and α and d_{Ch} are the absorption coefficient and the thickness of the undoped chalcogenide layer respectively. In the calculation R was considered to be constant.

The decrease of the absorbing $As_{40}S_{60}$ film thickness during reaction means that the magnitude of the actinic irradiation increases with time. However, because of the sample geometry used in the experiments ($d_{Ch}=1.14\mu$m, silver layer thickness $l=0.04$ μm), only a ~6% increase in the actinic light intensity occurs during photodissolution (see Figure 6.4) which can be neglected. However, the effect of the absorption of the *initial* chalcogenide film thickness on the different wavelengths does have to be considered (see Figure 6.2). For this reason a normalized laser power was always used when the light intensity and wavelength dependences of the silver photodissolution rate were evaluated.

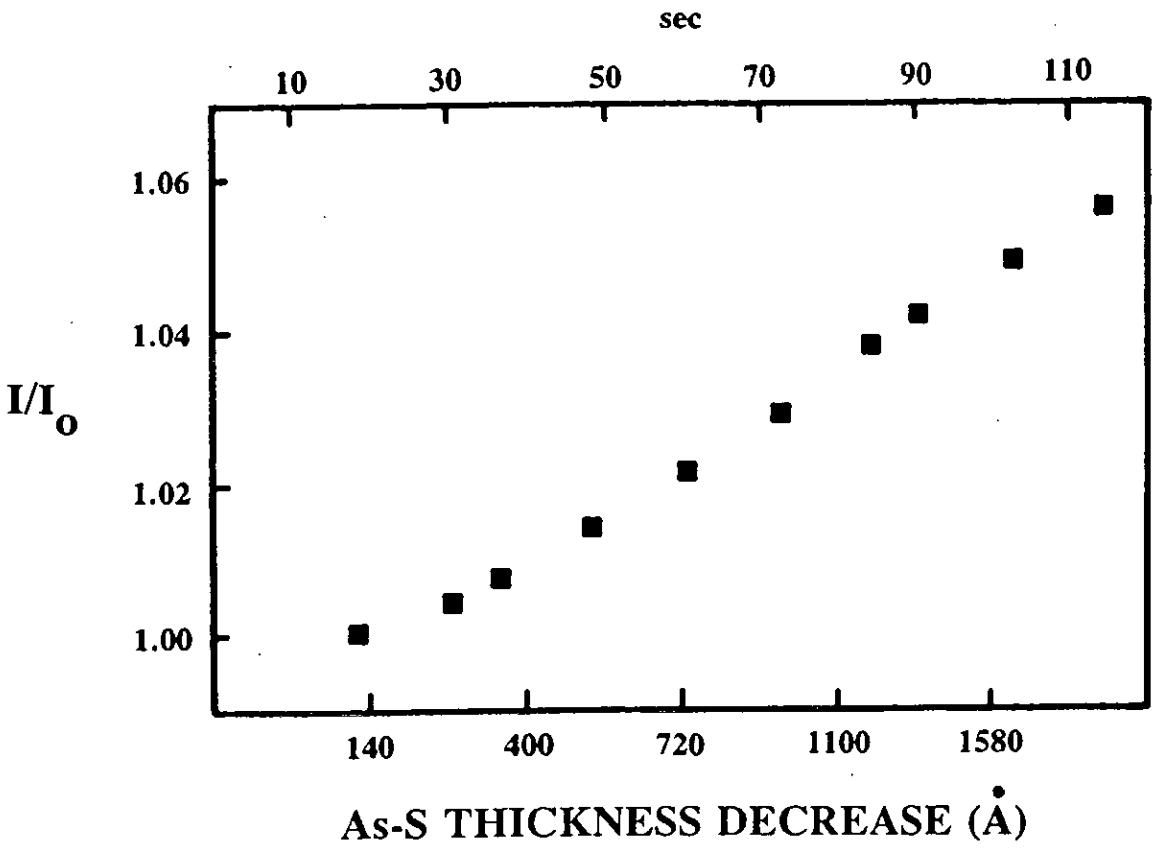

Figure 6.4 Relative intensity change of the actinic light, I/I_o, reaching the undoped / doped chalcogenide interface as a function of the decrease of undoped chalcogenide thickness.

6.1 TIME DEPENDENCE OF THE SILVER PHOTODISSOLUTION

Figure 6.3 shows that the intensity of the reflected monitoring light changes periodically, due to interference between the reflected light coming from the surface of the sample and the reflected light from the undoped / doped chalcogenide interface (R_1 and R_2 in Figure 6.1). By recording the reflected intensity change of the monitoring light with respect to time, it is possible to gain information about the change in the thickness of the undoped $As_{40}S_{60}$ film, and hence the rate of the reaction [3]. Using the interference condition equation the thickness change, d, of the undoped $As_{40}S_{60}$ between two consecutive interference maxima (or minima) is:

$$d = \frac{\lambda}{2n} \qquad (2)$$

where λ is the wavelength of the monitoring light (0.6328 μm), and n is the refractive index of the spin-coated $As_{40}S_{60}$ film at this wavelength (n=2.24).

By measuring the time between consecutive interference maxima and minima (corresponding to a thickness change of d/2), it was found that for every incident power and wavelength examined, an increasingly longer time was needed for the undoped / doped interface to progress the same distance as the reaction developed. Figures 6.5, 6.6, and 6.7 show the change in the undoped $As_{40}S_{60}$ thickness with respect to time, obtained for illumination with λ=0.4658, 0.4880 and 0.5145 μm light with different normalized incident powers. These curves are non-linear, showing a decreasing reaction rate with time.

It was also found, as Figures 6.8, 6.9, and 6.10 show, that for a given light intensity, the thickness of the undoped spin-coated $As_{40}S_{60}$ film changes linearly with the square root of the illumination time, suggesting a diffusion controlled reaction. Similar results have been obtained for silver photodissolution in spin-coated $As_{40}S_{60}$ films when the Ag-doped layer thickness change was measured [4]. This observation indicates that, similarly to the case of vacuum-evaporated As-S films [5], the rate of the silver photodissolution process in the spin-coated $As_{40}S_{60}$ films might also be controlled by the rate at which the Ag^+ ions or electrons can diffuse through the photodoped reaction product.

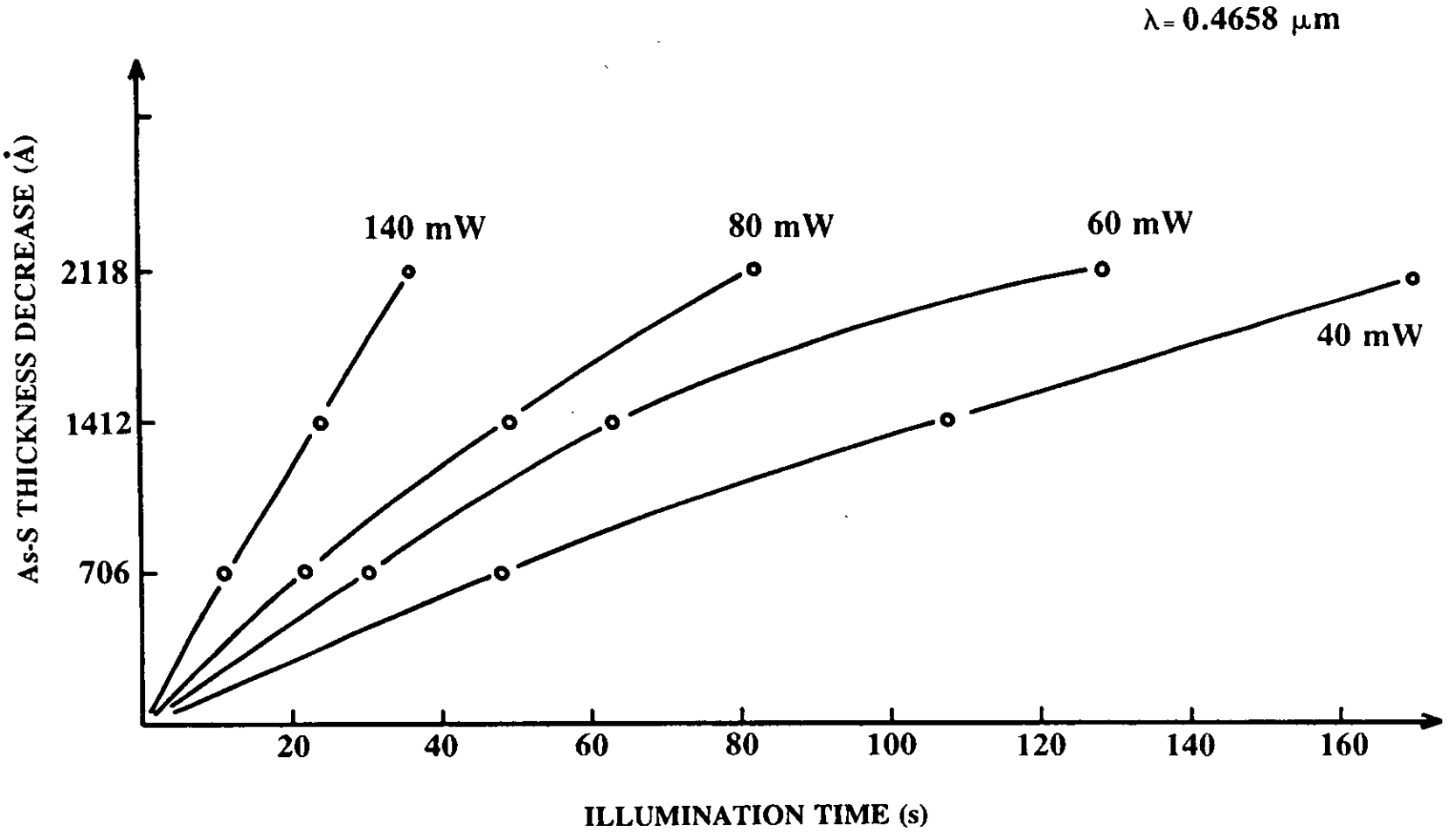

Figure 6.5 $As_{40}S_{60}$ thickness decrease vs. illumination time obtained for different normalized powers of $\lambda = 0.4658$ μm illumination wavelength.

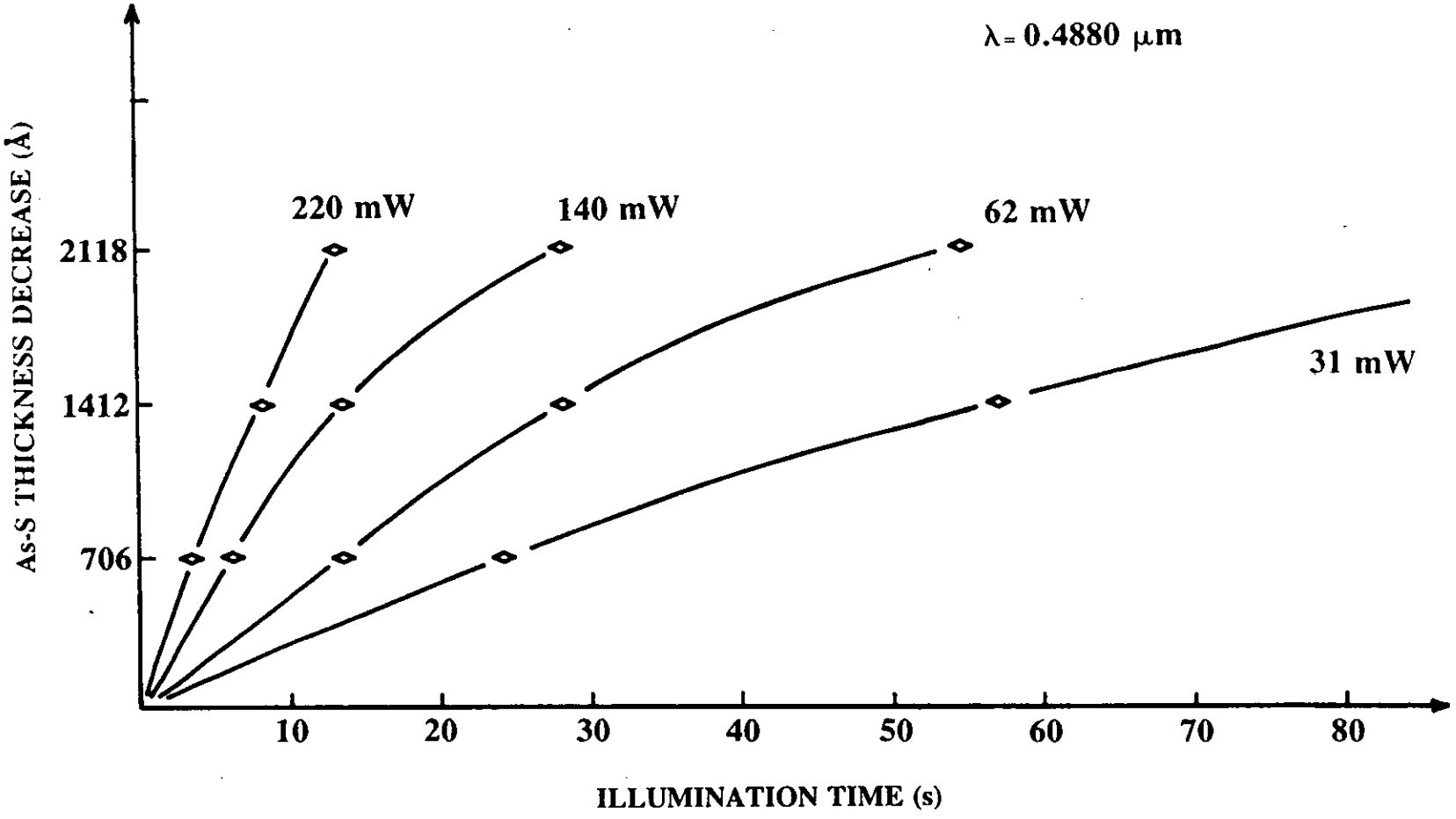

Figure 6.6 As Figure 6.5 but for different normalized powers of $\lambda = 0.4880$ μm illumination wavelength.

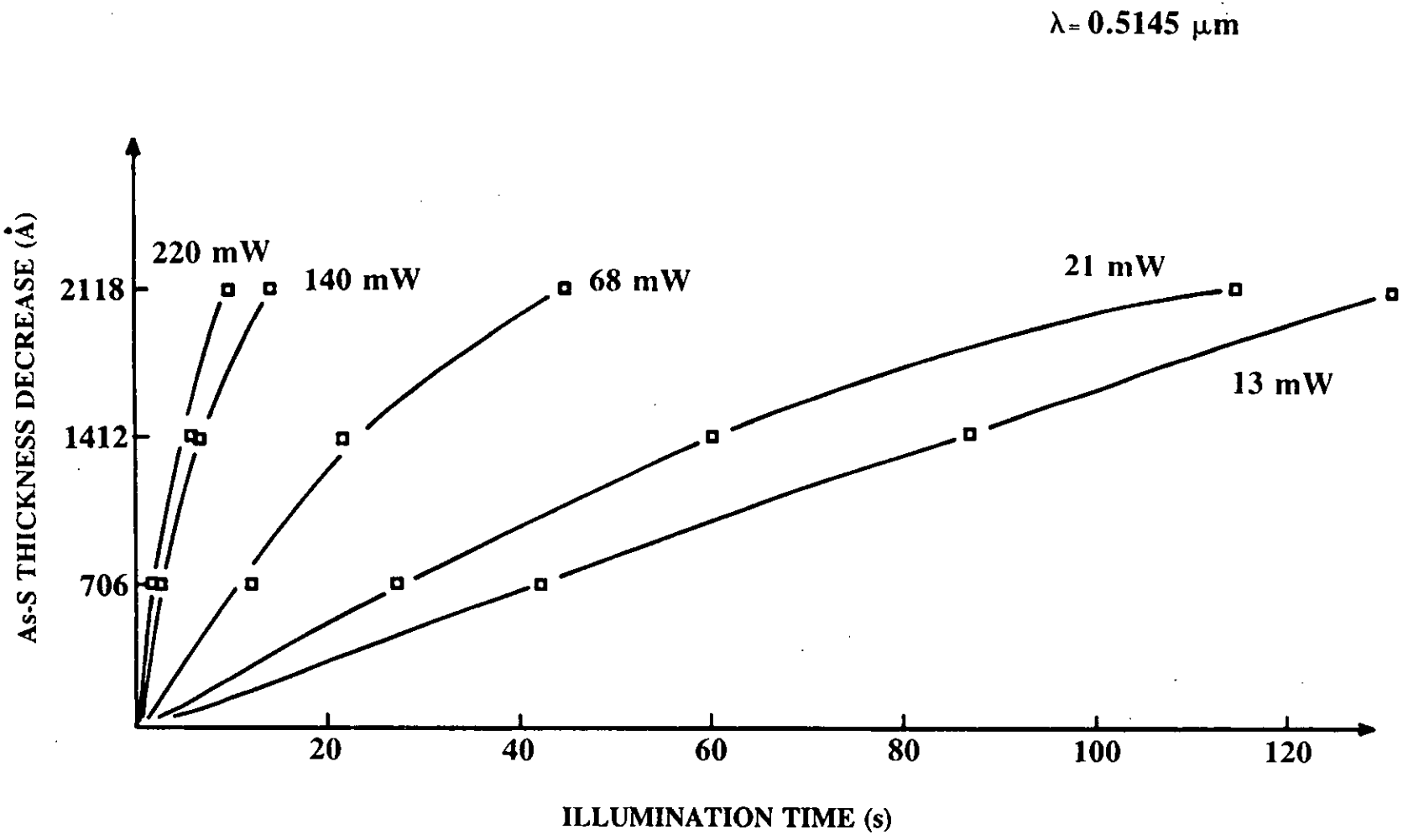

Figure 6.7 As Figure 6.5 but for different normalized powers of $\lambda = 0.5145$ μm illumination wavelength.

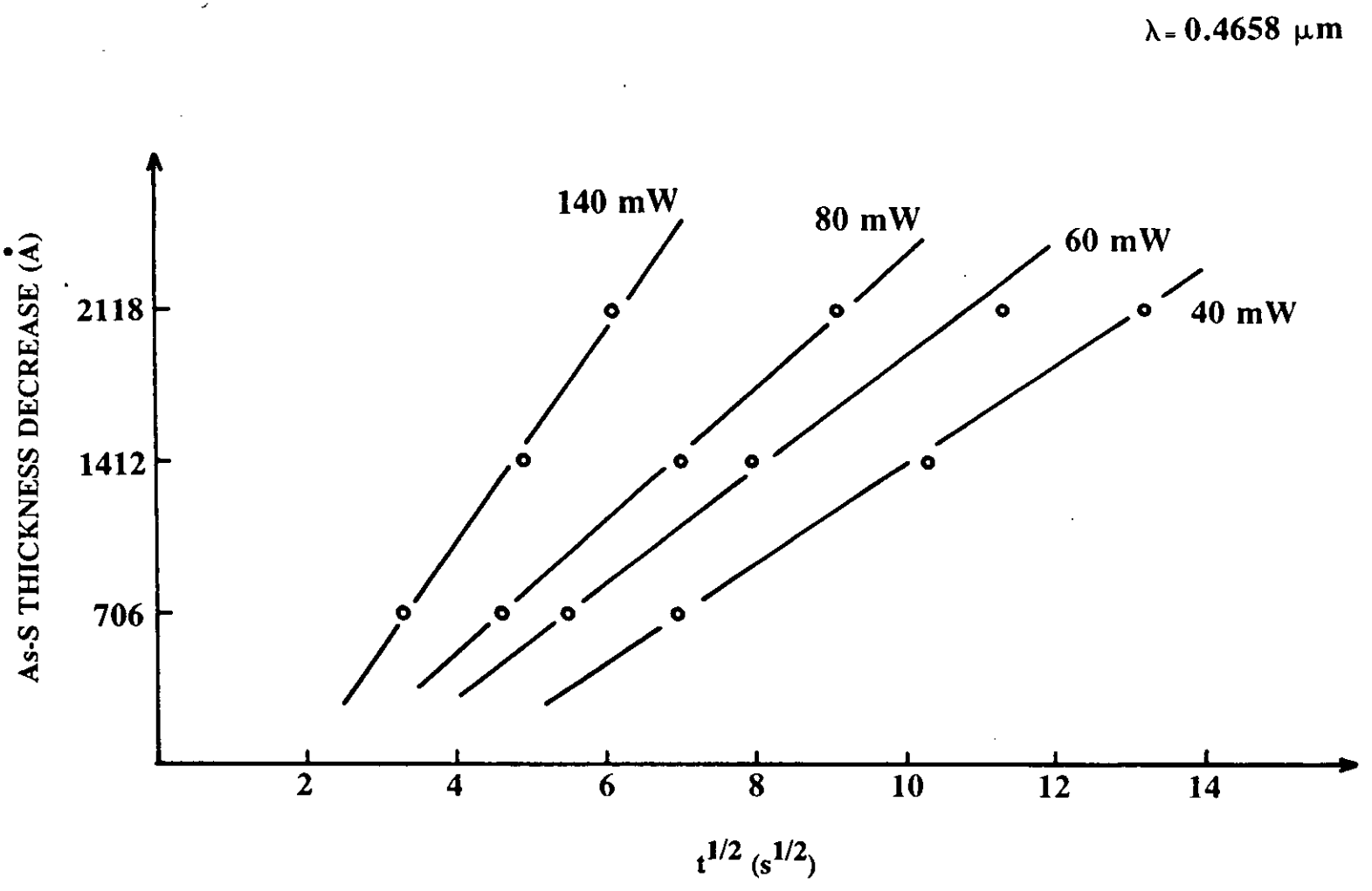

Figure 6.8 $As_{40}S_{60}$ thickness decrease vs. $t^{1/2}$ for different normalized powers of $\lambda = 0.4658$ μm illumination wavelength.

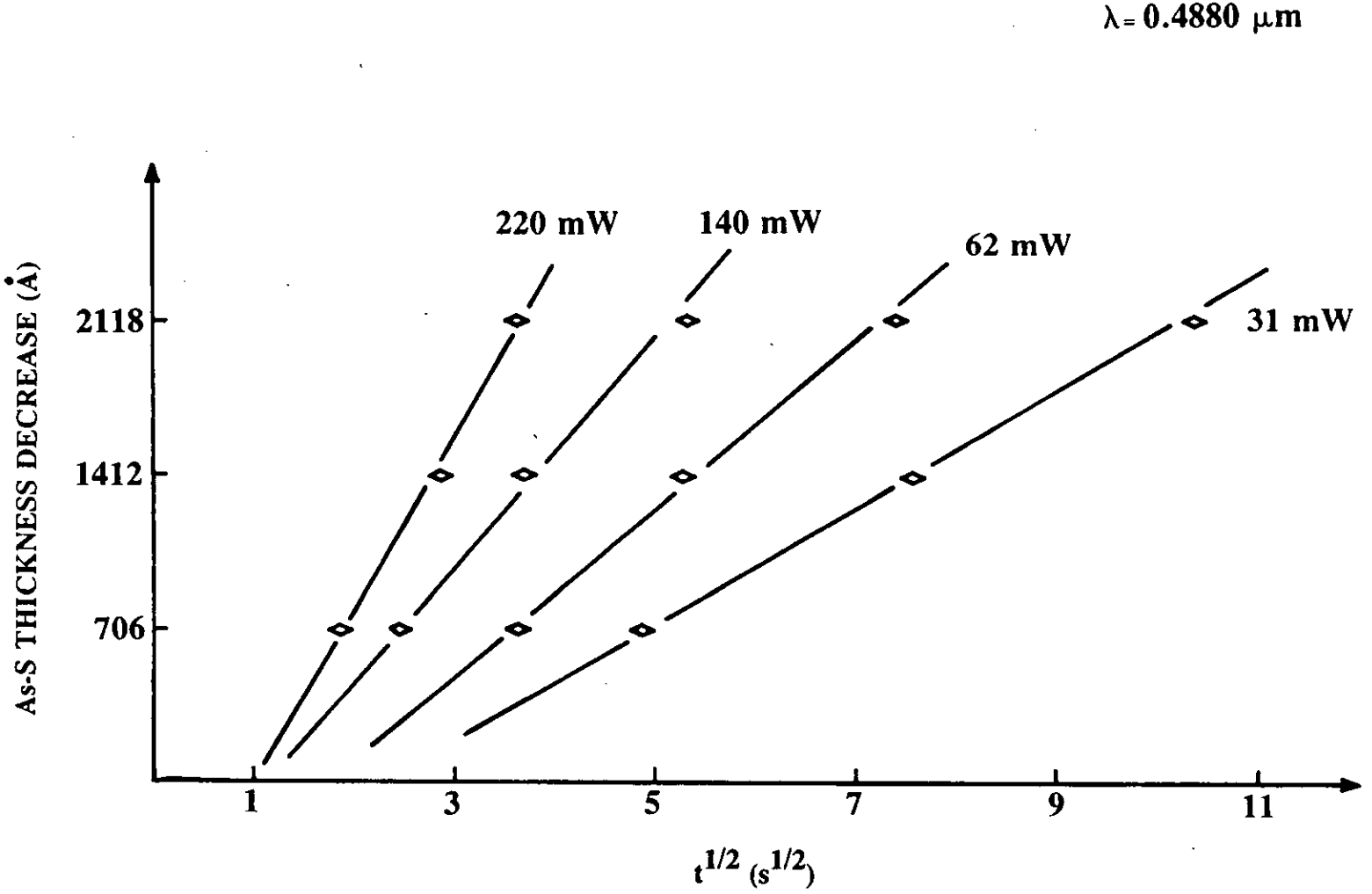

Figure 6.9 As Figure 6.8 but for different normalized powers of $\lambda = 0.4880$ μm illumination wavelength.

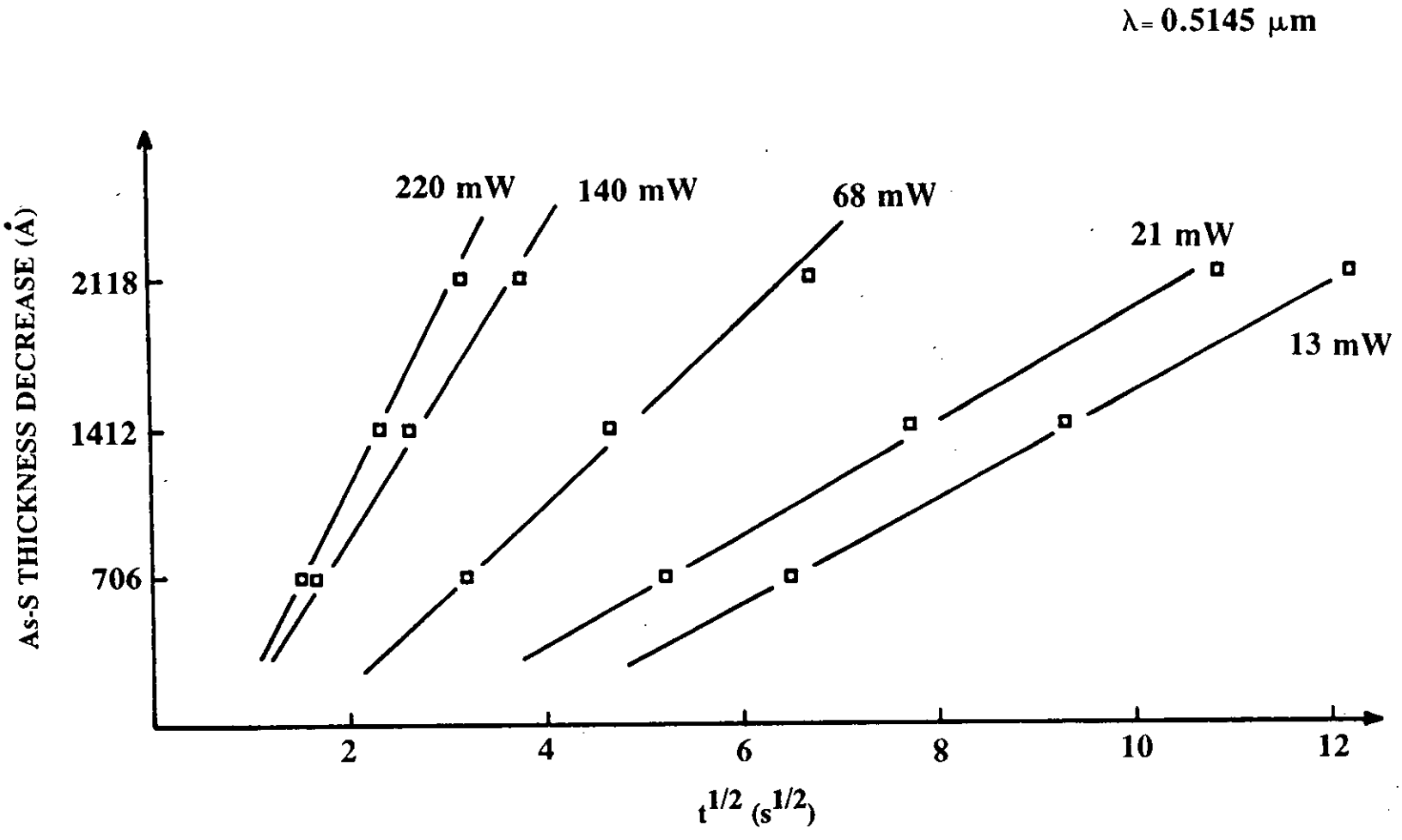

Figure 6.10 As Figure 6.8 but for different normalized powers of $\lambda = 0.5145$ μm illumination wavelength.

6.2 EFFECT OF ILLUMINATION INTENSITY AND WAVELENGTH ON THE RATE OF THE SILVER PHOTODISSOLUTION

The dependence of the photodissolution rate on the actinic light intensity and wavelength are important parameters, both for technological purposes and for understanding the underlying mechanism of the process. Silver photodissolution experiments were carried out using various illumination wavelengths with different incident laser powers and the obtained reaction rates were compared. Reaction rates were calculated by evaluating both the reflected and the transmitted intensity changes of the monitoring beam during the silver photodissolution reaction.

It was shown in Section 6.1 that the reaction rate changes with time during the diffusion process, thus only the reaction rates obtained at the same stage can be compared in order to obtain accurate information on the intensity and wavelength dependence of the process. For this reason, when evaluating the reflected intensity changes, the reaction rates were calculated between the first and second reflected interference maxima (Max_1 and Max_2 in Figure 6.3) for each reaction generated by different incident powers of $\lambda=0.5145$ μm, 0.4880 μm and 0.4658 μm illumination. In Figure 6.11 the logarithm of the rates, v, obtained this way is plotted against the logarithm of the incident (normalized) powers, P, for each different illumination wavelength. The slopes of the plots for all the examined wavelengths are $\sim$1 (0.97). This indicates that the reaction rate is linearly dependent on the illumination intensity.

Figure 6.11 also shows that the plots are shifted to smaller values of power when shorter wavelength illumination is used to induce the photodissolution reaction. For example, at 10 mW incident power, the rate of the reaction increases from $v_1=19.1$ Å/sec using $\lambda_1=0.5145$ μm illumination to $v_2=25.1$ Å/sec using $\lambda_2=0.4880$ μm illumination, and further increases to $v_3=79.4$ Å/sec using $\lambda_3=0.4658$ μm illumination. This shows that the more energetic photons increase the rate of the silver photodissolution.

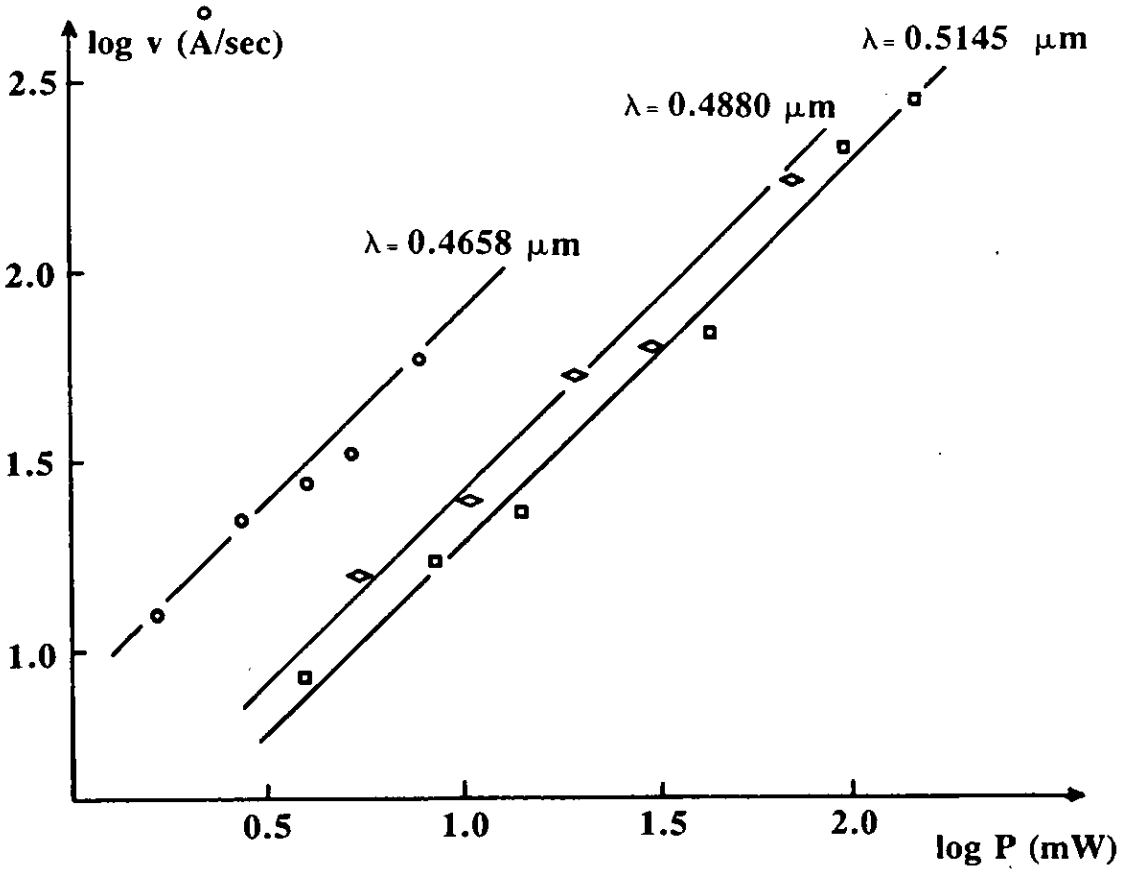

Figure 6.11 Log-log plot of reaction rate vs. incident power for three different illumination wavelengths. The rates were derived from the reflectance curves.

As stated above, the reaction rates in Figure 6.11 are associated with the $As_{40}S_{60}$ thickness decrease measured between the first and second interference maxima of the reflected monitoring beam. However, the intensity and wavelength dependence of the photodissolution rate can also be measured by monitoring the transmitted light intensity change during the reaction. Because the wavelength of the monitoring light

has a negligible absorption in the undoped and the Ag-doped As-S films, the sample transmittance, Tr, (after correction for reflection losses) is mainly a function of the Ag film thickness:

$$Tr = (1-R)\exp^{-\alpha l} \tag{3}$$

where α is the absorption coefficient of silver (constant at a fixed wavelength), and l is the Ag film thickness. The Ag-dissolution rate, v, can be written as:

$$v = \frac{dl}{dt} \tag{4}$$

Rearranging Equation 3:

$$\ln Tr = -\alpha l + \ln(1-R) \tag{5}$$

$$l = -\frac{\ln Tr}{\alpha} - \frac{\ln(1-R)}{\alpha} \tag{6}$$

Differentiating l with respect to time:

$$\frac{dl}{dt} = \frac{1}{Tr}\frac{dTr}{dt} = v \tag{7}$$

In addition to the change in the reflected intensity of the monitoring light, Figure 6.3 also shows the change in transmitted intensity recorded during the reaction. By differentiating the transmitted intensities with respect to time, the thickness decrease of the Ag film can be analyzed. A similar technique has also been used to measure the rate of photodissolution of zinc in chalcogenide glasses [6].

Figure 6.12 compares two first derivative curves of the transmitted intensity change of the monitoring light recorded during silver photodissolution in spin-coated $As_{40}S_{60}$ films. The samples were illuminated with P=6 mW of λ=0.5145 μm light (curve A in Figure 6.12) and P=60 mW of λ=0.4658 μm light (curve B in Figure 6.12). The curves have the same shape suggesting that the same type of reaction takes place regardless of the illuminating light wavelength and intensity.

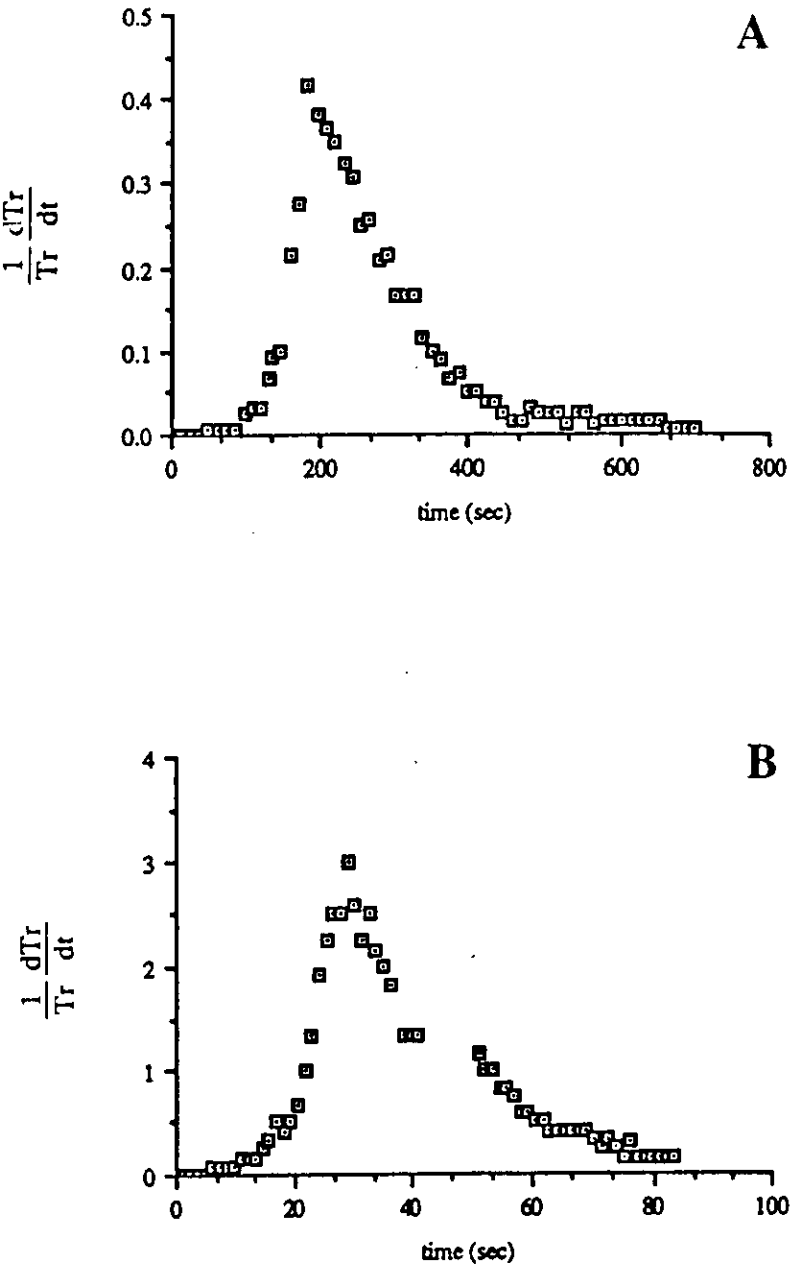

Figure 6.12 Comparison of the first derivatives of the transmitted intensity changes for photodissolution induced with: (A) 6 mW incident power of $\lambda = 0.5145$ μm illumination; (B) 60 mW incident power of $\lambda = 0.4658$ μm illumination.

The curves in Figure 6.12 can be divided into three different parts which can be associated with the different stages of the reaction [7] . All the observed curves start with a short period where the transmitted light intensity does not change much. Because the silver film thickness used in these experiments was ~0.04 μm, the samples were slightly transparent even at the beginning of the photodissolution process. Therefore the slow rise of the first derivative curves might be associated with the "induction" period which is often observed during the silver photodissolution process in vacuum-evaporated $As_{40}S_{60}$ films [8]. Figure 6.13 shows that the length of the induction period observed during the silver photodissolution process in spin-coated $As_{40}S_{60}$ films was found to be inversely proportional to the illumination intensity. This result is also in a good accordance with similar measurements obtained in vacuum-evaporated $As_{40}S_{60}$ films [7].

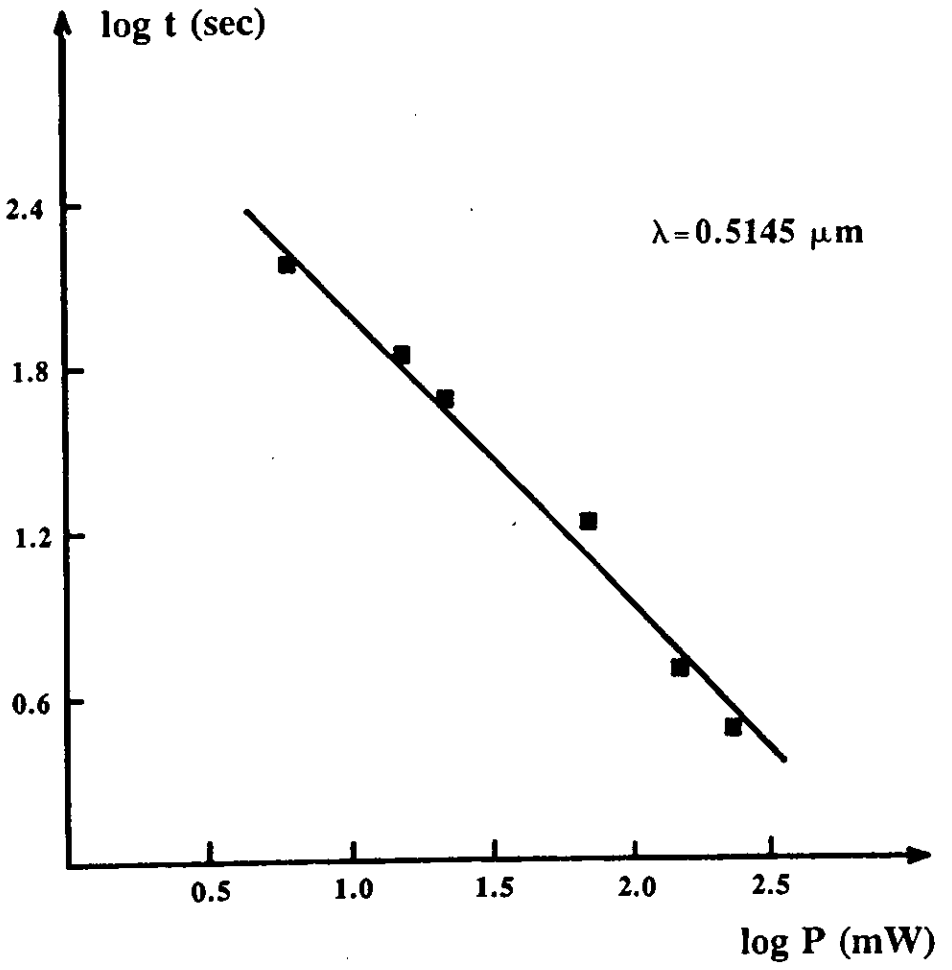

Figure 6.13 Log-log plot of the length of the induction period vs. incident power for λ=0. 5145 μm illumination.

Figure 6.12 also shows that after the short induction period, the rate of the silver layer thickness change increases rapidly. This part of the photodissolution is often referred to as stage II of the process [6, 8]. This is the stage during which the effective photodissolution occurs. After reaching a maximum point the reaction rate decreases until it finally approaches zero (stage III).

Figure 6.14 compares the first derivative curves of the transmitted intensity change during photodissolution obtained with different incident powers of $\lambda = 0.5145$ μm illumination. As the incident power increases, the maximum points of the first derivative curves occur at shorter times and a larger transmission change can be obtained in a given time with higher incident power. This indicates that at the same illumination wavelength, the reaction rate increases with increasing incident power.

The reaction rates at the maximum point of the first derivative curves were compared in order to gain information about the effect of the illumination intensity and wavelength on the rate. The obtained data are presented in Figure 6.15 where the logarithm of the reaction rate (at the maximum point) is plotted versus the logarithm of the incident light power for different illumination wavelengths. These plots are very similar to the intensity and wavelength dependence results obtained from analyzing the reflected light intensity changes, presented in Figure 6.11. In both figures the slopes of the log v versus log P plots are close to 1 suggesting that the rate of the silver photodissolution in spin-coated $As_{40}S_{60}$ films is linearly proportional to the illumination intensity (in the 6-220 mW power range, which corresponds to 0.41-7.0 Wcm^{-2} intensity range) at each examined wavelength. This observation indicates a monomolecular photochemical reaction between silver and spin-coated As-S films [9].

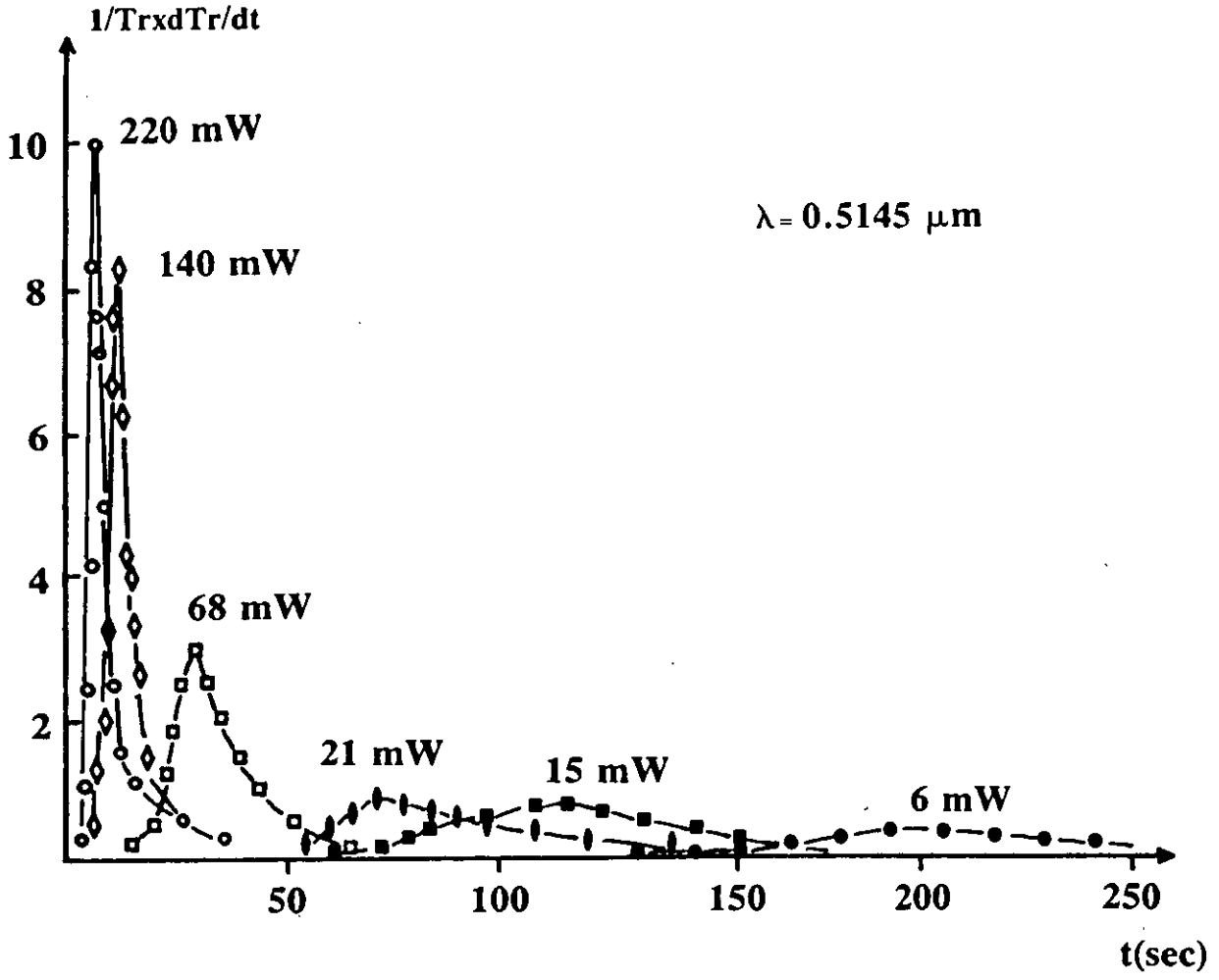

Figure 6.14 First derivative curves of the transmitted intensities changes vs. illumination time for different incident powers of $\lambda = 0.5145$ μm illumination.

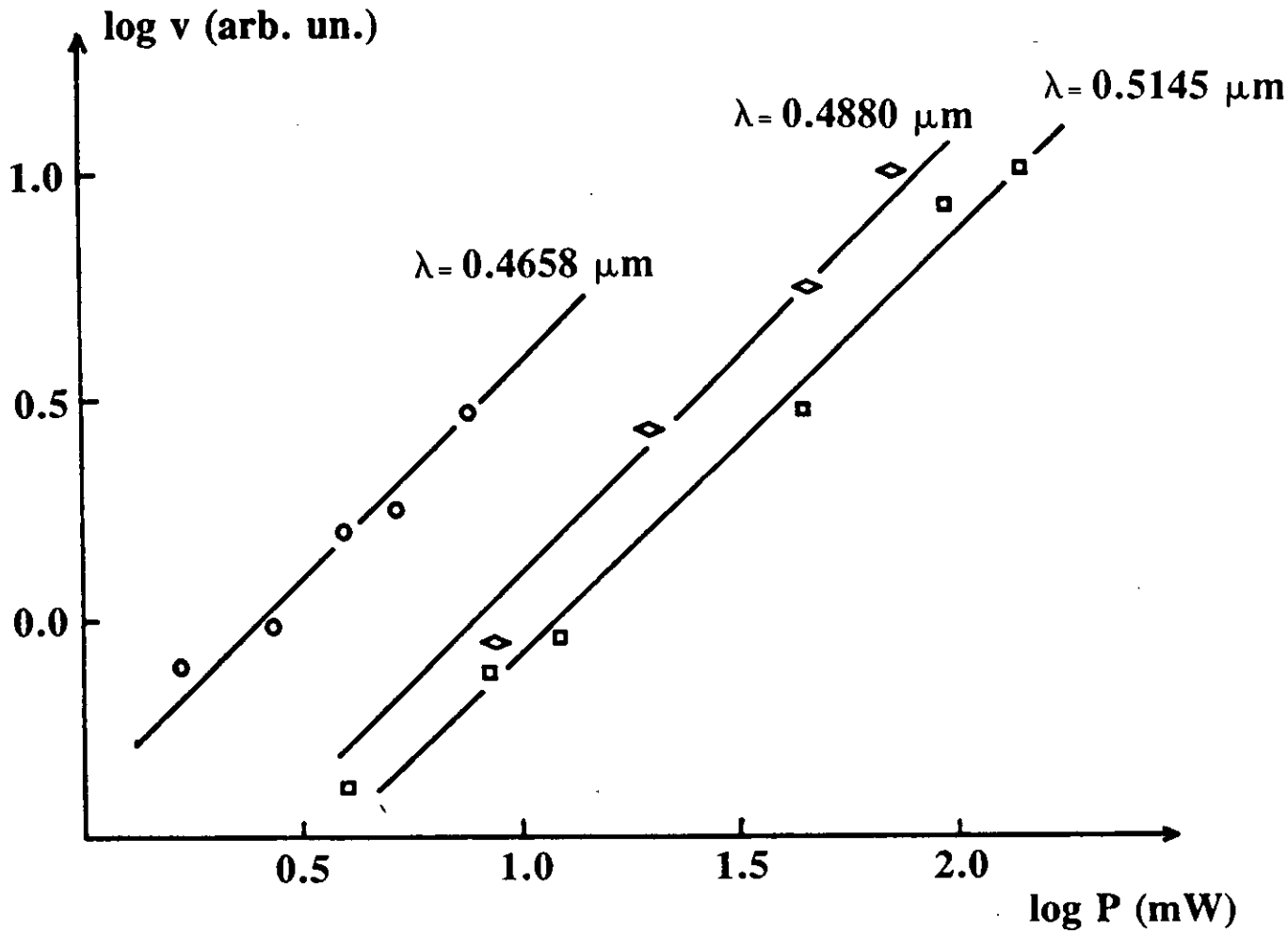

Figure 6.15 Log-log plot of reaction rate vs. incident power for three different wavelengths. The rates are derived from the transmittance curves.

6.3 SENSITIVITY OF Ag / SPIN-COATED As-S SYSTEM

By further analyzing the optical changes of the sample occurring during silver photodissolution in terms of the number of the incident photons it is possible to evaluate the sensitivity of the silver / spin-coated $As_{40}S_{60}$ double layer structure to actinic exposure. The number of the incident quanta, n_q, was calculated using the equation:

$$n_q = \frac{E}{h\nu} \tag{8}$$

where E is the illumination energy (obtained as normalized incident intensity x illumination time), h is Planck's constant and ν is the illumination frequency. The transmittance change of the monitoring beam gives direct information about the thickness change of the Ag film during reaction. The Ag thickness change during the silver photodissolution process was calculated using the calibration curve seen in Figure 6.16. This curve was constructed using Equation 3 in Section 6.2, where Tr is the transmittance of a silver film, α and l are the absorption coefficient and the thickness of the silver film respectively ($\alpha = 7.99 \times 10^5$ cm^{-1} at $\lambda = 0.6328$ μm).

Figure 6.17 shows the magnitude of the photodissolved Ag thickness as a function of the number of incident photons of the actinic light using $\lambda = 0.5145$ μm, 0.4880 μm and 0.4658 μm illumination. It can be seen that the photodissolved silver thickness is dependent on the number of incident photons and their energy. All the curves can be divided into three parts with different slopes. These parts again can be associated with the different stages of the silver photodissolution process. Figure 6.17 also shows that the more energetic photons increase the reaction rate at a fixed value of incident photon number.

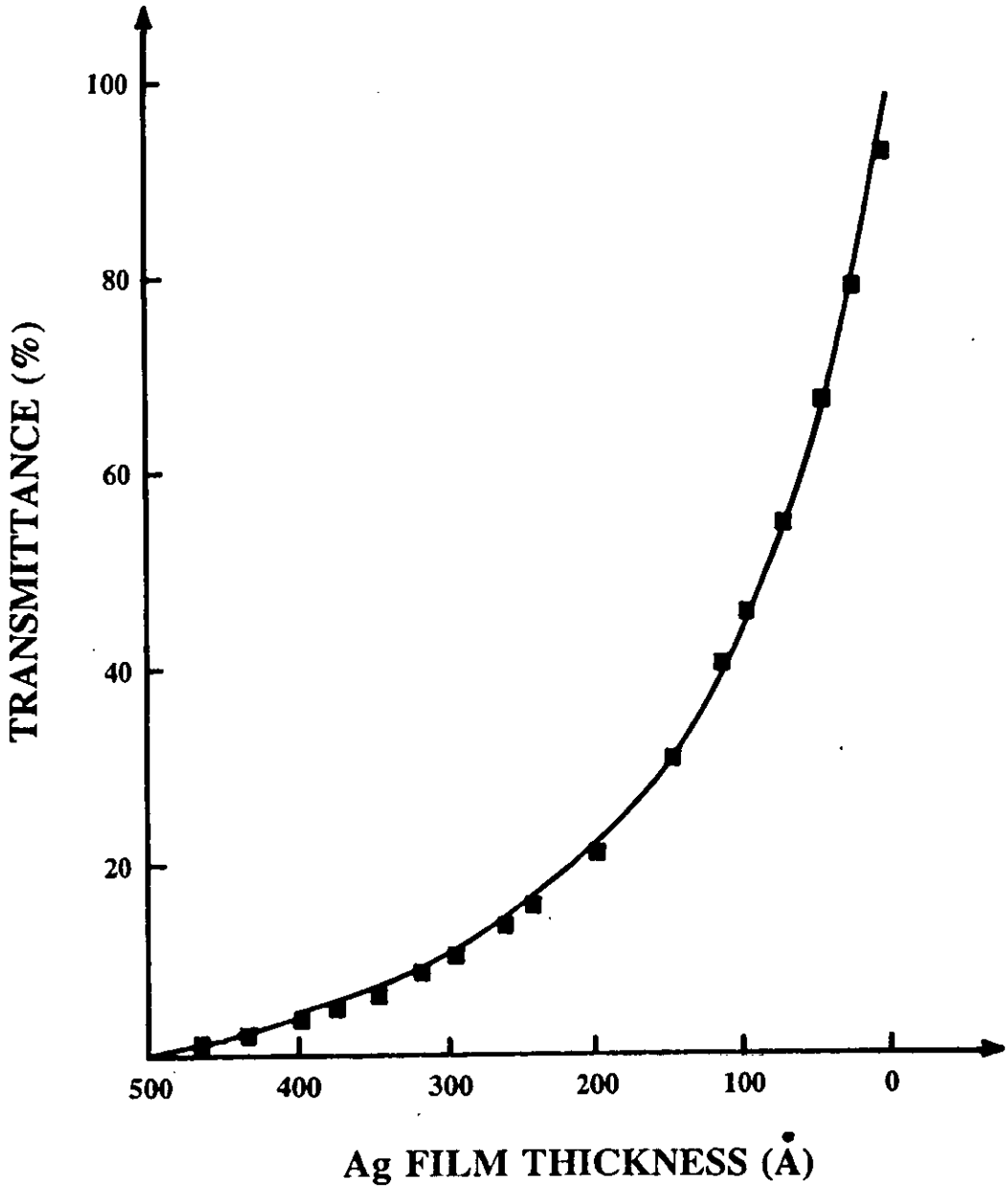

Figure 6.16 Transmittance curve of silver single layer.

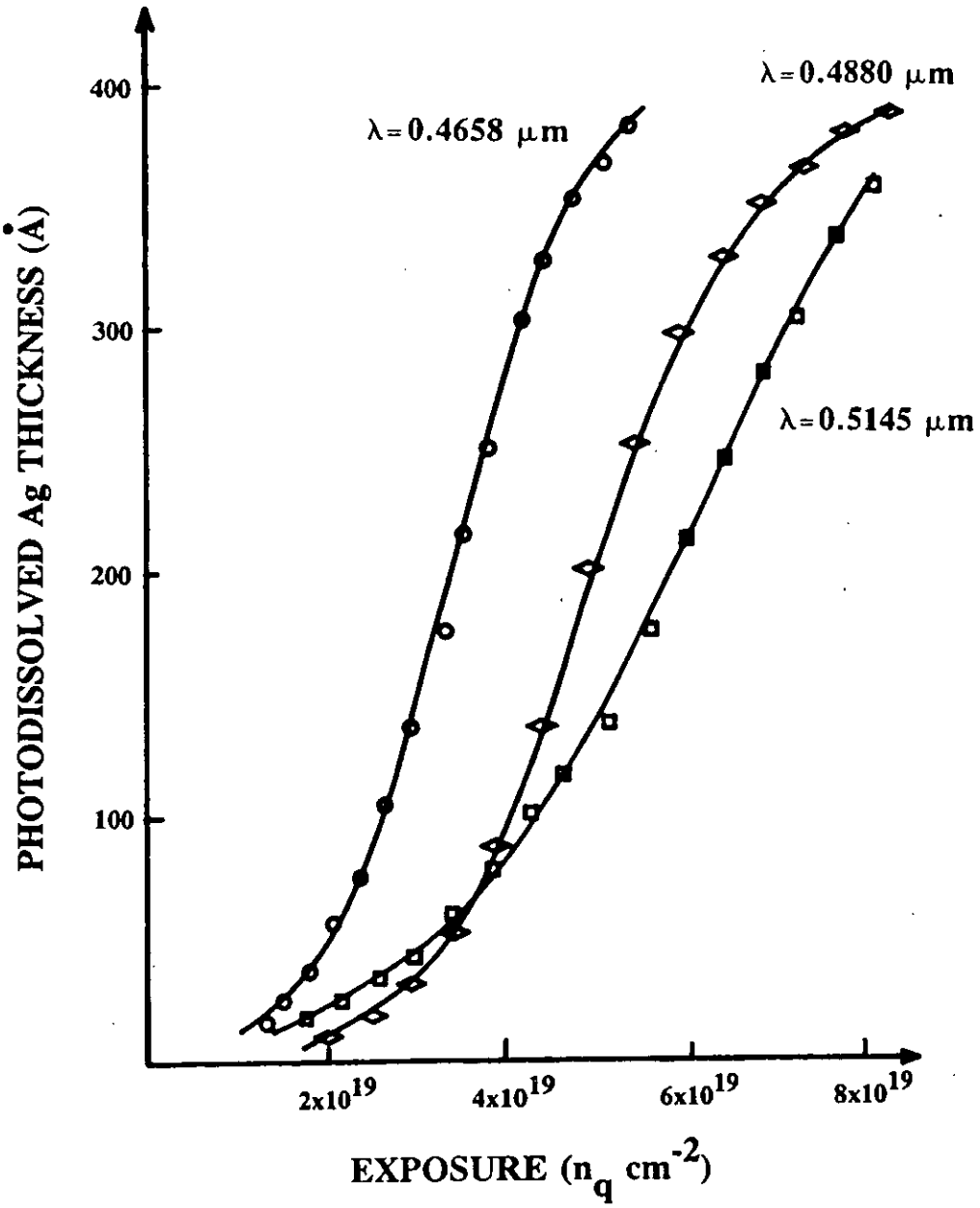

Figure 6.17 Photodissolved Ag thickness vs. number of incident photons.

6.4 SUMMARY OF RESULTS OBTAINED ON THE KINETICS OF SILVER PHOTODISSOLUTION IN SPIN-COATED As-S FILMS

In summary, it can be concluded that considerable information on the reaction kinetics, and the dependence of the reaction rate on the illumination wavelength and intensity can be obtained by monitoring the changes occurring in the optical properties of the sample during photodissolution. The photon energies used to induce the reaction in these experiments were near the band gap of the chalcogenide, therefore a separate monitoring beam (with energy smaller than the band gap) was used, i.e. with a wavelength at which the $As_{40}S_{60}$ film and also the reaction product were transparent. The transmitted and reflected intensities of the monitoring light were measured and analyzed to provide information on the rates at which the Ag and $As_{40}S_{60}$ films decrease in thickness during the reaction.

The time dependence of the reaction measured at a fixed light intensity was determined by measuring the time intervals between consecutive interference maxima and minima in the reflectance curves. Using this technique it was found that the reaction rate changes linearly with the square root of the reaction time, suggesting a diffusion controlled reaction between Ag and spin-coated $As_{40}S_{60}$ films.

The effect of the illumination intensity and wavelength on the rate of the silver photodissolution was also investigated. Since it was found that the reaction rate is not constant during the reaction, rates measured at the same stages of the reaction were compared when different illumination intensities and wavelengths were used to induce photodissolution. The reaction rates were calculated between the first and second interference maxima of the reflected monitoring light. It was found that the log v versus log P curves are linear with a slope of ~ 1 at each ~~examined~~ wavelength examined. The same relationship was found by monitoring the transmitted light intensity changes during the reaction. The transmitted intensities were differentiated with respect to time and the reaction rates at the maximum points of the first derivative curves were compared. Again, it was found that the reaction rate changes linearly with illumination intensity, the log-log plots having a slope of ~ 1 (in the 0.41-7.0 Wcm^{-2} intensity range examined) at each wavelength examined, showing that the rate of the silver photodissolution process in spin-coated $As_{40}S_{60}$ is linearly proportional to the illumination intensity. This suggests that the Ag photodissolution reaction might

be associated with a monomolecular photochemical reaction [9].

The first derivative curves of the sample transmittance were used to identify the different stages of the photodissolution process in spin-coated $As_{40}S_{60}$ films. It was found that the process is similar to that in samples prepared by vacuum-evaporation and consists of three parts. It was also found that the induction period measured in spin-coated $As_{40}S_{60}$ films is inversely proportional to the incident illumination intensity.

By evaluating the photodissolved Ag thickness as a function of the number of incident photons, the sensitivity of the silver / spin-coated $As_{40}S_{60}$ double layer system to actinic radiation was determined. Comparison of these data with that obtained for the silver / vacuum-evaporated $As_{40}S_{60}$ double layer systems [7, 10] shows that the sensitivity is slightly less for the spin-coated chalcogenide films. This is possibly due to the differences in the structure, already discussed in Chapters 4 and 5.

6.5 REFERENCES

[1] A. V. Kolobov and S. R. Elliott, Phyl. Mag. B, 1990, Vol. 6, No. 5, 859-865.

[2] O. S. Heavens, "Optical Properties of Thin Solid Films", 1955, Butterworths Scientific Publications London.

[3] A. P. Firth, P. J. S. Ewen and A. E. Owen, J. of Non-Cryst. Solids, 1985, 77 & 78, pp. 1153-1156.

[4] R. E. Belford, E. Hajto and A. E. Owen, Thin Solid Films, 1989. Vol. 173, pp. 129-137.

[5] P. J. S. Ewen, A. Zakery, A. P. Firth and A. E. Owen, Philos. Mag. B, 1988, Vol. 57, No. 1, pp. 1-12.

[6] A. V. Kolobov, B. T. Kolomiets, V. M. Lyubin and M. A. Tagirdzhanov, Solid State Comm. 1985, Vol. 54, No. 5, pp. 379-382.

[7] D. Goldschmidt and P. S. Rudman, J. Non-Cryst. Solids, 1976, Vol. 22, pp. 229-243.

[8] A. V. Kolobov and S. R. Elliott, Adv. Phys. in print.

[9] R. P. Wayne, "Photochemistry" 1970, published by Butterworth London.

[10] T. Yaji and S. Kurita, J. Appl. Phys. 1983, 54(2), p. 647.

CHAPTER 7

ETCHING PROPERTIES

OF SPIN-COATED As-S FILMS

7.1 ETCHING PROPERTIES OF CHALCOGENIDES

It has been demonstrated that band-gap illumination and metal photodissolution cause changes in the structure of chalcogenide glasses which result in significant changes in their physical and chemical properties [1, 2, 3]. The solubility difference between the illuminated and unilluminated parts of the amorphous chalcogenide films is of technological interest as the amorphous structure can yield high resolution patterns. The more drastic change in the solubility of chalcogenide glasses occurs as a result of metal photodissolution. The Ag-doped area of chalcogenide films has been found to be resistant to most chemicals, while the undoped region can be dissolved in alkaline solutions of NaOH, NH_4OH, KCN, K_2CO_3, Na_2CO_3 or Na_3PO_4 [1, 2, 3, 4]. This selective etching property has made it possible to use chalcogenide thin films in VLSI technology as inorganic resist materials [1, 3] and also to prepare surface relief type optical elements [5]. The solubility of undoped chalcogenides has been widely studied, and was found to be dependent on a variety of factors such as: type of etchant, chalcogenide composition, deposition conditions etc. [4, 5, 6]. The wet etching characteristics of evaporated As-S films have been found to be dependent on the composition of the chalcogenide, the pre-treatment (annealing, illumination) of the films, and the pH and temperature of the etchant [4, 7]. The etching rate difference between the as-deposited and illuminated evaporated As-S films, using the same etchant, was explained in terms of their structure [4]. The slower etch rate of the as-deposited films was assigned to the presence of As_4S_4 structural units (or As-As bonds) in the film. Under band-gap illumination these fragments can be polymerized and the resulting film structure is very similar to the structure of glassy As_2S_3. The dissolution of As_2S_3 and As_4S_4 in alkaline solutions proceed differently as described in Equation 1

and 2. Furthermore, the reaction rates are different for the above reactions, and As_4S_4 has been found to be insoluble for low OH^- concentration [4].

$$As_2S_3 + 6OH^- = AsO_3^{3-} + AsS_3^{3-} + 3H_2O \quad (1)$$

$$3As_4S_4 + 24OH^- = 4AsS_3^{-3} + 4AsO_3^{-3} + 4As + 12H_2O \quad (2)$$

The difference in the dissolution rate between the exposed and unexposed parts of As-S films has been found to vary with the composition of the chalcogenide [4]. It has been found that as the S content of the composition increases, fewer As_4S_4 molecules are present in the as-deposited film so illumination has less effect on the structure and hence on the etching properties.

The identification of selective dry etchants for chalcogenides further extended their potential use in lithography and imaging applications. Dry processing is important from the technological point of view, since it offers clean and more controllable etching conditions. Different etch rates have been measured for as-deposited, illuminated and Ag-doped vacuum deposited As-S films using CF_4 plasma [8]. Spin-coated As_2S_3 ($As_{40}S_{60}$) films have been successfully removed by plasma etching using CF_4 gas and also using $SF_6 + O_2$ gas mixture [9, 10]. The Ag-doped material is resistant to most wet etchants, although it can be removed by hot concentrated acids. However, it has recently been shown that a sulphur plasma will efficiently remove Ag-doped As-S films [11].

7.2 ETCHING PROPERTIES OF SPIN-COATED As-S FILMS

In the previous chapters it was shown that under the influence of light Ag^+ ions move into the structure of spin-coated As-S films thereby changing their original properties. It was found that the structure of spin-coated As-S films changes as a result of band gap illumination and also silver photodissolution. The optical properties of spin-coated As-S films were also found to change after silver photodissolution: higher refractive index and absorption coefficient values were obtained for Ag-doped spin-

coated As-S films.

The work described in this chapter is concerned with obtaining quantitative information on the etching properties of spin-coated As-S films in order to prepare surface relief structures in these films. In the present study CF_4 plasma was used as an etchant, and the etching rate of spin-coated As-S films was measured. Plasma etching is widely used in VLSI technology since it offers the advantages of: uniform, controlled etching; clean and simple processing; and reduced etchant material and handling costs. Most parts of the plasma etching process are not yet well understood because the reactions taking place during etching are complex. Plasma etching is the selective etching of material by reaction with chemically active radicals formed in a glow discharge. The plasmas used in plasma etching are ionized gases containing highly reactive ions, and free radicals. The plasmas are characterized by their relatively low temperatures (50–250° C), low pressure (0.09-3.0 Torr), and by etch gas flow rates of 50-500 cm^3/min. These conditions are typically achieved by exciting the plasma with rf power into a continuously evacuated reaction chamber into which an appropriate etch gas is bled through a needle valve [12]. Plasma etching is a chemical process, and etching occurs only if free radicals, formed in the plasma, can react chemically with the material to be etched to form a volatile compound that can be swept away by the gas flow. The etch rate in plasma etching usually depends on the etch gas composition, the rate of generation of etching radicals and their rate of arrival at the sample. The material being etched and its temperature, as well as the rate of volatilization and removal of the reaction products are also important factors [12].

This chapter describes how illumination alone and also silver photodissolution affects the etching properties of the spin-coated As-S films. The etching rates in a CF_4 plasma were measured for spin-coated $As_{40}S_{60}$ films having different treatments prior to etching. Among the films investigated were annealed and annealed and subsequently illuminated spin-coated $As_{40}S_{60}$ films. The plasma etching of Ag-doped spin-coated films was also investigated. The sample preparation and the experimental arrangement used for measuring the etching rates are described in Section 3.6. Different CF_4 plasma conditions were tried in order to obtain a constant etch rate during measurements. The reflected light intensity of the monitoring He-Ne laser beam was recorded during etching and the etching rate was evaluated from the time interval between the consecutive interference maxima and minima, using the interference condition (Equation 22 in Section 3.2).

Figure 7.1 shows the plots of the reflected light intensity changes as a function of etching time obtained during etching the annealed and the annealed and subsequently illuminated films. As Figure 7.1 shows, using the CF_4 plasma the etching time required to remove the annealed and illuminated film is shorter than that for the unilluminated spin-coated $As_{40}S_{60}$ film of the same thickness. It was also observed that etching of the as-deposited (unannealed) spin-coated $As_{40}S_{60}$ films using the CF_4 plasma does not occur. This observation might suggest that the structural units which are responsible for the etching, i.e. reaction with the CF_4 plasma and formation of volatile products, are blocked by the solvent residue in the film. There was no interference pattern observed during etching of the Ag-doped $As_{40}S_{60}$ films, showing that the thickness of this film does not change in the CF_4 plasma.

The calculated etching rates for the differently treated samples are presented in Figure 7.2. It was found that the thickness of the undoped spin-coated As-S films changes linearly with the etching time, indicating constant etch rates for the annealed and also for the annealed and subsequently illuminated films in the given CF_4 plasma conditions. There was no thickness reduction observed during etching of the Ag-doped spin-coated $As_{40}S_{60}$ films. The slope of the plot obtained for the annealed and subsequently illuminated $As_{40}S_{60}$ film is higher by a factor of 2.6 than that of the annealed film. The measured etch rate difference indicates that, as for vacuum-evaporated As-S films, light-induced structural changes also occur in spin-coated As-S films.

The illumination-induced etch rate difference in vacuum-evaporated chalcogenide films has made it possible to use these films as negative-type photoresists [1]. An illuminated and differentially etched vacuum-evaporated $As_{40}S_{60}$ film has been used as the photo-recording medium in the process of photomask preparation [7]. In the present study surface relief gratings were prepared in spin-coated $As_{40}S_{60}$ films using the etching rate difference between the illuminated and unilluminated parts of the films. The films were illuminated by UV light through a contact mask having 6 μm lines and spaces and the pattern developed in a CF_4 plasma. Figure 7.3 shows a photograph of the resulting surface relief grating.

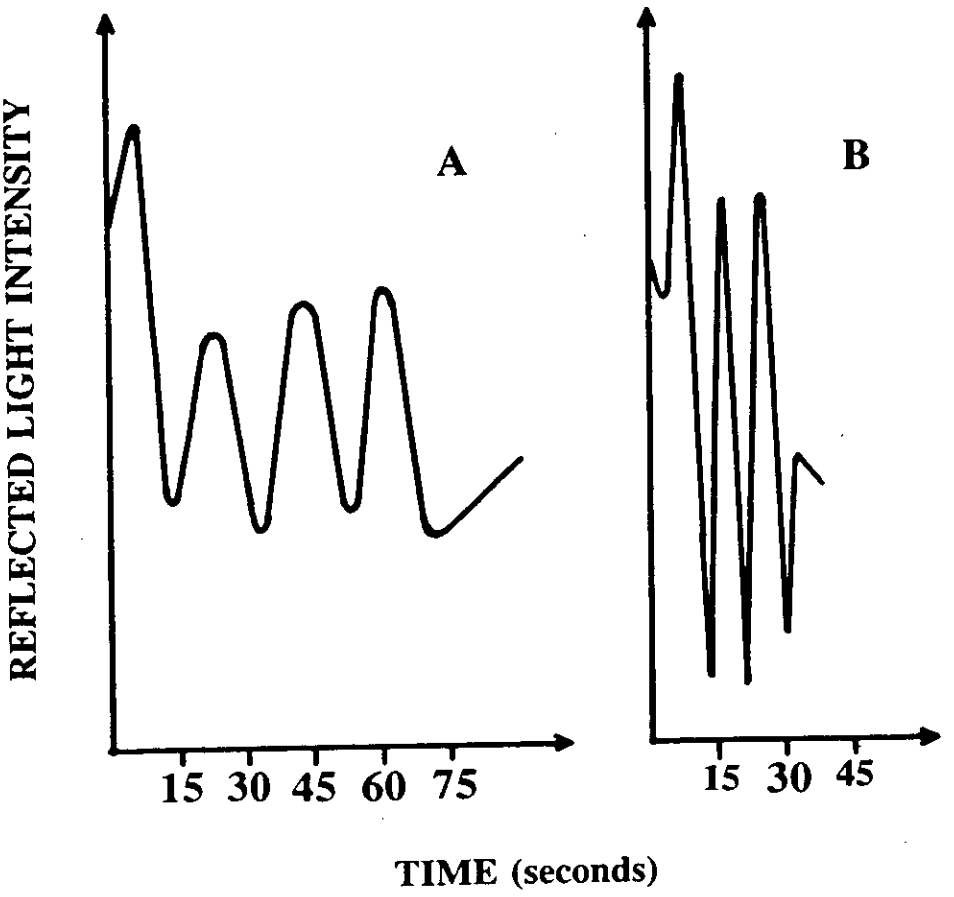

Figure 7.1 Reflected light intensity change as a function of etching time for: (A) annealed; and (B) annealed and illuminated spin-coated $As_{40}S_{60}$ films.

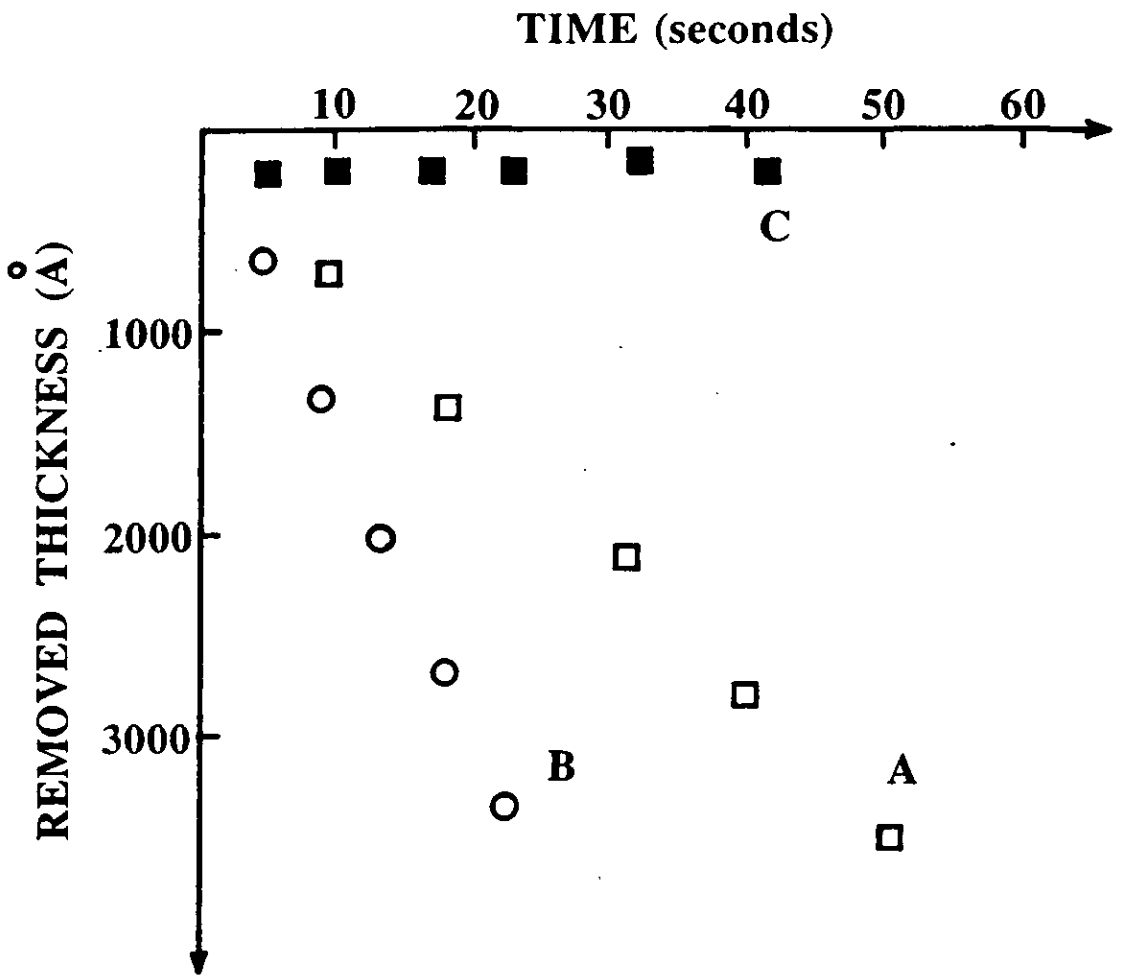

Figure 7.2 Removed film thickness as a function of etching time for: (A) annealed; (B) annealed and illuminated; and (C) Ag-doped spin-coated $As_{40}S_{60}$ films using CF_4 plasma.

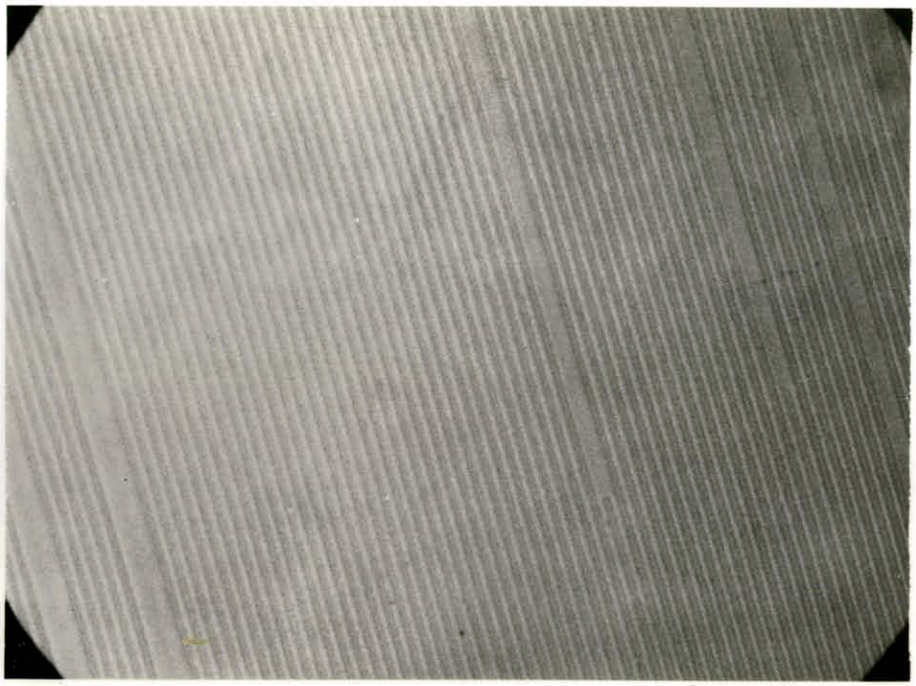

Figure 7.3 Photograph of a surface relief diffraction grating prepared in a spin-coated $As_{40}S_{60}$ film using the illumination-induced etch rate difference ($\Lambda = 6\ \mu m$).

7.3 REFERENCES

[1] Y. Mizushima and A. Yoshikawa, Jap. Ann. Review in Electronics, Computers and Telecomm. 1982, edited by Y. Hamakawa, pp. 277-295.

[2] E. Inoue, H. Kokado and I. Shimizu, Proceedings of the 5th Conference on Solid State Devices, Tokio, 1973, Supplement to the Journal of the Japan Society of Applied Phys. Vol. 43, p. 101.

[3] B. Singh, S. P. Beaumont P. G. Bower and C. D. W. Wilkinson, Appl. Phys. Lett. 1982, 41(9), pp. 889-891.

[4] M. Vlcek, M. Frumar, M. Kubovy and V. Nevsimalova, in the Proc. of 14. ICAS 1991, in press.

[5] Y. Utsugi and S. Zembutsu, Appl. Physics Letters, 1975, Vol. 27, No. 9, pp.508-509.

[6] B. Singh, S. Rajagopalan and K. L. Chopra, J. Appl. Physics, 1980, 51(3), pp. 1768-1772.

[7] A. G. Poleshchuk, E. G. Churin and Y. I. Yurlov, Journal of Imaging Science, 1986, Vol. 30, No. 3, pp.132-135.

[8] M. S. Chang, T. W. Hou, J. T. Chen, K. D. Kolwicz and J. N. Zemmel, J. Vac. Sci. Technol. 1979, 16(6), pp. 1973-1976.

[9] K. Kase, G. C. Chern and I. Lauks, Thin Solid Films, 1984, 116, L53-L54.

[10] B. Singh, G. C. Chern and I. Lauks, J. Vac. Sci. Technol. 1985, B3(1), pp. 327-330.

[11] R. E. Belford, E. Hajto and A. E. Owen, Thin Solid Films, 1989, 173, pp. 129-137.

[12] R. G. Poulsen, J. Vac. Sci. Technol. 1977, Vol. 14, No. 1, pp. 266-274.

CHAPTER 8

DIFFRACTION GRATING PREPARATION IN SPIN-COATED As-S FILMS

The high transparency of chalcogenide glasses in the infrared part of the optical spectrum enables these materials to be employed in the fabrication of various optical elements to be used in a broad spectral region [1]. In addition to their good transmission in the infrared, chalcogenide glasses exhibit light-induced effects which can be used to produce microstructures in these films [2, 3].

In previous chapters it was shown that the basic optical properties of the spin-coated As-S films are very similar to those of films prepared by vacuum-evaporation. It was also shown how the optical properties change as a result of silver photodissolution. In Chapter 4 it was seen that photodissolution of Ag causes the characteristic vibration band in the far-infrared region to shift from 310 cm^{-1} to 340 cm^{-1}. In the visible part of the spectrum (discussed in Chapter 5) the absorption edge of the Ag-doped spin-coated As–S film is shifted to smaller energies after silver photodissolution. It was shown that Ag-doped spin-coated As-S films, similarly to vacuum-evaporated films with the same composition, are highly transparent between these two regions of absorption. The loss (i.e. the lower transmittance) in this "window" is due to the reflectance. Chapter 7 showed that the CF_4 plasma is a suitable selective etchant for the fabrication of surface-relief structures in spin-coated As-S films, subsequent to the silver photodissolution process.

Very few materials have similar high transparency over such a broad region of the spectrum along with a range of light-induced effects which enable them to be easily patterned. Patterning spin-coated As-S films using the photodissolution of Ag could therefore be used in principle to produce diffractive optical elements. Spin-coating is a common technique for depositing materials such as dichromated gelatin, which are

used to produce diffractive optical elements for visible operation. This chapter describes how diffraction gratings can be prepared in chalcogenide films deposited by the same technique. The preparation of Ag / spin-coated As-S double layer systems is described in Section 3.7. Grating patterns were generated in the samples by silver photodissolution using a holographic illumination arrangement, detailed also in Section 3.7.

8.1 DIFFRACTION GRATING FORMATION IN SPIN-COATED As-S FILMS BASED ON THE Ag PHOTO-DISSOLUTION EFFECT

Figure 8.1 shows the basic steps required to produce surface relief gratings in a spin-coated $As_{40}S_{60}$ film using the silver photodissolution effect and subsequent selective etching.

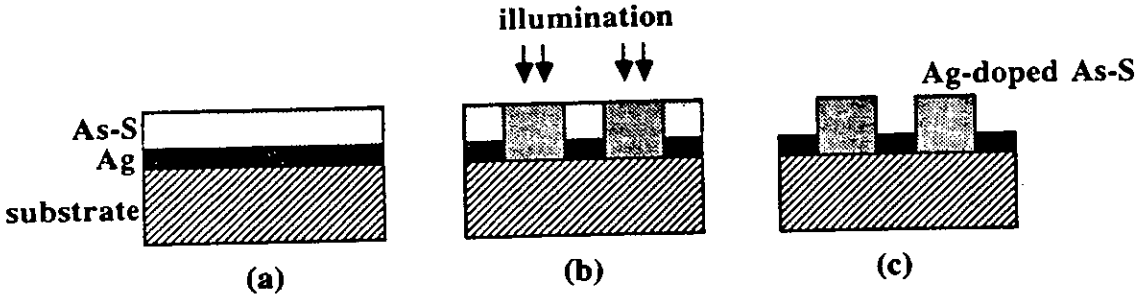

Figure 8.1 Schematic illustration of the sample structure and the principal steps in the formation of a surface relief grating in an $As_{40}S_{60}$ film using the Ag photodissolution effect.

When the $Ag/As_{40}S_{60}$ double layer structure, (a), is illuminated with the appropriate intensity pattern, (b), the silver layer diffuses into the structure of the $As_{40}S_{60}$ film in the illuminated areas changing their physical and chemical properties. After illumination, a suitable etchant can be applied for developing the surface relief pattern by removing the undoped part of the chalcogenide film, leaving the Ag-doped part unchanged (c).

In the present study the silver photodissolution was induced by using a holographic illumination arrangement. In this experiment the simplest form of interference grating was produced in which the samples were exposed to a sinusoidal intensity pattern generated by two interfering beams of light. An Argon-ion laser was used for illumination, operating at a single wavelength of $\lambda=0.5145$ μm. For the experiment a new type of holographic illumination arrangement was devised which provided more stable illumination conditions for the relatively long illumination time required for the Ag-diffusion. Instead of the usual holographic arrangement, involving beam splitter and mirrors, a prism was used to divide the beam into two parts with the same intensity and deflect them onto the surface of the sample.

The grating period which can be produced in a light sensitive material by holographic illumination [4] is determined only by the wavelength and the angle of incidence of the illuminating light, as described by Equation 24 in Section 3.7. In the present project the grating period was changed by altering the angle of incidence of the illuminating beams. The wavelength of the light was fixed at $\lambda=0.5145$ μm and the angle of incidence was changed by using prisms with different apex angles. Two prisms were available, the first provided an angle of incidence of $\theta=20^{o}$ and the second an angle of incidence of $\theta=0.7^{o}$.

Figure 8.2 is a SEM micrograph of a surface relief grating produced by the silver photodissolution in a spin-coated $As_{40}S_{60}$ film and subsequent selective etching using a CF_4 plasma. In this experiment the sample was illuminated through the prism which provided an angle of incidence of $\theta=20^{o}$. According to Equation 24 in Section 3.7, this illumination arrangement should produce a standing wave interference pattern with the distance between the neighbouring interference maxima (the grating period, Λ) $\sim$0.76 μm. The SEM micrograph in Figure 8.2 shows that the period of the standing wave pattern reproduced in the film as a surface relief grating after selective etching, is in good agreement with the calculated value. The applied laser power was 13.5 mW

and the illuminated area was 1.84 cm^2, resulting in a laser power density of $7.34x10^{-3}$ Wcm^{-2}. The duration of the illumination was 10 min, giving an illumination energy of 4.4 Jcm^{-2}. At this illumination energy the silver diffused to a depth of ~ 0.6 μm, as can be estimated from the grating profile shown in Figure 8.3, which is a SEM micrograph of a grating prepared in the same way, but in this case the photograph was taken in a tilted position with an angle close to 90^o with respect to the normal to the grating plane. Since the groove profile is basically a sine wave, it can be concluded that the silver diffusion depth, which determines the profile of the surface relief grating, is governed primarily by the light intensity profile.

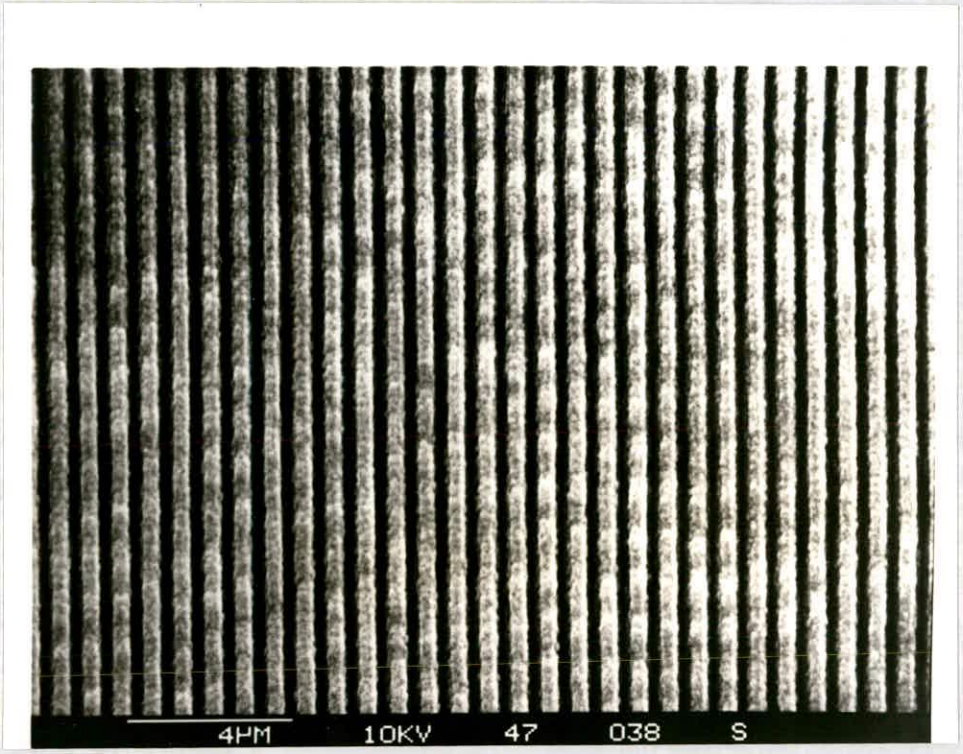

Figure 8.2 SEM micrograph of a holographic diffraction grating produced in a spin-coated $As_{40}S_{60}$ film.

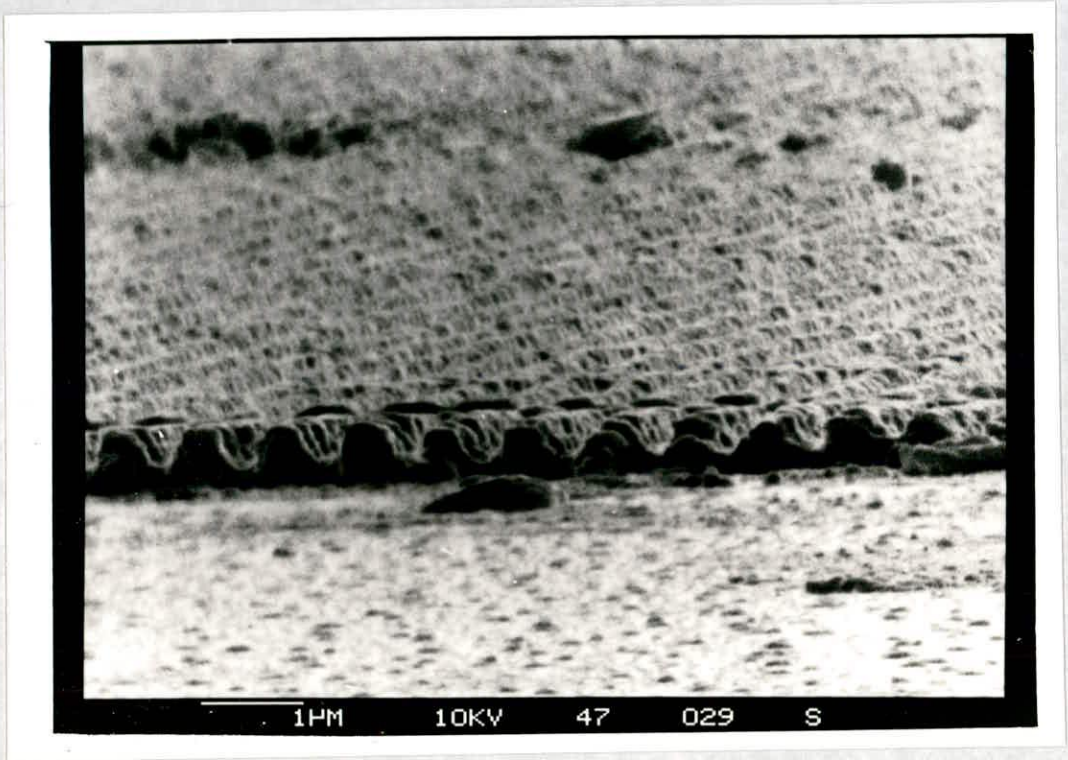

Figure 8.3 SEM micrograph of the profile of a holographic grating with a grating period of ~0.76 μm.

Figure 8.4 shows a SEM micrograph of one of the best quality gratings obtained in a spin-coated $As_{40}S_{60}$ film using the silver photodissolution effect. The 0.76 μm grating period recorded in the film gives a resolution of 1428 line/mm. The surface of the grating is smooth, all lines are parallel, straight, and equispaced, showing that the disturbing multiple interference effects apparent in Figure 8.3 can be eliminated by improving the stability of the optical arrangement.

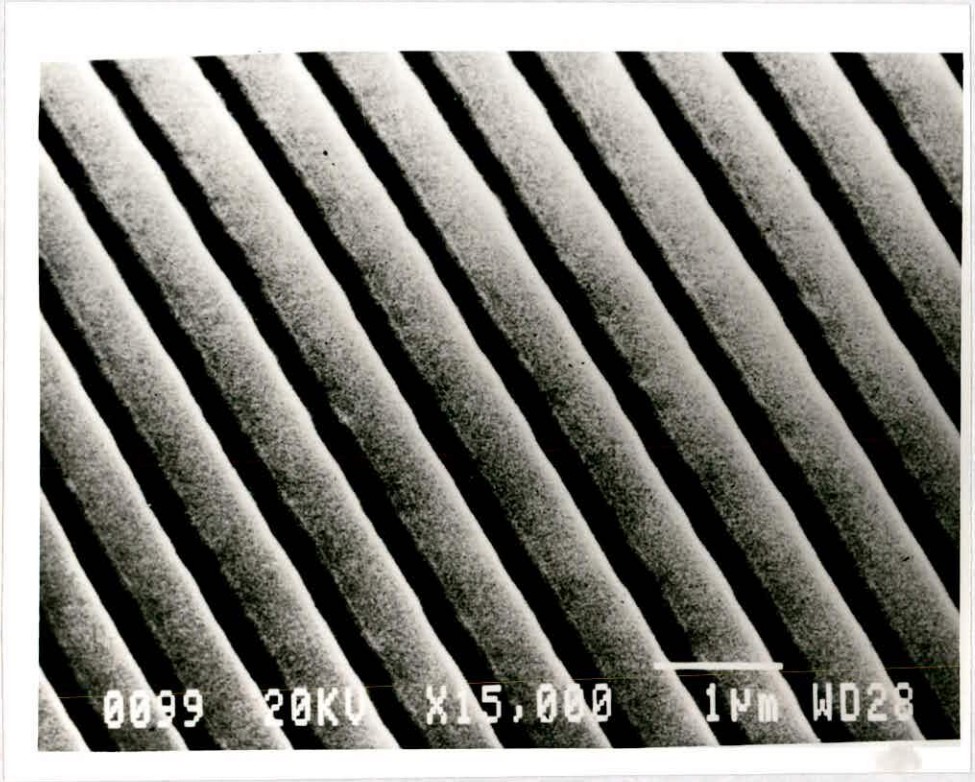

Figure 8.4 SEM micrograph of a holographic diffraction grating with a grating period of ~0.76 μm.

The period of the recorded fringes was increased by using a smaller angle of incidence for illumination with the same wavelength. This was achieved by using a different prism which provided an angle of incidence of $\theta = 0.7^{o}$ for the two intersecting beams. This resulted in a grating period of $\Lambda \sim 22$ μm as seen in Figure 8.5.

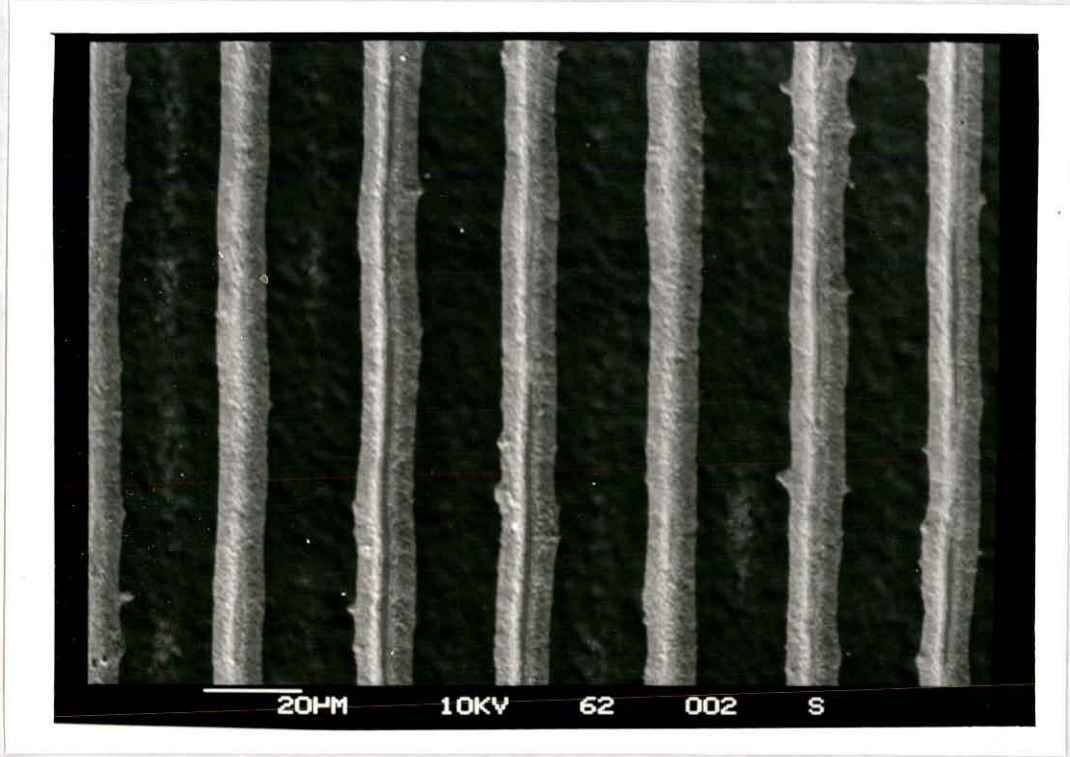

Figure 8.5 SEM micrograph of a surface relief grating with a grating period of $\Lambda = 22$ μm.

8.2 PERFORMANCE OF THE DIFFRACTION GRATINGS

The diffraction gratings, produced in spin-coated As-S films by the improved holographic arrangement, were assessed for their performance. The main features of diffraction gratings which determine their performance are: resolving power, spectral purity and diffraction efficiency [5].

8.2.1 Resolving power

The resolving power of a diffraction grating is its ability to separate two close neighbouring spectral lines. This is determined primarily by the total number of grooves on the grating and hence by the grating period and the area of the grating [6]. The period of a holographic grating can vary over a wide range and depends on the illuminating light wavelength and the angle of incidence used when exposing the photosensitive film. The finest grating period achieved in the experiments described above was $\Lambda = 0.76$ μm due to the limitation of the instrumentation. This is neither the final resolution of the holographic illumination technique nor of the material itself. In Section 3.7. it was stated that in practice 0.6λ resolution can be achieved without difficulty, λ being the illumination wavelength; this occurs when the angle of incidence $\theta = 60^{o}$. This illumination arrangement would have resulted in a grating period of $\Lambda = 0.268$ μm using illumination of wavelength $\lambda = 0.4658$ μm (calculated with Equation 24 in Section 3.7.) The necessary equipment to test this arrangement was not available. The highest resolution achieved in the amorphous As-S system using the silver photodissolution effect was the 30 nm wide linear gaps fabricated in evaporated As_2S_3 doped from a chemically deposited Ag_2S film, using electron beam exposure [7].

The final resolving power of a diffraction grating, R_g, is given by [6]:

$$R_g = \frac{\lambda'}{\Delta\lambda'} = mN \qquad (1)$$

where λ' and $\Delta\lambda'$ are the wavelengths of the spectral lines which can be separated, m is

the diffraction order number and N is the total number of lines in the grating. The surface relief grating shown in Figure 8.4 has a line density of 1428 lines mm^{-1} with a useful area 15 mm long, giving a total number of lines N=21420. This implies the smallest wavelength difference in the first diffracted order (m=1) which can be resolved is $\Delta\lambda' = 2.9 \times 10^{-5}$ μm at $\lambda' = 0.6328$ μm.

8.2.2 Spectral purity

Another parameter describing the quality of a diffraction grating is spectral purity. An ideal grating diffracts light only into the angles determined by the grating equation [5]:

$$\Lambda(\sin\alpha + \sin\beta) = M\lambda \qquad (2)$$

where Λ is the grating period, α and β are the angles of incidence and diffraction, M is the order number and λ is the wavelength of the incident light. Any light which is observed between the main diffracted orders constitutes spectral impurity and arises from defects in the grating. The prepared holographic grating with a period of $\Lambda = 0.76$ μm was tested as a reflection grating using a low intensity (2 mW) He-Ne laser with a wavelength of $\lambda = 0.6328$ μm. It was found that if the measuring light is used at normal incidence relative to the grating plane, the diffracted beams exit the surface at angles of $\beta = \pm 56^{o}$. There were no other diffracted orders observed in this measuring configuration, and the symmetry of the diffracted angles suggests a symmetrical groove profile, which is in good accordance with the SEM micrograph of Figure 8.3 showing the profile of the diffraction grating.

The grating period can also be determined from the grating equation using the measured angles of incidence and diffraction. Taking the angle of incidence $\alpha = 0^{o}$, the angle of diffraction $\beta = 56^{o}$, and the wavelength of the measuring light $\lambda = 0.6328$ μm, a grating period of $\Lambda = 0.76$ μm can be calculated, which again is in good agreement with the SEM micrographs of the surface relief gratings seen in Figures 8.2 and 8.3.

8.2.3 Diffraction efficiency

Another important grating parameter which determines its performance is the diffraction efficiency. The efficiency of a diffraction grating is defined as the fraction of the incident radiation that is diffracted into the required order. For the reflection grating the diffraction efficiency is determined by the properties of the surface (the reflectance of the surface or the surface coating) and the groove profile. For these measurements the sample was covered with a thin aluminium layer in order to increase its reflectance. The efficiency in this case is determined primarily by the groove profile.

If the grating is illuminated at normal incidence with respect to the surface of the grating, the diffraction efficiency cannot be higher than 50% in any diffraction order because of the symmetry. In practice the efficiency seldom exceeds 33% in this configuration [8]. The diffraction efficiency of the holographic grating prepared with a grating period of $\Lambda = 0.76$ μm was measured at normal incidence using a 2 mW He-Ne laser operating at $\lambda = 0.6328$ μm. Figure 8.6 shows that ~18% efficiency was measured at the ± 1 diffraction orders, at $\beta = \pm 56^{o}$ diffraction angles, indicating that the profile of the surface relief grating is symmetrical and close to the "ideal" sinusoidal profile as seen in Figure 8.3. Similar diffraction efficiencies have been reported for the best holographic gratings produced in a vacuum-evaporated chalcogenide / silver double layer system [9].

8.2.4 Q parameter

The surface relief gratings prepared in this way are considered as thin holographic gratings. The distinction between thick and thin holographic gratings is usually made with the aid of the Q-parameter [10] defined as:

$$Q = 2\pi\lambda d / (n\Lambda^2) \qquad (3)$$

where λ is the illuminating wavelength, n is the refractive index of the material, d is

the film thickness and Λ is the spacing of the recorded interference fringes (grating period). The holographic grating is considered thick when $Q \geq 10$ and thin otherwise. In the case of the first sample, where a grating period of $\Lambda = 0.76\ \mu m$ was produced, a value $Q_1 = 1.47$ is obtained using the experimentally determined parameters of $\lambda = 0.6328\ \mu m$, $n = 2.8$, $d = 0.6\ \mu m$ and $\Lambda = 0.76\ \mu m$. In the case of the second sample (grating period $\Lambda = 22\ \mu m$ as seen in Figure 8.5), a value of $Q_2 = 2.64 \times 10^{-3}$ is obtained. Therefore the gratings produced in the experiments described above are of the thin type.

8.2.5 Mechanism of the diffraction

Holographic gratings are also classified according to the mechanism by which the illuminating light is diffracted. In the phase grating a phase modulation occurs when the illuminating wave passes through the film. In the amplitude grating, the recorded interference pattern acts as a density variation of the recording medium and the amplitude of the illuminating wave is modulated.

Generally the change in the phase, $\Delta\phi$, is given by [11]:

$$\Delta\phi = \frac{2\pi}{\lambda}\Delta n + (n-1)\Delta d \qquad (4)$$

where λ is the wavelength of the illuminating light, d is the thickness of the grating, n is the refractive index of the grating material, Δd and Δn are the thickness and the refractive index variations in the grating. Therefore phase modulation can be achieved either by having a periodically changing refractive index across the grating or by producing a periodic thickness variation in the film. In the present work diffraction gratings were obtained using the silver photodissolution followed by selective etching. This process resulted in a sinusoidal variation of the film thickness, but the refractive index of the silver doped film was constant across the grating. Therefore the phase change, $\Delta\phi$, in the case of the surface relief grating can be given by:

$$\Delta\phi = \frac{2\pi}{\lambda} (n-1)\, \Delta d \qquad (5)$$

where λ is the wavelength of the illuminating light, n is the refraction index of the grating material and Δd is the depth of the profile in the surface relief grating. Using the experimentally determined values of $\lambda = 0.6328$ μm, $n = 2.8$ (at the given wavelength), $\Delta d = 0.6$ μm, a phase difference of $\Delta\phi = 1.4\pi$ is obtained. It can also be seen that this phase shift is primarily determined by the depth of the profile of the surface relief grating, therefore different phase modulations can be achieved by varying the intensity and/or time of illumination in order to alter Δd.

Phase modulation occurs when the grating is illuminated with wavelengths which have negligible absorption in the grating material. If the absorption of the material is larger than zero, amplitude modulation occurs [12]. In the amplitude grating the ratio of the transmissivities (t_1/t_2) of the two halves (the two different thickness d_1, d_2 in the profile) of the surface relief grating can be approximated by:

$$t_1/t_2 = \exp -\alpha(d_2 - d_1) \qquad (6)$$

where α is the absorption coefficient of the Ag-doped layer. Using the experimentally determined values of: $d_1 = 1$ μm, $d_2 = 0.4$ μm for the two halves of the prepared surface relief grating, a ratio of 1.33 can be obtained for $\lambda = 0.6328$ μm illuminating light. However, due to the exponentially rising absorption edge in this spectral region (discussed in Section 5.2.2) the amplitude modulation increases when shorter wavelength light is used. For example, using the $\lambda = 0.4658$ μm light of the Ar-ion laser a transmissivity ratio of $t_1 / t_2 = 4 \times 10^2$ can be obtained for the same surface relief grating because the absorption coefficient of the Ag-doped $As_{40}S_{60}$ film at the given wavelength is $\alpha = 10^5$ cm^{-1}.

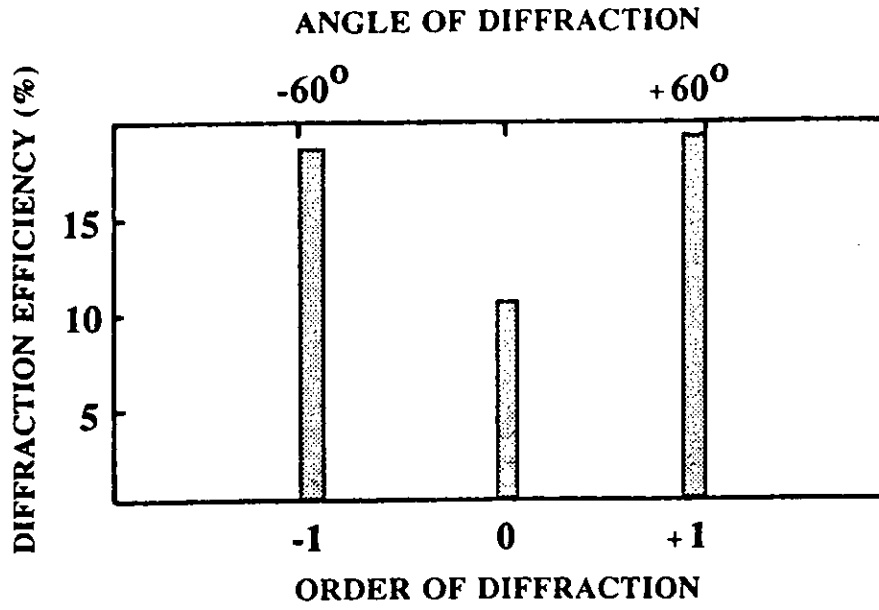

Figure 8.6 Diffraction efficiency of the holographic grating prepared in a spin-coated $As_{40}S_{60}$ film ($\Lambda = 0.76$ μm), measured at normal incidence.

8.3 SUMMARY OF THE RESULTS OBTAINED ON DIFFRACTION GRATING PREPARATION

The optical constants and the solubility of spin-coated As-S films change significantly after silver is incorporated into the film by photodissolution. The Ag / spin-coated $As_{40}S_{60}$ sample structures were illuminated with a spatially periodic intensity pattern using a holographic illumination arrangement. Instead of the usual holographic arrangement where beam splitter and mirrors are used to divide and to deflect the beams, in this project prisms have been used in order to increase the stability of the illumination system. Interference gratings were prepared with 0.76 μm and 22.0 μm grating periods by varying the angle of incidence of the illuminating light. Subsequent to the illumination, the grating patterns were developed by selective etching, using CF_4 plasma. This process resulted in surface relief type diffraction gratings.

The quality and the performance of the prepared diffraction gratings were assessed using different techniques. The morphology of the surface relief gratings have been studied by scanning electron microscopy. It was found that using equal writing beam intensities, the profile of the gratings were sinusoidal, suggesting that the silver diffusion depth is determined primarily by the light intensity profile. The performance of the prepared surface relief gratings was determined from their resolving power, spectral purity and diffraction efficiency. The measured grating periods, diffraction angles, and the diffraction efficiency were found in good accordance with the theoretical values. It was shown that the observed changes in the optical constants of the spin-coated As-S films as a result of Ag photodissolution enable the material to modulate the phase and the amplitude of the light, hence the recording of amplitude or phase holograms in Ag / spin-coated As-S sample structures is possible.

8.4 REFERENCES

[1] A. M. Andriesh, V. V. Ponomar, V. L. Smirnov and A. V. Mironos, Sov. J. Quantum Electron, 1986, 16(6), pp. 721-736.

[2] Y. Mizushima and A. Yoshikawa, "Japan Annual Reviews in Electronic, Computers and Telecommunications", 1982, edited by Y. Hamakava, pp. 277-295.

[3] K. D. Kolwicz and M. S. Chang, J. Electrochem. Soc. 1980, Vol. 127, No. 1, pp. 135-138.

[4] M. C. Hutley, "Diffraction Gratings", Academic Press, London, 1982, p. 18.

[5] M. C. Hutley, Journal of Physics E: Scientific Instr. 1976, Vol. 9, pp. 513-520.

[6] A. Sommerfeld, "Optics" Academic Press, 1954, p. 228.

[7] B. Singh, S. P. Beaumont, P. G. Bower and C. D. W. Wilkinson, Appl. Phys. Lett. 1982, 41(9), pp. 889-891.

[8] M. C. Hutley, "Diffraction Gratings", Academic Press, London, 1982, p. 109.

[9] T. Fukaya, S. Matsuma, J. Tsujiuchi, E. Inoue and H. Kokado, Opt. Commun. 1973, 7. pp. 98-102.

[10] H. M. Smith, Topics in Applied Physics, 1977 Vol. 20 Holographic Recording Materials, Springer-Verlag, Berlin.

[11] H. M. Smith, "Holographic Recording Materials", 1977, Springer, Berlin, p. 5.

[12] A. Sommerfeld, "Optics" Academic Press, 1954, p. 229.

CHAPTER 9

CONCLUSIONS

The deposition of chalcogenide films from their solutions by the spin-coating technique is important not only from the point of view of chemistry (there was very little known about the possible dissolution of arsenic chalcogenides in solvents of the homologous series $R-NH_2$ [1]), but also because it offers a new possibility for preparing the technologically useful chalcogenide thin films more easily. The spin-coating technique seems a more suitable method of deposition to obtain thin films of chalcogenides for applications such as high resolution lithography (using these films as X-ray-, electron- or ion-beam resists), and optical imaging, including holographic recording.

In this study the optimal deposition and annealing conditions were established for preparing different compositions of As-S films from solutions, with reproducible properties. The structure of the spin-coated films was investigated by IR spectroscopy, and their optical properties were analysed and compared with those of vacuum-evaporated films of the same composition. The kinetics of silver photodissolution in spin-coated $As_{40}S_{60}$ films was also investigated and the sensitivity of the effect determined. Finally, using the silver photodissolution process and subsequent dry development, surface relief gratings with different grating periods were produced in spin-coated $As_{40}S_{60}$ films by employing a holographic illumination arrangement.

9.1 COMPOSITION AND STRUCTURE OF SPIN-COATED As-S FILMS

Although the techniques of vacuum-evaporation or sputtering offer clean conditions to obtain thin films of chalcogenides, it has been reported that they

generally result in a composition, morphology and microstructure that are difficult to control [1]. In contrast, it has been claimed that chalcogenide films can be prepared with controlled stoichiometry using the spin-coating deposition technique [1]. In the present work spin-coated As-S films were successfully deposited from solutions prepared with propylamine in a broad thickness range (0.02-6 μm, depending on the concentration of the solution, the spinning time and rate). Examination by optical and scanning electron microscopy showed the films to be continuous, uniform and free of microstructure. The spin-coating technique involves various processes (e.g. dissolution, drying) which might affect the composition of the deposited films, therefore it was important to determine the actual composition of the deposited films compared to the source materials. A wide composition range of spin-coated As-S films was analysed using wavelength dispersive X-ray microprobe analysis, and it was found that in most cases the film composition deviated from that of the bulk glass within only 1 at. %. A larger deviation of ~4 at. % was found only in the case of spin-coated $As_{25}S_{75}$ and this was attributed to some sulphur loss occurring during annealing.

It was also found that the as-deposited spin-coated films contain solvent residue, which can affect the physical and chemical properties of the films. Although propylamine is volatile at atmospheric pressure (its boiling point is 48° C), the middle- to far-IR absorption spectra showed that drying the films during spinning at room temperature is not sufficient to totally remove the solvent. Annealing at 160° C for 1 hour produced nearly solvent-free spin-coated As-S films.

In the present study, the structure of the spin-coated As-S films was investigated using IR spectroscopy. It has been established in previous studies that the short range order in the structure of bulk As-S glass and annealed vacuum-evaporated films is essentially the same as that in the crystalline network [2, 3]. It was shown that the characteristic IR active lattice vibration can be found at 310 cm^{-1} and this was assigned to an intramolecular bond stretching mode of the AsS_3 "molecular" units in the structure [4]. In the present work the extreme far-IR spectra of the annealed spin-coated As-S films were also found to be dominated by an absorption band at 310 cm^{-1}. In addition to this band, another absorption band was observed in the spectra of the as-deposited films at 420 cm^{-1}, which is not a characteristic vibration of the propylamine molecules. From the observation that the magnitude of this absorption band was dependent on the temperature and the duration of annealing, and also that it was observed in the spectra of spin-coated sulphur films, it was concluded that this absorption band can be associated with the bond formed between the solvent molecules

and the sulphur atoms of the AsS_3 structural units during dissolution.

It was also observed that UV illumination causes the main absorption band at 310 cm^{-1} to split resulting in the appearance of the 340 cm^{-1} absorption peak, which can be eliminated by annealing. This change in the spectrum was associated with the irreversible structural changes which occur in the amorphous $As_{40}S_{60}$ film under illumination [5].

Silver photodissolution in spin-coated $As_{33}S_{67}$ caused the main absorption band to shift from 310 cm^{-1} to 340 cm^{-1}. A similar change in the Raman spectra of vacuum-evaporated $As_{40}S_{60}$ films was observed as a result of silver photodissolution, and was found to be characteristic of crystalline Ag_3AsS_3 [5, 6]. It was concluded that the structure of the Ag-doped spin-coated As-S films prepared in this work was similar to that of films prepared by vacuum-evaporation. The shift of the main absorption band, as a result of silver photodissolution, was attributed to the possible linking of the AsS_3 structural units of the spin-coated film by the silver atoms.

Analysis of the infrared spectra provided information about the mechanism of the dissolution process of As-S glass in propylamine. Middle- to far-infrared spectra indicated that the amine group in the propylamine molecule plays a significant role in the dissolving process. A broad absorption band, characteristic of amine salts, was observed in the spectra of freshly deposited spin-coated As-S films, while the characteristic bands for aliphatic C-H stretching and bending vibrations remained unchanged. Extreme far-infrared spectra showed that the solvent / chalcogenide interaction occurs at the S sites of the AsS_3 structural units of the chalcogenide.

9.2 OPTICAL PROPERTIES OF SPIN-COATED As-S FILMS

As-S glasses are well known for their high transparency over a broad band of the optical spectrum [7]. This property makes these materials suitable for the fabrication of optical elements for use in their low absorption spectral region [7, 8]. Very few materials have similar optical properties and also exhibit light-induced effects which can be used to pattern their thin films. The modelling of the applications of these

materials and also the interpretation of the kinetics data require a knowledge of the optical constants (refractive index, n, and absorption coefficient, α) of spin-coated As-S films. Comparison of the optical constants of spin-coated films with those of the vacuum-evaporated material also provides some information on the purity and the possible structure of the films. The optical absorption edge of the spin-coated films also yields information on the absorbing region of the spectrum, which has an influence on the silver photodissolution process in the films.

The dispersion of the refractive index of spin-coated As-S films was determined from their transmittance spectra using the method suggested by Swanepoel et al. [9]. It was found that the refractive index of spin-coated As-S films is constant in the infrared region ($\sim$1 μm-10 μm), but in the shorter wavelength region it increases due to the onset of optical absorption. The refractive index dispersion curves had the same shape for all compositions but they were displaced to higher values with increasing As content. In general, the refractive index dispersion for the spin-coated As-S films was found to be the same as that for the vacuum-evaporated films but slightly lower n values were obtained for the spin-coated As-S films (n=2.14 for spin-coated $As_{40}S_{60}$ and n=2.32 for vacuum-evaporated $As_{40}S_{60}$ films [10] measured at λ=1 μm). This result indicates that the densities of spin-coated As-S films might be smaller than those of the vacuum-evaporated films.

The refractive index data in the transparent region were fitted with the single oscillator expression, and the oscillator energy, E_o, and the oscillator dispersion energy, E_d, for different compositions of spin-coated As-S films were determined. It was found that E_o decreases and E_d increases with increasing As content. These compositional dependences can be explained by the fact that the E_o is determined primarily by the chemical bonding energies, but E_d is determined mainly by the valency and coordination number of the constituent atoms. At the stoichiometric composition of $As_{40}S_{60}$ the structure is dominated by threefold coordinated AsS_3 pyramidal units. In the sulphur rich compositions extra twofold coordinated S atoms are incorporated probably between the AsS_3 structural units in chain-like form and creats S-S homobonds with higher bond strength thus decreasing the average coordination and increasing the chemical bond strength of the network. Experimental results also showed that slightly higher E_o and lower E_d values were obtained for spin-coated As-S films compared with those for the vacuum-evaporated films of the same composition [11].

The β value (which is a parameter describing the type of chemical bond in the solid and is calculated from E_d) for different compositions of spin-coated As-S films yielded "covalent" values. It was also found that the value of β decreases with decreasing As content indicating that beside the AsS_3 "molecular" units, other, differently coordinated structural units are present in the structure of the spin-coated films. It was found that the E_g values were approximately half of the corresponding optical gap energy, E_g, values in the case of spin-coated As-S films.

The refractive index dispersion for the Ag-doped spin-coated $As_{40}S_{60}$ film was found to be similar to that obtained for the undoped films but displaced to higher values (n=2.19 and n=2.74 for undoped and Ag-doped spin-coated $As_{40}S_{60}$ films respectively, measured at $\lambda=1$ μm). The increase of refractive index as a result of silver photodissolution was found to be less than calculated from the additive law, suggesting a compound formation rather than alloying. It was also found that E_o decreased and E_d increased after silver photodissolution.

The absorption coefficient values for the undoped and Ag-doped spin-coated $As_{40}S_{60}$ films were determined near the optical absorption edge. The $\alpha(\lambda)$ values were calculated from the transmittance and the reflectance spectra of the films, using the method suggested by Ticha et al. [12]. The absorption edges of spin-coated As-S films with different compositions were determined and were found to rise exponentially with increasing photon energy as in the case of vacuum-evaporated As-S films, although the exponential region was restricted to a smaller energy range and the slopes obtained were smaller (~9 eV^{-1} for spin-coated $As_{40}S_{60}$) than the slope reported for vacuum-evaporated films of the same composition (~19 eV^{-1} [13]). The shape of the absorption edge at low absorption constant values, and the smaller slopes of the absorption edges for different compositions of spin-coated As-S films are consistent with the structural differences of the films.

In the higher energy part of the spectrum the measured absorption coefficient was found to be linearly proportional to the square of the photon energy and the value of the optical energy gap, E_g, was obtained for different compositions of the spin-coated As-S films. It was found that E_g decreases with increasing As content. The compositional dependence of E_g measured for spin-coated As-S films was explained by the effect of different bond strengths for the As-As, As-S and S-S bonds in the structure. Experimental results also showed that silver photodissolution decreases the

value of E_g in the case of spin-coated $As_{40}S_{60}$ from 2.3 eV to 2.19 eV for a doping level of ~22 at. % Ag indicating more "metallic" like properties for silver-doped spin-coated As-S films. This result is in good accordance with the electrical conductivity measurements on bulk silver-doped As-S glasses [14, 15].

9.3 KINETICS OF SILVER PHOTODISSOLUTION IN SPIN-COATED As-S FILMS

The kinetics of silver photodissolution in chalcogenide films have been widely studied in order to obtain a better understanding of the process and also to investigate the sensitivity of these systems for imaging applications. Various measuring techniques have been reported for obtaining information on the kinetics of silver photodissolution (e.g. electrical [16] or optical [17, 18]). In this study the reflectivity and transmissivity changes in the sample were monitored simultaneously during photodissolution for the first time and the time dependence and sensitivity of the process to the illumination wavelength and to the number of incident photons were determined.

It was found that the rate of the silver photodissolution process in spin-coated $As_{40}S_{60}$ films is not constant. The thickness of the undoped chalcogenide layer was found to decrease linearly with the square root of the exposure time (at a fixed incident intensity and wavelength). This result is in good accordance with results reported earlier for spin-coated As-S films, but obtained using a different measuring technique [19]. Similar time dependence has also been reported for the silver photodissolution process in vacuum-evaporated As-S films [20]. This type of time dependence for the silver photodissolution was explained by a diffusion controlled reaction rate, as the process involves the movement of Ag^+ ions and electrons through the host chalcogenide layer [22]. The overall form of the silver photodissolution reaction (which consists of three stages) in spin-coated films was found to be the same as that observed in vacuum-evaporated films [16], suggesting a similar type of process in both cases. Experimental results showed that in the case of spin-coated $As_{40}S_{60}$ films the length of the induction period is inversely proportional to the illumination intensity.

The rate of decrease of the spin-coated chalcogenide layer thickness and the rate of photodissolution of the silver were both found to be linearly dependent on the illumination intensity (at constant wavelength), suggesting a monomolecular photochemical reaction for the process [21]. This indicates that one photon is needed to produce one Ag^+ ion at the metal / chalcogenide interface.

On the other hand, the sensitivity of the photodissolution process (that is, the speed at which the silver layer is consumed under illumination) was found to increase if more energetic photons are used to induce the process. All of the illumination energies used in these experiments were equally highly absorbed in the silver layer and they were also in the absorption edge region for the spin-coated As-S films. From the fact that the sensitivity curves were displaced to different energy values depending on the incident wavelength, it can be concluded that the role of illumination is not only to produce Ag^+ ions from the silver layer; light absorption in the As-S film (possibly through the excitation of the chalcogen atoms) is also important for the silver photodissolution process. Similar considerations were applied in the recent theoretical models explaining the mechanism of the silver photodissolution process [22, 23].

Comparison of the photodissolution sensitivity in terms of the number of incident photons shows that the spin-coated films are less sensitive (by a factor of $\sim$10) to actinic radiation than vacuum-evaporated films of the same composition [16]. This is possibly due to differences in the structure of the chalcogenide films prepared by the different deposition techniques (as discussed in Chapters 4 and 5).

9.4 ETCHING PROPERTIES OF SPIN-COATED As-S FILMS

A knowledge of the etching properties of the As-S films deposited by the spin-coating technique is of technological importance since it affects the use of such films as lithographic materials or the recording of surface relief type images in the film. A different etch rate has been reported for the exposed and unexposed areas of vacuum-evaporated As-S films using either wet chemical etching (using, for example, NH_4OH or NaOH solutions [24, 25]) or plasma etching (using, for example, CF_4 or SF_6 plasmas [26]). It was also reported that the Ag-doped As-S film is not soluble in these

chemicals [24, 27]. The etching rate of spin-coated $As_{40}S_{60}$ has been compared with that of the organic photoresists in SF_6+O_2 plasma, and a spin-coated chalcogenide film was used as a barrier layer in a high resolution trilayer resist system [28]. Spin-coated As_2S_3 films, deposited from ethylenediamine, have been removed by plasma etching using CF_4 gas [29].

In this study the etching properties of spin-coated $As_{40}S_{60}$ films, deposited from solutions prepared with propylamine, were investigated using CF_4 plasma as the etchant. It was found that the films exposed to UV illumination had an etch rate faster by a factor of 2.6 compared to that of the unexposed material. The thickness of Ag-doped spin-coated $As_{40}S_{60}$ films remained unchanged in the CF_4 plasma. Using the light-induced differential etch rate, a surface relief grating was prepared in spin-coated $As_{40}S_{60}$.

9.5 DIFFRACTION GRATING PREPARATION IN SPIN-COATED As-S FILMS

The optical constants and the solubility of As-S films change significantly after silver is incorporated into the structure by photodissolution. These changes are the basis of the reported applications of As-S films as holographic recording materials [7] or as high resolution inorganic resists [23].

In this work surface relief diffraction gratings were prepared in spin-coated $As_{40}S_{60}$ films using selective etching subsequent to silver photodissolution. The spin-coated $As_{40}S_{60}$ / Ag sample structures were illuminated with a spatially periodic intensity pattern using a holographic illumination arrangement. A new type of arrangement was developed to improve the stability of the illumination system. Interference gratings were prepared with 0.76 μm and 22.0 μm grating periods by varying the angles of incidence of the illuminating beams while the illumination wavelength was fixed at $\lambda=0.5145$ μm.

The quality and performance of the diffraction gratings prepared were assessed using different techniques. The morphology of the surface relief gratings was studied by scanning electron microscopy. The performance of the gratings was evaluated from

their resolving power, spectral purity and diffraction efficiency. The measured values were found to be in good agreement with the theoretical values. The diffraction efficiency achieved with the gratings prepared in spin-coated films was similar to that reported for the gratings prepared in vacuum-evaporated samples [30, 31].

It was shown that the observed changes in the optical constants (refractive index and absorption coefficient) of the spin-coated As-S films as a result of silver photodissolution enables the material to modulate the phase and the amplitude of the light, thereby allowing the recording of amplitude or phase holograms.

9.6 SUGGESTIONS FOR FUTURE WORK

The applications of chalcogenide glasses for different optical elements and also for VLSI lithography are mainly based on patterning thin films of these materials using the metal photodissolution effect, since it produces more significant changes in the properties of the chalcogenides such as the refractive index and etch resistance. For both typesof applications it is necessary to increase the speed of the photodissolution process. Further work is needed in order to improve the sensitivity of the Ag / spin-coated As-S system. This could be achieved by studying the photodissolution process in different metal / chalcogenide systems. The deposition of chalcogenides other than As-S using the spin-coating technique could be one point of interest. Another method for improving sensitivity might be the co-deposition of chalcogenides with a silver-containing compound soluble in the same solvent as the chalcogenide.

The investigation of the performance of both phase and surface relief gratings should be extended to the IR region because the chalcogenide glasses are well known for their transparency in this region. The preparation of different diffractive optical elements (for example gratings with various profiles, lenses) for use in the IR region could be another interesting research area. The long term stability of such optical elements should also be investigated in order to obtain information on any possible redistribution of silver atoms in the amorphous chalcogenide network.

The refractive index of As-S films can be varied over a wide range by changing the silver concentration of the photodissolution product. This property should be particularly useful for fabricating thin film waveguides operating either in the visible or the IR region.

The silver photodissolution process in chalcogenide glasses can also be used quite effectively in lithographic applications, because of the superior resolution of these materials compared with organic resists, due to the smaller dimensions of its structural units (only a few Angstroms). Submicron resolution was achieved in a Ag / spin-coated $As_{40}S_{60}$ structure using visible illumination [32]. The investigation of the lithographic performance of spin-coated As-S films using X-ray, e-beam or ion-beam techniques would be interesting. For these illumination techniques very thin film structures would be needed, yielding not only a very high resolution but also an improved sensitivity.

9.7 REFERENCES

[1] G. C. Chern and I. Lauks, J. Appl. Phys. 1982, Vol. 53, No. 10, pp.6979-6982.

[2] I. Cervinka, "The Structure of Non-Crystalline Materials" 1982, Edited by P. H. Gaskell, pp. 255-285.

[3] R. Zallen, "The Physics of Amorphous Solids" 1983, John Willey & Sons pp. 93.

[4] G. Lucovsky, Phys. Rew. B, 1972, Vol. 6. No. 4. pp. 1480-1489.

[5] P. J. S. Ewen, W. T. Taylor and G. L. Paul 1983, J. Phys. C, 16, 6475.

[6] A. P. Firth, P. S. Ewen and A. E. Owen "The Structure of Non-Crystalline Materials", 1982, Edited by P. H. Gaskell, Taylor & Frances Ltd, pp. 286-293.

[7] M. I. Kostyishin, E. P. Krasnojov, V. A. Makeev and G. A. Sobolev Proceeding of the Intern. Symposium of Holography, Ed. by J. C. Vienot (France 1970).

[8] C. W. Slinger, A. Zakery, P. J. S. Ewen and A. E. Owen to be published in Applied Optics.

[9] R. Swanepoel, J. Phys. E: Sci. Instrum. 1983 Vol. 16. pp. 1214-1222.

[10] P. J. S. Ewen, C. W. Slinger, A. Zakery, A. Zekak and A. E. Owen Proc. of the Int. Congress on Optical Science and Engineering, The Hague 1991 in press.

[11] K. Tanaka, Thin Solid Films 1980, 66. 271

[12] H. Ticha, L. Tichy and M. Frumar Phys. Stat. Sol. 1979 (a) 54, K163.

[13] N. F. Mott and E. A. Davis Electronic Processes in Non Crystalline Materials Clarendon Press Oxford 1979, p. 273.

[14] J. Plocharski, J. Przyluski and M. Teodorczyk, J. Non-Cryst. Solids, 1987, 93, pp. 303-310.

[15] E. Hajto, R. E. Belford, P. J. S. Ewen and A. E. Owen, in Proc. of 14th Int. Conf. on Amorphous and Liquid Semicond. 1991, in press.

[16] D. Goldschmidt and P. S. Rudman 1976, J. Non-Cryst. Solids, 22. 229.

[17] T. Kavaguchi and K. Masui 1987, Jap. J. Appl. Phys. 26, 15.

[18] A. P. Firth, P. J. S. Ewen and A. E. Owen 1985, J. of Non-Cryst. Solids 77 & 78 pp. 1153-1156.

[19] R. E. Belford, E. Hajto and A. E. Owen, 1989, Thin Solid Films, 173, pp. 129-137.

[20] P. J. S. Ewen, A. Zakery, A. P. Firth and A. E. Owen 1988 Phil. Mag. B 57. 1.

[21] R. Wayne, "Photochemistry" Butterworth London 1970, Chapt. 5.

[22] G. Kluge 1987, Phys. Stat. Sol. (a) 101, pp. 105-114.

[23] S. R. Elliott to be published in Journ. of Non-Cryst. Solids.

[24] Y. Mizushima and A. Yoshikawa Japan Annual Rew. in Electronic Computers and Telecommun. 1982, Edited by Y. Hamakava pp. 277-295.

[25] M. Vlcek, M. Frumar, M. Kubovy and V. Nevsimalova, in proceeding of 14th ICAS 1991, in press.

[26] M. S. Chang and J. T. Chen Appl. Phys. Lett. 1978, 33(10), pp. 892-895.

[27] B. Singh, S. P. Beaumont, P. G. Bower and C. D. W. Wilkinson Appl. Phys. Letters, 1982, 41(9), pp. 889-891.

[28] B Singh, G. C. Chern and I. Lauks 1984, Appl. Phys. Letters, 45(1), pp. 74-76.

[29] K. Kase G. C. Chern and I. Lauks 1984, Thin Solid Films, L53-L54.

[30] T. Fukaya, S. Matsumara, J. Tsujiuchi, E. Inoue and H. Kokado Optics Communications, 1972, Vol. 7. No. 2, pp. 98-103.

[31] Yasushi Utsugi and Sakae Zembutsu, Appl. Phys. Letters, 1975, Vol. 27, No. 9 pp. 508-509.

[32] E. Hajto, P. J. S. Ewen, R. E. Belford and A. E. Owen, 1991, Thin Solid Films, 200, pp. 229-237.

APPENDICES

LIST OF COMPUTER PROGRAM

FOR CALCULATION OF OPTICAL CONSTANTS

```
1 PRINTER IS 1
2 PRINTER IS 701
10 INPUT "SUBSTRATE TRANSMISSION (0-1)?",Ts
20 INPUT "SAMPLE TRANSMISSION MAX(0-1)?",Tmax
30 INPUT "SAMPLE TRANSMISSION MIN(0-1)?",Tmin
40 INPUT "SAMPLE THICKNESS (CM)?",D
41 INPUT "WAVELENGTH (CM)?",L
50 P=SQR((1/(Ts)^2)-1)
60 S=(1/Ts)+P
70 M=(2*S/Tmin)-(((S^2)+1)/2)
80 N1=M+(SQR((M^2)-(S^2)))
90 N=SQR(N1)
100 C=(2*S*((Tmax-Tmin)/(Tmax*Tmin)))+(((S^2)+1)/2)
110 Nn=C+(SQR((C^2)-(S^2)))
120 N2=SQR(Nn)
130 Em=((8*(N2^2)*S)/Tmax)+((N2^2-1)*((N2^2)-(S^2)))
140 A=(((N2^2)-1)^3)*((N2^2)-(S^4))
150 Aa=(((N2^2)-1)^3)*(N2-(S^2))
160 X=(Em-(SQR((Em^2)-A)))/Aa
170 Ta=SQR(Tmax*Tmin)
180 Gg=(((N2^2)-1)^2)*(((N2^2)-(S^2))^2)
190 Tt=(N2^2)*(((N2^2)-1)^2)*(((S^2)-1)^2)
200 G=(((128*(N2^4)*(S^2))/(Ta^2))+(Tt+Gg)
210 Xx=SQR((G^2)-((((N2^2)-1)^6)*(((N2^2)-(S^4))^2)))
220 X1=SQR(G-Xx)
223 Xa=X1/(((N2-1)^3)*(N2-((S^2))))
240 PRINT "SUBSTRATE REFRACTIVE INDEX :      ",S
250 PRINT "REFRACTIVE INDEX SAMPLE TR REGION :      ",N
251 PRINT "REFRACTIVE IND SAMPLE WEAK ABS REG. :          ",N2
261 A0=(ABS(LOG(Xa)))/D
262 PRINT "ABS COEFF.(CM-1)WEAK ABS SAMPLE FROM Eqs 18-19 :          ",A0
263 J=(A0*L)/(4*(PI))
265 PRINT "EXTINCTION COEFF K WEAK ABS SAMPLE FROM Eqs 18-19:          ",J
270 R3=((S-1)/(S+1))^2
280 R2=((N2-S)/(N2+S))^2
290 R1=((1-N2)/(1+N2))^2
300 Pp=(R1-1)*(R2-1)*(R3-1)
310 Qq=2*Ta*((R1*R2)+(R1*R3)-(2*R1*R2*R3))
320 Bb=SQR((Pp^2)+(2*Qq*Ta*(1-(R2*R3))))
330 X3=(Pp+Bb)/Qq
360 A1=(ABS(LOG(X3)))/D
370 PRINT "ABS COEFF.(CM-1) WEAK ABS SAMPLE FROM Eq.A3 :          ",A1
371 J1=(A1*L)/(4*(PI))
390 PRINT "EXTINCTION COEFF. K WEAK ABS SAMPLE FROM Eq.A3 :          ",J1
400 PRINT "WAVELENGTH (CM) :          ",L
410 PRINT "-------------------------------------------------------------"
420 PRINT "-------------------------------------------------------------"
430 END
```

PUBLICATIONS

Journal of Non-Crystalline Solids 97&98 (1987) 1191-1194
North-Holland, Amsterdam

OPTICAL PROPERTIES OF SPIN-COATED AMORPHOUS CHALCOGENIDE THIN FILMS

E. HAJTO, P.J.S. EWEN, R. BELFORD, J. HAJTO and A.E. OWEN

Department of Electrical Engineering, Kings Buildings, University of Edinburgh, Edinburgh

Optical spectra of spin-coated amorphous As-S thin films are given. These indicate different bondind structure compared to the vacuum evaporated thin films.

1. INTRODUCTION

Recent studies have shown that a broad range of chalcogenide thin films can be prepared from organic solutions using spin deposition techniques[1]. Some of the materials have been demonstrated to be potentially useful for high resolution microlithography.[2] For this application it is required that the thin film of chalcogenide material should be sensitive to the photodiffusion of metals such as silver and should also have a uniform thickness in the range of 0.02 to 2μm. It is also important that the material should have a large absorption coefficient for the irradiation commonly used in standard microlithographic techniques.

The present paper is concerned with the optical properties of thin films prepared by spin coating from solutions of As-S chalcogenide glasses dissolved in n-propylamine.

2. EXPERIMENTAL

The bulk materials (As_xS_{100-x}) were prepared by direct synthesis from 5N purity elements in evacuated quartz ampoules at 800 ^oC for 12 hr. After synthesis the ampoules were air quenched. Solutions of the chalcogenides were made by dissolving the powdered glass in anhydrous n-propylamine. The solution was filtered, using a 0.5 μm pore size filter on deposition, this ensured that the solution was free from solid material. The resulting film thickness varies with the concentration of the solution, the spinning time and speed. It was found for example that 2gms $As_{40}S_{60}$ dissolved in 10 ml n-propylamine (i.e. 0.81M solution) and spin-deposited onto a glass substrate (3000rpm for 20sec) resulted in a uniform film of $\sim$ 1μm thickness. The spin coated chalcogenide films were annealed for $\sim$ 1 hour at 90 ^oC in order to remove the remains of the solvent.

The optical transmittance and reflectance of thin films for a broad range of As_x-S_{100-x} compositions were measured in the spectral region of 0.2 to 2.5 μm using an UV-VIS-NIR spectrophotometer (Perkin-Elmer Lambda 9). The optical constants, refractive index n and absorption coefficient α, were calculated from the transmittance and the reflectance data using the methods suggested by Swanepoel[3] and Abeles[4].

3. RESULTS

The compositional dependence of the refractive index (measured at photon energy $\hbar\omega = 1.23$ eV) for spin-coated As_x-S_{100-x} films is depicted in Figure 1.

0022-3093/87/$03.50

It can be seen that the value of refractive index gradually increases towards the composition $As_{40}S_{60}$ (i.e. the molecular composition As_2S_3.) Similar compositional dependence was observed for vacuum evaporated As-S films[5].

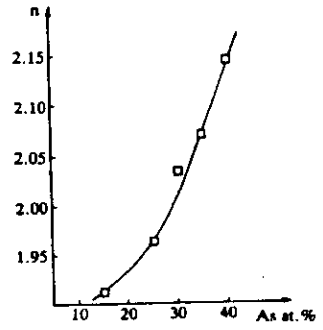

Figure 1.,Compositional dependence of n for spin coated As-S films

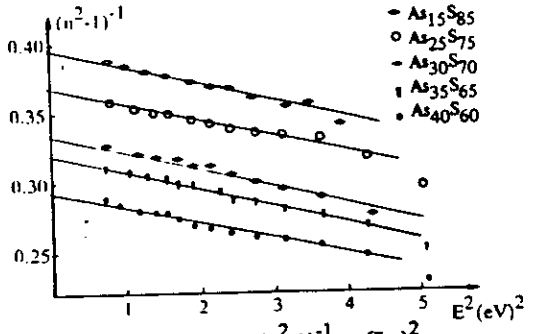

Figure 2.,Plot of $(n^2-1)^{-1}$ vs $(\hbar\omega)^2$ for spin coated As-S films

The energy dependence of the refractive index n(E) can be fitted by the Wemple-Di Domenico [6] dispersion relationship;

$$\epsilon_1(\omega)=n^2(\omega)=1+E_oE_d/[E_o^2-(\hbar\omega)^2] \quad (1)$$

where $\hbar\omega$ is the photon energy, E_o is the single oscillator energy and E_d is the dispersion energy. By plotting $(n^2-1)^{-1}$ versus $(\hbar\omega)^2$ (see Figure 2.) and fitting the data with a straight line, E_d and E_o can be directly determined from the intercept (E_o/E_d) and the slope $(-1/E_oE_d)$. The negative curvature deviation which is observed in the higher energy portion in Figure 2 is due to the onset of interband optical absorption. The dependences of the single oscillator energy E_o and its dispersion energy E_d on composition are plotted in Figure 3.a,b. Also plotted are data for vacuum evaporated As-S films obtained by various authors[7].

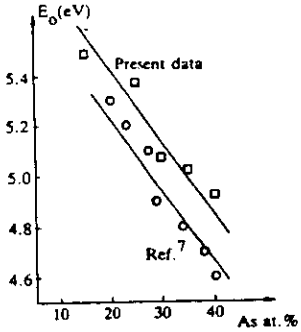

Figure 3.a. Compositional dependence of the single oscillator energy E_o

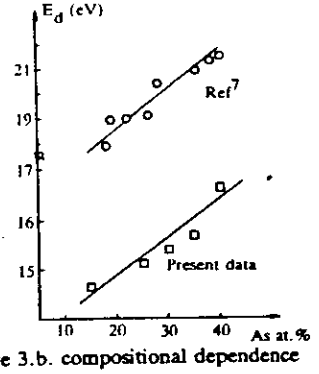

Figure 3.b. compositional dependence of dispersion energy E_d

The common features of these data are the maximum in E_d and the minimum in E_o at the stoichiometric composition ($As_{40}S_{60}$). However the values of the oscillator dispersion energy E_d for spin-coated films are considerably lower than those obtained for vacuum evaporated films. It was demonstrated[6] that E_d obeys a simple empirical relationship $E_d = \beta N_c Z_a N_e$, where β is a constant, N_c is the number of the nearest neighbour cations to the anion, Z_a is the formal chemical valency of the anion and N_e is the effective number of valence electrons per anion. Therefore the smaller E_d suggest a different bonding structure for those films prepared by spin-coating compared to those prepared by vacuum evaporation. The optical absorption spectra for spin coated As-S films are depicted in Figure 4. It is a salient feature that films of identical composition give different absorption spectra solely depending on their mode of deposition i.e. spun or vacuum evaporated. In the case of vacuum evaporated As-S films the absorption coefficient rises exponentially with photon energy over the region 1.5 to 2.7 eV according to the Urbach rule;

$$\alpha = \alpha_o \exp[B(\hbar\omega - \hbar\omega_o)] \qquad (2)$$

where B and α_o are constants. This exponential absorption edge is typical for vacuum evaporated amorphous chalcogenide films[8]. In the case of spin coated As_xS_{100-x} films the exponential region is restricted to a smaller energy region (2.4 to 2.6 eV) and the slopes are smaller (B is ranging from 5 to 9 eV^{-1}) than the slopes measured for the vacuum evaporated films[8] (B ~ 19 eV^{-1}). Also a broad absorption band is present for $\alpha \leq 10^3$ cm^{-1} and in the photon energy range 1.2 to 2.3 eV. This band is not present in the vacuum evaporated films.

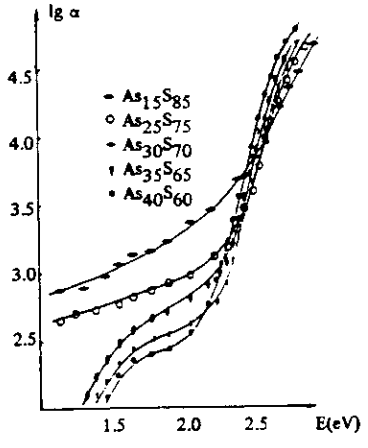

Figure 4., α vs photon energy for spin coated As-S films

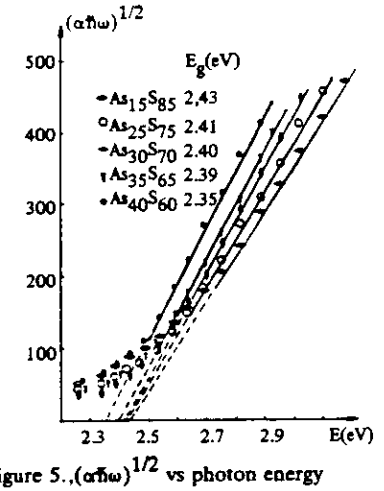

Figure 5., $(\alpha\hbar\omega)^{1/2}$ vs photon energy for spin coated As-S films

The broad absorption band might be associated with light scattering from inhomogeneities of the order of hundreds of angstroms in diameter[9]. At higher values of the optical absorption coefficient, its exponential dependence on photon energy ceases to hold and the absorption coefficient rises less steeply. Figure 5 shows that for this region the α values can be linearised as;

$$\alpha^{1/2} \sim (\alpha\hbar\omega)^{1/2} = C(\hbar\omega - E_g)^2 \quad (3)$$

Such spectral dependence of the absorption coefficient can be attributed to interband electronic transitions since one can write[8].

$$\alpha = \text{const}\frac{M^2}{\hbar\omega} \int_0^{\hbar\omega - E_g} g_v(E) g_c(\hbar\omega - E_g - E)dE \quad (4)$$

where g_v and g_c are the densities of states in valence and conduction bands. Assuming that $g(E) \sim E^{1/2}$ and that the transition matrix element M is constant in the energy range under consideration, equation (4) takes on the form expressed by equation (3). The value of the optical energy gap E_g can be obtained by extrapolating $\alpha^{1/2}$ towards zero (see Figure 5.). The value of the optical energy gap E_g decreases with the As content. The slope C on the other hand increases towards the stoichiometric composition indicating a narrowing of the conduction band and the valence band (i.e. increasing order in the chemical bond statistics). Similar compositional dependences were found for vacuum evaporated As-S films[7].

4.CONCLUSION

Varying the composition of spin coated As-S films induces changes in E_g through modifications of the average bonding energy (i.e. by varying the chemical bond statistics.) This is consistent with changes in E_g observed in vacuum evaporated As-S films[7]. As the composition became increasingly sulphur rich, the trends shown in E_d, E_o, B and C are attributed to either an increasing disorder or to chemical changes resulting in a redistribution of the density of states within a certain energy gap. Furthermore, the broad absorption band and the fact that E_d, B and C are smaller than the corresponding parameters for vacuum evaporated films[7], indicate a different bonding structure in the amorphous network for the films prepared by spin-coating and vacuum evaporation. Measurements are currently underway to study the photodissolution of metals in spin-coated films.

REFERENCES

1) G.C.Chern, I.Lauks, J.Appl.Phys. 53(10) Oct. (1982) 6979
2) A.P.Firth, P.J.S.Ewen, A.E.Owen, C.M.Huntley, Advances in Resist Technology and Processing II. Vol.539. (1985) 160
3) R.Swanepoel, J.Phys. E: Sci Instrum., 16 (1983) 1214
4) F. Abeles, Optical Properties of Solids, Amsterdam North-Holland Publ. Co. (New York American Elsevier 1972)
5) Z.U.Borisova, Glassy Semiconductors, (Plenum Press New York 1981) p.136
6) S.H.Wemple, Jr. DiDomenico, Phys Rew.B3 (1971) 1338
7) K.Tanaka, Thin Solid Films, 66 (1980) 271
8) N.F.Mott, E.A. Davis, Electronic Processes in Non Cryst. Materials (Clarendon Press Oxford 1979) p.273
9) A.Vancu, St.Sladaru and R.Grigorovici, in Proc. of 5th Int.Conf. on Am. and Liquid Semiconductors, (Taylor and Francis London 1974) p.631

phys. stat. sol. (a) **114**, 587 (1989)

Subject classification: 78.65; 68.55; S8

Department of Electrical Engineering (a)
and Department of Geology (b), University of Edinburgh[1])

Spectroscopic Investigation of Spin-Deposited As–S Amorphous Films

By

E. HAJTO (a), P. J. S. EWEN (a), P. G. HILL (b), and A. E. OWEN (a)

The structure of spin-deposited As-S films and its dependence on annealing, illumination, and silver-doping are studied by optical and infrared spectroscopy. The films are prepared by spin deposition from organic solution onto substrates held at room temperature. The analysis of refractive index data indicate different bonding arrangements compared to vacuum evaporated films. Infrared transmittance spectra over the range of 4000 to 200 cm^{-1} show new features previously unreported in the literature. The infrared data above 600 cm^{-1} suggest that the structure of the as deposited film is influenced by the remains of the organic solvent while the data below 600 cm^{-1} suggest that molecular type units are present in the freshly deposited films. Upon annealing the solvent related peaks are significantly reduced and AsS_3 pyramidal units become the dominant structural elements of the amorphous network. Infrared data is also obtained for silver doped As-S films.

Die Struktur von As-S-Schichten nach Spinabscheidung und ihre Abhängigkeit von Temperung, Belichtung und Silberdotierung werden mittels optischer und IR-Spektroskopie untersucht. Die Schichten werden mittels Spin-Abscheidung aus organischer Lösung auf Substraten aufgebracht, die bei Zimmertemperatur gehalten werden. Die Analyse der Werte des Brechungsindex zeigen im Vergleich zu vakuumaufgebrachten Schichten unterschiedliche Bindungsanordnungen. Infrarot-Transmissionsspektren im Bereich 4000 bis 200 cm^{-1} zeigen neue, bisher nicht veröffentlichte Charakteristiken. Die Infrarotdaten oberhalb 600 cm^{-1} zeigen, daß die Struktur der Schichten unmittelbar nach der Abscheidung durch Reste des organischen Lösungsmittels beeinflußt werden, während die Werte unterhalb 600 cm^{-1} darauf hinweisen, daß Moleküleinheiten in frisch aufgebrachten Schichten vorhanden sind. Nach Temperung werden die Lösungsmittel-verknüpften Maxima signifikant verringert und AsS_3-Pyramideneinheiten werden die dominierenden Strukturelemente des amorphen Netzwerks. Infrarotwerte werden auch für silberdotierte As-S-Schichten aufgenommen.

1. Introduction

Recent studies have shown that a broad range of chalcogenide thin films can be used for high resolution microlithography based on the light-enhanced metal dissolution effect [1, 2]. It has been demonstrated that 0.03 μm resolution can be obtained by electron-beam microlithography [3]. In addition to the good resolution capability, chalcogenide glasses might have some other advantages in microlithographical applications. Thin and uniform films can be prepared not only by vacuum evaporation or sputtering, but also by the spin-coating technique commonly used for depositing organic polymer photoresists.

In recent publications [4, 5] the preparation, properties, and some applications of spin-coated amorphous chalcogenide films have been described. It has been demon-

[1]) King's Buildings, Edinburgh EH9 3JL, Great Britain.

strated that thin films of amorphous materials can be deposited from organic solutions of As_2S_3, As_2Se_3, As_2Te_3, and GeSe solutes dissolved in n-propylamine or n-butylamine. The structure of spin-deposited films was investigated in these studies by infrared spectroscopy, NMR spectroscopy, and thermogravimetry, and was suggested to consist of As_2S_3 glass domains terminated at their surfaces by excess negatively charged sulphur and charge compensating alkyl-ammonium ions. Removal of the amine ions by annealing (i.e. by thermal decomposition) resulted in a material which is essentially a "network glass" containing only arsenic and sulphur [5]. X-ray diffraction measurements of spin-deposited films showed that the structure was amorphous i.e. no sign of crystalline peaks could be observed [4]. However, the position of the first peak is slightly different from the position observed for vacuum-evaporated films suggesting a different bonding structure i.e. different first neighbour distances.

In this paper we present a systematic investigation of the optical properties and structure of spin-deposited As–S films of different composition by infrared spectroscopy: middle- and far-infrared spectra (4000 to 600 cm^{-1}) provide information about the chalcogenide-solvent interaction and extreme infrared spectra (600 to 200 cm^{-1}) give information about the nature of the bonding structure in the amorphous network. Section 2 outlines the method of sample preparation and the experimental technique used for the spectroscopic measurement, Section 3 contains the experimental results and discussion and Section 4 summarises the conclusions.

2. Preparation and Experimental Technique

The studied materials (As_xS_{100-x}) were prepared by direct synthesis from elements of 5N purity heated together in evacuated quartz ampoules at 850 °C for 12 h. After synthesis the melts were air-quenched, resulting in bulk glasses of the required compositions.

Solutions of the chalcogenides were made by dissolving the powdered glass in anhydrous n-propylamine. Before deposition a 0.5 μm pore size filter was used to ensure that the solution did not contain solid particles. The film thickness was dependent on the concentration of the solutions, the spinning time and the spinning rate. Typically, 2 g of glass dissolved in 10 ml n-propylamine and spin-deposited at 3000 r.p.m. for 20 s resulted in a uniform film of about 1 μm thickness. The spin coated films were investigated both by optical and electron microscopy and found to be uniform and free of microstructure i.e. no grain boundaries had been observed on the 1 μm scale.

The compositions of the spin coated As–S films were determined by X-ray microprobe analysis and were generally found to be close to the composition of the corresponding bulk glass used as the solute (Table 1). It can be seen that the difference between the bulk glass and the corresponding film composition is somewhat larger for the $As_{25}S_{75}$ film which was the most sulphur-rich composition with respect to the

Table 1
Results of X-ray microprobe analysis of bulk and spin-deposited As–S materials

nominal composition of bulk glasses (at%)	actual composition of bulk glasses (at%)	actual composition of annealed spun films (at%)
$As_{40}S_{60}$	$As_{39.4}S_{60.6}$	$As_{38.2}S_{61.8}$
$As_{35}S_{65}$	$As_{34.3}S_{65.7}$	$As_{33.2}S_{66.8}$
$As_{30}S_{70}$	$As_{29.5}S_{70.5}$	$As_{29.4}S_{70.6}$
$As_{25}S_{75}$	$As_{23.9}S_{76.1}$	$As_{27.9}S_{72.1}$

stoichiometric $As_{40}S_{60}$. The deviation in the sulphur content might be due to an increased sulphur loss during the annealing step (160 °C for one hour) after spin deposition.

The optical transmittance and reflectance of the spin-deposited films were measured in the spectral region 0.2 to 2.5 μm using a UV-VIS-NIR spectrophotometer (Perkin-Elmer Lambda 9). For this purpose the As–S films were spun onto 7059 Corning glass substrates. Si wafers and CsI discs were used as substrates for the middle and far infrared measurements (2.5 to 50 μm i.e. equivalent of 4000 to 200 cm^{-1}) using a Perkin-Elmer 598 Infrared Spectrophotometer.

In order to investigate the effect of illumination on the structure, some samples were illuminated with a UV light source for two hours and transmittance spectra were subsequently recorded.

The effect of silver doping was also studied. For this purpose silver films (thickness ≈ 0.2 μm) were first vacuum evaporated onto CsI substrates and then As–S films (thickness ≈ 1 μm) were spin deposited on top of the silver. The silver-chalcogenide structures were illuminated with UV light for 1 h using a Carl Suss Illumination System. As a result of illumination, the silver layer diffused into the chalcogenide film. The optical spectra of the silver doped As–S films were then recorded.

3. Experimental Results and Discussion

3.1 Refractive indices of spin-deposited As-S films

The optical constants (absorption coefficient α, refractive index n) were calculated from the measured transmittance and reflectance spectra of spin-deposited As–S films, using the methods suggested by Swanepoel [6] and Abeles [7]. The absorption constant data were described in a previous paper [8]. Fig. 1 shows the refractive index data for spin-deposited As–S films. The measurements were obtained on samples annealed at 160 °C for 1 h. The value of refractive index is nearly constant in the infrared region ($\lambda = 3$ to 15 μm) indicating that the films are suitable for optical applications (i.e. no significant absorption present). All the curves are similar in shape but are displaced to higher values of n as the As content increases.

At higher photon energy ($\lambda \approx 1$ μm) n increases rapidly due to the onset of optical absorption [9]. Fig. 2 shows the dispersion of the refractive index for As–S films of different compositions according to the theoretical model suggested by Wemple and Di Domenico [10]. The data can be fitted with the single oscillator expression

$$n^2(h\nu) - 1 = \frac{E_0 E_d}{E_0^2 - (h\nu)^2}, \tag{1}$$

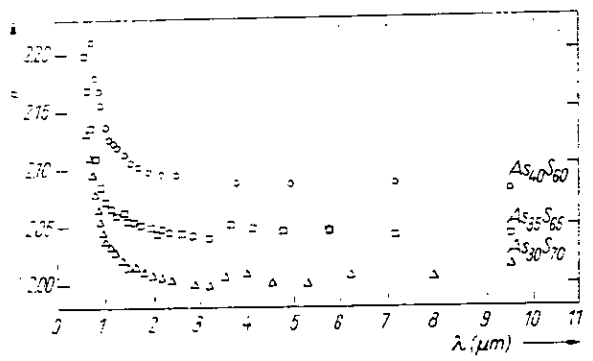

Fig. 1. Wavelength dependence of refractive indices for different compositions of spin-deposited As–S films

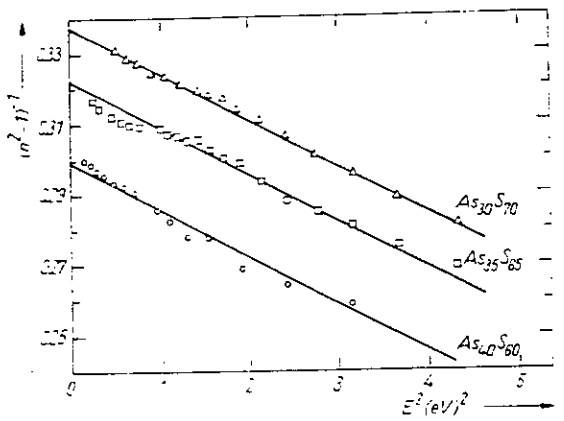

Fig. 2. Dispersion of refractive indices for different compositions of spin-deposited As–S films

where $h\nu$ is the photon energy. E_0 is the single oscillator energy, and E_d is the dispersion energy. It should be emphasized that (1) can be applied to the extended infrared range (0.8 to 15 μm) suggesting that the dispersion over the transparent region is controlled by the single absorption peak in the high energy region (characterised by E_0). This indicates that in the infrared region (0.8 to 15 μm) the term describing the contribution of vibrational transitions to the refractive index is very small in comparison to the term describing the contribution of interband optical transitions and therefore can be neglected in the dispersion formulae (i.e. a single oscillator model applies).

Fig. 3 shows the Wemple-Di Domenico relationship for undoped and silver doped $As_{33}S_{67}$ films. It can be seen that the single oscillator model can also be applied for the silver doped sample despite the large shift in the refractive index.

The dependencies of E_0 and E_d on composition are summarised in Table 2. Also included is data for the silver doped $As_{33}S_{67}$ film. The observed changes are small: E_0 decreases while E_d slightly increases with increasing As content (i.e. towards $As_{10}S_{60}$ stoichiometric composition). Similar dependencies of E_0 and E_d on composi-

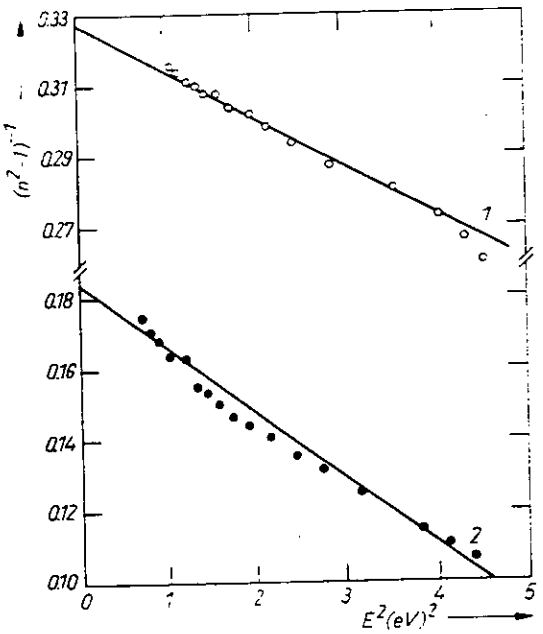

Fig. 3. Dispersion of refractive indices for undoped (1) and Ag-doped (2) spin-deposited $As_{33}S_{67}$ films

Table 2
E_0 and E_d data for spin-deposited As–S films of different compositions

composition (at%)	E_0(eV)	E_d(eV)
$As_{10}S_{60}$	4.71	15.76
$As_{35}S_{65}$	4.88	15.23
$As_{33}S_{67}$	4.98	15.19
$As_{30}S_{70}$	5.07	15.05
$Ag_{10}As_{30}S_{60}$	3.17	17.28

tion were published for vacuum evaporated As–S films [11]. However, the values of the oscillator dispersion energy E_d are considerably lower than those obtained for vacuum evaporated films. E_d is a measure of the strength of the interband optical transitions. It was demonstrated [10] that E_d obeys a simple empirical relationship $E_d = \beta N_c Z_a N_e$ where β is a constant. N_c is the the number of the nearest neighbour cations to the anion, Z_a is the formal chemical valency of the anion, and N_e is the effective number of valence electrons per anion. Therefore the differences in E_d values suggest a different bonding structure of the amorphous network depending on their mode of deposition.

The optical properties of the silver doped $As_{33}S_{67}$ film are quite different from those of the undoped films. The energy dependence of refractive index can also be described by the single oscillator relationship (Fig. 3) although the values of E_0 and E_d are rather different from those of the corresponding values for the undoped films (Table 2). This is due to the significant amount of silver ($\approx$ 10 at%) incorporated into the $As_{33}S_{67}$ which changes the coordination number and valency in the amorphous network.

3.2 Middle to far infrared transmittance spectra of spin-deposited As-S films

The 4000 to 600 cm^{-1} region of the infrared transmittance spectra (Fig. 4) of the freshly deposited spin coated As–S films contain a series of absorption bands associated with the organic solvent. These bands are not present in the vacuum evaporated

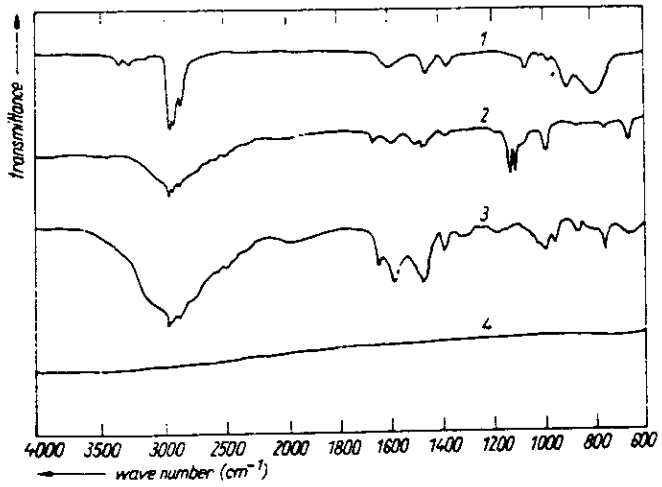

Fig. 4. Middle- and far-infrared absorption spectra of n-propylamine (1), spin-deposited sulphur (2), and spin-deposited $As_{40}S_{60}$ (3) films (vacuum evaporated $As_{40}S_{60}$ (4))

Table 3
Positions and assignment of the observed absorption bands in the 4000 to 600 cm^{-1} region for n-propylamine, spin-deposited sulphur, and spin-deposited $As_{40}S_{60}$

wave number (cm^{-1})	assignment	comment
3365 3290	NH_2 symmetric–asymmetric stretch (doublet)	observed in solvent, absent in spin-deposited sulphur and chalcogenide films.
900 800	NH_2 out of plane vibrations	observed in solvent, absent in spin-deposited sulphur and chalcogenide films.
2960 2920 2870	aliphatic C–H stretch	observed in both solvent and spin-deposited films.
1465 1390	C–H scissor bend	observed in both solvent and spin-deposited films.
1575	N–H scissor bend	observed in both solvent and spin-deposited films. peak frequency is slightly different for solvent (1608 cm^{-1}).
2200 to 3200	broad absorption band characteristic of amine salts	absent in solvent, present in spin-deposited films.
750	H–S stretch and wag	absent in solvent, present in spin-deposited films.

$As_{40}S_{60}$ film. Table 3 summarises the position and assignment of the absorption peaks present in the middle-far infrared transmittance spectra of propylamine. as-deposited sulphur film deposited from its solution of propylamine, and as-deposited $As_{40}S_{60}$ film. A comparison of the observed absorption bands reveals some evidence for the possible chemical bonding between the solvent and the chalcogenide glass during dissolution.

The 2960, 2920. 2870 cm^{-1} and 1465, 1390 cm^{-1} absorption bands are observed both in the solvent and spin-deposited films indicating that the aliphatic C–H chain is not taking part in the dissolving process.

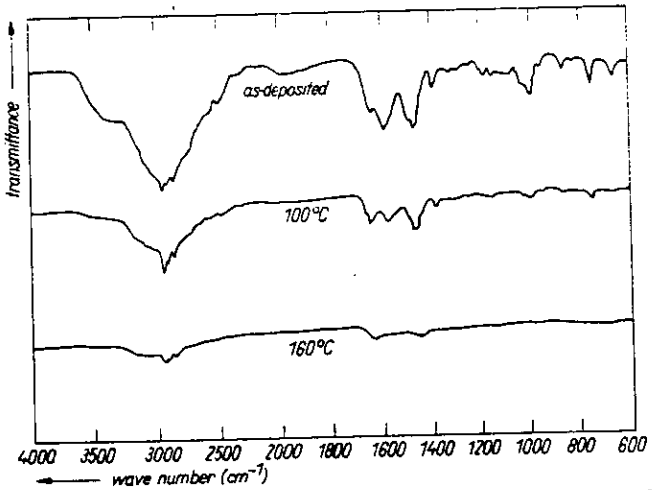

Fig. 5. Middle- and far-infrared absorption spectra of spin-deposited $As_{40}S_{60}$ films annealed at different temperatures

On the other hand the 3365, 3290 cm^{-1} and 900 to 800 cm^{-1} absorption peaks which are characteristic of $-NH_2$ stretch and out of plane vibrations are only present in the spectra of the pure solvent. However, a broad absorption band can be observed in the spin-deposited sulphur and the spin-deposited $As_{40}S_{60}$ films at 3200 to 2200 cm^{-1} which is characteristic of the NH_3^+ of the amine salt and absent in the solvent spectrum. This absorption band is identical for spin-deposited sulphur and chalcogenide glass indicating that the solvent–chalcogenide interaction occurs at the sulphur sites in the amorphous network possibly by creating S^-–NH_3^+ ionic bonds. This assumption is further supported by our observation that the solubility of the As–S glasses in n-propylamine increases with increasing sulphur concentration.

The spin coated As–S films were subjected to different temperature treatments in order to investigate the removal of the solvent from the chalcogenide films. A typical result is shown in Fig. 5 for $As_{40}S_{60}$ films. The magnitude of the solvent-related peaks substantially decreases indicating the evolution of organic content from the spin-coated films. However, for thicker films (thickness $\approx 2\,\mu m$) the removal of the organic solvent is not complete even after annealing at 160 °C for 2 h.

3.3 Extreme-infrared absorption spectra

Typical transmittance spectra over the range of 600 to 200 cm^{-1} for as deposited $As_{25}S_{75}$, $As_{30}S_{70}$, and $As_{40}S_{60}$ films are shown in Fig. 6. The transmittance spectrum of a spin-deposited sulphur film is also included. For all the compositions (except pure sulphur) a strong absorption band appears at 310 cm^{-1}, which was assigned by Lucovsky [12] to the r_3 asymmetric stretching mode in a pyramidal AsS_3 unit, indicating that the main structure of our spin-coated films is dominated by these molecular type units as in the case of vacuum evaporated $As_{40}S_{60}$ thin films.

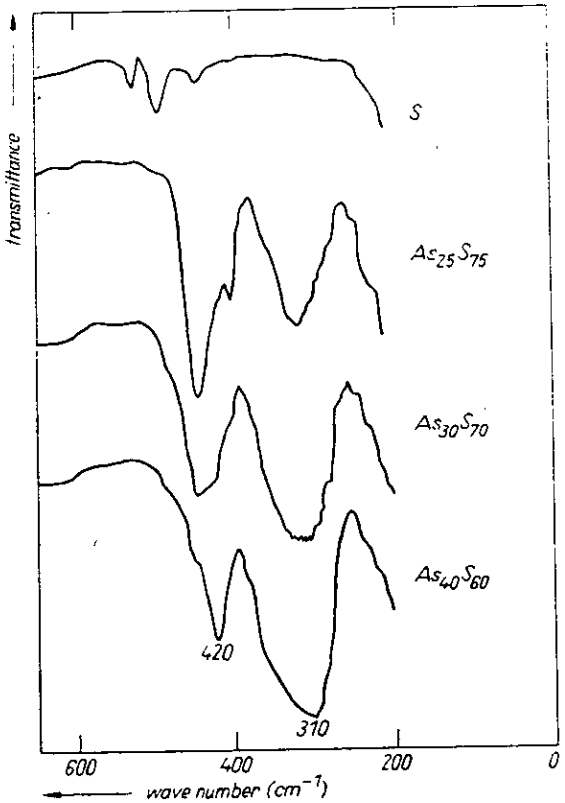

Fig. 6. Extreme infrared absorption spectra of spin-deposited sulphur and spin-deposited As–S films of different compositions

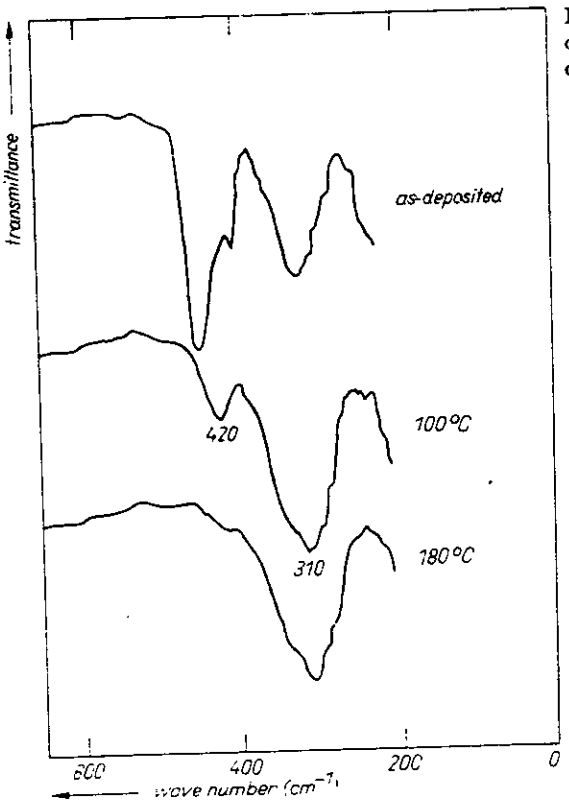

Fig. 7. Extreme infrared absorption spectra of spin-deposited $As_{25}S_{75}$ films annealed at different temperatures

However, in the unannealed spin-deposited As–S films, another absorption peak occurs at 420 cm^{-1} which is not observed in vacuum evaporated As–S films. It is interesting to note that the 310 cm^{-1} and 420 cm^{-1} peak amplitudes change asymmetrically with the chalcogenide composition i.e. the 420 cm^{-1} peak increases with increasing sulphur content of the chalcogenide film, while the 310 cm^{-1} peak increases with increasing arsenic content. We assume that the 420 cm^{-1} peak can be assigned to a bond formed between the sulphur atoms of the AsS_3 pyramidal units and the solvent molecules. This assumption is supported by the facts that the magnitude of the 420 cm^{-1} peak depends on the sulphur concentration of the chalcogenide film (Fig. 6) and it gradually disappears as a result of annealing (Fig. 7). Furthermore, the 420 cm^{-1} peak is not present in the spin-deposited pure sulphur film (Fig. 6).

Based on these observations we suggest that the continuous network of the bulk glass is fragmented by the solvent molecules possibly at the sulphur sites of the AsS_3 molecular units, resulting in a material which contains AsS glass fragments surrounded by propylamine molecules possibly to which they are ionically bonded, via their amine groups. The annealing process can remove most of the organic content of the film so that the continuous glass network becomes more extensive.

Spin coated $As_{40}S_{60}$ films were also subjected to illumination and annealing steps in order to investigate the light- and thermally-induced changes in the structure. As described earlier, the main feature of the spectra of the freshly deposited $As_{40}S_{60}$ films is the vibration of the AsS_3 pyramidal units at $\nu_3 = 310$ cm^{-1} (an AsS_3 intramolecular asymmetric bond-stretching mode). As a result of illumination with UV light the magnitude of this band decreases slightly and a relatively strong absorption peak appears at 340 cm^{-1} i.e. a band splitting occurs as seen in Fig. 8. It is also important to note that under the influence of illumination the solvent-related 420 cm^{-1} band

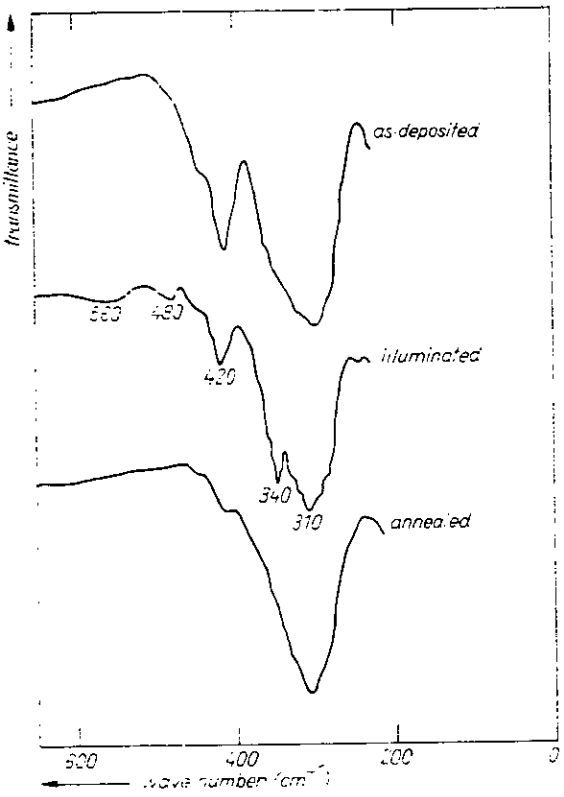

Fig. 8. Extreme infrared absorption spectra of spin-deposited and illuminated $As_{40}S_{60}$ films

decreases, i.e. some loss of organic content occurs. Furthermore, new features appear at 480 cm^{-1} and 560 cm^{-1} which can be associated with the presence of H_2S_2 units in the film [13]. In the subsequent experiment the illuminated $As_{40}S_{60}$ film was annealed at 160 °C for two hours. As a result of annealing, the 340 cm^{-1} peak disappears and the 310 cm^{-1} becomes dominant again.

It should be emphasized that the effect of illumination and annealing on the structure is different. Illumination produces the 340 cm^{-1} band while annealing restores the originally dominant 310 cm^{-1} band. The light enhanced infrared activity (i.e. the appearance of the 340 cm^{-1} band) due to intermolecular effects has been suggested in previous publications [12]. It is possible that in our case the illumination produces an intramolecular charge redistribution by a small displacement of As and/or S atoms which in turn leads to infrared activity in $\nu_1 = 340$ cm^{-1}. However, the appearance of the 340 cm^{-1} band can also be explained by light induced formation of a new type of molecular unit in the amorphous network such as As_4S_4 [14]. Based on the available experimental results, it is not possible to decide which type of structural transformations occur as a result of illumination.

The effect of light induced silver doping on the infrared spectra of spin-coated As–S films has also been studied. The far infrared transmission spectra of silver doped $As_{33}S_{67}$ films is different from those of the undoped ones (Fig. 9). The main absorption band (310 cm^{-1} in undoped films) shifts to 340 cm^{-1}, and no additional features are present. This change is similar to what was observed in the Raman experiments [15]. It is interesting to note that the magnitude of the band shifting is the same as the band splitting was in the case of the effect of light. On the other hand, we did not observe any absorption band for pure Ag_2S powder in this region. Silver atoms can incorporate into the main AsS_3 pyramidal units by displacing S atom(s), or they can break the relatively weak S–S bonds between the pyramidal units and create S–Ag–S

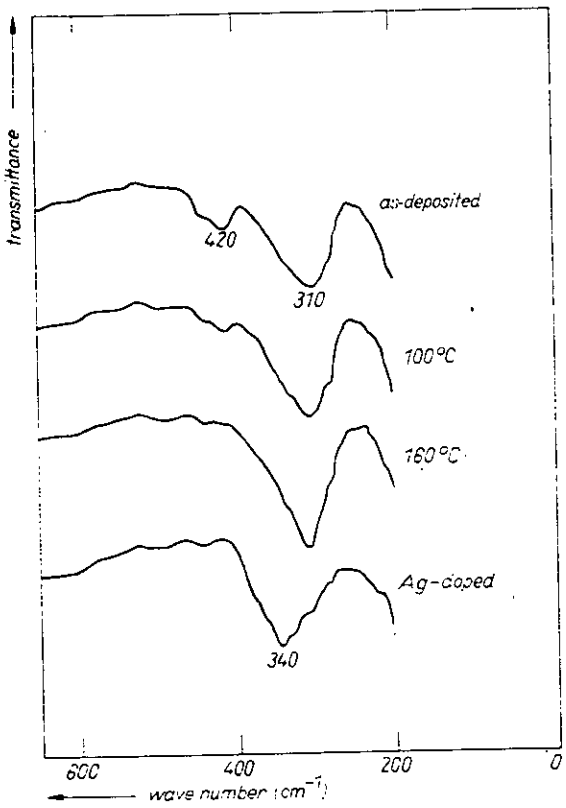

Fig. 9. Extreme infrared absorption spectra of spin-deposited and Ag-doped $As_{33}S_{67}$ films

bridges connecting them. It is quite possible that in a "real" amorphous system both types of transformations might occur depending on the chalcogenide composition, the circumstances of the film depositions and annealing. However, in the case of substitutional doping of the pyramid the symmetry of the unit would change considerably which should result in the appearence of more vibrational bands in the infrared spectrum. This was not observed in our experiments there fore the pyramidal-bridging process seems to be more favorable.

4. Conclusion

The values of refractive indices of spin-deposited As–S films are slightly lower than those of the vacuum evaporated film of identical compositions indicating a difference in the chemical bonding structure. The wavelength dependence of the refractive index suggets negligible absorption in the infrared region (4000 to 600 cm^{-1}) which makes the spin-deposited films suitable for optical applications.

On the other hand, middle- to extreme-infrared transmittance spectra provide new evidence for the possible chemical interaction between the organic solvent and As–S glasses. Infrared spectra in the region of 4000 to 600 cm^{-1} indicate that the amine group of the organic molecule plays the most significant part in the dissolving process.

Extreme infrared spectra (600 to 200 cm^{-1}) indicate that solvent-chalcogenide interaction occurs at the sulphur sites in the amorphous network possibly by creating S^{-}–NH_3^{+} ionic bonds (associated with the 420 cm^{-1}) band). Annealing substantially reduces the 420 cm^{-1} band and enhances the 310 cm^{-1} band. The resulting spectrum (with its dominant 310 cm^{-1} band) is very similar to the spectrum of the bulk well annealed glass. Illumination and annealing seem to have opposite effects on the structure (as evidenced by the 310 $cm^{-1} \rightarrow$ 340 cm^{-1} band splitting). The light induced

silver doping effect is also characterised by the 310 $cm^{-1} \rightarrow 340\ cm^{-1}$ band shift. This might indicate that the silver doping effect is accompanied by light induced structural changes in the amorphous network.

Acknowledgements

The authors wish to thank Prof. E. A. V. Ebsworth in the Chemistry Department of University of Edinburgh for providing access to their IR Spectrophotometer. This work was supported by the U.K. Science and Engineering Research Council and Pilkington Brothers plc.

References

[1] A. Yoshikawa, O. Ochi, H. Nagai, and Y. Mizushima, Appl. Phys. Letters **29**, 677 (1976).
[2] K. D. Kolwicz and M. S. Chang, J. Electrochem. Soc. **127**, 135 (1980).
[3] B. Singh, S. P. Beaumont, P. G. Bower, and C. D. W. Wilkinson, Appl. Phys. Letters **41**, 1002 (1982).
[4] G. C. Chern and I. Lauks, J. appl. Phys. **53**, 6979 (1982).
[5] G. C. Chern and I. Lauks, J. appl. Phys. **54**, 2701 (1983).
[6] R. Swanepoel, J. Phys. E **16**, 1214 (1983).
[7] F. Abeles (Ed.), Optical Properties of Solids. North-Holland Publ. Co., Amsterdam 1972.
[8] E. Hajto, P. J. S. Ewen, R. Belford, J. Hajto, and A. E. Owen, J. non-crystall. Solids **97/98**, 1191 (1987).
[9] I. Tauc, in: Optical Properties of Solids. Ed. F. Abeles. North-Holland Publ. Co., Amsterdam 1972 (p. 279).
[10] S. H. Wemple and M. DiDomenico, Phys. Rev. B **3**, 1338 (1971).
[11] K. Tanaka, Thin Solid Films **66**, 271 (1980).
[12] G. Lucovsky, Phys. Rev. B **6**, 1480 (1972).
[13] S. D. Ross, Inorganic Infrared and Raman Spectra. McGraw-Hill Publ. Co., New York 1972 (p. 188).
[14] U. Strom and T. P. Martin, Solid State Commun. **29**, 527 (1979).
[15] A. E. Owen, A. P. Firth, and P. J. S. Ewen, Phil. Mag. B **52**, 347 (1985).

(Received May 8, 1989)

Journal of Non-Crystalline Solids 115 (1989) 129-131
North-Holland

DRY ETCHED HIGH RESOLUTION POSITIVE AND NEGATIVE INORGANIC PHOTORESIST

E. HAJTO, R.E. BELFORD, P.J.S. EWEN and A.E. OWEN

Department of Electrical Engineering, University of Edinburgh, Edinburgh EH9 3JL, Scotland

The etching properties of spin coated As-S and Ag-As-S films are reported. Novel results obtained on both the light induced effects and the dry etching of these films opens real opportunities for their use as high resolution photoresists.

1. INTRODUCTION

Light induced changes in the properties of evaporated chalcogenide thin films have been studied for their potential use as inorganic photoresists [1-2]. The advantages of their use in fabricating integrated circuits (chemical and physical durability, broad spectral sensitivity, high resolution, edge sharpening and step-like function capabilities) have been described in recent pubications [3-6].

The technique of spin-coating offers the additional advantage that the layers can be deposited in the same way as conventional organic photoresists. The films deposited by this method have basically the same properties as those obtained by vacuum evaporation or sputtering techniques. Amorphous As-S films can be deposited in a wide range of thicknesses by spin coating, such films films are uniform and free of microstructure[7]. Their composition closely follows that of the bulk material. The annealed spin coated As-S film structure and optical properties have been investigated [8-9].

Patterns can be generated by two different methods: photo-darkening of the As-S film and photo-dissolution of Ag into the As-S film, the former being a single step process and the latter a bi-layer resist process involving the deposition of a Ag layer, as well as the chalcogenide film. Both negative and positive type resists are available using the above methods. The properties of these resists were investigated using standard IC processing techniques.

0022-3093/89/$03.50

2. EXPERIMENTAL METHODS

2.1. Sample preparation

Solutions of various strengths were made by dissolving the powdered As_2S_3 glass in n-propylamine, the resulting film thickness (200A - 2μm) was dependent on the concentration of the solution. Thin films were obtained by spinning these solutions onto substrates of either Si wafers or microscope slides. The spun films were annealed at 120°C for 1hr in order to eliminate the organic solvent from the film. For the silver photodissolution experiments, evaporated Ag films were used beneath the spin coated chalcogenide film as a silver source. A commercial wafer stepper (Optimetrix 8010 λ = 430-600nm, power density = 150mW.cm^{-2}) was used to illuminate the samples.

2.2. Plasma etching

Plasma etching experiments were carried out in an International Plasma Corporation 2000 series system, which is a basic barrel-type plasma etcher. The chamber pressure (atmospheric - 10^{-1} Torr) was the sole means of controlling the rate of flow of gas within the chamber. Etching was carried out with different plasma strengths (input powers) and barrel pressure combinations for each gas. The gases used were CF_4(g) for As-S material and S(g) for Ag-As-S material. Sulphur vapour was generated in vacuo from a solid source and sublimed before entry into the chamber.

An "in situ" optical technique was used to evaluate the etching rates using a He-Ne laser. The light is reflected from both the front (receding) and the back

(stationary) interfaces of the film, and the reflected light intensity is detected by a photodiode and plotted on a chart recorder.

3. RESULTS AND DISCUSSION

3.1. The single layer system: Photodarkening

It was observed that illumination caused photodarkening of the annealed spin coated films (associated with structural changes). This results in differences in the chemical etch rate, therefore the effect can be used for pattern generation in the film. A single As_2S_3 layer (thickness $\sim 0.5\mu m$) was deposited by spin coating and annealed at 120°C for 1 hour. Half of the layer was then illuminated for 10 min. The exposure time used here was for comparative work and is not a measure of sensitivity. A plasma of CF_4(g) was used to etch differentially the illuminated and unilluminated areas of the film. The optimum etching conditions were: CF_4 gas pressure 0.7 Torr, r.f. power 100W. The progress of the etching was monitored continuously by the in-situ technique described above. The recorded interference patterns are shown in Fig. 1.

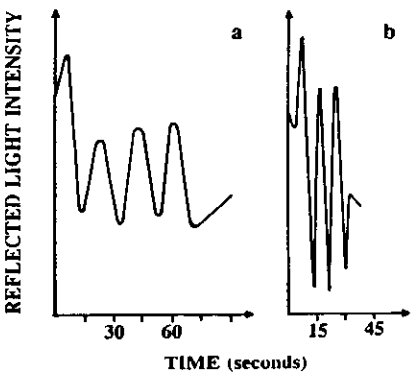

FIGURE 1
Reflected laser intensity curves as a function of etching time. (a) unilluminated (b) illuminated As_2S_3 film

The etching rates were calculated by the positions relative to time, of succesive maxima and minima. The amount of film removed at any given time is; $d = M\lambda/2n$ where M is an integer, λ is the wavelength of laser light used (6328Å) and n is the refractive index of the film. The refractive indices were found to be 2.24 for the unilluminated and 2.36 for the illuminated spin coated As_2S_3 (as determined by optical measurements). The etching time required to remove the illuminated film is significantly shorter than that required for the unilluminated areas. The calculated etch rate for illuminated spin coated As_2S_3 film is -230 Å/sec, and for the unilluminated film is -92 Å/sec. The results obtained for the etching kinetics are shown in Fig. 2.

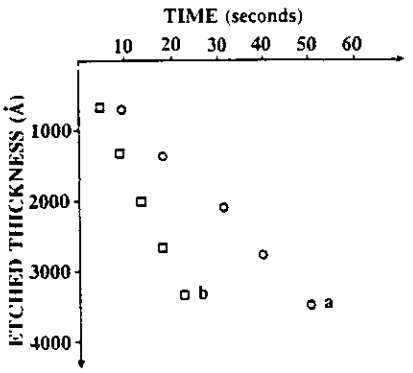

FIGURE 2
Etching kinetics for (a) unilluminated (b) illuminated As_2S_3 film

The etch rate is constant ie the plots are linear for both exposed and unexposed areas. The etch rate of the illuminated film is 2.5 times larger than that of the unilluminated areas. A differential etch rate of this magnitude makes spin coated As_2S_3 films suitable for pattern delineation, and thus use as a positive photoresist with all the advantages this material offers.

3.2 The bilayer system: Photo-dissolution of Ag into As-S

As demonstrated in the previous section As_2S_3 film can be etched in CF_4 plasma but no suitable etchant has been reported for the removal of the Ag doped material, this has restricted the use of Ag-As-S system as negative photoresist. A plasma of S(g) was found to be very effective and selective to the doped material, yielding an amphoteric resist system ie either negative

or positive depending on the etchant used. The etching was monitored in the same way as described above. The optimum etching conditions were: S(g) pressure = 0.65 Torr, r.f. power = 10W, and an etch rate of ~160 Å/sec was observed. Fig. 3 shows the experimentally obtained interference pattern and Fig. 4 shows the the etching kinetics for the Ag-As-S bilayer system.

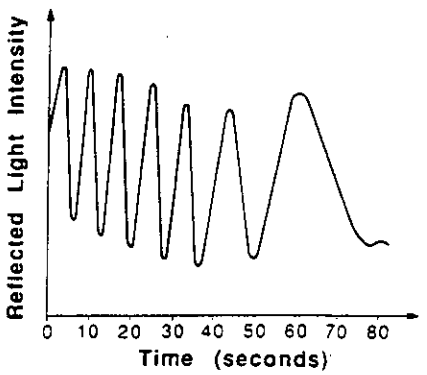

FIGURE 3
Reflected laser intensity curve as a function of etching time for Ag-As-S film.

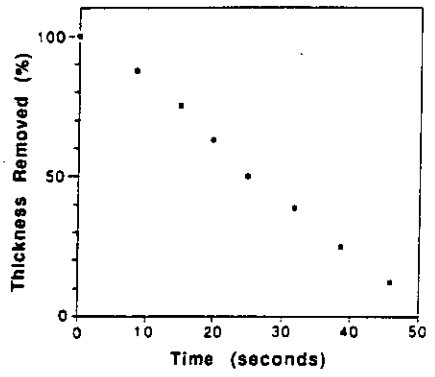

FIGURE 4
The information obtained from Fig. 3 in the form of thickness etched (%) vs. time.

In this case the samples were usee to obtain optical resolutions of 0.5μm, which is the limit of the wafer stepper used. The samples used were Si wafers with a vacuum evaporated Ag layer of 1000Å and a spun As-S film of 300Å. These very thin films[3] have the same etching characteristics as those shown in Figs. 3-4, but they are too thin to give infomation as regards etch rates and thus vacuum evaporated samples were used to obtain this data.

4. CONCLUSIONS

Both photodarkening and silver-photodiffusion effects in spin-coated films of As_2S_3 can be used for pattern generation. The photodarkening effect offers a factor of 2.5 in the etching rate difference for illuminated and unilluminated films. This affords a positive type photoresist involving only a single layer deposition. The Ag-As-S double layer system has the drawback of having two deposition steps, but can act as either a negative or positive photoresist with all the advantages described.

REFERENCES

1. Y.Mizushima and A.Yoshikawa, Jap. Ann. Rev. Comp. & Telecomm. Ed. Y.Hamakawa, (1982) 277-290

2. B.Singh, G.C.Chern and I.Lauks, J. Vac. Sci. Technol. 3(1) (1985) 327

3. R.E.Belford, E.Hajto and A.E.Owen, Thin Solid Films 173 (1989)

4. B.Singh, S.P.Beaumont, P.G.Bower and C.D.W.Wilkinson Appl. Phys. Lett. 41(9) (1982) 889

5. K.L.Tai, R.G.Vadimsky, C.T.Kemmerer, J.S.Wagner, V.E.Lambertii and A.G.Timko, J. Vac. Sci. Technol. 17(5) (1980) 1169

6. H.Kokado, I.Shimizu and E.Inoue, J. Non-Cryst. Sol. 20 (1976) 131

7. G.C.Chern and I.Lauks, J. Appl. Phys. 53 (1982) 6979

8. E.Hajto, P.J.S.Ewen, P.G.Hill and A.E.Owen, Phys. Stat. Sol. (in print)

9. E.Hajto, P.J.S.Ewen, R.E.Belford, J.Hajto and A.E.Owen, J. Non-Cryst. Sol. 96-97 (1987) 1191

Thin Solid Films, *200* (1991) 229–237
ELECTRONICS AND OPTICS

INTERFERENCE GRATING FABRICATION IN SPIN-COATED As_2S_3 FILMS

E. HAJTO AND P. J. S. EWEN
Department of Electrical Engineering, University of Edinburgh, Edinburgh EH9 3JL (U.K.)
R. E. BELFORD
Department of Physics, Napier College, Colinton Road, Edinburgh EH10 5DT (U.K.)
A. E. OWEN
Department of Electrical Engineering, University of Edinburgh, Edinburgh EH9 3JL (U.K.)
(Received August 29, 1990; revised November 16, 1990; accepted December 5, 1990)

The optical properties and solubility of spin-coated As_2S_3 films significantly change after silver is introduced by photodiffusion. The different types of holographic grating that can be fabricated in spin-coated Ag/As_2S_3 double film structures by photodiffusion and subsequent selective etching are described in this paper. The silver diffusion occurs under the influence of visible monochromatic light and the grating pattern is produced by a holographic arrangement.

1. INTRODUCTION

Light-induced changes in the physical and chemical properties of evaporated As–S and other chalcogenide thin films have been widely studied[1–3]. As–S films can also be deposited by the spin coating technique and such films have basically the same properties as those obtained by vacuum evaporation[4,5]. Amorphous As–S films can be deposited in a wide range of thicknesses by this technique and the resulting films are uniform[6]. Their composition closely follows that of the bulk material dissolved for spin coating and the structure and optical properties of the annealed, spin-coated As–S films are found to be very similar to those of the evaporated material[7]. Patterns can be generated in As–S films either by photodarkening, which produces a difference in etch rate between the illuminated and unilluminated part of the film[8], or by light-enhanced silver diffusion into the As–S film[9], which results in an even larger difference in the etch rate between the illuminated (*i.e.* silver-doped) and unilluminated film.

Since the chalcogenide glasses are also well-known IR transmitting materials, patterning based on these photo-induced effects can be used to produce diffractive optical elements for use in the IR region[10]. Such elements have potential applications in beam combining, filtering and spectral analysis and have advantages over conventional refractive components as regards weight, cost and ease of manufacture. Spin coating is a common technique for depositing materials, such as dichromated gelatin, which are used to produce diffractive optical elements for visible operation, and hence it would be useful to determine whether gratings can be created in chalcogenide films deposited by this technique.

0040-6090/91/$3.50

In this paper the light-induced diffusion of silver into spin-coated As_2S_3 films is studied. It is shown that, using a holographic illumination method and subsequent selective etching, a surface relief grating of submicron resolution can be obtained. It is also demonstrated that the optical constants (absorption coefficient α and refractive index n) of the silver-doped As_2S_3 films differ considerably from those of the undoped films, so that the changes can be used to record either amplitude or phase holograms in the Ag/As_2S_3 double film structures.

2. EXPERIMENTAL DETAILS

The Ag/As_2S_3 double film structures are prepared in two steps. First a thin (about 0.3 μm) silver layer is deposited by vacuum evaporation onto a glass substrate; then an amorphous As_2S_3 layer (about 1 μm) is deposited using the spin coating technique[11].

For spin coating, solutions of As_2S_3 were made by dissolving the powdered bulk As_2S_3 glass in propylamine. Thin films were obtained by spinning these solutions onto glass substrates previously covered with a silver film. Typically 2 g of As_2S_3 dissolved in 10 ml *n*-propylamine and spin deposited at 3000 rev min^{-1} for 20 s, produced an As_2S_3 film of about 1 μm thickness. The samples were annealed (in the dark) at 120 °C for 30 min in order to eliminate the remains of the organic solvent from the As_2S_3 film. The optical properties of the films were measured using a UV–visible–near-IR spectrophotometer (Perkin Elmer Lambda 9). The optical constants n and α were calculated from the transmittance and the reflectance data using the method suggested by Swanepoel[12] and Abeles[13]. For these measurements the samples were deposited onto Corning glass 7059 substrates with refractive index $n_{substrate} = 1.5049$. The effect of silver doping was also studied. For this purpose the Ag/As_2S_3 structures were illuminated from the As_2S_3 side (*i.e.* from the top of the double structure) with UV light using a Carl Suss mask aligner system. As a result of illumination, the silver layer completely diffused into the As_2S_3 film. The optical constants of the silver-doped As_2S_3 films were then measured.

The structure of the thin films and the principal steps in the formation of the surface relief grating are shown in Fig. 1. The Ag/As_2S_3 double structure is illuminated with the required pattern and the silver layer diffuses into the As_2S_3 layer in the illuminated areas. After illumination, methanol saturated with ammonia is used for developing the surface relief grating.

The optical arrangement for pattern generation is shown in Fig. 2. In this experiment we used the simplest form of interference grating in which the

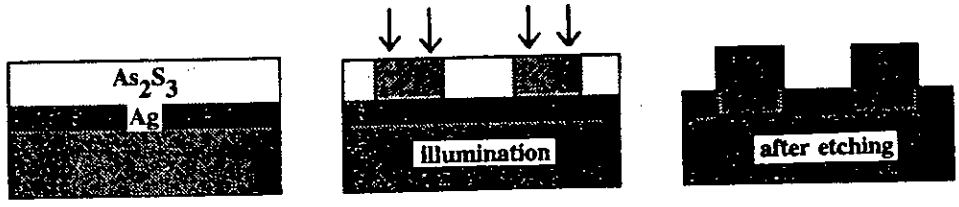

Fig. 1. Sample configuration used for holographic imaging.

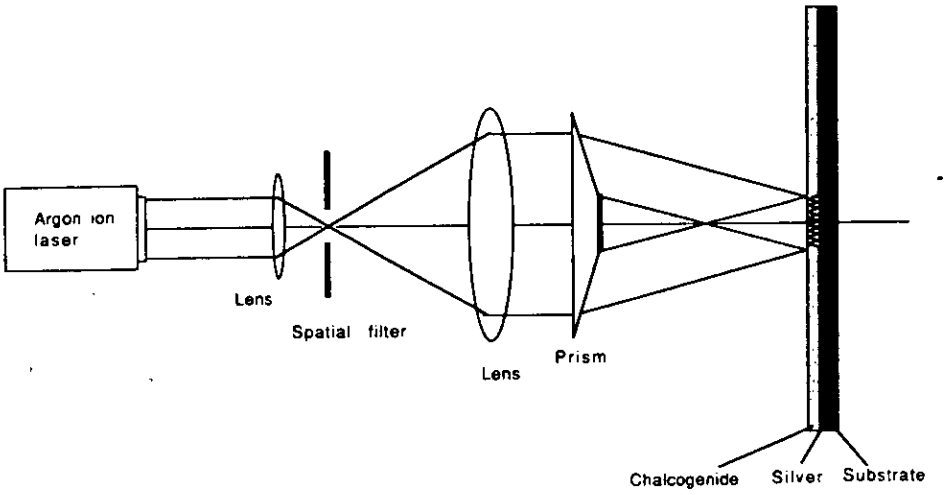

Fig. 2. Optical arrangement used for illumination.

photosensitive films are exposed to a sinusoidal fringe pattern generated by two interfering beams of light. A continuous-wave argon ion laser is used for illumination, operating at a single wavelength of 5145 Å. The laser beam is focused first through a spatial filter, and then expanded and collimated. The beam is divided into two parts of the same intensity using a prism, which is a more stable arrangement than the usual holographic method using a beam splitter and mirrors, because the optical path length is shorter and the number of optical elements is fewer. A stable optical arrangement is important in this case because of the relatively long exposure time required for the silver diffusion. When the two coherent beams of light intersect at an angle 2θ, they will generate interference fringes within the volume common to both beams with a spacing (also termed grating period) Λ given by[14]

$$\Lambda = \lambda/2 \sin\theta \tag{1}$$

where λ is the wavelength of the light and θ is the angle of incidence. Therefore the grating period in the Ag/As_2S_3 structure is determined by the wavelength λ of the illuminating light and the angle of incidence θ which is in turn determined by the angle of the prism. The finest spacing that can be obtained is $\lambda/2$ which corresponds to $\theta = 90^\circ$. This cannot be achieved in practice since it requires both beams to be incident along the surface of the sample, but a value of $\theta = 60^\circ$ yields a spacing of 0.6λ. In our experiments two different prisms were used: prism (1) provided an angle of incidence $\theta = 20^\circ$ and prism (2) provided an angle of incidence $\theta = 0.7^\circ$. The performance of the gratings produced (resolution, spectral purity, efficiency) was assessed using a low intensity He–Ne laser.

3. RESULTS AND DISCUSSION

Curve A of Fig. 3 shows the absorption coefficient of the undoped, spin-coated As_2S_3 films (*i.e.* without silver) as a function of a wavelength in the visible range of

the optical spectrum. Curve B of Fig. 3 shows the absorption coefficient for the silver-doped As_2S_3 films. The effect of silver doping on the refractive index is shown in Fig. 4 (curve A for the undoped As_2S_3 film, and curve B for the silver doped film). It can be seen that the absorption coefficient and the refractive index increase as a result of the silver incorporation into the As_2S_3 network. These results correspond

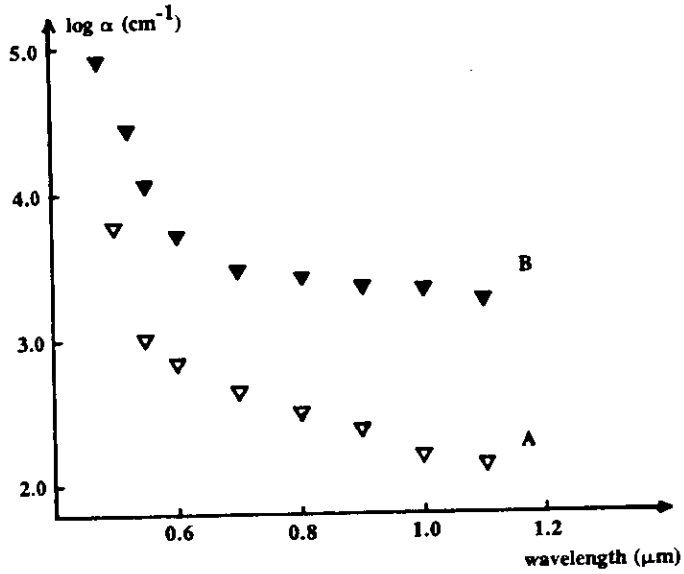

Fig. 3. Wavelength dependence of the absorption coefficient of spin-coated As_2S_3 films (curve A) and of silver-photodoped As_2S_3 films (curve B).

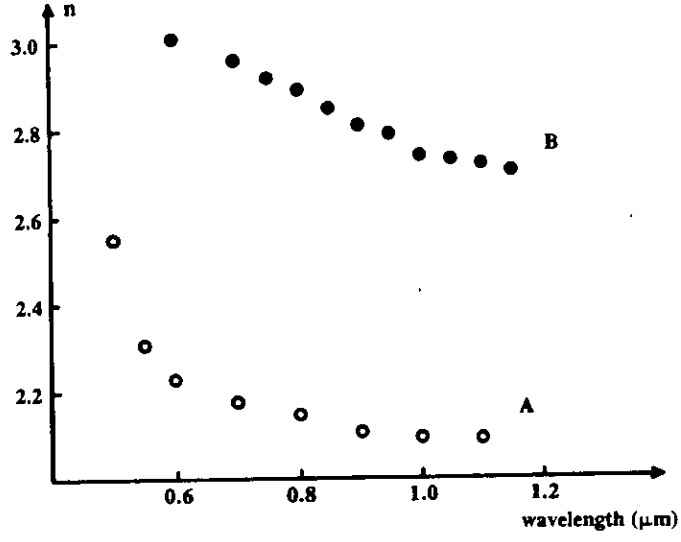

Fig. 4. Wavelength dependence of the refractive index of spin-coated As_2S_3 films (curve A) and of silver-photodoped As_2S_3 films (curve B).

to a silver concentration of about 22 at.% in the As_2S_3 films as calculated from the initial thickness of the silver and As_2S_3 films.

The large changes observed in the optical constants of the silver-rich (*i.e.* the illuminated) parts of the films are accompanied by a drastic change in other physicochemical properties, for example their solubility in a suitable solvent such as methanol saturated with ammonia. This agent dissolves the non-illuminated part of the As_2S_3 film but the silver-doped part becomes practically insoluble. Figure 5 is a scanning electron micrograph of the surface relief grating produced in a spin-coated As_2S_3 film by light-enhanced silver diffusion and subsequent selective etching using the above solvent. In this experiment the sample was illuminated with the holographic arrangement of Fig. 2 using prism (1), *i.e.* the intersecting beams reach the surface of the sample with an angle of incidence $\theta = 20°$. According to eqn. (1) this will produce a standing wav. with the distance Λ between the neighbouring interference maxima (the grating period) of about 0.75 μm. The electron micrograph in Fig. 5 shows that the standing wave pattern is reproduced as a surface relief grating after selective etching. The applied laser power was 13.5 mW and the illuminated area was 1.84 cm^2, resulting in a laser power density of 7.34×10^{-3} W cm^{-2}. The duration of the illumination was 10 min, *i.e.* an illumination energy of 4.4 J cm^{-2} was obtained. This illumination energy caused the silver to diffuse to a depth of about 0.6 μm, as can be estimated from the surface profile shown in Fig. 6 which is an electron micrograph of the grating taken in a tilted position with an angle close to 90°. Since the groove profile is basically a sine wave, it can be concluded that the silver diffusion depth (which determines the profile of the surface relief grating) is governed primarily by the light intensity profile.

The period of the recorded fringes can be increased significantly if a small angle of incidence is used for illumination with the same wavelength (see eqn. (1)). This is achieved by using prism (2) which produces an angle of incidence $\theta = 0.7°$ for the two intersecting beams. This resulted in a grating period $\Lambda \approx 22$ μm as seen in Fig. 7.

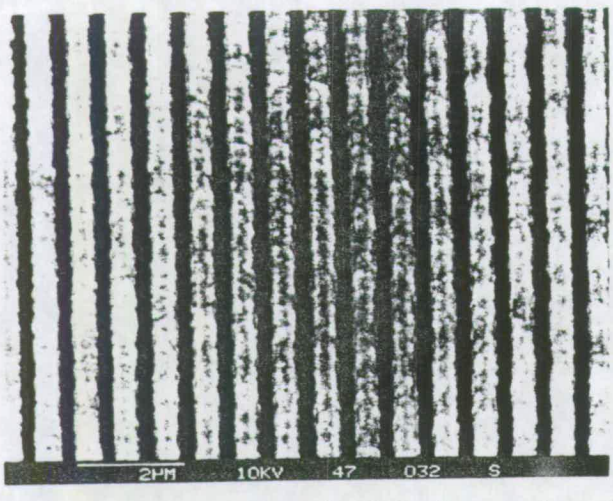

Fig. 5. Scanning electron micrograph of the interference grating produced in spin-coated As_2S_3 by silver photodiffusion.

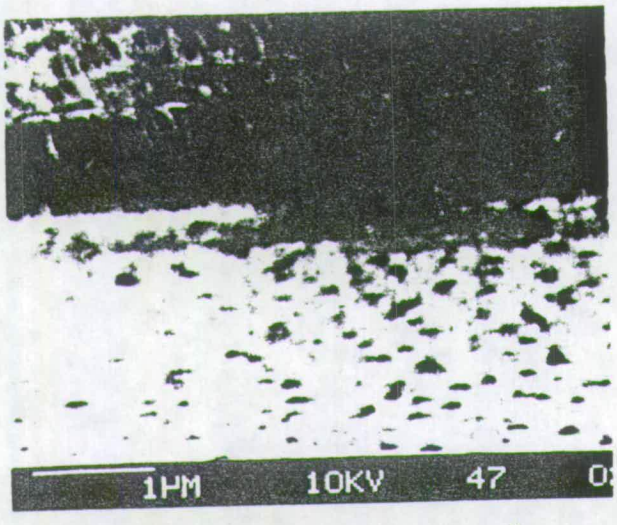

Fig. 6. Scanning electron micrograph of the grating profile.

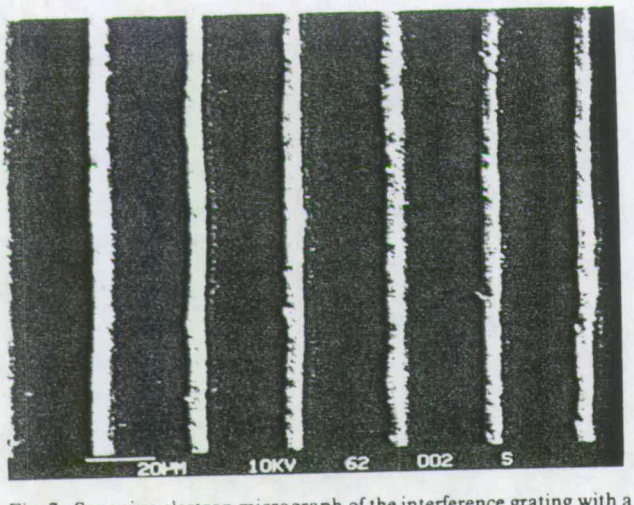

Fig. 7. Scanning electron micrograph of the interference grating with a grating period of about 22 μm.

The surface relief gratings prepared in this way are considered as thin holographic gratings. The distinction between thick and thin holographic gratings is usually made with the aid of the Q parameter[15] defined as

$$Q = 2\pi\lambda d/n\Lambda^2 \tag{2}$$

where λ is the illuminating wavelength, n is the refractive index, d is the thickness and Λ is the spacing of the recorded fringes. The holographic grating is considered thick when $Q \geq 10$ and thin otherwise. In our case a value $Q \approx 1.4$ can be obtained using the experimentally determined parameters of $\lambda = 0.6\,\mu m$, $n = 3.0$ (see Fig. 4), $d = 0.56\,\mu m$ (see Fig. 6) and $\Lambda = 0.7\,\mu m$ (see Fig. 6).

Holographic gratings are also classified by the mechanism by which the illuminating light is diffracted. In the amplitude grating, the interference pattern is

recorded as a density variation of the recording medium and the amplitude of the illuminating wave is modulated. In the phase grating a phase modulation occurs when the illuminating wave passes through the film. In our case it is primarily the phase of the illuminating wave which is modulated and diffracted from the surface relief grating. The change $\Delta\phi$ in the phase is given by

$$\Delta\phi = \frac{2\pi}{\lambda}\{d\,\Delta n + (n-1)\,\Delta d\} \tag{3}$$

where Δn is the difference in the refractive index, Δd is the difference in the thickness and λ is the illuminating wavelength. If the hologram is physically thin, d is very small and the contribution to $\Delta\phi$ from the term $d\,\Delta n$ is negligible so that

$$\Delta\phi = \frac{2\pi}{\lambda}(n-1)\,\Delta d \tag{4}$$

suggesting that the surface relief modulates the light by the differences in the thickness of the film[15].

For an ideal sinusoidal grating one would expect the light to be diffracted only into the angles determined by the grating equation[14]

$$\Lambda(\sin\alpha + \sin\beta) = m\lambda \tag{5}$$

where Λ is the grating period, α and β are the angles of incidence and diffraction, m is the order number and λ is the wavelength of the light used. Therefore the grating period Λ can be determined from the measured angle of the diffracted beam. It was found that if the measuring light ($\lambda = 0.6328$ μm) is used at normal incidence relative to the surface relief grating, the diffracted beams exit the surface at angles $\beta = \pm 56.4°$. This gives $\Lambda = 0.76$ μm for the period of the grating, in good agreement with the micrographs of the surface relief grating (seen in Figs. 5 and 6).

The efficiency of a grating is defined as the fraction of the incident radiation that is diffracted into the required order. Figure 8 shows the measured efficiency of the surface relief grating using an He–Ne laser ($\lambda = 0.6328$ μm) at normal incidence. These measurements were obtained on the same surface relief grating but used in reflection mode. (For these measurements the sample was covered with a thin aluminium layer in the order to increase the reflectivity.) The efficiency is determined

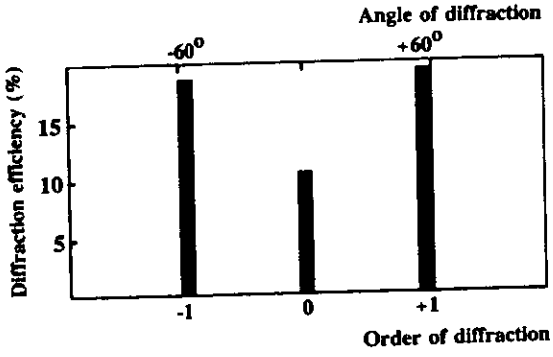

Fig. 8. Diffraction efficiency of the grating with 0.7 μm period as measured with 6328 Å light at normal incidence.

primarily by the groove profile and if the grating is illuminated at normal incidence it cannot be higher than 50% in any order because of the symmetry. In practice the efficiency seldom exceeds 33% in this configuration[14]. Figure 8 shows that approximately 18% efficiency is measured at the diffracted orders of ± 1 (at angles $\beta = \pm 56.4°$), suggesting that the profile of the surface relief grating is close to the "ideal" sinusoidal profile. Similar diffraction efficiencies were obtained in a vacuum-evaporated chalcogenide–silver double-layer system[16]. The roughness of the surface (see Fig. 5) might introduce a random variation in phase and amplitude of the diffracted light which might generate diffuse scattering. However, according to the theoretical analysis[17] the spectral image of the diffracted light does not change significantly; the efficiency may decrease slightly but the distribution of light among the diffracted orders is much the same. It should also be emphasized that we did not observe spurious diffracted orders or diffuse scatter which might arise from periodic errors or imperfections across the surface of the grating.

We suggest that the large variation observed in the optical constants of the As_2S_3 films as a result of light-enhanced silver diffusion could also be used for recording thin amplitude or phase holograms. In this process no selective etching is necessary because the hologram can be recorded as changes in the absorption coefficient or the refractive index, which are in turn determined by the amplitude and the phase of the illuminating beam. It can be seen from Fig. 3 that silver doping increases the absorption coefficient (measured at 0.6 μm) from $\alpha = 1.35 \times 10^3\ cm^{-1}$ to $\alpha = 4.67 \times 10^3\ cm^{-1}$, which can be used for recording an amplitude hologram. In addition, the refractive index (measured at 0.6 μm) increases from $n = 2.22$ to $n = 3$ (see Fig. 4) as a result of light-induced silver diffusion. This effect can be used to produce a phase shift of the illuminating wave, *i.e.* to record a phase hologram. In our case these two effects occur simultaneously, indicating that the amplitude transmittance of such a hologram will be a complex function that describes the change in the amplitude and the phase of an illuminating wave on transmission through the material.

4. CONCLUSIONS

The optical constants and solubility of spin-coated As_2S_3 films significantly change after silver is incorporated by photodiffusion and these changes can be used to record grating patterns in the films. The silver diffusion depth, which determines the profile of the surface relief grating, is governed primarily by the light intensity profile. The recorded pattern can be developed using selective etching or, alternatively, the observed changes in the optical constants as a result of silver photodiffusion can enable the material to modulate the amplitude and the phase of the transmitted light, thereby facilitating the recording of amplitude or phase holograms.

ACKNOWLEDGMENT

E. H. is grateful to the U.K. Science and Engineering Research Council and Pilkington Brothers plc. for the provision of a CASE studentship.

REFERENCES

1 A. Matsuda and M. Kikuchi, *J. Jpn. Soc. Appl. Phys.*, *42* (1973) 239–248.
2 A. E. Owen, A. P. Firth and P. J. S. Ewen, *Philos. Mag. B*, *52* (1985) 347–362.
3 A. V. Kolobov, S. R. Elliott and M. A. Taguirdzhanov, *Philos. Mag. B*, *61* (1990) 859–865.
4 G. C. Chern and I. Lauks, *J. Appl. Phys.*, *54* (1983) 4596–4601.
5 E. Hajto, P. J. S. Ewen, R. Belford, J. Hajto and A. E. Owen, *J. Non-Cryst. Solids*, *97–98* (1987) 1191–1194.
6 G. C. Chern and I. Lauks, *J. Appl. Phys.*, *54* (1983) 2701–2705.
7 E. Hajto, P. J. S. Ewen, P. G. Hill and A. E. Owen, *Phys. Status Solidi A*, *114* (1989) 587–597.
8 E. Hajto, R. E. Belford, P. J. S. Ewen and A. E. Owen, *J. Non-Cryst. Solids*, *115* (1989) 129–131.
9 K. Kase, G. C. Chern and I. Lauks, *Thin Solid Films*, *116* (1984) L53–L54.
10 A. Zakery, C. W. Slinger, P. J. S. Ewen, A. P. Firth and A. E. Owen, *J. Phys. D*, *21* (1988) S78–S81.
11 G. C. Chern and I. Lauks, *J. Appl. Phys.*, *53* (1982) 6979–6982.
12 R. Swanepoel, *J. Phys. E*, *16* (1983) 1214.
13 F. Abeles, *Optical Properties of Solids*, North-Holland, Amsterdam.
14 M. C. Hutley, *Diffraction Gratings*, Academic Press, London, 1982.
15 H. M. Smith (ed.), *Holographic Recording Materials*, Topics in Applied Physics, Vol. 20, Springer, Berlin, 1977.
16 T. Fukaya, S. Matsumura, J. Tsujiuchi, E. Inoue and H. Kokudo, *Opt. Commun.*, *7* (1973) 98–102.
17 M. C. Hutley, *J. Physics E*, *9* (1976) 513–520.